

MODERN WELL TEST ANALYSIS

A Computer-Aided Approach



Roland N. Horne

MODERN WELL TEST ANALYSIS

A Computer-Aided Approach

Roland N. Horne

Stanford University

OVERVIEW

During the 1980's, there were several major advances in the science of well test interpretation. These have been associated with: (i) the use of pressure derivative plots, (ii) the common availability of computer software for rapid graphical presentation, (iii) the use of non-linear regression (automated type curve matching), (iv) the availability of higher precision, high frequency data, both for pressure and flow rate, and (v) the development of new interpretation models, such as for multiphase flow and for multilayered reservoirs. This book emphasizes well test interpretation in this new computerized environment. During the book, emphasis is on problem solving, using computerized tools.

COPYRIGHT

Copyright © 1990, by Petroway, Inc
926 Bautista Court
Palo Alto, CA 94303
(415)494-2037
fax: (415)494-8160

Fourth Printing

ISBN 0-9626992-0-9

All rights reserved. Reproduction or use, without express permission, of editorial or pictorial content, in any manner, is prohibited. No patent liability is assumed with respect to the use of the information contained herein. While every precaution has been taken in the preparation of this book, neither the publisher or the author assumes responsibility for errors or omissions. Neither is any liability assumed for damage resulting from the use of the information contained herein.

Cover design by Yoshimi Segawa

Printed in the United States of America

Acknowledgements

This book brings together traditional material from earlier sources, together with new material prepared specifically for this work. In particular, I have made use of personal notes of Henry J. Ramey, Jr., and Matt Mavor, as well as the many references listed in the text. The work of these earlier authors who have collected material on well test analysis is gratefully acknowledged.

This is a book about computer-aided engineering, and has made extensive use of computer software throughout. The well test interpretation software used in the book was AUTOMATE-II, of which I am a co-author. However, most of the descriptions and explanations contained here are not specific to that software, and may be applied similarly to other packages. Examples of other software that could be used in similar ways would be INTERPRET, by SSI, WELLTEST, by ECL, and PAN/System, by Edinburgh Petroleum Services.

This manuscript was produced entirely electronically, including all of the diagrams. None of the figures were drawn by hand, and no paste-up was required. Typesetting and sketch diagrams were done using the software EROFF, by Elan Computer Group, Inc. Most of the well test diagrams were produced directly by the AUTOMATE-II software, and converted from HPGL to Postscript using PSPLOT by Legend Communications, Inc. Three figures in Section 2 were drawn using AutoSketch by Autodesk, Inc. The engineering calculations and typesetting were performed on an IBM PS/2 Model 80, and draft printed on an Apple LaserWriter II-NTX. Final printing used a Linotronic 300 printer at 1800 dpi.

Much of this manuscript was written while I was a guest of the Petroleum Engineering Department at Heriot-Watt University in Edinburgh, Scotland, and I am indebted to Prof. Jim Peden and his faculty and staff for their hospitality and support during my visit. The first draft of this material was originally prepared for a short course organized in Jakarta, Indonesia, by Jamin Djuang of P.T. Loka Datamas Indah in February 1990. Subsequent to this first "test flight", corrections and expansions brought the manuscript to its present form. Based on its origins as course material, this book is intended as a tutorial on well testing, rather than a full textbook or comprehensive reference.

This book is dedicated to my friend and mentor, Hank Ramey, who truly deserves the title of "the father of modern well test analysis".

*Roland N. Horne
Palo Alto, California
May 1990*

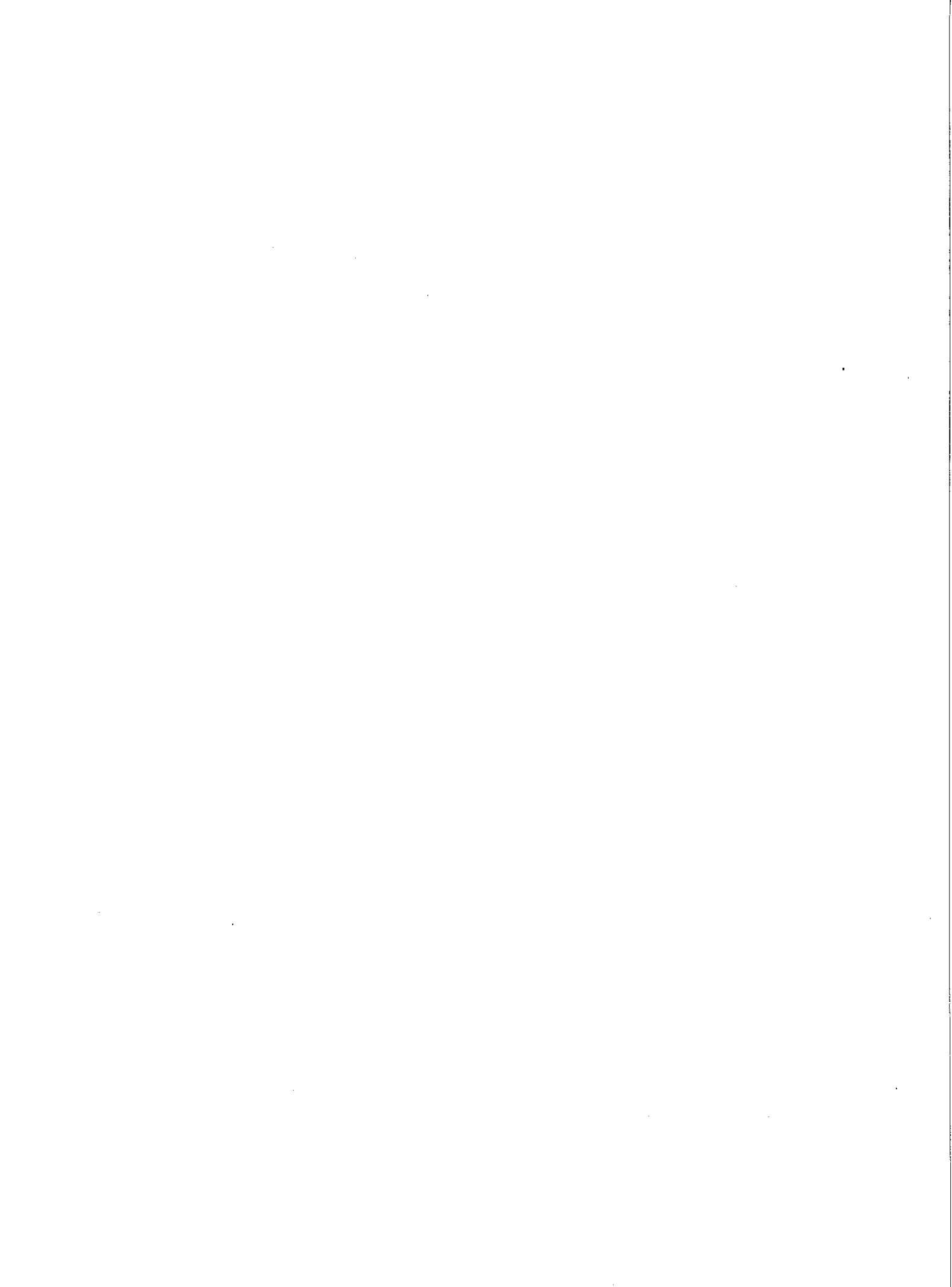


Table of Contents

TABLE OF CONTENTS

1. WELL TEST OBJECTIVES	1
1.1 Introduction.....	1
1.2 Reservoir Evaluation.....	1
1.3 Reservoir Management	2
1.4 Reservoir Description	2
1.5 Decline Curve Analysis	3
1.6 Types of Tests	3
1.6.1 Drawdown Test.....	3
1.6.2 Buildup Test.....	4
1.6.3 Injection Test.....	4
1.6.4 Falloff Test.....	5
1.6.5 Interference Test	5
1.6.6 Drill Stem Test (DST).....	6
1.7 References.....	6
2. WELL TEST CONCEPTS	7
2.1 Basics of Reservoir Models.....	7
2.2 Dimensionless Variables	8
2.3 Log-Log Type Curves	9
2.4 The Skin Effect	10
2.4.1 Flow Efficiency	13
2.5 Wellbore Storage	13
2.6 Infinite Acting Radial Flow	19
2.7 Reservoir Boundary Response	20
2.7.1 Closed Boundaries.....	21
2.7.2 Fault Boundaries	25
2.7.3 Constant Pressure Boundaries	25

Table of Contents

2.8 Fractured Wells.....	26
2.8.1 Finite Conductivity Fractures	27
2.8.2 Infinite Conductivity Fractures	28
2.8.3 Uniform Flux Fractures	30
2.9 Double Porosity Behavior	31
2.10 Summary of Responses in Time Sequence.....	35
2.11 Superposition	36
2.12 References	42
3. INTRODUCTION TO COMPUTER-AIDED ANALYSIS.....	43
3.1 Graphical Representations	43
3.2 The Derivative Plot	44
3.3 Diagnostic Plot Evaluation	51
3.4 Data Preparation	52
3.4.1 Number and Frequency of Data.....	52
3.4.2 Datum Shifting	54
3.5 Nonlinear Regression	55
3.5.1 Confidence Intervals.....	55
3.5.2 Initial Pressure	60
3.5.3 Multirate and Variable Rate Tests	61
3.6 Desuperposition	63
3.7 Interpretation Sequence	63
3.8 Non-Ideality	64
3.9 References.....	66
4. INTERPRETATION EXAMPLES - HOMOGENEOUS RESERVOIRS.....	68
4.1 Drawdown Example	68
4.1.1 Traditional Graphical Analysis	68

Table of Contents

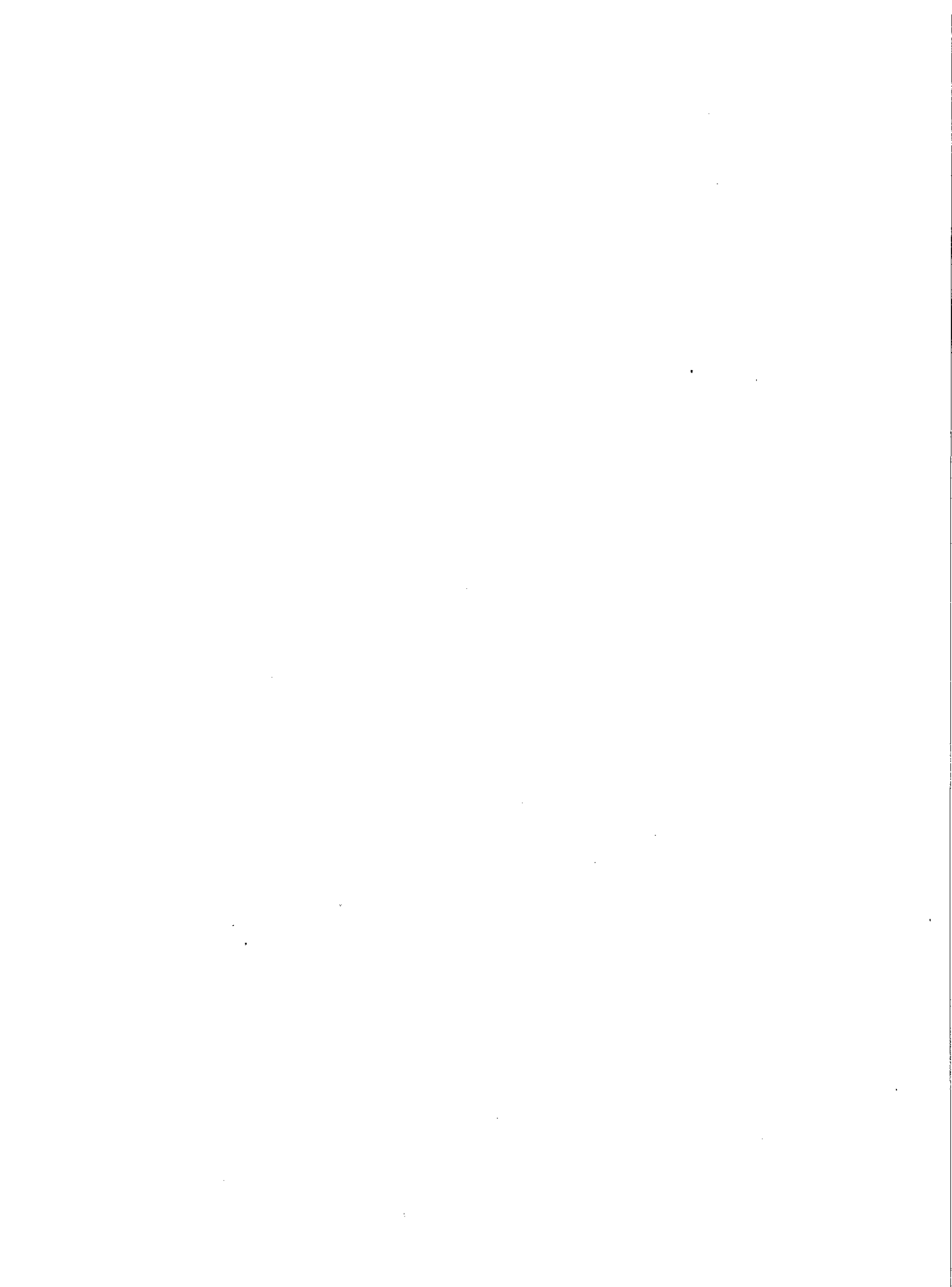
4.1.1.1 Identifying Flow Periods	68
4.1.1.2 Estimating Parameters	69
4.1.1.3 Type Curve Match	72
4.1.1.4 Comparison of Graphical Estimates	74
4.1.1.5 Time Shift Errors.....	75
4.1.1.6 Confidence Intervals	77
4.1.2 Nonlinear Regression	78
4.1.3 Boundary Effects.....	80
4.1.4 Ambiguity.....	84
4.1.5 Truncated Data.....	86
4.1.6 Simultaneous Rate-Pressure Data.....	89
4.2 Buildup Example	91
4.2.1 Test Without Boundary Effects	91
4.2.2 Effects of Boundaries.....	93
4.2.3 Knowledge of p_{wf}	96
4.2.4 Average Reservoir Pressure	96
4.2.5 Treating Buildups as Drawdowns.....	98
4.3 References.....	99
5. INTERPRETATION EXAMPLES - FRACTURED WELLS	100
5.1 Finite Conductivity Fracture Example.....	100
5.2 Infinite Conductivity Fracture Example	106
6. INTERPRETATION EXAMPLES - DOUBLE POROSITY RESERVOIRS	112
6.1 Drawdown Example.....	112
6.2 Buildup Example	118
6.3 References.....	120

Table of Contents

7. INTERPRETATION EXAMPLES - INTERFERENCE TESTS	121
7.1 Single Well Pair Example	121
7.2 Multirate Example	123
8. GAS WELL TESTS	127
8.1 Real Gas Pseudopressure and Pseudotime	127
8.2 Calculating Pseudopressure	129
8.3 Using Pseudopressure in Graphical Interpretation.....	129
8.4 Rate Dependent Skin Effect	131
8.5 Example Interpretation.....	131
8.6 References.....	135
9. MULTIPHASE WELL TESTING	137
9.1 Perrine's Approach	138
9.2 Pressure Squared Approach	140
9.3 References.....	141
10. DESIGNING WELL TESTS.....	142
10.1 Variable Dependency	142
10.2 Test Duration	143
10.3 Flow Rate Considerations.....	144
11. CALCULATING PROPERTIES	146
11.1 Oil Properties	146
11.2 Gas Properties	148
11.3 Water Properties	151
11.4 Rock Properties	152
11.5 Total Properties.....	152
11.6 References	153

Table of Contents

APPENDIX - Example Data	155
Example 4.1	155
Example 4.2	158
Example 5.1	161
Example 5.2	164
Example 6.1	167
Example 6.1(a).....	170
Example 6.2	172
Example 7.1	176
Example 7.2	178
Example 8.1	180



1. WELL TEST OBJECTIVES

1.1 Introduction

During a well test, the response of a reservoir to changing production (or injection) conditions is monitored. Since the response is, to a greater or lesser degree, characteristic of the properties of the reservoir, it is possible in many cases to infer reservoir properties from the response. Well test interpretation is therefore an inverse problem in that model parameters are inferred by analyzing model response to a given input.

In most cases of well testing, the reservoir response that is measured is the pressure response. Hence in many cases well test analysis is synonymous with pressure transient analysis. The pressure transient is due to changes in production or injection of fluids, hence we treat the flow rate transient as input and the pressure transient as output.

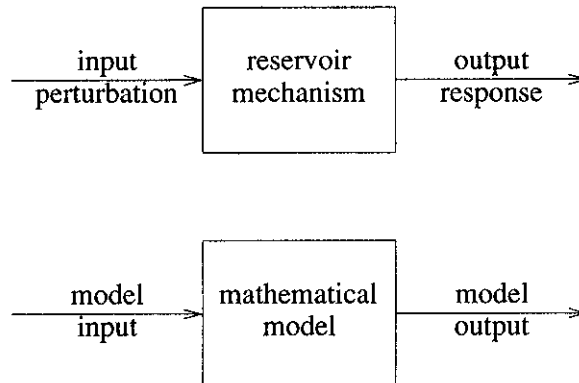


Figure 1.1

In well test interpretation, we use a mathematical model to relate pressure response (output) to flow rate history (input). By specifying that the flow rate history input in the model be the same as that in the field, we can infer that the model parameters and the reservoir parameters are the same if the model pressure output is the same as the measured reservoir pressure output. Clearly, there can be major difficulties involved in this process, since the model may act like the actual reservoir even though the physical assumptions are entirely invalid. This ambiguity is inherent in all inverse problems, including many others used in reservoir engineering (e.g., history matching in simulation, decline curve analysis, material balance). However, the dangers can be minimized by careful specification of the well test in such a way that the response is most characteristic of the reservoir parameters under investigation. Thus in most cases, the design and the interpretation of a well test is dependent on its objectives.

The objectives of a well test usually fall into three major categories: (i) reservoir evaluation, (ii) reservoir management, and (iii) reservoir description.

1.2 Reservoir Evaluation

To reach a decision as to how best to produce a given reservoir (or even whether it is worthwhile to spend the money to produce it at all) we need to know its deliverability, properties, and size. Thus we will attempt to determine the reservoir conductivity (kh , or permeability-thickness product), initial

reservoir pressure, and the reservoir limits (or boundaries). At the same time, we will sample the fluids so that their physical properties can be measured in the laboratory. Also, we will examine the near wellbore condition in order to evaluate whether the well productivity is governed by wellbore effects (such as skin and storage) or by the reservoir at large.

The conductivity (kh) governs how fast fluids can flow to the well. Hence it is a parameter that we need to know to design well spacing and number of wells. If conductivity is low, we may need to evaluate the cost-effectiveness of stimulation.

Reservoir pressure tells us how much potential energy the reservoir contains (or has left) and enables us to forecast how long the reservoir production can be sustained. Pressures in the vicinity of the wellbore are affected by drilling and production processes, and may be quite different from the pressure and the reservoir at large. Well test interpretation allows us to infer those distant pressures from the local pressures that can actually be measured.

Analysis of reservoir limits enables us to determine how much reservoir fluid is present (be it oil, gas, water, steam or any other) and to estimate whether the reservoir boundaries are closed or open (with aquifer support, or a free surface).

1.3 Reservoir Management

During the life of a reservoir, we wish to monitor performance and well condition. It is useful to monitor changes in average reservoir pressure so that we can refine our forecasts of future reservoir performance. By monitoring the condition of the wells, it is possible to identify candidates for workover or stimulation. In special circumstances, it may also be possible to track the movement of fluid fronts within the reservoir, such as may be seen in water flooding or in-situ combustion. Knowledge of the front location can allow us to evaluate the effectiveness of the displacement process and to forecast its subsequent performance.

1.4 Reservoir Description

Geological formations hosting oil, gas, water and geothermal reservoirs are complex, and may contain different rock types, stratigraphic interfaces, faults, barriers and fluid fronts. Some of these features may influence the pressure transient behavior to a measurable extent, and most will affect the reservoir performance. To the extent that it is possible, the use of well test analysis for the purpose of reservoir description will be an aid to the forecasting of reservoir performance. In addition, characterization of the reservoir can be useful in developing the production plan.

Examples of the use of well test analysis for reservoir description can be found in Britt et al. (1989), Myers et al. (1980), Lee (1982), Currier (1988) and Roest et al. (1986). However, it is important to acknowledge that there is a limit to the level of detail that can be achieved in a reservoir description. This is because pressure transmission is an inherently *diffusive* process, and hence is governed largely by average conditions rather than by local heterogeneities. For example, Grader and Horne (1988) showed that it is possible to have a "hole" in the reservoir that is as large as half the distance between a production well and an observation well, without that "hole" making any discernable difference in an interference test. This observation appears discouraging at first, however it underlines the overall usefulness of well test analysis -- well tests can be interpreted to estimate bulk reservoir properties *because* they are insensitive to most local scale heterogeneities.

1.5 Decline Curve Analysis

The discussions above have referred to pressure transient analysis, in which the pressure transient is considered to be the response of a system to a specific flow rate history. It should be clear however that it is equally valid to consider a flow rate response to a specific pressure history. This case, in which well flowing pressure is usually treated as constant and production rate declines, is commonly known as decline curve analysis. Fundamentally, there is no difference between pressure transient analysis and decline curve analysis, however, there are practical considerations that usually separate the two applications. Since flow rate is the easier of the two functions to control in a short term test, pressure transient tests (such as drawdown, buildup and interference tests) are usually conducted over only a few hours or days. Hence pressure transient tests are usually used to diagnose near wellbore conditions, such as kh , storage and skin. During long term production, pressure is often controlled by production equipment requirements, and production rates are monitored in the long term (over months and years) for decline curve analysis. Hence decline curve analysis is more diagnostic of long term effects, such as reservoir volume.

In general terms, both flow rate and pressure are interdependent, and both are governed by reservoir characteristics. Thus pressure transient analysis and decline curve analysis are specific examples of the same process, although traditionally each has been developed somewhat differently. In this book, the distinction between them will be removed. Any time that flow rate and pressure both are measured it is possible to specify one and match the other. Because of the diffusive nature of pressure transmission mentioned earlier, it is often easier to match pressures than it is to match flow rates.

1.6 Types of Tests

In some cases, the type of test performed is governed by the test objectives. In other cases the choice is governed by practical limitations or expediencies. For the purpose of later discussion, the various types of test will be defined in this section.

1.6.1 Drawdown Test

In a drawdown test, a well that is static, stable and shut-in is opened to flow. For the purposes of traditional analysis, the flow rate is supposed to be constant (Figure 1.2).

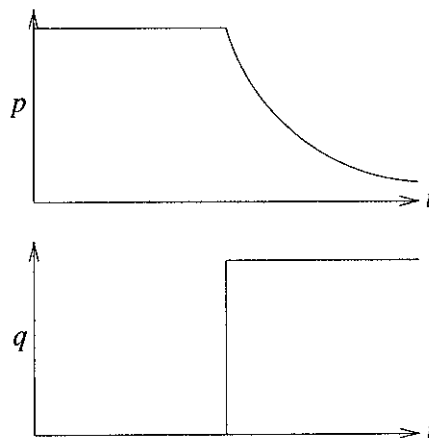


Figure 1.2

Many of the traditional analysis techniques are derived using the drawdown test as a basis (including many of the derivations in Section 2). However, in practice, a drawdown test may be rather difficult to achieve under the intended conditions. In particular: (a) it is difficult to make the well flow at constant rate, even after it has (more-or-less) stabilized, and (b) the well condition may not initially be either static or stable, especially if it was recently drilled or had been flowed previously.

On the other hand, drawdown testing is a good method of reservoir limit testing, since the time required to observe a boundary response is long, and operating fluctuations in flow rate become less significant over such long times.

1.6.2 Buildup Test

In a buildup test, a well which is already flowing (ideally at constant rate) is shut in, and the downhole pressure measured as the pressure builds up (Fig. 1.3). Analysis of a buildup test often requires only slight modification of the techniques used to interpret constant rate drawdown test. The practical advantage of a buildup test is that the constant flow rate condition is more easily achieved (since the flow rate is zero).

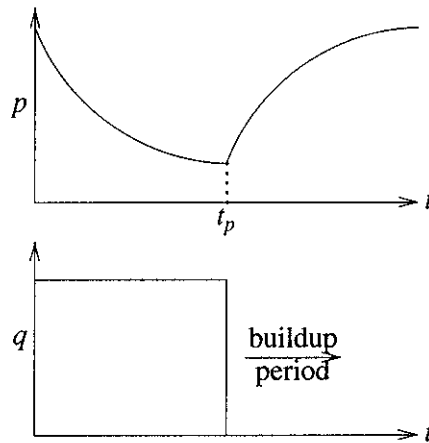


Figure 1.3

Buildup tests also have disadvantages:

- (a) It may be difficult to achieve the constant rate production prior to the shut in. In particular, it may be necessary to close the well briefly to run the pressure tool into the hole.
- (b) Production is lost while the well is shut in.

1.6.3 Injection Test

An injection test is conceptually identical to a drawdown test, except that flow is into the well rather than out of it (Fig. 1.4).

Injection rates can often be controlled more easily than production rates, however analysis of the test results can be complicated by multiphase effects unless the injected fluid is the same as the original reservoir fluid.

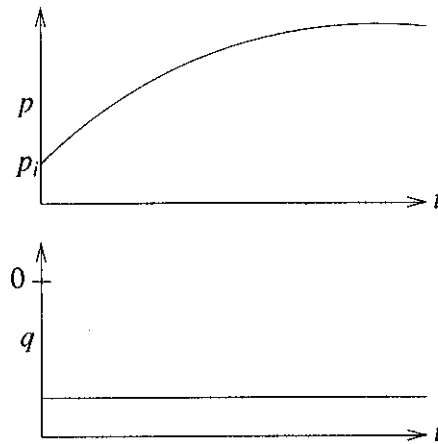


Figure 1.4

1.6.4 Falloff Test

A falloff test measures the pressure decline subsequent to the closure of an injection (Fig. 1.5). It is conceptually identical to a buildup test.

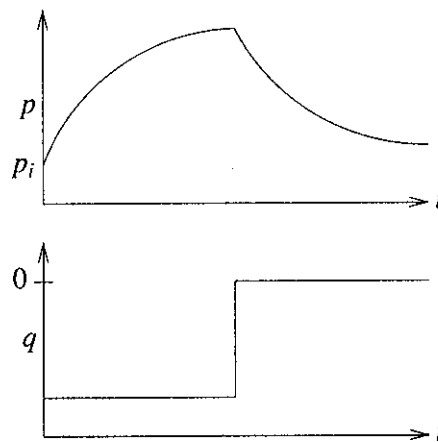


Figure 1.5

As with injection tests, falloff test, interpretation is more difficult if the injected fluid is different from the original reservoir fluid.

1.6.5 Interference Test

In an interference test, one well is produced and pressure is observed in a different well (or wells). An interference test monitors pressure changes out in the reservoir, at a distance from the original producing well. Thus an interference test may be useful to characterize reservoir properties over a greater length scale than single-well tests. Pressure changes at a distance from the producer are very much smaller than in the producing well itself, so interference tests require sensitive pressure recorders and may take a long time to carry out. Interference tests can be used regardless of the type of pressure change induced at the active well (drawdown, buildup, injection or falloff).

1.6.6 Drill Stem Test (DST)

A drill stem test is a test which uses a special tool mounted on the end of the drill string. It is a test commonly used to test a newly drilled well, since it can only be carried out while a rig is over the hole. In a DST, the well is opened to flow by a valve at the base of the test tool, and reservoir fluid flows up the drill string (which is usually empty to start with). A common test sequence is to produce, shut in, produce again and shut in again. Drill stem tests can be quite short, since the positive closure of the downhole valve avoids wellbore storage effects (described later). Analysis of the DST requires special techniques, since the flow rate is not constant as the fluid level rises in the drill string. Complications may also arise due to momentum and friction effects, and the fact that the well condition is affected by recent drilling and completion operations may influence the results.

References

Britt, L.K., Jones, J.R., Pardini, R.E., and Plum, G.L.: "Development of a Reservoir Description Through Interference Testing of the Clayton Field, Prairie du Chien Formation", paper SPE 19846, *Proceedings SPE 64th Annual Fall Technical Conference and Exhibition*, San Antonio, TX, Oct 8-11, (1989), 787-800.

Currier, B.H.: "Lisburne Reservoir Limited Drainage Test: A Pilot Test Case History", paper SPE 18277, presented at SPE 63rd Annual Fall Technical Conference and Exhibition, Houston, TX, Oct 2-5, (1988).

Grader, A., and Horne, R.N.: "Interference testing: Detecting an Impermeable or Compressible Sub-Region," *SPE Formation Evaluation*, (1988), 428-437.

Lee, B.O.: "Evaluation of Devonian Shale Reservoirs Using Multiwell Pressure Transient Testing Data," paper SPE/DOE 10838, presented at the SPE/DOE Unconventional Gas Recovery Symposium, Pittsburgh, PA, May 16-18, (1982).

Myers, G.A., Johnson, R.D., and Mainwaring, J.R.: "Simulation of Prudhoe Bay Field Interference Test" paper SPE 9456, presented at SPE 55th Annual Fall Technical Conference and Exhibition, Dallas, TX, Sept 21-24, (1980).

Roest, J.A., Jolly, D.C., and Rogriguez, R.A.: "Pulse Testing Reveals Poor Lateral and Vertical Continuity in a Reservoir Consisting of Distributary Channel Sands", paper SPE 15613, presented at SPE 61st Annual Fall Technical Conference and Exhibition, New Orleans, LA, Oct 5-8 (1986).

2. WELL TEST CONCEPTS

2.1 Basics of Reservoir Models

In the process of testing a well, we provide an input *impulse* (usually a change in flow rate) and we measure the *response* (usually a change in pressure). The reservoir response is governed by parameters such as permeability, skin effect, storage coefficient, distance to boundaries, fracture properties, double porosity coefficients, etc. Based on an understanding of the reservoir physics, we develop a mathematical model of the dependence of the response on these reservoir parameters. Then by matching the *model response* to the measured *reservoir response* we infer that the model parameters take the same values of the reservoir parameters. This process is illustrated in Fig. 2.1.

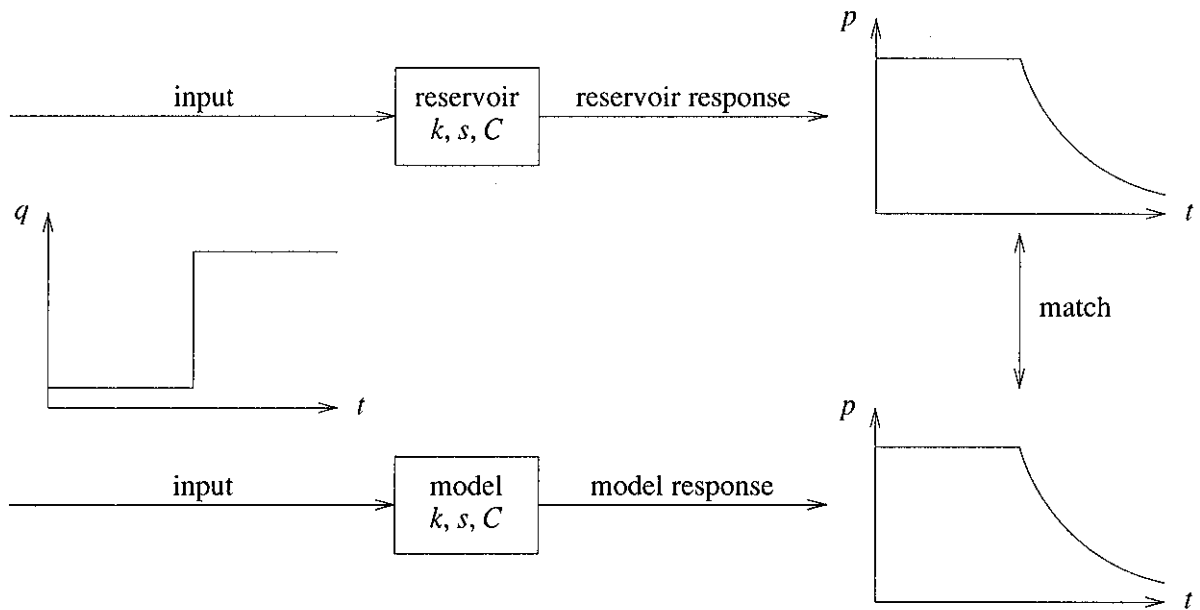


Figure 2.1

The mathematical model can be either analytical or numerical (i.e., a reservoir simulator), but is usually analytical. The remainder of this section will discuss the basis of these analytical reservoir models.

The mathematical equation governing pressure transmission in a porous medium filled by slightly compressible fluid is given by (in cylindrical coordinates):

$$\frac{\partial^2 p}{\partial r^2} + \frac{1}{r} \frac{\partial p}{\partial r} + \frac{k_\theta}{k_r} \frac{1}{r^2} \frac{\partial^2 p}{\partial \theta^2} + \frac{k_z}{k_r} \frac{\partial^2 p}{\partial z^2} = \frac{\phi \mu c_t}{k_r} \frac{\partial p}{\partial t} \quad (2.1)$$

Assumptions inherent in this equation are:

- Darcy's Law applies,
- Porosity, permeabilities, viscosity and compressibility are constant,
- Fluid compressibility is small (this equation is not usually valid for gases),
- Pressure gradients in the reservoir are small (this may not be true in high rate wells or for gases),

- (e) Flow is single phase,
 (f) Gravity and thermal effects are negligible.

If permeability is isotropic, and only radial and vertical flow are considered, then this equation reduces to:

$$\frac{\partial^2 p}{\partial r^2} + \frac{1}{r} \frac{\partial p}{\partial r} + \frac{\partial^2 p}{\partial z^2} = \frac{\phi \mu c_t}{k} \frac{\partial p}{\partial t} \quad (2.2)$$

This equation is recognizable as the diffusion equation, which appears in many fields of science and engineering. This underlines the importance of the diffusion process in well test interpretation, and emphasizes the underlying significance of the hydraulic diffusivity parameter $k/\phi\mu c_t$.

For the purposes of this book (and for the application of well test interpretation in general), it is not necessary for us to understand the process of solution of the pressure transmission equation (Eq. 2.2). Solutions to this equation have been developed for a wide variety of specific cases, covering many reservoir configurations. These specific reservoir solutions are the models that we will use to match reservoir behavior, thereby inferring reservoir parameters that we do not know in advance.

2.2 Dimensionless Variables

Well test analysis often makes use of dimensionless variables. The importance of dimensionless variables is that they simplify the reservoir models by embodying the reservoir parameters (such as k), thereby reducing the total number of unknowns. They have the additional advantage of providing model solutions that are independent of any particular unit system. It is an inherent assumption in the definition that permeability, viscosity, compressibility, porosity, formation volume factor and thickness are all constant.

The dimensionless pressure p_D is defined (in oilfield units) as

$$p_D = \frac{kh}{141.2qB\mu} (p_i - p_{wf}) \quad (2.3)$$

where k	=	permeability (md)
h	=	thickness (feet)
p_i	=	initial reservoir pressure (psi)
p_{wf}	=	well flowing pressure (psi)
q	=	production rate (STB/d)
B	=	formation volume factor (res vol/std vol)
μ	=	viscosity (cp)

In a consistent unit set, p_D is defined as

$$p_D = \frac{2\pi kh}{qB\mu} (p_i - p_{wf}) \quad (2.3a)$$

The dimensionless time t_D is defined (in oilfield units) as

$$t_D = \frac{0.000264kt}{\phi\mu c_t r_w^2} \quad (2.4)$$

where t	=	time (hours)
ϕ	=	porosity (pore volume/bulk volume)
c_t	=	total system compressibility (/psi)
r_w	=	wellbore radius (ft)

In a consistent unit set, t_D is defined as

$$t_D = \frac{kt}{\phi\mu c_t r_w^2} \quad (2.4a)$$

This is only one form of the dimensionless time. Another definition in common usage is t_{DA} , the dimensionless time based upon reservoir area:

$$t_{DA} = \frac{0.000264kt}{\phi\mu c_t A} \quad (2.5)$$

where A	=	reservoir area = πr_e^2
r_e	=	reservoir radius (ft)

Clearly there is a direct relationship between t_D and t_{DA}

$$t_D = t_{DA} \frac{A}{r_w^2} = t_{DA} \pi \frac{r_e^2}{r_w^2} \quad (2.6)$$

We can also define a dimensionless radius, r_D , as

$$r_D = \frac{r}{r_w} \quad (2.7)$$

This definition is independent of any particular set of units.

2.3 Log-Log Type Curves

Having just defined dimensionless pressure and time, it is worthwhile to discuss log-log type curves since this is one of the primary uses of dimensionless variables in well test interpretation. Since, by definition, dimensionless pressure and time are *linear* functions of actual pressure and time (recall Eqs. 2.3 and 2.4), then the logarithm of actual pressure drop will differ from the logarithm of dimensionless pressure drop *by a constant amount*.

$$\log \Delta p = \log p_D - \log \frac{kh}{141.2qB\mu} \quad (2.8)$$

similarly

$$\log \Delta t = \log t_D - \log \frac{0.000264k}{\phi\mu c_t r_w^2} \quad (2.9)$$

Hence a graph of $\log \Delta p$ versus $\log t$ will have an *identical shape* to a graph of $\log p_D$ versus $\log t_D$, although the curve will be shifted by $\log kh/141.2qB\mu$ vertically (in pressure) and $\log 0.000264k/\phi\mu c_t r_w^2$ horizontally (in time). Matching the two curves will give us estimates of kh from $kh/(141.2qB\mu)$ (assuming q , B and μ are known) and ϕh (from $0.000264(kh)/(\phi h)\mu c_t r_w^2$, assuming μ , c_t and r_w^2 are known). This process provides a useful method of estimating two very important reservoir parameters, the transmissivity or ability to flow, and the storativity or quantity of fluid contained. Type curves can also be used to estimate other parameters -- this will be illustrated in examples later on.

2.4 The Skin Effect

Pressure transmission does not take place uniformly throughout the reservoir, since it is affected by local heterogeneities. For the most part, these do not affect the pressure change within the well, except those reservoir heterogeneities which are in the immediate vicinity of the wellbore. In particular, there is often a zone surrounding the well which is invaded by mud filtrate or cement during the drilling or completion of the well -- this zone may have a lower permeability than the reservoir at large, and thereby acts as a "skin" around the wellbore, causing higher pressure drop. This is shown in Fig. 2.2.

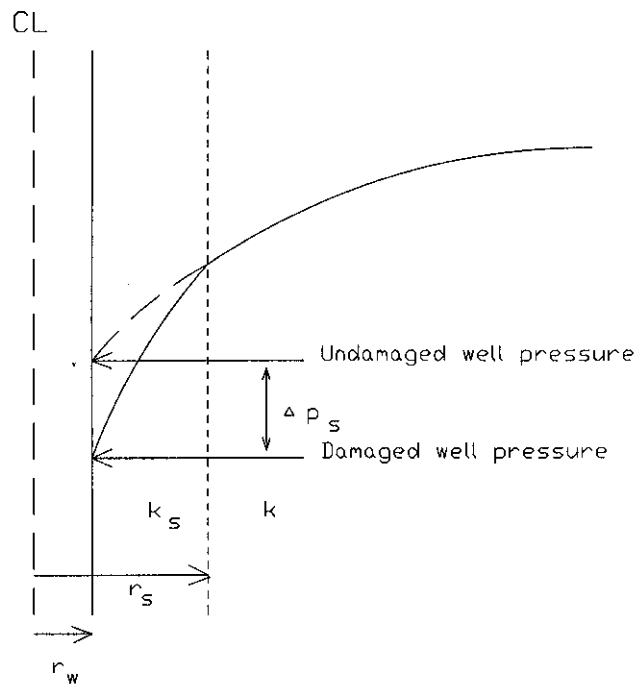


Figure 2.2

The pressure drop across the skin Δp_s is the difference between the actual pressure in the well when it is flowing, and the pressure that would have been seen if the well were undamaged. The skin factor is a dimensionless variable used to quantify the magnitude of the skin effect. The skin factor is defined (in oilfield units) as:

$$s = \frac{kh}{141.2qB\mu} \Delta p_s \quad (2.10)$$

In consistent units, the skin effect would be defined

$$s = \frac{2\pi kh}{qB\mu} \Delta p_s \quad (2.11)$$

If we imagine that the skin effect is due to a damaged zone of radius r_s and reduced permeability k_s , then the skin effect can be calculated from

$$s = \left[\frac{k}{k_s} - 1 \right] \ln \frac{r_s}{r_w} \quad (2.12)$$

We can also describe the skin effect in terms of an effective wellbore radius. This is the smaller radius that the well appears to have due to the reduction in flow caused by the skin effect. This effective radius is given by

$$r_{weff} = r_w e^{-s} \quad (2.13)$$

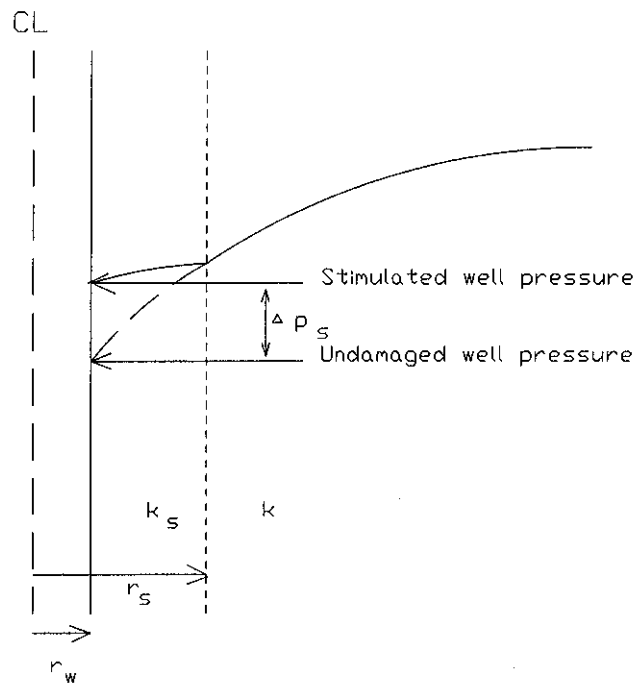


Figure 2.3

It can be seen from Eq. 2.12 that if the skin zone permeability k_s is higher than that of the reservoir (as can happen due to acidization or stimulation), then the skin effect can be negative. In the case of negative skin, the effective wellbore radius, given by Eq. 2.13, will be greater than the actual radius. The pressure distribution in this case would appear as in Fig. 2.3.

Clearly there is a limit as to how negative a negative skin effect can be, and in practice skin factors less than -5 are rarely seen. This is not the case for positive skin effects, which can have any magnitude (although they are rarely greater than 20).

Example 2.1

A 12 inch diameter hole has a damaged region 48 inches deep. The permeability in this region is one tenth that of the undamaged region. The skin effect can be estimated as follows

$$r_w = 0.5 \text{ feet}$$

$$r_s = r_w + 4 = 4.5 \text{ feet}$$

from Eq. 2.12

$$s = \left[\frac{k}{k_s} - 1 \right] \ln \frac{r_s}{r_w} = (10 - 1) \ln \frac{4.5}{0.5}$$

$$\underline{s = 19.78}$$

If, on the other hand, the 48 inch deep zone were stimulated instead of damaged, and the permeability enhancement was a factor of 10, then the skin factor would be

$$s = \left[0.1 - 1 \right] \ln \frac{4.5}{0.5}$$

$$\underline{s = -1.98}$$

From these two numerical examples, it can be seen that the numerical values of positive and negative skins are quite different. A tenfold *decrease* in permeability gives rise to a positive skin factor of about 20, whereas a tenfold *increase* in permeability produces a negative skin factor of only -2.

It is interesting also to look at the effective wellbore radii for the two cases just described. For the positive skin factor of 19.78, the effective wellbore radius will be

from Eq. 2.13

$$r_{weff} = 0.5 e^{-19.78}$$

$$r_{weff} = 1.28 \times 10^{-9} \text{ feet}$$

From this we can see that a skin of 19.78 is very large indeed! For the negative skin factor of -1.98, the effective wellbore radius will be

$$r_{weff} = 0.5 e^{1.98}$$

$$r_{weff} = 3.62 \text{ feet}$$

2.4.1 Flow Efficiency

A term sometimes used to describe the wellbore damage is flow efficiency, the ratio of the theoretical pressure drop if no skin had been present to the actual pressure drop measured during the test. The flow efficiency parameter can be used to calculate the flow rate that could be achieved if the wellbore damage were removed (by stimulation) since it is also the ratio of the ideal (zero skin) flow rate to the actual flow rate.

$$FE = \frac{\Delta p_{(zero\ skin)}}{\Delta p_{(actual)}} = \frac{q_{(actual)}}{q_{(zero\ skin)}} \quad (2.14)$$

In practice, flow efficiency is time dependent, not because the well damage is changing, but simply due to its mathematical definition. Thus it is not as definitive a parameter as skin factor, which is a constant for all time.

2.5 Wellbore Storage

We have understood that, in most cases, well test analysis is the interpretation of the pressure response of the reservoir to a given change in the rate (from zero to a constant value for a drawdown test, or from a constant value to zero for a buildup test). However, for many well tests, the only means of controlling the flow rate is at the wellhead valve or flow line. Hence although the well may produce at constant rate at the wellhead, the flow transient within the wellbore itself may mean that the flow rate from the reservoir into the wellbore (the "sand face" flow rate, q_{sf}) may not be constant at all. This effect is due to wellbore storage.

Wellbore storage effect can be caused in several ways, but there are two common means. One is storage by fluid expansion, the other is storage by changing liquid level.

Consider the case of a drawdown test. When the well is first open to flow, the pressure in the wellbore drops. This drop causes an expansion of the wellbore fluid, and thus the first production is not fluid from the reservoir but is fluid that had been stored in the wellbore volume. As the fluid expands, the wellbore is progressively emptied, until the wellbore system can give up no more fluid, and it is the wellbore itself which provides most of the flow during this period. This is wellbore storage due to fluid expansion.

The second common kind of wellbore storage is due to a changing liquid level. This is easily envisaged in the case of a completion consisting of a tubing string without a packer, as in Fig. 2.4.

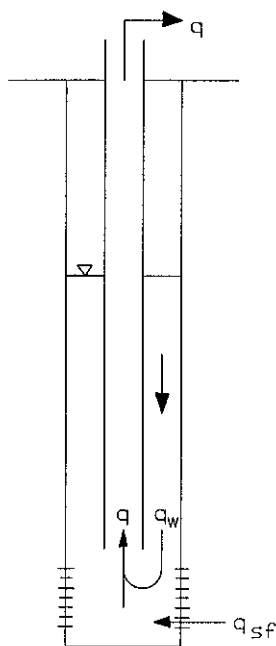


Figure 2.4

When the well is open to flow during a drawdown test, the reduction in pressure causes the liquid level in the annulus to fall. The liquid extracted from the annulus joins that from the reservoir and makes up a proportion of the total flow from the well. The falling liquid level is generally able to supply much more fluid than is possible simply from expansion of the fluid alone, thus wellbore storage effects are usually much more prominent in this type of completion.

The wellbore storage coefficient, C , is a parameter used to quantify the effect. C is the volume of fluid that the wellbore itself will produce due to a unit drop in pressure:

$$C = \frac{V}{\Delta p} \quad (2.15)$$

where V is the volume produced, and Δp is the pressure drop. C has units STB/psi (or sometimes MCF/psi in the case of gas wells). It is also common to use a dimensionless wellbore storage coefficient, C_D , defined as

$$C_D = \frac{5.615 C}{2\pi\phi c_f h r_w^2} \quad (2.16)$$

where C is in STB/psi.

Assuming the fluid is of constant density, conservation of mass requires that the total flow rate q be equal to the flow of fluid from the reservoir (q_{sf}) added to that which flows from the well itself (q_w):

$$q = q_s + q_w \quad (2.17)$$

Thus the fraction of the total flow that originates from the reservoir is given by:

$$\frac{q_{sf}}{q} = 1 - \frac{q_w}{q} \tag{2.18}$$

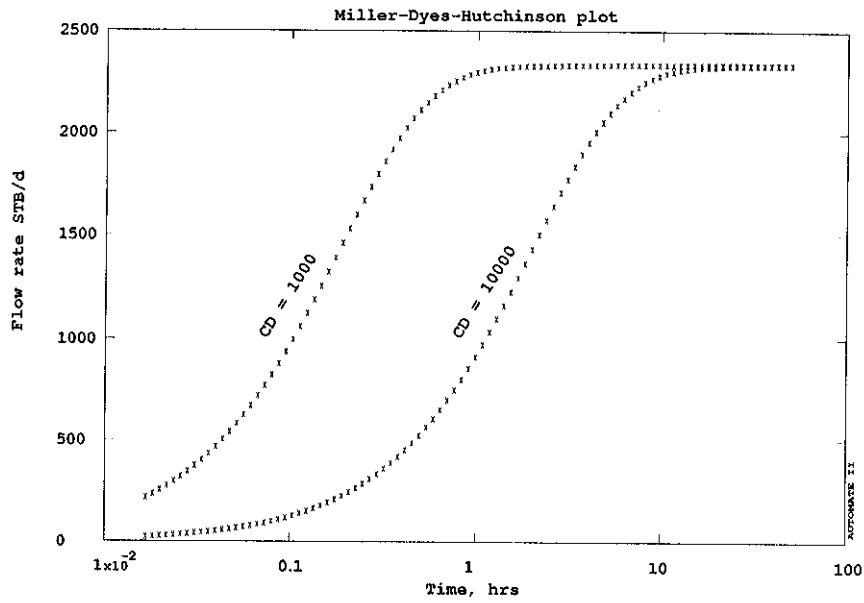


Figure 2.5

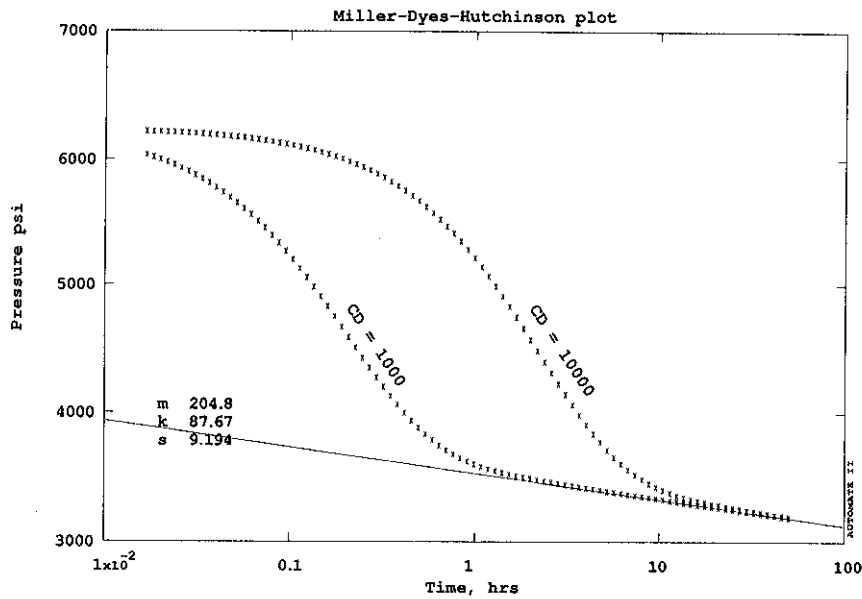


Figure 2.6

The overall effect of wellbore storage can be seen in Fig. 2.5. At early time the ratio q_{sf}/q is close to zero, as all the fluid produced at the wellhead originates in the wellbore. As this goes on, the wellbore storage is depleted, and eventually the reservoir produces all the fluid (as q_{sf}/q tends to one). The corresponding pressure transients due to the wellbore storage effects are seen in Fig. 2.6. It is important to recognize that, as a consequence of the wellbore storage effect, the early transient response during a well test is not characteristic of the reservoir, only of the wellbore. This means that a well test must be long enough that the wellbore storage effect is over and fluid is flowing into the wellbore from the reservoir. As we will see later, we can also overcome the problem of wellbore storage by specifically measuring the sandface flow rate q_{sf} down hole.

The value of the wellbore storage coefficient can be estimated based upon the configuration of the completion. For a fluid expansion storage coefficient,

$$C = c_w V_w \quad (2.19)$$

where V_w is the volume of the wellbore, and c_w is the compressibility of the fluid in the wellbore. In principle, the wellbore compressibility includes the volume changes in the tubing and casing, however, these are usually small. Nonetheless, the compressibility is different from c_r , the total reservoir compressibility, since c_r includes the rock compressibility and will be under different pressure, temperature and saturation conditions than the wellbore.

For a falling liquid level storage coefficient

$$C = \frac{144 A_w}{\rho} \text{ ft}^3/\text{psi} \quad (2.20)$$

where A_w is the cross-sectional area of the wellbore in the region where the liquid level is falling (in ft^2) and ρ is the density of the fluid (in lbm/ft^3).

Example 2.2

A 1000 ft deep pumping well has a 2 inch tubing inside a 7-5/8 inch casing. Without a packer, the liquid level will be pumped down over the annular space. This space has a cross sectional area of

$$A_w = \frac{\pi (7.675^2 - 2^2)}{4} \frac{1}{144}$$

$$A_w = 1.1812 \text{ ft}^2$$

If the oil in the well has a density of $58 \text{ lbm}/\text{ft}^3$, then the storage coefficient will be (using Eq. 2.20):

$$C = \frac{144 \times 1.1812}{58} = 2.93 \text{ ft}^3/\text{psi}$$

$$C = 0.522 \text{ STB}/\text{psi}$$

If the same well were filled with a gas (of compressibility $2 \times 10^{-4} \text{ psi}^{-1}$), then instead of the falling liquid level effect we would see a fluid expansion storage effect of:

using Eq. 2.19

$$C = 2 \times 10^{-4} V_w$$

where the wellbore volume is:

$$V_w = \pi (7.625^2) \frac{1000}{144} \text{ ft}^3$$

$$\text{So, } C = 2 \times 10^{-4} \pi (7.625^2) \frac{1000}{144} = 0.254 \text{ ft}^3/\text{psi.}$$

$$C = 0.045 \text{ STB/psi.}$$

Notice that even though the gas is much more compressible, the falling liquid level storage coefficient is very much larger than the fluid expansion storage coefficient.

Wellbore storage is a major nuisance to well test interpretation, since it disguises the reservoir response until late in the test. One way to overcome this problem is to measure the flow rates downhole instead of at the surface. Such flow rate measurements have become more common during the 1980's, but are still by no means standard. Measuring flow rates adds to the cost of the test, and is difficult in multiphase, inclined and pumping wells. Reservoir engineers still need to be prepared to analyze well test results in the presence of wellbore storage.

From material balance, the pressure in the wellbore is directly proportional to time during the wellbore storage dominated period of the test

$$p_D = \frac{t_D}{C_D} \tag{2.21}$$

On a log-log plot of pressure drop versus time, this gives a characteristic straight line of unit slope (Fig. 2.7).

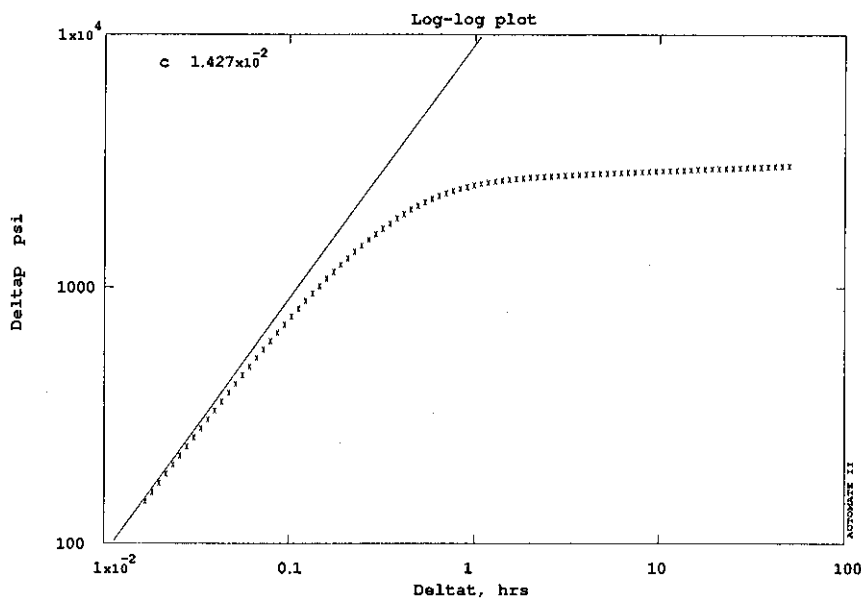


Figure 2.7

The straight line response continues up to a time given approximately by

$$t_D = C_D (0.041 + 0.02 s) \quad (2.22)$$

provided that the skin factor s is positive. However, the storage effect is not over at this time, as there is a period (roughly one and a half log cycles long) during which the response undergoes a transition between wellbore response and reservoir response. Thus the reservoir response does not begin until a time

$$t_D = C_D (60 + 3.5 s) \quad (2.23)$$

During the design of a test, care should be taken to ensure that the test is at least this long (and usually very much longer, even if nonlinear regression techniques are to be used for the interpretation).

Example 2.3

The pumping well in Example 2.2 produces from a reservoir with the following properties:

Permeability $k = 20$ md
 Thickness $h = 5$ feet
 Porosity $\phi = 20\%$
 Compressibility $c_t = 5 \times 10^{-6}$ /psi
 Wellbore radius $r_w = 0.32$ feet
 Viscosity $\mu = 2$ cp

We can estimate that the time required for wellbore storage effects (and transition) to disappear as follows:

(from Example 2.2)

$$C = 2.93 \text{ ft}^3/\text{psi}.$$

(from Eq. 2.16)

$$C_D = \frac{2.93}{2\pi(0.2)(5 \times 10^{-6})(5)(0.32)^2}$$

$$C_D = 9.24 \times 10^5$$

If skin factor s is zero, then the time when the wellbore storage influenced response ends is

$$t_D = 9.24 \times 10^5 (60 + 0) = 5.544 \times 10^7$$

In real terms, using Eq. 2.5:

$$t = \frac{\phi \mu c_t r_w^2}{0.000264 k} t_D$$

$$t = \frac{(0.2)(2)(5 \times 10^{-6})(0.32)^2}{0.000264 (20)} 5.544 \times 10^7$$

$$t = 2150.4 \text{ hrs}$$

This is clearly an impossibly long time, and we could not even consider attempting to test this well without a downhole flow rate measurement. If the skin effect is as large as 10, this time would be about 50% larger (from Eq. 2.23).

Based on this example, it can be seen that the time affected by wellbore storage is independent of porosity, wellbore radius and system compressibility. In fact Eqs. 2.23, 2.16 and 2.5 can be combined to give the storage-influenced time as

$$t = \frac{3385 C (60 + 3.5s)}{kh/\mu} \quad (2.24)$$

From this we can see that wells with greater deliverability (related to kh/μ) are less strongly influenced by wellbore storage effects. It is also important to note that the storage effect is independent of the flow rate q .

2.6 Infinite Acting Radial Flow

Once the wellbore storage effects are over, the wellbore pressure transient reflects the pressure transmission out in the reservoir. As time proceeds, the response is characteristic of conditions further and further away from the wellbore. At very late time, the pressure response is affected by the influence of reservoir boundaries, but prior to those late times the pressure response does not "see" the reservoir boundaries, and the reservoir acts as if it were infinite in extent. This intermediate time response, between the early wellbore-dominated response and the late time boundary-dominated response, is known as the infinite acting period. Although modern well test interpretation identifies several different types of flow during the infinite acting period, one of the most common and easily identified is radial flow. Infinite acting radial flow has been the basis of very many well test interpretation techniques, and it is worthwhile to discuss it in some detail.

In the absence of wellbore storage and skin effects, the pressure transient due to infinite acting radial flow into a line source wellbore producing at constant flow rate is given by

$$p_D = -\frac{1}{2} Ei \left[-\frac{r_D^2}{4t_D} \right] \quad (2.25)$$

Here Ei represents the exponential integral function. This solution is valid throughout the reservoir ($r_D > 1$), including at the wellbore ($r_D = 1$). Thus it can be used for interference tests as well as drawdown and buildup tests. Fig. 2.8 shows the exponential integral solution plotted in semilog coordinates.

From this graphical presentation, it can be seen that the infinite acting radial flow response is directly proportional to the logarithm of time for all but early times. Examination of the solution numerically confirms this to be true. For $t_D > 10$, the exponential integral solution at $r_D = 1$ can be well approximated by

$$p_{wD} = \frac{1}{2} [\ln t_D + 0.80907] + s \quad (2.26)$$

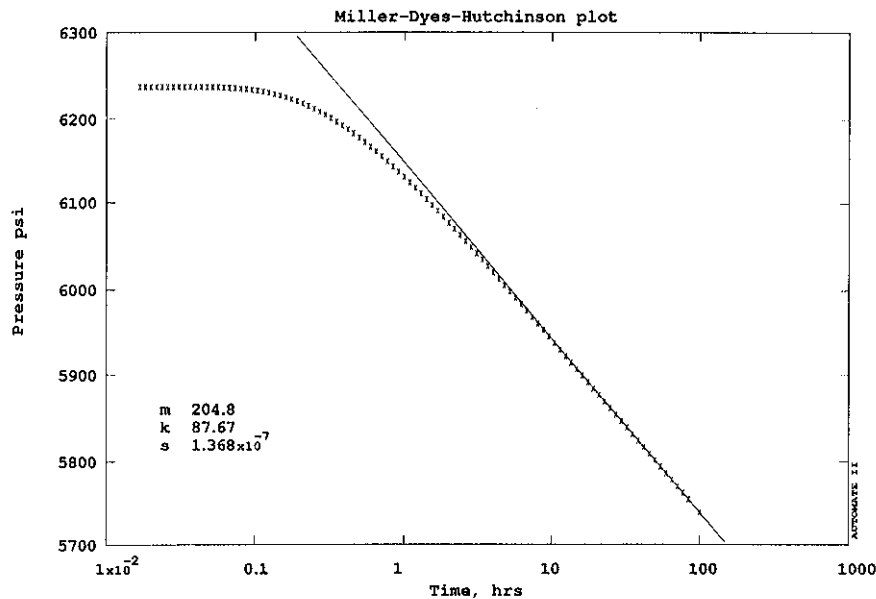


Figure 2.8

Writing this in dimensional variables:

$$p_{wf} = p_i - 162.6 \frac{qB\mu}{kh} \left[\log t + \log \frac{k}{\phi\mu c_r r_w^2} + 0.8686s - 3.2274 \right] \quad (2.27)$$

where the natural logarithm (ln) has been replaced by a logarithm to base 10 (log). From this equation it is seen that a plot of pressure drop against the logarithm of time should contain a straight line with slope

$$m = 162.6 \frac{qB\mu}{kh} \quad (2.28)$$

Hence the recognition of this slope makes it possible to estimate the permeability (k) or the permeability-thickness product (kh). Many traditional well test interpretation techniques are based on this "semilog approach" and the recognition of the "correct semilog straight line" is a crucial aspect of this type of analysis. We shall examine this further in Section 3.

2.7 Reservoir Boundary Response

Obviously, reservoirs are not really infinite in extent, thus the infinite acting radial flow period cannot last indefinitely. Eventually the effects of the reservoir boundaries will be felt at the well being tested. The time at which the boundary effect is noticed is dependent on several factors, including the distance to the boundary and the properties of the permeable formation and the fluid that fills it. The two types of reservoir boundary that are most commonly considered are (a) impermeable and (b) constant pressure. An impermeable boundary (also known as a closed boundary) occurs where the reservoir is sealed and no flow occurs. No flow boundaries can also arise due to the interference between wells. A constant

pressure boundary rarely occurs exactly in practice, however, in many cases aquifer support, a balanced injection pattern or the presence of a large gas cap can cause an effect that closely approximates a constant pressure boundary.

2.7.1 Closed Boundaries

When a reservoir (or a well's own "drainage region") is closed on all sides, the pressure transient will be transmitted outwards until it reaches all sides, after which the reservoir depletion will enter a state known as pseudosteady state. In this state, the pressure in the reservoir will decline at the same rate everywhere in the reservoir (or drainage region). Thus a pseudosteady state is not at all steady, and corresponds to the kind of pressure response that would be seen in a closed tank from which fluid was slowly being removed. This is illustrated in Fig. 2.9.

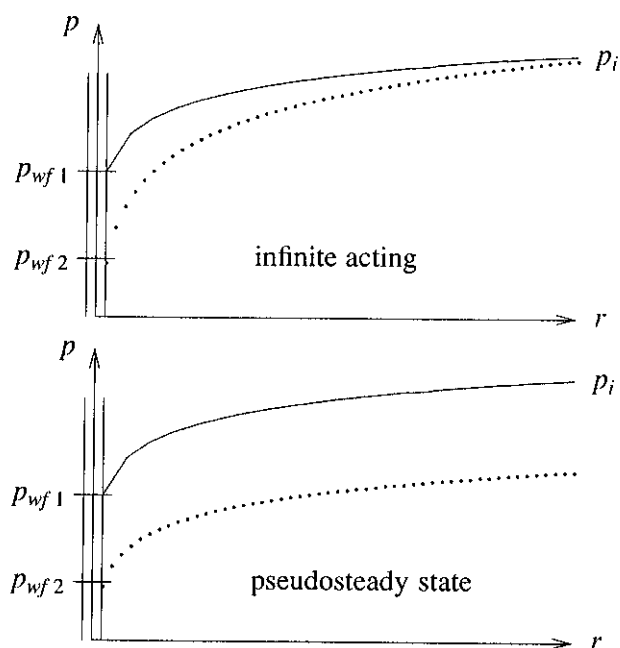


Figure 2.9

The condition of the reservoir during pseudosteady state is that pressure drop (everywhere) is due to the decompression of the reservoir fluid as fluid is produced from the well. This "volumetric" pressure loss is given simply from the definition of compressibility

$$c_l = -\frac{1}{V} \frac{\Delta V}{\Delta p} \quad (2.29)$$

$$\text{or, } \Delta p = \frac{1}{V} \frac{q \Delta t}{c_l} \quad (2.30)$$

where V is the total reservoir fluid volume, and the cumulative production ΔV is replaced by $q \Delta t$.

From Eq. 2.30 we can see that, during pseudosteady state, the pressure drop is:

2

- (a) directly proportional to time -- hence is identifiable as a straight line on a Δp vs. t or $\log(\Delta p)$ vs. t (Δt),
- (b) dependent on reservoir volume -- hence is extremely useful as a means of estimating reservoir size

In terms of the dimensionless variables defined earlier, and incorporating the effects of skin on reservoir shape, the pressure drop can be written:

$$p_D = 2\pi t_{DA} + \frac{1}{2} \ln \left[\frac{2.2458A}{C_A r_w^2} \right] + s \quad (2.3)$$

where A is the area of the reservoir (or drainage region), and C_A is a shape factor that depends on the shape of the region and the position of the well. C_A has been determined for a variety of drainage shapes shown in Table 2.1, which is reproduced from Earlougher (1977).

If we treat the reservoir or drainage region as a circle of radius r_e , with the well at the center, then $A = \pi r_e^2$ and $C_A = 31.62$. In this case

$$p_D = 2\pi t_{DA} + \frac{1}{2} \ln \left[0.472 \frac{r_e}{r_w} \right] + s \quad (2.32)$$

Whatever the boundary shape, either Eq. 2.31 or 2.32 allow us to estimate the drainage area by determining the slope of the appropriate straight line found on a plot of Δp versus t . Substituting the definitions of p_D and t_{DA} in Eq. 2.31:

$$\Delta p = \frac{0.2342 qB}{(\phi c_t h) A} t + 70.65 \frac{qB\mu}{kh} \left[\ln \left[\frac{2.2458A}{C_A r_w^2} \right] + 2s \right] \quad (2.33)$$

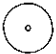


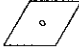
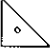


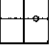
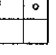

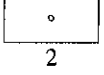
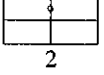
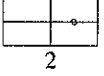
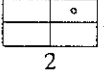
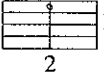
Thus the slope of the line Δp (psi) versus t (hrs) will be

$$m_{\text{Cartesian}} = \frac{0.2342 qB}{(\phi c_t h) A} \quad (2.34)$$

Notice the groupings $\phi c_t h$, which is known as the "storativity," and $\phi h A$, which is the total pore volume within the drainage region.

Before seeking a straight line on a Cartesian pressure versus time graph, it is important to note that the pseudosteady state response does not appear until a certain value of t_{DA} . Recognition of this fact may be helpful to prevent the analysis of an improper Cartesian straight line. In Table 2.1 the time given as "Use infinite system solution with less than 1% error for t_{DA} less than" can be considered the end of the infinite acting behavior (the end of the semilog straight line); the time given as "less than 1% error for t_{DA} greater than" can be considered as the start of pseudosteady state (the start of the Cartesian straight line). For the circular reservoir with the well at the center, the pseudosteady state starts exactly at the time the infinite acting behavior ends ($t_{DA} = 0.1$), hence the two times appear to overlap slightly (because of the 1% tolerance). However for more elongated shapes, or eccentric well locations, the infinite acting response ends long before pseudosteady state begins. The intervening period is a transition period.

Table 2.1: Shape factors for various reservoir shapes (from Earlougher, 1977)

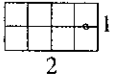
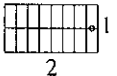
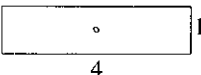
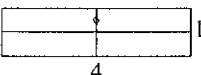
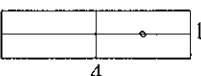
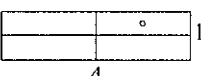
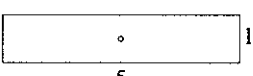
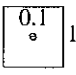
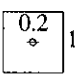
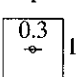
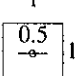
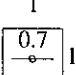
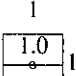
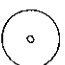
Reservoir shape	C_A	$\ln C_A$	$\frac{1}{2} \ln[2.2458/C_A]$	Exact for t_{DA} greater than	Less than 1% error for t_{DA} greater than	Use infinite system solution with less than 1% error for t_{DA} less than
Bounded reservoirs						
	31.62	3.4538	-1.3224	0.1	0.06	0.10
	31.6	3.4532	-1.3220	0.1	0.06	0.10
	27.6	3.3178	-1.2544	0.2	0.07	0.09
	27.1	3.2995	-1.2452	0.2	0.07	0.09
	21.9	3.0865	-1.1387	0.4	0.12	0.08
	0.098	-2.3227	+1.5659	0.9	0.60	0.015
	30.8828	3.4302	-1.3106	0.1	0.05	0.09
	12.9851	2.5638	-0.8774	0.7	0.25	0.03
	4.5132	1.5070	-0.3490	0.6	0.30	0.025
	3.3351	1.2045	-0.1977	0.7	0.25	0.01
	21.8369	3.0836	-1.1373	0.3	0.15	0.025
	10.8374	2.3830	-0.7870	0.4	0.15	0.025
	4.5141	1.5072	-0.3491	1.5	0.50	0.06
	2.0769	0.7309	+0.0391	1.7	0.50	0.02
	3.1573	1.1497	-0.1703	0.4	0.15	0.005

Copyright © 1977, Society of Petroleum Engineers

Earlougher, Robert C.: "Advances in Well Test Analysis", Monograph Series, SPE, Richardson, TX (1977) 5, 203-204

Reprinted with permission.

Table 2.1 (continued):

Reservoir shape	C_A	$\ln C_A$	$\frac{1}{2} \ln[2.2458/C_A]$	Exact for t_{DA} greater than	Less than 1% error for t_{DA} greater than	Use infinite system solution with less than 1% error for t_{DA} less than
	0.5813	-0.5425	+0.6758	2.0	0.60	0.02
	0.1109	-2.1991	+1.5041	3.0	0.60	0.005
	5.3790	1.6825	-0.4367	0.8	0.30	0.01
	2.6896	0.9894	-0.0902	0.8	0.30	0.01
	0.2318	-1.4619	+1.1355	4.0	2.00	0.03
	0.1155	-2.1585	+1.4838	4.0	2.00	0.01
	2.3606	0.8589	-0.0249	1.0	0.40	0.025
Vertically fractured reservoirs		Use $(x_e/x_f)^2$ in place of A/r_w^2 for fractured systems				
	2.6541	0.9761	-0.0835	0.175	0.08	cannot use
	2.0348	0.7104	+0.0493	0.175	0.09	cannot use
	1.9986	0.6924	+0.0583	0.175	0.09	cannot use
	1.6620	0.5080	+0.1505	0.175	0.09	cannot use
	1.3127	0.2721	+0.2685	0.175	0.09	cannot use
	0.7887	-0.2374	+0.5232	0.175	0.09	cannot use
Water drive reservoirs						
	19.1	2.95	-1.07	--	--	--

Sometimes this transition period can be very long (see for example the 5-to-1 rectangle, where it is sixteen times longer than the entire infinite acting response). Hence it would be a mistake to assume that the pseudosteady state response (Cartesian straight line) occurs immediately at the end of the infinite acting response (semilog straight line).

2.7.2 Fault Boundaries

Fault boundaries usually act as impermeable barriers, and therefore the pressure response of a well close to a single linear fault can begin to look like the response of a closed reservoir. However, the response is actually different. Since the well responds to only one boundary instead of being completely closed in on all sides, there is no pseudosteady state (at least not initially). Due to the influence calculable by superposition (described later), the well "sees itself in the mirror", and the net late time response is that of two identical wells. The semilog straight line of the original infinite acting response will therefore undergo a doubling in slope at the time the boundary effect is felt. This will be described later.

2.7.3 Constant Pressure Boundaries

When the reservoir pressure is supported by fluid encroachment (either due to natural influx from an aquifer or gas cap, or by fluid injection) then a constant pressure boundary may be present. Such a boundary may completely enclose the well (as, for example, for a production well surrounded by injectors) or may be an open boundary to one side of the well (for example, in the case of an isolated producer/injector well pair).

The effect of *any* constant pressure boundary will ultimately cause the well pressure response to achieve steady state, at which the well pressure will be the same constant pressure as the boundary, as in Fig. 2.10.

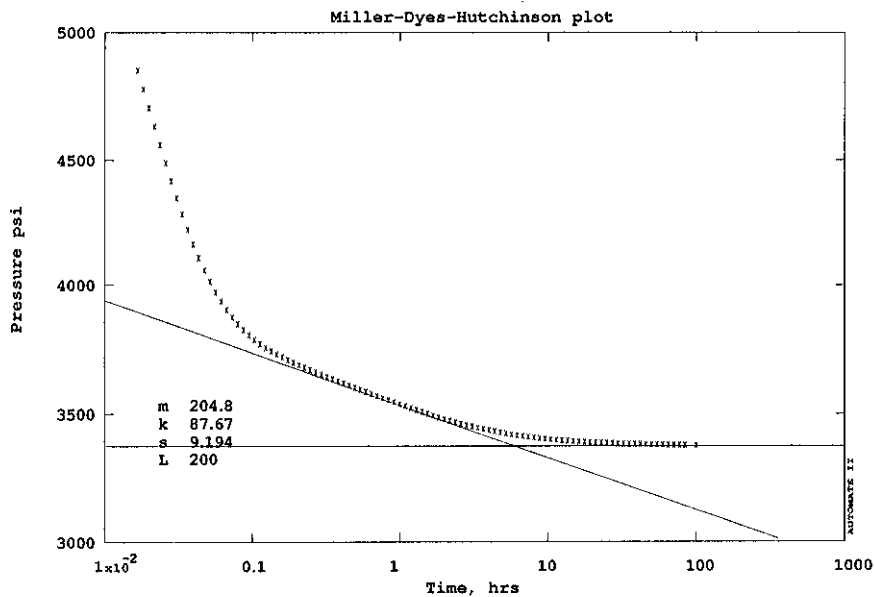


Figure 2.10

For the case of a circular constant pressure boundary with the well at the center, the wellbore pressure response will depart from the semilog straight line (infinite acting radial flow) response at a time t_{DA} of 0.08, pass through a transition period, and achieve steady state at a time t_{DA} of 0.3. Notice that this is rather later than the time required to achieve pseudosteady state in the case of impermeable boundaries. The time required to reach the steady state response will be different for drainage regions of different shape, and steady state will generally be reached sooner if some part of the constant pressure boundary is closer to the well.

2.8 Fractured Wells

In the U.S., the *majority* of new oil and gas wells are hydraulically fractured as a routine part of their completion. In such a hydraulic fracturing procedure, the usual objective is the production of a single vertical fracture that completely penetrates the thickness of the productive formation and which extends some distance from the well. In other kinds of reservoir (for example geothermal wells which are commonly drilled in volcanic rocks) such major fractures may occur naturally and may be intersected by the well during drilling.

The fracture has much greater permeability than the formation it penetrates, hence it influences the pressure response of a well test significantly. Due to the *linear* geometry of the fracture, we will observe a pressure response other than the infinite-acting *radial* flow behavior discussed in Section 2.5, at least for part of the response. The interpretation of well tests from such wells must therefore consider the effects of the fracture; indeed, often tests of fractured wells are conducted specifically to determine fracture properties so that the effectiveness of the fracture stimulation operation can be evaluated.

The case of common practical interest is of a vertical fracture of length x_f , fully penetrating the formation (Figure 2.11).

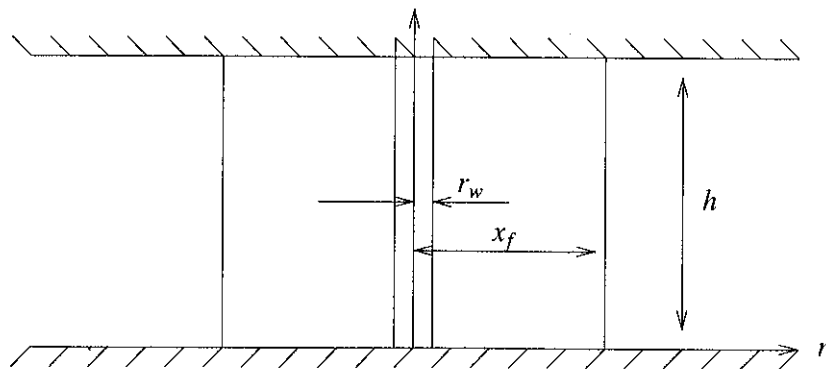


Figure 2.11

For the purposes of fractured well analysis, we often make use of a dimensionless time t_{Dxf} based on the fracture length x_f :

$$t_{Dxf} = \frac{0.000264 kt}{\phi\mu c_f x_f^2} \quad (2.35)$$

Notice that this is directly related to the usual dimensionless time t_D as follows:

$$t_{Dxf} = t_D \frac{r_w^2}{x_f^2} \quad (2.36)$$

In well test analysis, three main fracture types are commonly considered: (a) finite conductivity factors, (b) infinite conductivity fractures, and (c) uniform flux fractures.

2.8.1 Finite Conductivity Fractures

The most general case of a finite conductivity fracture was considered by Cinco, Samaniego and Dominguez (1978) and Cinco and Samaniego (1981). Due to the linear flow in the fracture, several different flow regimes can be observed at different times (Figure 2.12).

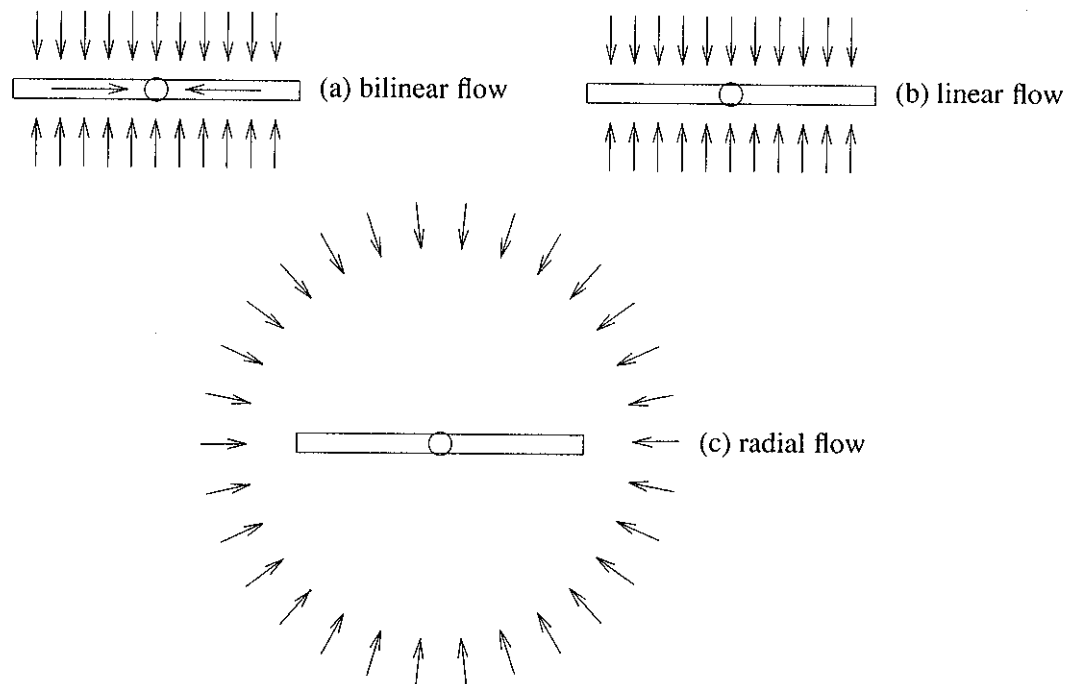


Figure 2.12

At early time, there is linear flow within the fracture and linear flow into the fracture from the formation (Figure 2.12 a). The combination of these two linear flows gives rise to the bilinear flow period. This part of the response is characterized by a straight line response with slope $\frac{1}{4}$ on a log-log plot of pressure drop against time (Figure 2.13) since the pressure drop during this period is given by

$$p_D = \frac{2.451}{\sqrt{k_{fD} w_{fD}}} t_{Dxf}^{1/4} \quad (2.37)$$

where the dimensionless fracture permeability and width are given respectively by

$$k_{fD} = \frac{k_f}{k} \quad (2.38)$$

$$w_{fD} = \frac{w}{x_f} \quad (2.39)$$

where w is the width (or aperture) of the fracture.

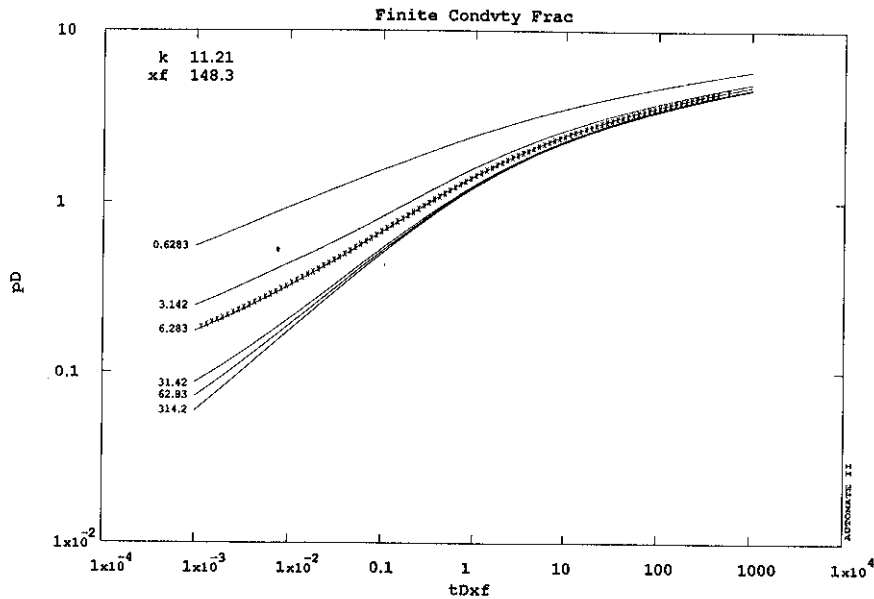


Figure 2.13

Following the bilinear flow period, there is a tendency towards linear flow (Figure 2.12 b), recognizable by the upward bending in Fig. 2.13 towards a $\frac{1}{2}$ slope on the log-log plot. In practice, the $\frac{1}{2}$ slope is rarely seen except in fractures where the conductivity is infinite. Finite conductivity fracture responses generally enter a transition after bilinear flow ($\frac{1}{4}$ slope), but reach radial flow (Fig. 2.12 c) before ever achieving a $\frac{1}{2}$ slope (linear flow). Fig. 2.14 shows an example of such a response.

2.8.2 Infinite Conductivity Fractures

If the product $k_{fD}w_{fD}$ (defined by Eqs. 2.38 and 2.39) is larger than 300, then the fracture conductivity can be considered to be infinite. Such highly conductive fractures are quite possible in practice, especially in formations with lower permeability. The pressure response of a well intersecting an infinite conductivity fracture is very similar to that of the more general finite conductivity fracture case, except that the bilinear flow period is not present. An infinite conductivity fracture response is characterized by a truly linear flow response (Fig. 2.11 b), during which the pressure drop is given by

$$p_D = (\pi t_{Dxf})^{1/2} \quad (2.40)$$

Such a response shows as a $\frac{1}{2}$ slope straight line on a log-log plot of pressure drop against time (Fig. 2.15), as shown by Gringarten, Ramey and Raghavan (1974).

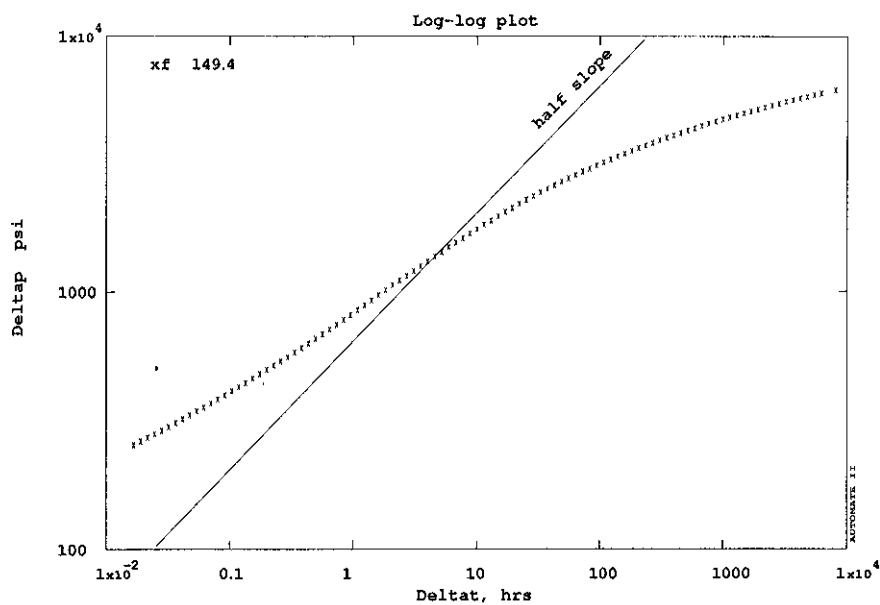


Figure 2.14

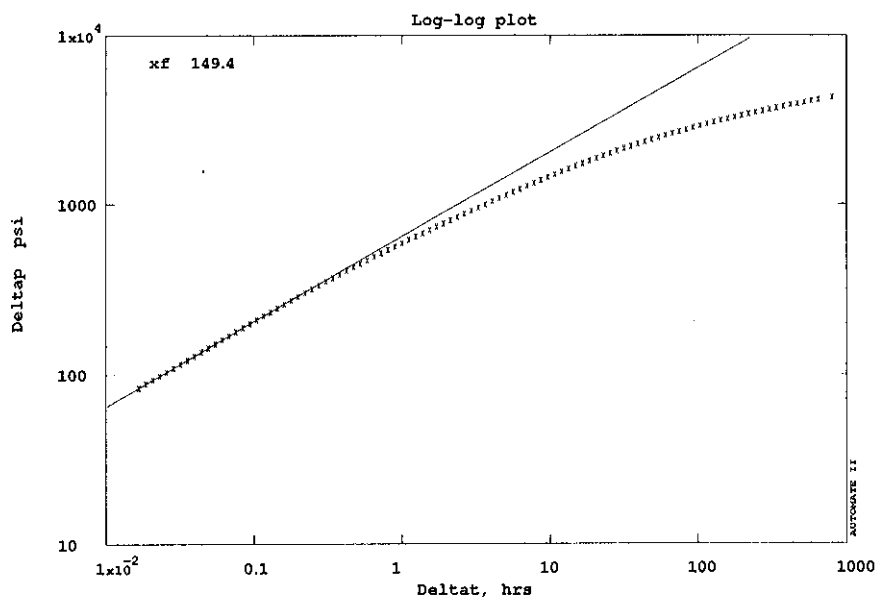


Figure 2.15

Beyond the linear flow period, the response will pass through a transition to infinite acting radial flow (semilog straight line behavior).

2.8.3 Uniform Flux Fracture

One of the earliest mathematical solutions to a fractured well problem assumed that the flow into the fracture was uniform along its length (Gringarten, Ramey and Raghavan, 1972). This was a mathematical convenience only, and it is known that the flux distribution along a fracture is far from uniform (Fig. 2.16).

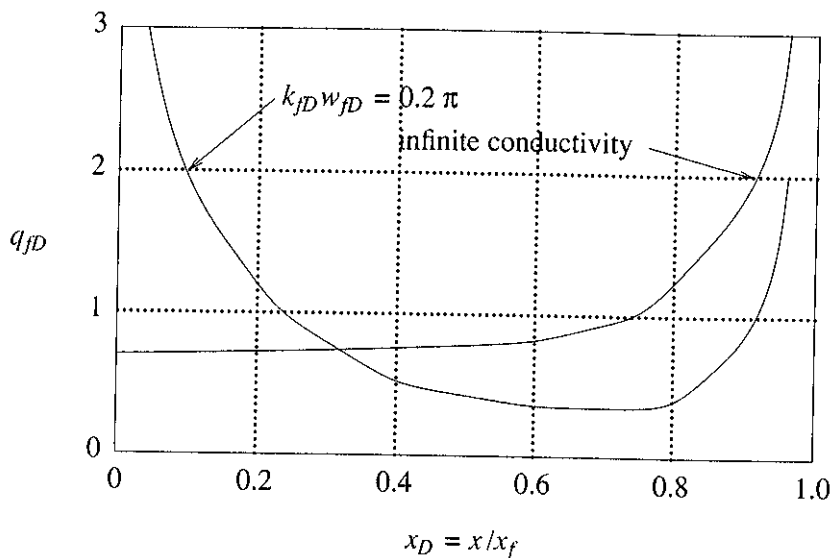


Figure 2.16

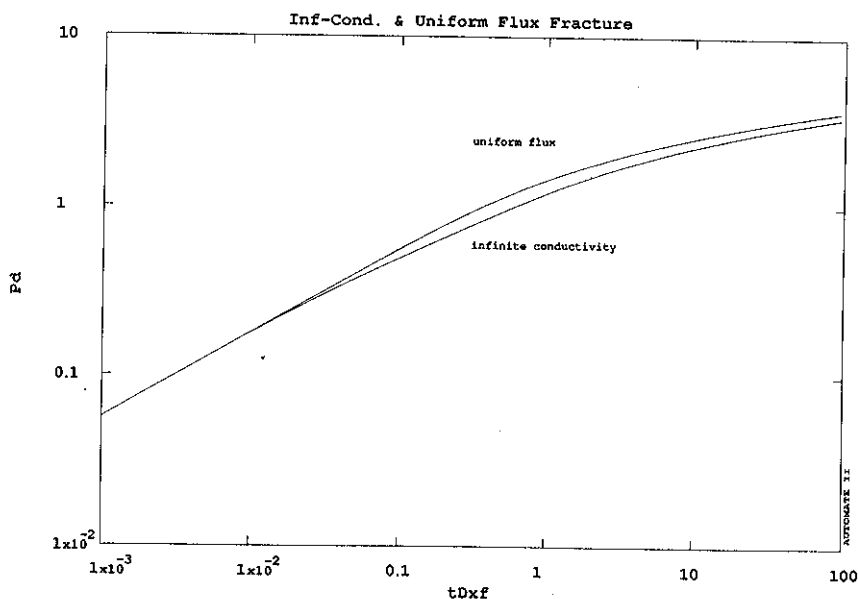


Figure 2.17

The only practical case in which the fracture flux distribution approaches uniformity is when there is a significant fracture "skin", caused by a lower permeability region between the fracture and the reservoir (Cinco and Samaniego, 1981b). Whether this "damaged fracture" case is common or not is unclear,

however, it is true that some wells appear to fit the uniform flux fracture response better than the infinite conductivity fracture response. In fact, there is only a rather small difference between the two flow situations (Fig. 2.17).

2.9 Double Porosity Behavior

Discussion in previous sections has been focused on reservoirs with homogeneous properties. Because of the diffusive nature of pressure transmission, many reservoirs do indeed behave as if they were homogeneous, even though it is certain that the reservoir properties must be non-uniform to some extent. However, there is a type of reservoir heterogeneity that is noticeable in pressure transients in reservoirs that have distinct primary and secondary porosity. These pressure effects are known as double porosity or dual porosity behavior, and are quite commonly seen, particularly in naturally fractured reservoirs.

In a dual porosity reservoir, a porous "matrix" of lower transmissivity (primary porosity) is adjacent to higher transmissivity medium (secondary porosity), as in Figure 2.18.

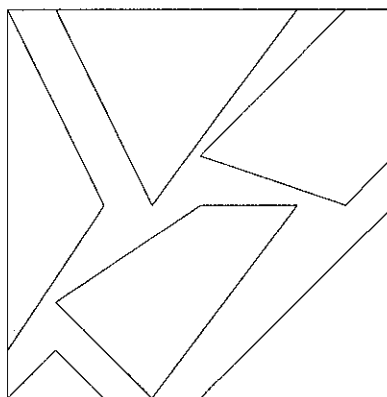


Figure 2.18

For the most part, we will discuss dual porosity reservoirs in terms of fractures and porous matrix blocks, however it is important to recognize that thin stratigraphic sequences of differing permeability can also give rise to dual porosity effects. Although there are variations, a common model is to associate fluid *storativity* with both the fractures (secondary porosity) and the matrix (primary porosity), but to assume *transmissivity* mainly in the fractures. In such a dual porosity model, fluid flows to the wellbore through the fractures alone, although may flow from the matrix blocks into the fractures.

Since there are now two interconnected media, we must define properties for each. The matrix permeability, porosity and total system compressibility are k_m , ϕ_m and c_m respectively, while those for the fracture are k_f , ϕ_f and c_f . In fractured systems, the fracture porosity ϕ_f may be very low, since the fracture volume is usually only a very small part of the total. Fracture compressibility c_f is often very large due to the inflation/deflation effect as pressure changes in the fracture.

Based on the mathematical development (not shown here) of the equations of flow in the two media the normal dimensionless pressure and time are somewhat modified. Dimensionless pressure is based on fracture transmissivity, while dimensionless time is based on total (fracture plus matrix) storativity:

$$p_D = \frac{k_f h}{141.2 q B \mu} \Delta p \quad (2.41)$$

$$t_D = \frac{0.000264 k_f t}{(\Phi_f c_{if} + \Phi_m c_{im}) \mu r_w^2} \quad (2.42)$$

The dual porosity effects are described in terms of two parameters that relate primary and secondary properties. The first of the two parameters is the storativity ratio, ω , that relates the secondary (or fracture) storativity to that of the entire system:

$$\omega = \frac{\Phi_f c_{if}}{\Phi_f c_{if} + \Phi_m c_{im}} \quad (2.43)$$

The second parameter is dependent on the transmissivity ratio, and is designated as λ :

$$\lambda = \alpha \frac{k_m}{k_f} r_w^2 \quad (2.44)$$

Here α is a factor that depends on the geometry of the interporosity flow between the matrix and the fractures:

$$\alpha = \frac{A}{xV} \quad (2.45)$$

where A is the surface area of the matrix block, V is the matrix volume, and x is a characteristic length. If the matrix blocks are cubes or spheres, then the interporosity flow is three-dimensional and λ is given by

$$\lambda = \frac{60}{x_m^2} \frac{k_m}{k_f} r_w^2 \quad (2.46)$$

where x_m is the length of a side of the cubic block, or the diameter of the spherical block. If the matrix blocks are long cylinders, then the interporosity flow is two-dimensional and λ is given by

$$\lambda = \frac{32}{x_m^2} \frac{k_m}{k_f} r_w^2 \quad (2.47)$$

where x_m is now the diameter of the cylindrical block. If the matrix blocks are slabs overlying each other with fractures in between (this kind of dual porosity often occurs in layered formations), then the interporosity flow is one-dimensional, and λ is given by

$$\lambda = \frac{12}{h_f^2} \frac{k_m}{k_f} r_w^2 \quad (2.48)$$

where h_f is the height of the secondary porosity slab (i.e., the thickness of the high permeability layer).

Values of ω can be less than or equal to one. The special case of $\omega=1$ occurs when the matrix porosity is zero, hence refers to a reservoir that is single porosity -- this means that the standard single porosity reservoir behaviors already discussed are simply special cases of dual porosity behavior with $\omega=1$. In naturally fractured reservoirs, ϕ_f is usually very small, however, the large fracture compressibility c_{if} means that ω is commonly less than 0.1 but not necessarily many orders of magnitude less.

Values of λ are usually very small (for example, 10^{-3} to 10^{-10}). If λ is larger than 10^{-3} , the level of heterogeneity is insufficient for dual porosity effects to be of importance, and again the reservoir acts as a single porosity.

Due to the two separate "porosities" in the reservoir, the dual porosity system has a response that may show characteristics of both of them. The secondary porosity (fractures), having the greater transmissivity and being connected to the wellbore, responds first. The primary porosity does not flow directly into the wellbore and is of lower transmissivity, therefore responds much later. The combined effect of the two gives rise to two separate semilog straight line responses, Figure 2.19.

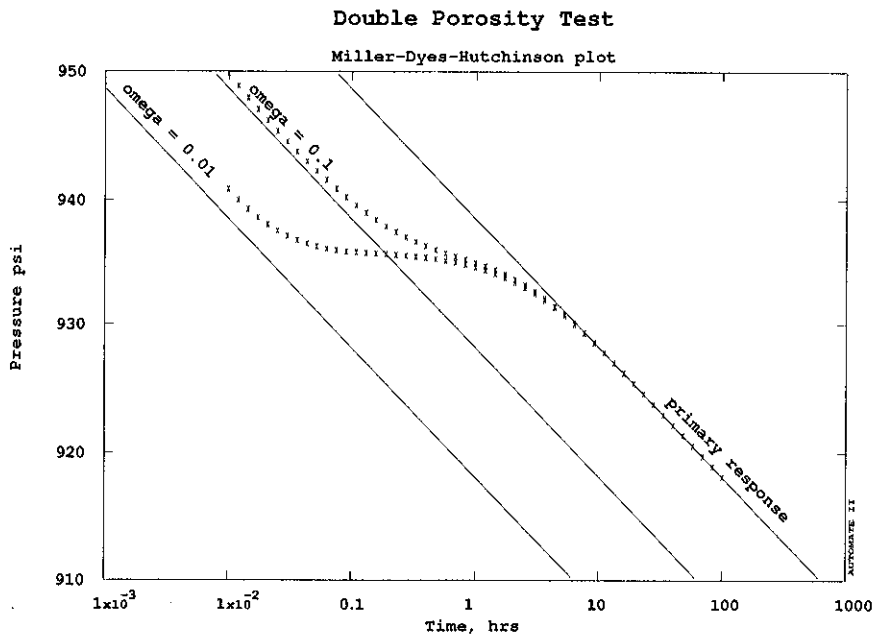


Figure 2.19

The separation between the straight lines is dependent on ω . For each log cycle that separates the two lines, ω is reduced by a factor of 10. Thus in Fig. 2.19 the lines for $\omega = 0.1$ are separated by one log cycle in time, and the lines for $\omega = 0.01$ are separated by two log cycles in time. The time at which the transition between them occurs is dependent on λ , Fig. 2.20. The value of λ can be estimated by locating the transition line, and then examining the *start* of the primary straight line (which is the later one) given by $t_D = (1 - \omega)/7\lambda$.

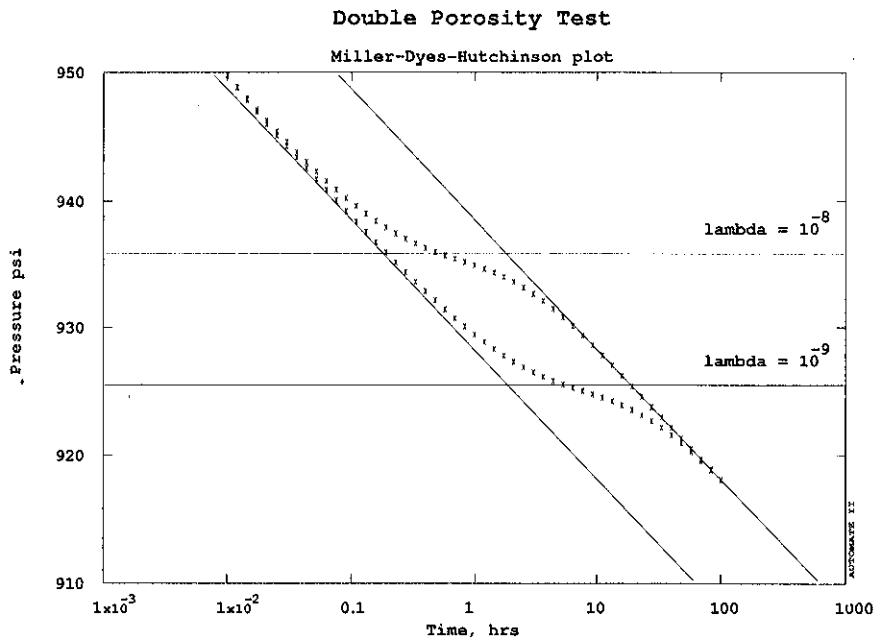


Figure 2.20

It should be stressed that this double straight line behavior is easily disguised by effects of wellbore storage (which may hide the primary porosity transient completely) or by boundary effects (which may have an effect on the primary transient before the secondary porosity behavior is evident).

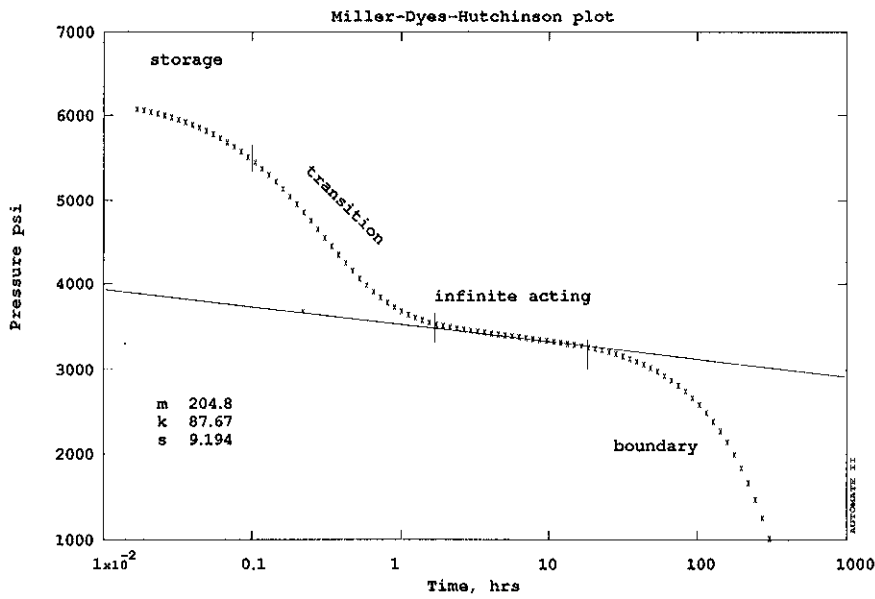


Figure 2.21

2.10 Summary of Responses in Time Sequence

As has been discussed in the preceding five sections, a well test response may have different behavior at different times. The earliest time response is usually wellbore storage. Somewhat later, the response of fractures or primary porosity may be evident. At intermediate times, infinite acting radial flow may appear. Finally, late time responses may show the effects of reservoir boundaries. This combination of responses may give rise to an overall transient such as in Figure 2.21. Clearly there are many possible combinations of effects, as can be imagined by examination of Table 2.2.

Table 2.2

	Early time		Intermediate time			Late time
radial flow	storage		infinite acting radial flow			closed boundary sealing fault constant pressure
fractures	storage	bilinear flow	radial flow			closed boundary sealing fault constant pressure
double porosity	storage		double porosity behavior	transition	radial flow	closed boundary sealing fault constant pressure

Recognition and appropriate analysis of these different responses is the key to proper interpretation of a well test. Data from a real well test can start and end at any time, so one or more of the responses can be missing. Also, depending on parameter values, one response may overlap and hide another. For example, in a dual porosity reservoir, the first semilog straight line characteristic of the primary porosity may be completely hidden by wellbore storage (Figure 2.22).

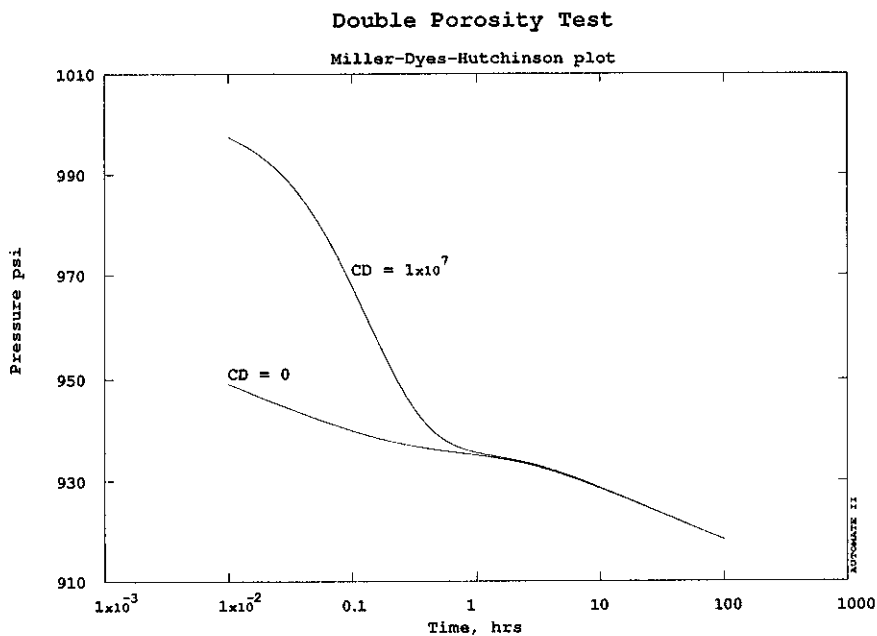


Figure 2.22

2.11 Superposition

One of the most powerful techniques in reservoir engineering is superposition. This approach makes it possible to construct reservoir response functions in complex situations, using only simple basic models. Superposition is especially useful in well test analysis, since we can use it to represent the response due to several wells by adding up the individual well responses. By appropriate choice of flow rate and well location, we can also represent various reservoir boundaries. In addition, we can use superposition in time to determine the reservoir response to a well flowing at variable rate, by using only constant rate solutions.

The principle of superposition is very simple. It says that the response of the system to a number of perturbations is exactly equal to the sum of the responses to each of the perturbations as if they were present by themselves. It should be noted in passing that the principle of superposition only holds for linear systems (in the mathematical sense), however these include most of the standard response functions used in well test analysis, such as the constant rate radial flow, double porosity, fractured and bounded well solutions described earlier.

To begin to understand use of superposition, consider the pressure drop in the reservoir at point A due to the production of two wells at B and C (Figure 2.23).



Figure 2.23

Assuming that wells B and C are both line source wells without wellbore storage, the pressure drop at A due to the production of both wells is (assuming $t_D > 10$):

$$\Delta p = \frac{141.2q_B B \mu}{kh} \left[\frac{1}{2} \left[\ln \frac{kt}{\phi \mu c_i r_B^2} + 0.80908 \right] \right] + \frac{141.2q_C B \mu}{kh} \left[\frac{1}{2} \left[\ln \frac{kt}{\phi \mu c_i r_C^2} + 0.80908 \right] \right] \quad (2.49)$$

It can be confirmed from Eq. 2.49 that the total pressure drop is equal to the sum of the individual pressure drops. This is true for any number of wells.

Another interesting observation can be made if both wells produce at identical rate, and the point A is exactly midway between them. In this case the pressure *gradient* towards the other wells, thus the net flux towards either well is zero. Hence *any* point midway between the wells is a no flux point, and we can replace all such points by an impermeable barrier without affecting the flow distribution or the pressure field (Figure 2.24).

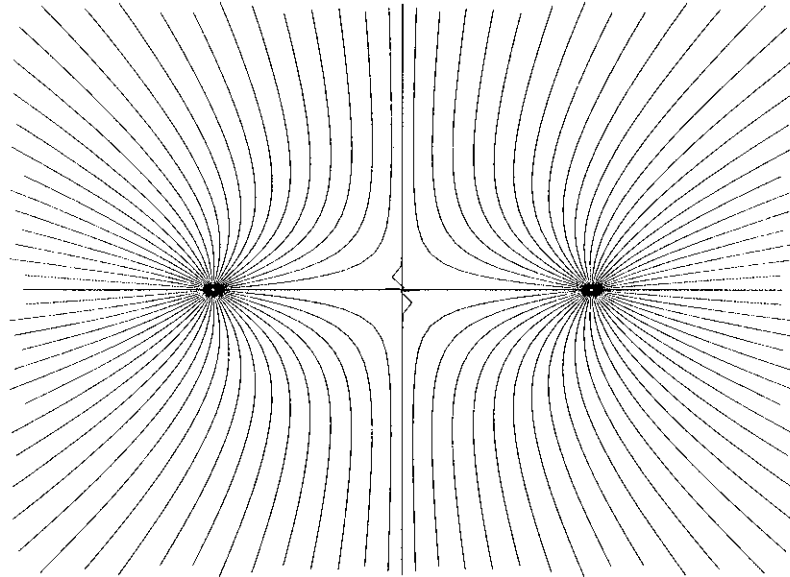


Figure 2.24

Alternatively, if the wells are equidistant, but have equivalent flow rates opposite in sign, then the pressure drop at the midpoint will be exactly zero, since the pressure drop due to one well will be exactly cancelled by the pressure rise due to the other. The net result is that all such midpoints remain at constant pressure, and the effect is identical to the situation in which a linear constant pressure boundary is present (Figure 2.25).

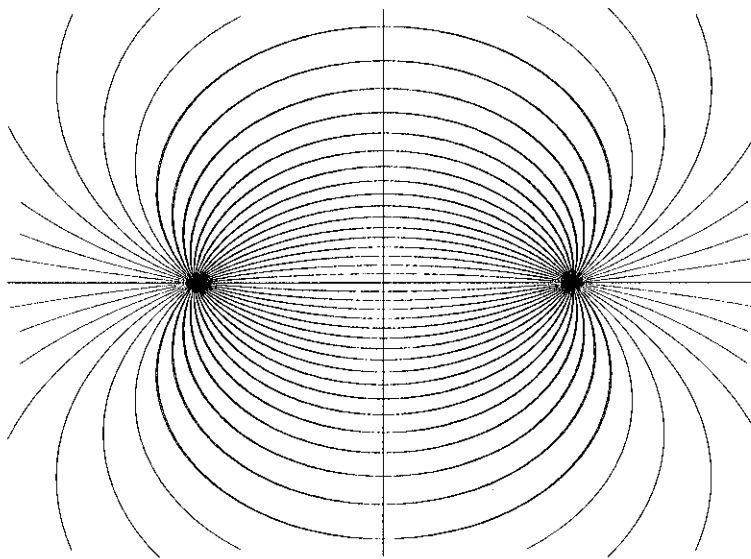


Figure 2.25

Thus we have discovered an important method of representing the effect of a boundary, using only very simple pressure drop solutions for wells *in an infinite reservoir*. The effect of an impermeable boundary can be replicated exactly by placing an "image" well at a distance from the original well that is exactly twice the distance of the boundary from the original well. Also, we can see from Eq. 2.49 that at late time the effect of two identical wells, measured at the original well, will be given by Eq. 2.50.

$$\Delta p = \frac{141.2q_B B \mu}{kh} \left[\frac{1}{2} \left(\ln \frac{kt}{\phi \mu c_t r_w^2} + \ln \frac{kt}{\phi \mu c_t (2r_e)^2} \right) + 0.80908 \right] \quad (2.50)$$

where r_e is the distance to the impermeable boundary. Hence we can understand why the slope of the semilog straight line doubles as the boundary effect becomes significant (as was described earlier in Section 2.6.2, and is shown in Figure 2.26).

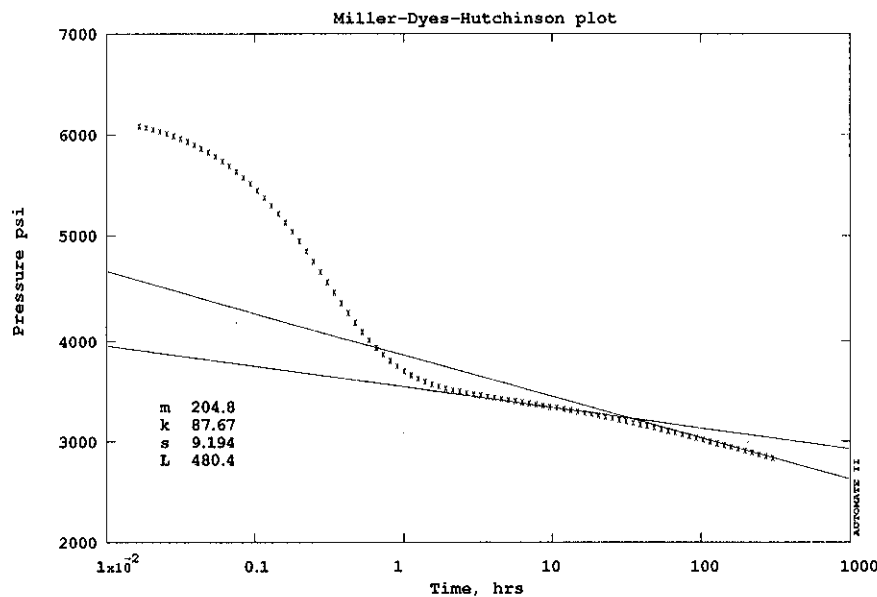


Figure 2.26

Why is the semilog slope not doubled for all time? Since r_e^2 is so much larger than r_w^2 , the second well effect does not become significant until time t becomes large (recall that the logarithmic approximation to the exponential integral function is only valid for $t_D > 10$).

Using the image well concept, it is very simple to create the effect of quite complex boundary shapes, including mixtures of impermeable and constant pressure boundaries, even in three dimensions. Consider for example the images that can be used to create the effect of a rectangular boundary (Fig. 2.27).

A second important use of superposition is to add together the effects of wells at different *times*. Consider for example the case of Fig. 2.22 where A, B and C are all at the same point. The pressure drop of two wells *at the same location*, one with flow rate q_B and the other with flow rate q_C , is identical to the pressure drop due to a single well with flow rate $q_B + q_C$. We can imagine replacing two small pumps by

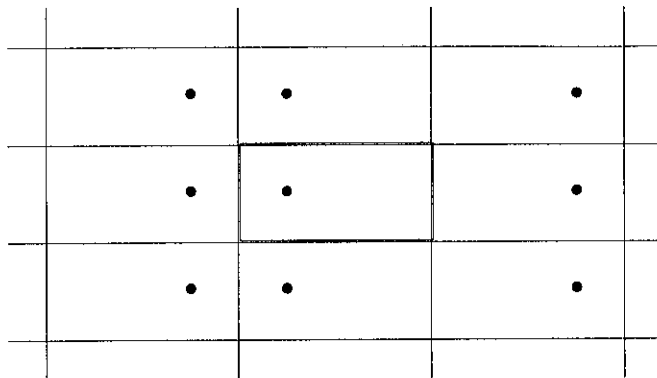


Figure 2.27

one big pump. However, let us go on to consider the case where the first well starts flowing at time zero, and the second well does not start flowing until time t_p (Fig. 2.28).

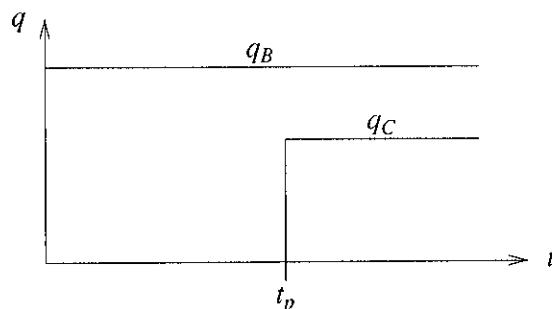


Figure 2.28

The net effect is of a single well flowing at rate q_B for time t_p , and at rate $q_B + q_C$ thereafter (Fig. 2.29).

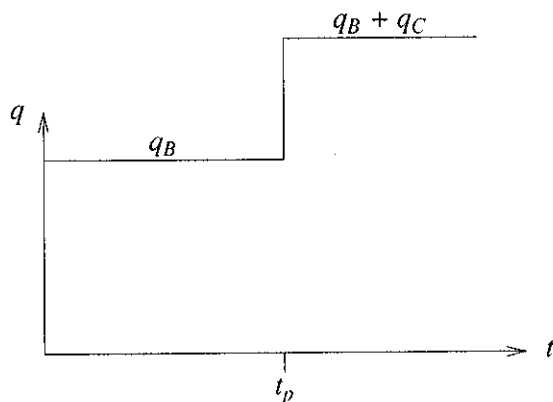


Figure 2.29

This same superposition can be used for any number of "wells", each with constant flow rates starting at different times, thus it is possible to generate the reservoir response to a single well flowing at variable rate, using only the same constant rate solutions described already. The variable rate is approximated by a series of "stairsteps," as in Fig. 2.30.

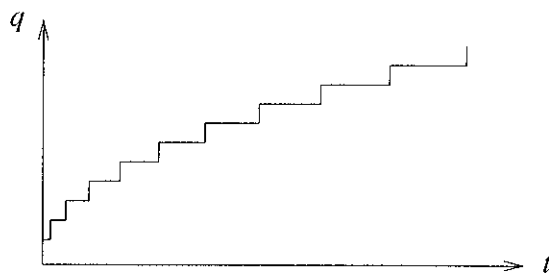


Figure 2.30

A particular case of practical importance is where q_B is q , starting at time zero, and q_C is $-q$, starting at the time t_p .

The effect of these two flow rates is the representation of a well which is produced for a time t_p , at rate q , and then shut in (Figure 2.31).

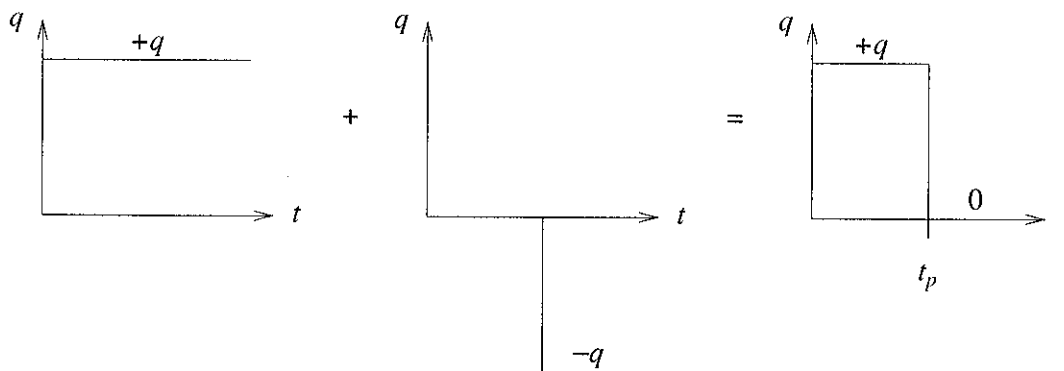


Figure 2.31

This gives us a means to generate the pressure response during a buildup test, using the simple constant rate solutions generated for drawdown tests (as in Eq. 2.51).

$$p_D = p_D(t_D + \Delta t_D) - p_D(\Delta t_D) \tag{2.51}$$

This is illustrated in Fig. 2.32, and is true regardless of the reservoir model used.

While discussing this point, we can observe that this time superposition leads to a particularly simple result during infinite acting radial flow. During this flow regime:

$$p_{ws} = p_i - \frac{141.2qB\mu}{kh} \left[\frac{1}{2} \left[\ln \frac{k(t_p + \Delta t)}{\phi\mu c_i r_w^2} - \ln \frac{k\Delta t}{\phi\mu c_i r_w^2} \right] \right] \tag{2.52}$$

$$\text{or, } p_{ws} = p_i - \frac{162.6qB\mu}{kh} \log \frac{t_p + \Delta t}{\Delta t} \tag{2.53}$$

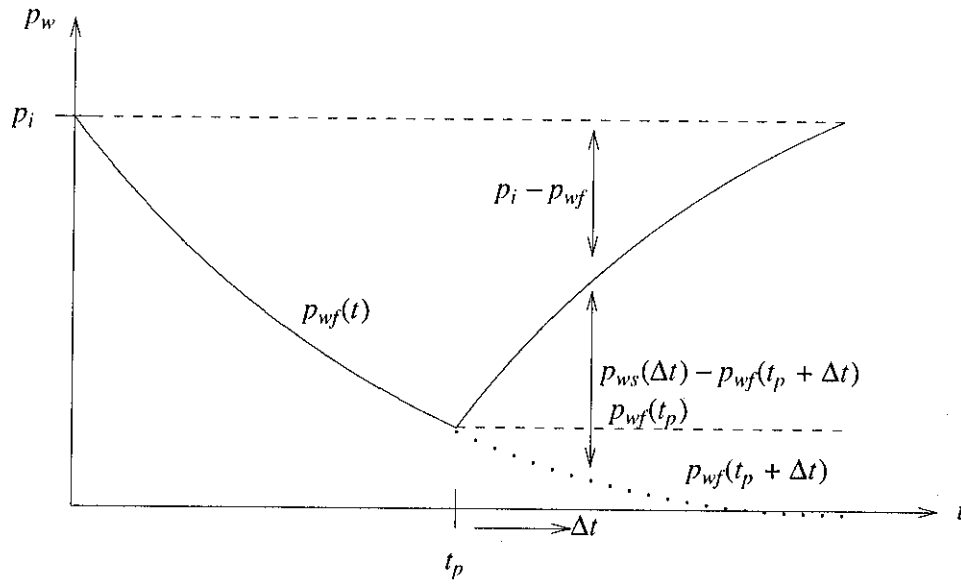


Figure 2.32

Thus a plot of pressure against the logarithm of $(t_p + \Delta t) / \Delta t$ will show a straight line of slope

$$m = 162.6 \frac{qB\mu}{kh} \tag{2.54}$$

Such a plot is known as a Horner plot, and we refer to $(t_p + \Delta t) / \Delta t$ as the Horner time (Fig. 2.33)

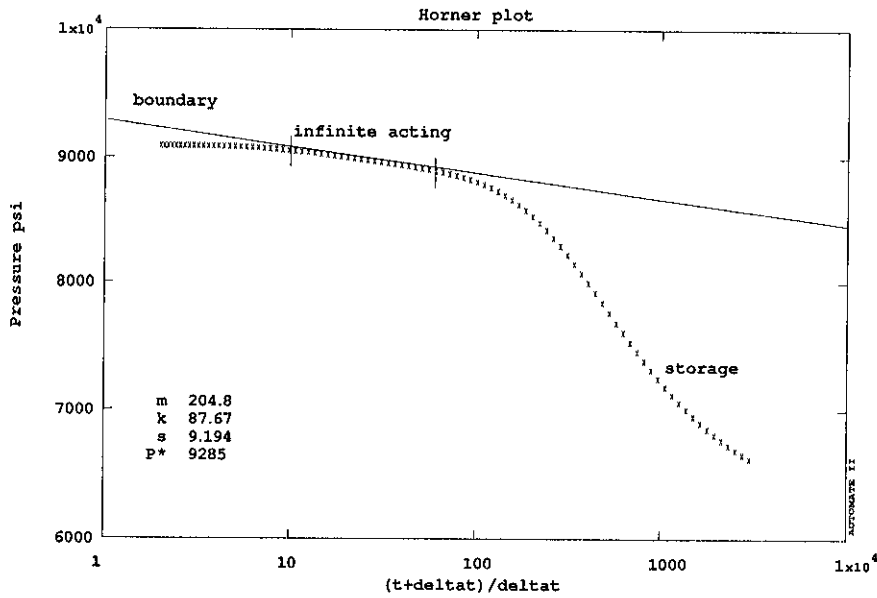


Figure 2.33

The Horner time is useful for semilog analysis, however we still have problems with log-log (type curve) analysis. This is because in type curve analysis of a drawdown test, we plot $\log(p_i - p_{wf})$ against $\log \Delta t$. We could do this correctly for shut-in tests if we could plot the logarithm of $p_{ws}(\Delta t) - p_{wf}(t_p + \Delta t)$ (see Fig. 2.32), by subtracting the "would have been" flowing pressure from the measured well pressure. Unfortunately we do not know what this "would have been" pressure is. Agarwal (1980) developed the concept of an "equivalent time" (which is known as the Agarwal equivalent time) as a time at which the measurable pressure difference $p_{ws}(\Delta t) - p_{wf}(t_p)$ is equal to the correct pressure difference $p_{ws}(\Delta t) - p_{wf}(t_p + \Delta t)$. This equivalent time can be determined exactly for infinite acting radial flow, when the log approximation is valid (i.e., when $t_D > 10$). For the time to be equivalent, we require that

$$p_{ws}(t_{equiv}) - p_{wf}(t_p) = p_{ws}(\Delta t) - p_{wf}(t_p + \Delta t) \quad (2.55)$$

As long as each pressure varies as $\log t$, then we can determine that

$$t_{equiv} = \frac{t_p \Delta t}{t_p + \Delta t} \quad (2.56)$$

This is the Agarwal equivalent time, and using it in place of Δt will allow drawdown type curves to be used for buildup. This is strictly true only for infinite acting radial flow without wellbore storage, however has been shown to work well even in tests which contain storage or fracture effects.

2.12 References

- Agarwal, R.G.: "A New Method to Account for Producing Time Effects When Drawdown Type Curves are Used to Analyze Pressure Buildup and Other Test Data", paper SPE 9289 presented at the 55th SPE Annual Technical Conference and Exhibition, Dallas, TX, Sept 21-24, (1980).
- Cinco, H., Samaniego, F., and Dominguez, N.: "Transient Pressure Behavior for a Well with a Finite Conductivity Vertical Fracture", *Soc. Petr. Eng. J.*, (August 1978), 253-264.
- Cinco, H., Samaniego, F.: "Transient Pressure Analysis for Fractured Wells", *J. Pet. Tech.*, (September 1981).
- Cinco, H., Samaniego, F.: "Transient Pressure Analysis: Finite Conductivity Fracture Case Versus Damaged Fracture Case", paper SPE 10179 presented at the 56th SPE Annual Technical Conference and Exhibition, San Antonio, TX, Oct 5-7, (1981b).
- Earlougher, R.C., Jr.: "Advances in Well Test Analysis", Society of Petroleum Engineers Monograph 5, Dallas, TX, (1977).
- Gringarten, A.C., Ramey, H.J., Jr., and Raghavan, R.: "Pressure Analysis for Fractured Wells", paper SPE 4051 presented at the 47th SPE Annual Technical Conference and Exhibition, San Antonio, TX, Oct 8-11, (1972).
- Gringarten, A.C., Ramey, H.J., Jr., and Raghavan, R.: "Unsteady State Pressure Distribution Created by a Well with a Single Infinite Conductivity Vertical Fracture", *Soc. Petr. Eng. J.*, (August 1974), 347-360.

3. INTRODUCTION TO COMPUTER-AIDED ANALYSIS

Well test analysis by traditional methods makes considerable use of graphical presentations. Much of the theory of the field has concentrated on procedures to aid graphical analysis. Much of this traditional theory has been explained in Section 2. It can be seen that many of the underlying principles are based upon the following restrictions:

- (a) Drawdown in a single well
- (b) Constant rate production

Using approximations that are often associated with log (time) behavior (i.e., infinite acting radial flow) there are some useful extensions that can be made to graphical techniques (for example to allow analysis of buildup tests).

The first objective in computer-aided analysis is to speed up the traditional graphical techniques by allowing rapid presentation of graphs and by performing the standard estimation calculations. However a more important objective is to extend the analysis beyond the restrictions inherent in traditional methods. Specifically, a computer-aided interpretation can accommodate situations that are either only approximated in traditional methods, or which cannot be handled at all, such as:

- (a) Continuously varying rate
- (b) Multiple wells
- (c) Complex geometries
- (d) Downhole measurements of flow rate
- (e) Indefinite initial pressure

Thus a computer-aided interpretation allows the reservoir engineer to obtain better results in less time, to a wider range of field conditions. Economides, Joseph, Ambrose, and Norwood (1989) and Gringarten (1986) have both summarized modern approaches to well test analysis using computers.

The procedure in many computer-aided analyses is to follow traditional lines of approach as far as they are applicable, and then to extend the interpretation using the additional capabilities permitted by the computer-aided approach. The advantage of starting the analysis along traditional lines is that the techniques are familiar to the engineer engaged in the work and the expertise gained over many years of traditional well interpretation is not abandoned.

Thus computer-aided interpretation remains dependent on graphical presentations (in fact the simplest of computer assistance may be restricted to that).

3.1 Graphical Presentations

Data presented in a pictorial (graphical) form are much easier to understand than a simple table of numbers. A useful "toolbox" of graphing functions are therefore an essential part of a computer-aided well test interpretation system.

The objective in examining a series of graphical presentations of the data is to correctly identify the different characteristic flow periods occurring during the well test. The various different flow periods described earlier in Section 2 are summarized in Table 3.1, along with their characteristic signature and the plot on which this signature is best recognized.

Flow Period	Characteristic	Plot
Infinite acting radial flow (drawdown)	Semilog straight line	p vs $\log \Delta t$ (MDH plot)
infinite acting radial flow (buildup)	straight line p vs $\log(t_p + \Delta t)/\Delta t$	p vs $\log(t_p + \Delta t)/\Delta t$ (Horner plot)
wellbore storage	straight line p vs t unit slope $\log \Delta p$ vs $\log \Delta t$	$\log \Delta p$ vs $\log \Delta t$ (log-log type curve)
finite conductivity fracture	straight line slope $1/4$ $\log \Delta p$ vs $\log \Delta t$	$\log \Delta p$ vs $\log \Delta t$, or Δp vs $\Delta t^{1/4}$
infinite conductivity fracture	straight line slope $1/2$ $\log \Delta p$ vs $\log \Delta t$	$\log \Delta p$ vs $\log \Delta t$, or Δp vs $\Delta t^{1/2}$
double porosity effects	S-shaped transition between semilog straight lines	p vs $\log \Delta t$ [difficult]
closed boundary	pseudosteady state, pressure linear with time	p vs Δt (Cartesian plot)
impermeable boundary	doubling of slope on semilog straight line	p vs $\log \Delta t$ (MDH plot)
constant pressure boundary	constant pressure flat line on all p/t plots	any

Table 3.1

3.2 The Derivative Plot

From Table 3.1 it can be appreciated that different plots are used for different purposes, and most analysis will require the consideration of several plots.

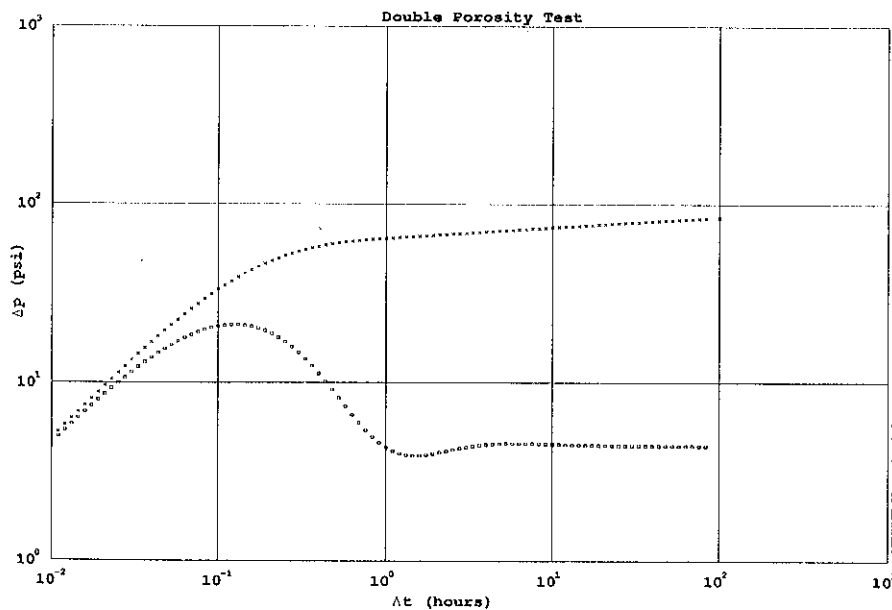


Figure 3.1

Modern analysis has been greatly enhanced by the introduction of the derivative plot by Bourdet, Whittle, Douglas and Pirard (1983) (also discussed in Bourdet, Ayoub, and Pirard, 1989). The derivative plot provides a simultaneous presentation of $\log \Delta p$ versus $\log \Delta t$ and $\Delta t \log \partial p / \partial t$ versus $\log \Delta t$, as in Figure 3.1.

The advantage of the derivative plot is that it is able to display in a single graph many separate characteristics that would otherwise require different plots. These characteristics are shown in Figures 3.2 - 3.9, compared to their traditional plots (as listed in Table 3.1).

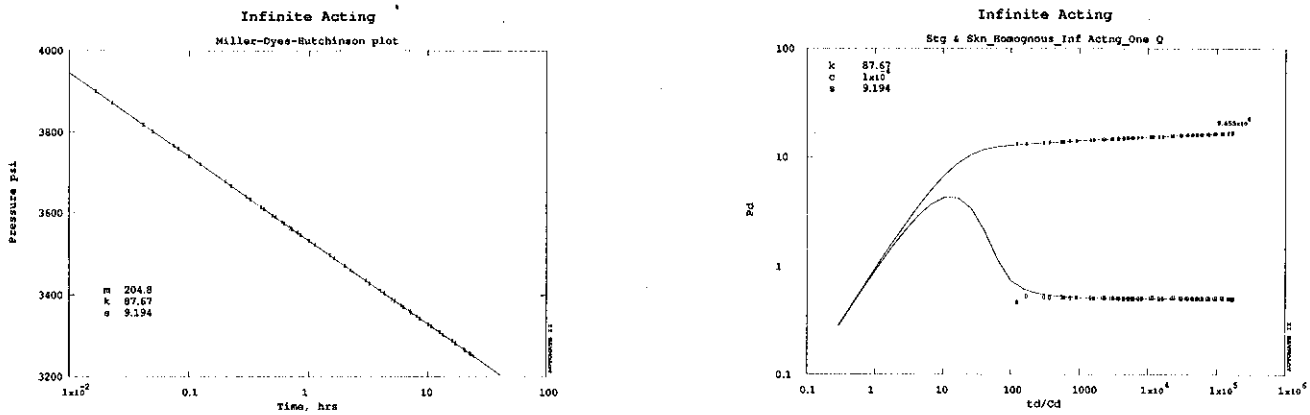


Figure 3.2: Infinite acting radial flow shows as semilog straight line on a semilog plot, as a flat region on a derivative plot

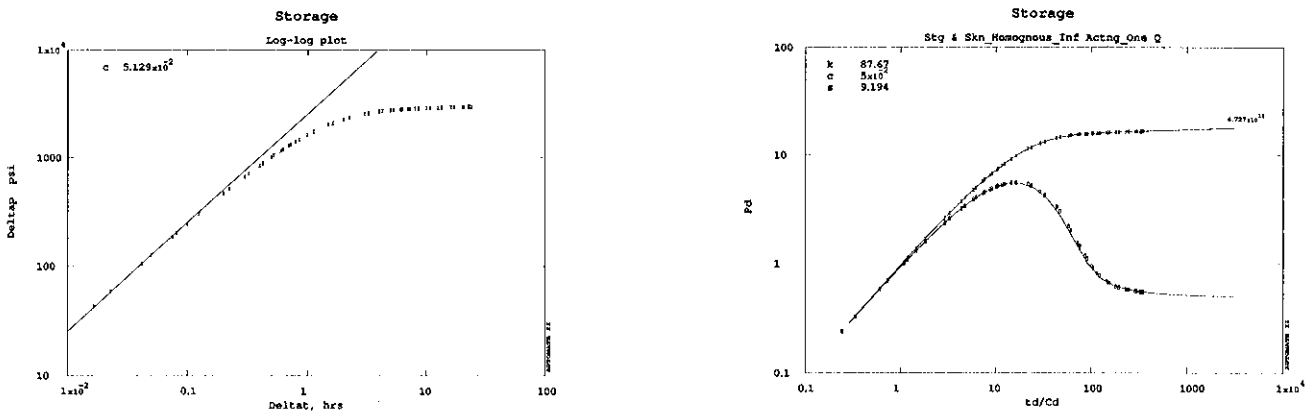


Figure 3.3: Storage shows as a unit slope straight line on a log-log plot, as a unit slope line plus a hump on a derivative plot

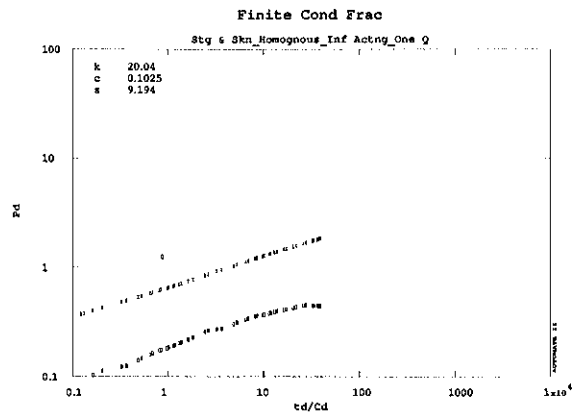
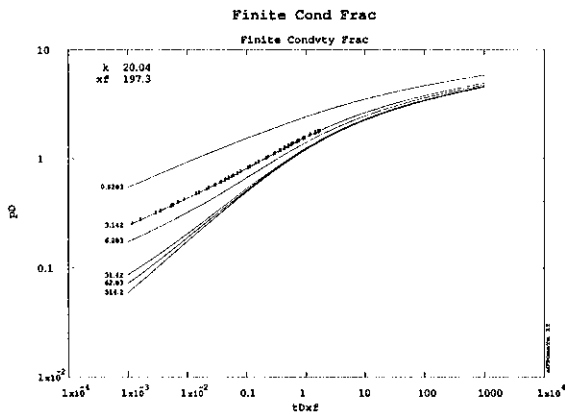


Figure 3.4: A finite conductivity fracture shows as a 1/4 slope line on a log-log plot, same on a derivative plot

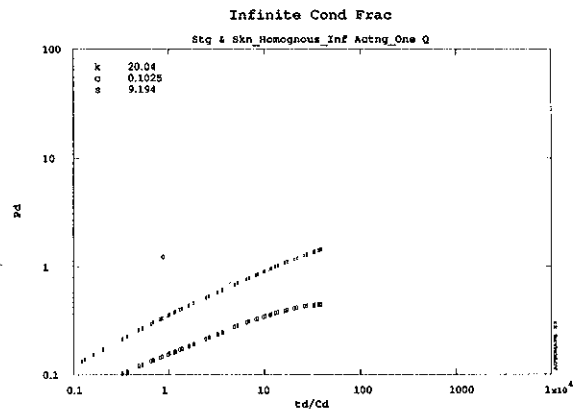
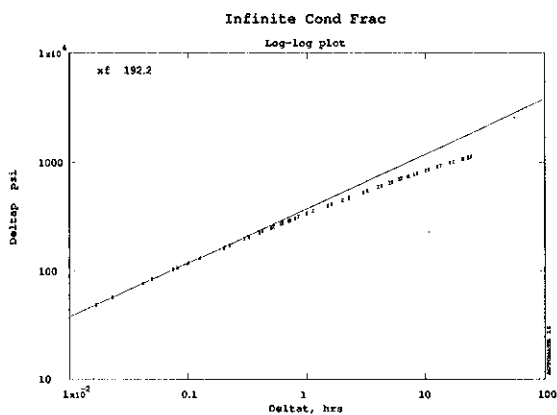


Figure 3.5: An infinite conductivity fracture shows as a 1/2 slope line on a log-log plot, same on a derivative plot

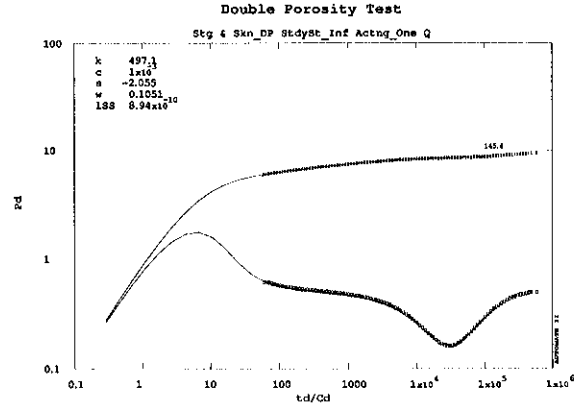
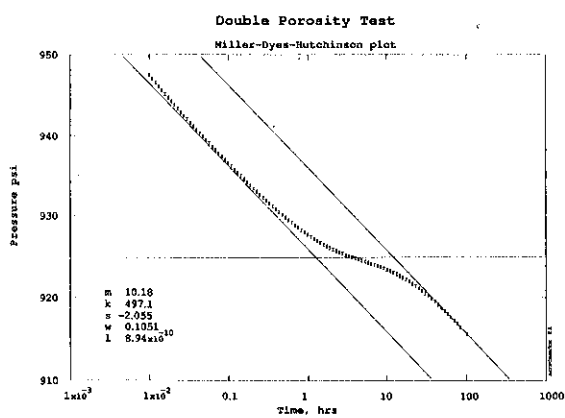


Figure 3.6: Double porosity behavior shows as two parallel semilog straight line on a semilog plot, as a minimum on a derivative plot

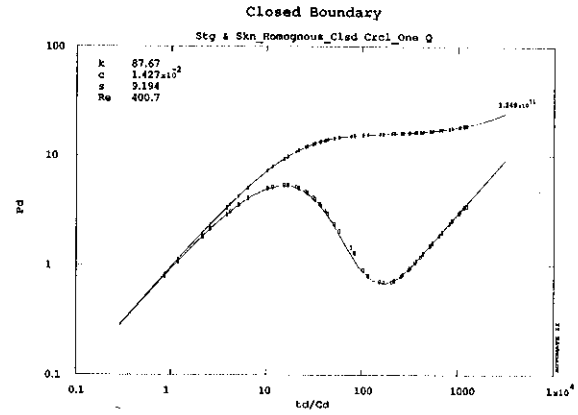
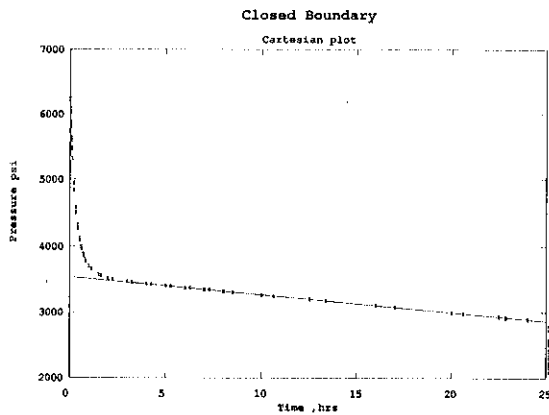


Figure 3.7: A closed outer boundary (pseudosteady state) shows as a straight line on a Cartesian plot, as a steep rising straight line on a derivative plot

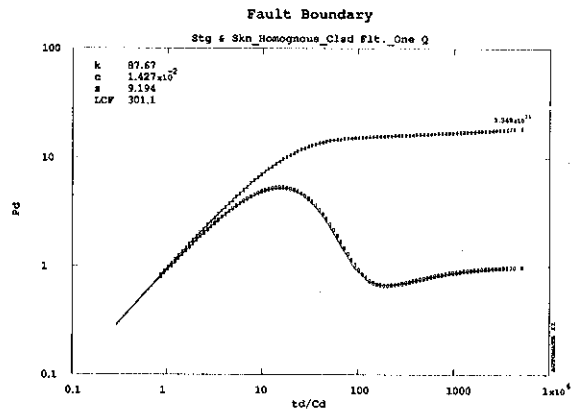
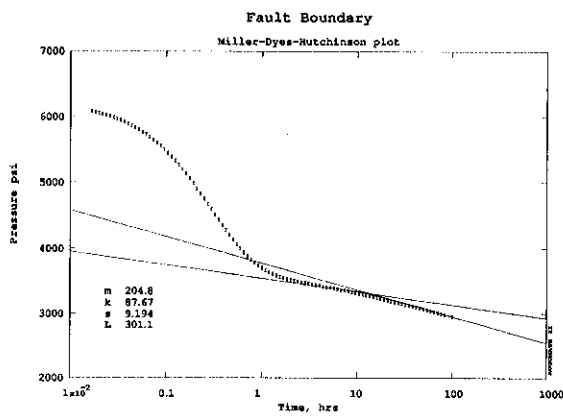


Figure 3.8: A linear impermeable boundary shows as semilog straight line with a doubling of slope on a semilog plot, as a second flat region on a derivative plot

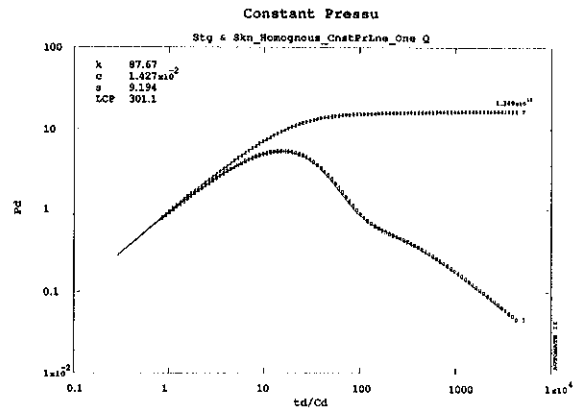
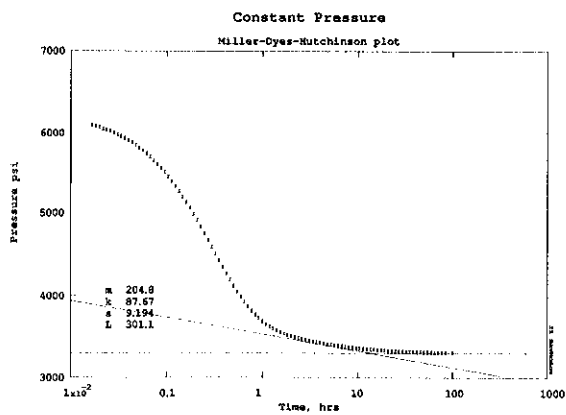


Figure 3.9: A constant pressure boundary shows as flat region on most p vs. t plots, as a continuously decreasing line on a derivative plot

In particular, double porosity behavior is much easier to see on a derivative plot (Fig. 3.6) even when the first semilog straight line is obscured by wellbore storage.

Even though the derivative plot is by far the most useful for diagnosis, it is not necessarily the most accurate for calculation when it comes to estimating parameters. Hence the other plots (particularly the semilog plots) are still required.

Calculating the pressure derivative requires some care, since the process of differentiating the data amplifies any noise that may be present. A straightforward numerical differentiation using adjacent points (Eq. 3.1) will produce a very noisy derivative (Fig. 3.10).

$$t \left[\frac{\partial p}{\partial t} \right]_i = t_i \left[\frac{(t_i - t_{i-1}) \Delta p_{i+1}}{(t_{i+1} - t_i)(t_{i+1} - t_{i-1})} + \frac{(t_{i+1} + t_{i-1} - 2t_i) \Delta p_i}{(t_{i+1} - t_i)(t_i - t_{i-1})} - \frac{(t_{i+1} - t_i) \Delta p_{i-1}}{(t_i - t_{i-1})(t_{i+1} - t_{i-1})} \right] \quad (3.1)$$

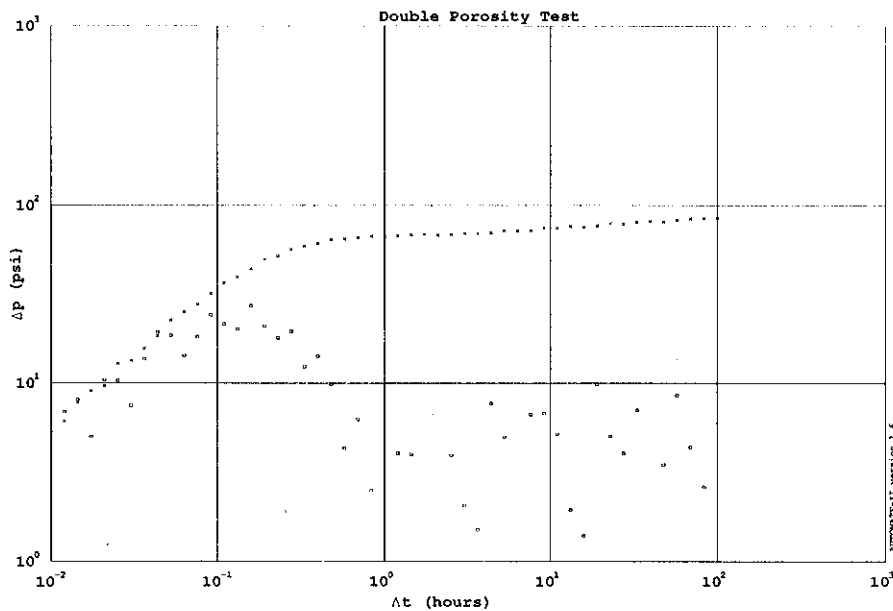


Figure 3.10

If the data are distributed in geometric progression (with the time difference from one point to the next becoming greater as the test proceeds), then the noise in the derivative can be reduced somewhat by using a numerical differentiation with respect to the logarithm of time:

$$t \left[\frac{\partial p}{\partial t} \right]_i = \left[\frac{\partial p}{\partial \ln t} \right]_i$$

$$\begin{aligned}
&= \frac{\ln(t_i/t_{i-1})\Delta p_{i+1}}{\ln(t_{i+1}/t_i) \ln(t_{i+1}/t_{i-1})} \\
&+ \frac{\ln(t_{i+1}t_{i-1}/t_i^2)\Delta p_i}{\ln(t_{i+1}/t_i) \ln(t_i/t_{i-1})} \\
&- \frac{\ln(t_{i+1}/t_i)\Delta p_{i-1}}{\ln(t_i/t_{i-1}) \ln(t_{i+1}/t_{i-1})}
\end{aligned} \tag{3.2}$$

However, even this approach leads to a noisy derivative. The best method to reduce the noise is to use data points that are separated by at least 0.2 of a log cycle, rather than points that are immediately adjacent. Hence:

$$\begin{aligned}
t \left[\frac{\partial p}{\partial t} \right]_i &= \left[\frac{\partial p}{\partial \ln t} \right]_i \\
&= \frac{\ln(t_i/t_{i-k})\Delta p_{i+j}}{\ln(t_{i+j}/t_i) \ln(t_{i+j}/t_{i-k})} \\
&+ \frac{\ln(t_{i+j}t_{i-k}/t_i^2)\Delta p_i}{\ln(t_{i+j}/t_i) \ln(t_i/t_{i-k})} \\
&- \frac{\ln(t_{i+j}/t_i)\Delta p_{i-k}}{\ln(t_i/t_{i-k}) \ln(t_{i+j}/t_{i-k})}
\end{aligned} \tag{3.3}$$

$$\ln t_{i+j} - \ln t_i \geq 0.2 \tag{3.4}$$

$$\ln t_i - \ln t_{i-k} \geq 0.2 \tag{3.5}$$

The value of 0.2 (known as the differentiation interval) could be replaced by smaller or larger values (usually between 0.1 and 0.5), with consequent differences in the smoothing of the noise. Figs. 3.11a through c compare the different amount of smoothing achieved. Notice that if a very wide interval is used (0.5 in Fig. 3.11c), then the shape of the calculated derivative curve (represented by the points in Figs. 3.11a-c) may be distorted. In Fig. 3.11c, the points to the right of the storage "hump" are displaced to the right, by comparison with Figs. 3-11a and b.

It should be noted that the use of the differentiation interval may cause problems determining the derivative of the last part of the derivative curve, since the data "runs out" within the last differentiation interval. Some noise is therefore to be expected at the end of the data. Also, the differentiation interval approach may overly flatten the early time derivative, and since this part of the data is not prone to noise anyway, it is often better to use the arithmetic differentiation for the early points (Eq. 3.2).

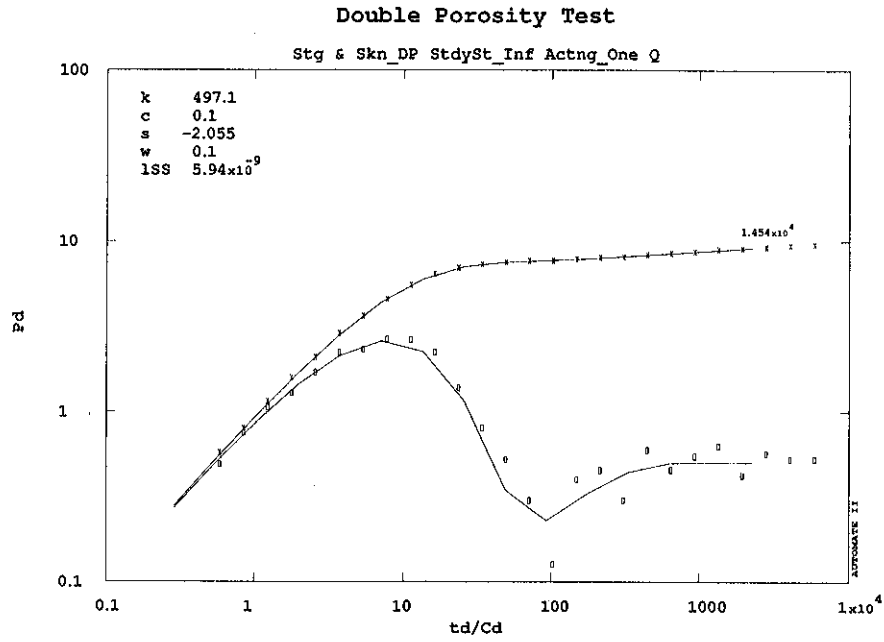


Figure 3.11a: Differentiation interval 0.1

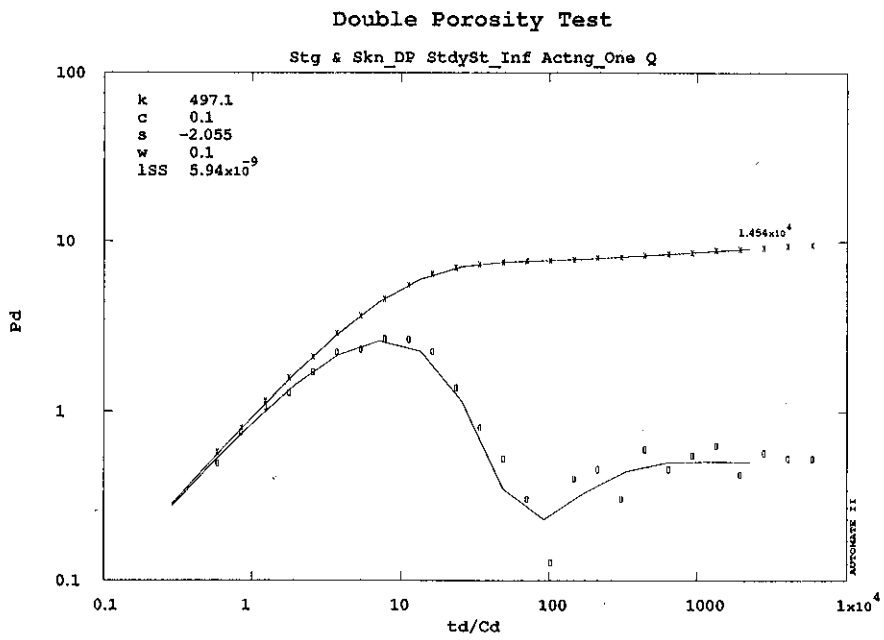


Figure 3.11b: Differentiation interval 0.2

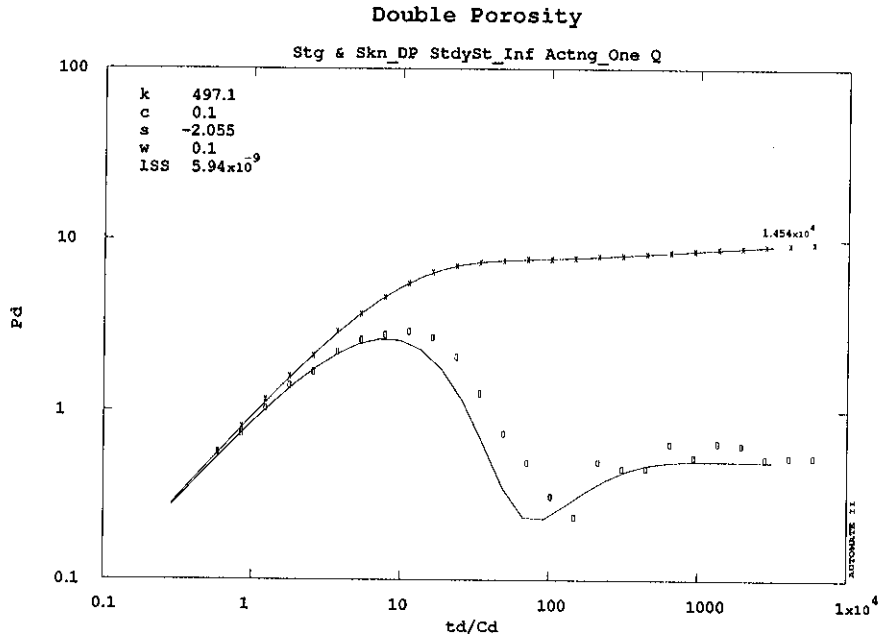


Figure 3.11c: Differentiation interval 0.5

3.3 Diagnostic Plot Evaluation

As has been described in the previous two sections, different parts of the reservoir response are recognizable by their characteristics or particular graphical presentations. This enables the engineer to separate one part of the response from another. It is absolutely critical to the final interpretation that this distinction be made. Why is it so important? Consider, for example, the estimation of reservoir permeability from the slope of the semilog straight line characteristic of infinite acting radial flow -- there may be other parts of the response which may at first appear to show a semilog straight line, but which would give totally erroneous estimates of the permeability. Such false straight lines could be due to boundary effects, or may be due to external effects completely unrelated to the reservoir response (for example temperature response of the instrument, removal of drilling fluids from the invaded zone, etc.). Since certain specific portions of the response are used to estimate specific reservoir parameters, it is clearly necessary to identify each portion precisely.

Often a good indication of a particular reservoir response can be obtained by considering the responses preceding and following it, since the different responses do come in a certain chronological order (this was summarized in Table 2.2). Thus we would not look for infinite acting radial flow before wellbore storage, nor would we look for it after a pseudosteady state response. It is often useful to "tag" particular response regions (e.g., storage, semilog straight line, boundary effect) to confirm that the identified responses appear in the correct order, and do not overlap each other (Fig. 3.12). There are also useful indicators in some of the transitions between flow regimes, for example, the $1\frac{1}{2}$ log cycles between storage and infinite acting radial flow, which gives rise to the $1\frac{1}{2}$ log cycle rule.

The specific response characteristics have already been illustrated in Figs. 3.2 - 3.9, and will be discussed in more detail in specific examples later.

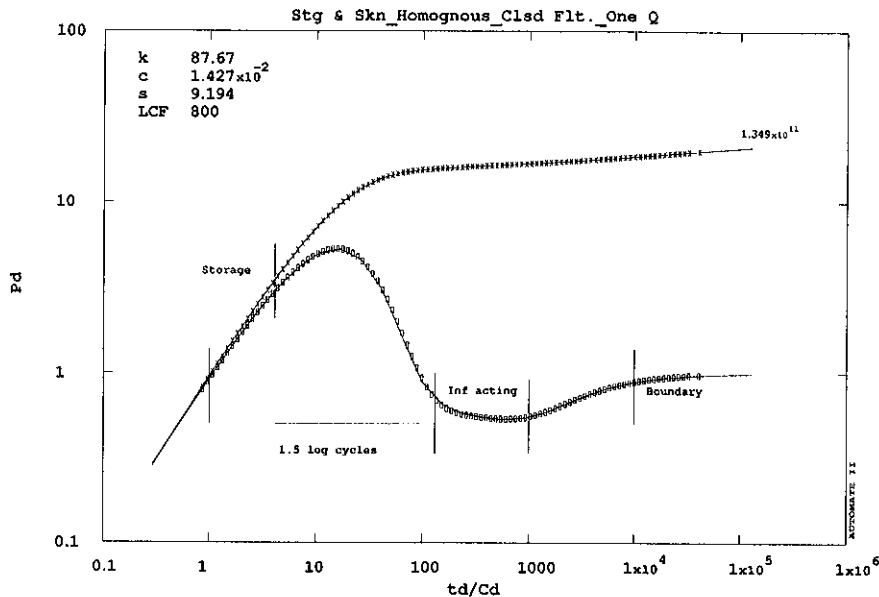


Figure 3.12

3.4 Data Preparation

If we are to be able to correctly identify regions of the data, it is clearly important that the data itself be correct. Since real data collection is sometimes subject to both physical and human error, it is worthwhile to consider the preparation of data prior to beginning the analysis. Some preparation may be necessary to extract the pressure data in the correct format, units and datum from service company output files, however this is relatively mundane. Two specific items of data preparation that require special care are discussed in detail here, namely (a) number and frequency of data, and (b) datum shifting.

3.4.1 Number and Frequency of Data

Modern electronic pressure gauges are capable of high precision measurements at high frequency, making digital pressure measurements faster than one per second if required. These measurements can be recorded magnetically at surface (in surface recording tools) or may be stored electronically within the downhole tool itself (in memory tools). In either case, the total number of data points can be many thousands during the time of a test. In permanently installed gauges, data can accumulate to millions of points. Plotting and manipulating so many data can be a monstrous task, even for a computer, and it is usually desirable to reduce the total data set to a more manageable size by sampling a representative subset of at most a few hundred data.

The main objectives in sampling data are: (a) to capture essential features of the response; (b) to apply roughly equal weight to each of the separate response regions; (c) to reduce the total number of data to speed up plotting and calculation.

If our objective were only to reduce the number of data, it would be legitimate to sample data at fixed intervals (for example sampling every tenth point in 2000 data, to end up with 200 data). However, if the data were measured at regular intervals, this would tend to provide an excessive number of late time points and too few early time points, since we know that the most rapid changes take place at early time. This kind of sampling can be useful for preliminary reduction of very large data sets, or when the data were actually recorded with reducing frequency at later time.

If data were recorded at a uniform spacing in time, a more suitable sampling would be *logarithmic*. This approach includes more data at early time and fewer at late time (Fig. 3.13). This achieves the correct weighting for infinite acting responses, which we have already observed are logarithmically dependent on time. However this would not be a good method to use when the data includes several different flow periods, since the logarithmic cycle needs to be restarted at each major flow change -- Fig. 3.14 shows an example of a logarithmic sampling in a multirate test, demonstrating that insufficient data points are included after the rate change.

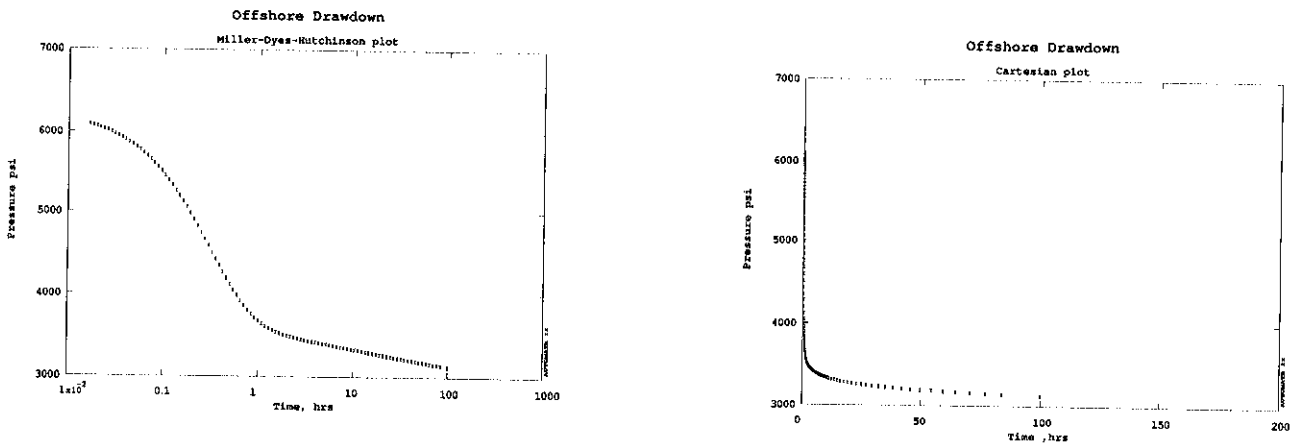


Figure 3.13

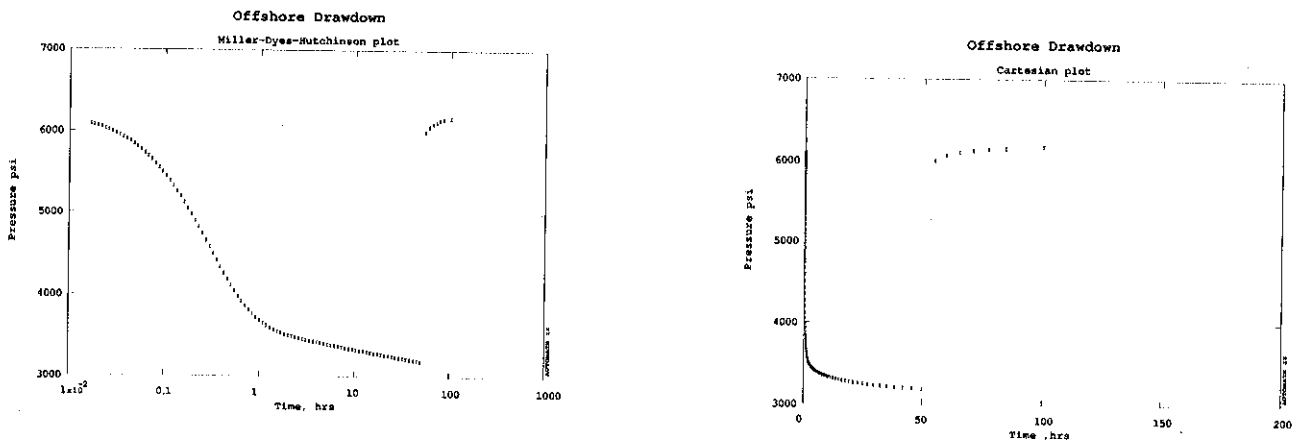


Figure 3.14

A third sampling method which is more generally applicable is one which samples uniformly in *pressure* rather than in time. This ensures that more data are included at times where the pressure

changes most, which will usually result in more or less equivalent weighting of all flow regimes. Care must be taken in specific cases. Firstly, if the data contains flat regions (regions of constant pressure) then it is necessary to ensure that the region is not skipped altogether. Secondly, if the data is noisy in some places relative to others, then this sampling method will tend to emphasize the noisier data.

3.4.2 Datum Shifting

An instrument may measure pressures at one second intervals, and may record during a well test for several days. Hence data may be available from 1 second to 10^5 or 10^6 seconds, and may span six log cycles in a graphical presentation. However it must be remembered that a logarithmic presentation tends to hide errors at late time, and emphasize them at early time. It must also be remembered that the start of the test does not occur instantaneously, nor does the pressure gauge react immediately. Opening or closing a wellhead valve may take some minutes, and the pressure transducer may take up to a minute to stabilize (this is particularly true of capillary tube tools). For these various reasons, the actual time of the early data may be a minute or more different from the recorded time. Another way of looking at the situation is that at the indicated time, the pressure was not really that recorded at that same actual time. Errors of a few minutes in time, or a few psi in pressure drop may not seem significant, but because of the common use of logarithmic plots such differences can substantially alter the appearance of the data and can therefore impair the interpretation. Consider the effects of one minute changes in the specification of time zero in Figure 3.15.

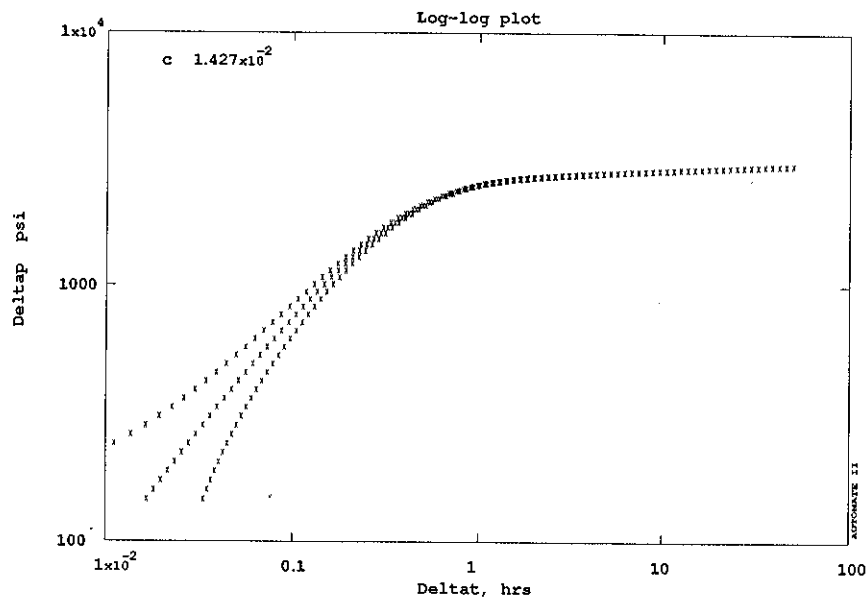


Figure 3.15

In this example it would be easy to mistake the wellbore storage region for some kind of fracture effect (in the case of the upper curve).

Thus it is important to be cautious with early time data, especially from modern electronic gauges. It may often be necessary to shift the time datum forward or backward to correct the appearance of the early time data. Another way of correcting the situation is to treat the initial pressure measured at the

start of the test as a variable (this would be p_i for a drawdown test, or p_{wf} for a buildup test). This will be discussed in more detail in Section 3.5.2.

3.5 Non-Linear Regression

One of the most powerful analytic tools made possible by computer-aided interpretation is non-linear regression (sometimes known as automated type curve matching).

This method is entirely different from graphical techniques in that it uses a mathematical algorithm to match the observed data to a chosen reservoir model. The matching is achieved by changing the values of the unknown reservoir parameters (such as permeability, skin, ω , λ , distance to boundary, etc.) until the model and the data fit as closely as possible (in a least squares sense) by minimizing the sum of squares of the differences between measured pressure and model pressure:

$$\sum_{i=1}^n [p_{measured}(t_i) - p_{model}(t_i, k, s, c, \dots)]^2$$

The nonlinear regression procedure is freed from the restrictions associated with graphical techniques (constant rate production and instantaneous shut-in) and can therefore be used to interpret more modern tests in which downhole rates were recorded or in which several different rates were used. The method fits all the data simultaneously, and therefore avoids the problem of inconsistently interpreting separate portions of the data, as can happen with graphical analysis. Also, the mathematical fitting process allows for the statistical determination of goodness of fit, thus providing not only a numerical answer but also a quantitative evaluation of how good the answer is. Finally, nonlinear regression is capable of estimating reservoir parameters from pressure responses that are in the transition regions which cannot directly be interpreted by graphical methods. Thus there are significant cases of tests which are interpretable by nonlinear regression but not by graphical techniques, such as those that terminated prior to reaching the semilog straight line.

To summarize the advantages of using nonlinear regression, they are:

- (a) Analyzes multi-rate or variable rate tests,
- (b) Avoids inconsistent interpretations,
- (c) Provides confidence estimate on answer,
- (d) Can interpret "uninterpretable" tests.

At the same time, nonlinear regression requires the specification of the reservoir model to be matched; the algorithm itself does not select the model which is appropriate. Thus a nonlinear regression analysis must be complemented by a visual diagnosis of the data so that the engineer can select the correct reservoir model. At the same time as selecting the reservoir model the engineer can also speed up the nonlinear regression by making first estimates of the reservoir parameters. Most computer-aided well test software will do this automatically.

3.5.1 Confidence Intervals

To understand the evaluation of statistical goodness of fit, it is useful to discuss the concept of confidence intervals. Suppose that we estimate the reservoir permeability by fitting a semilog straight line through data from a pressure transient test, as in Fig. 3.16.

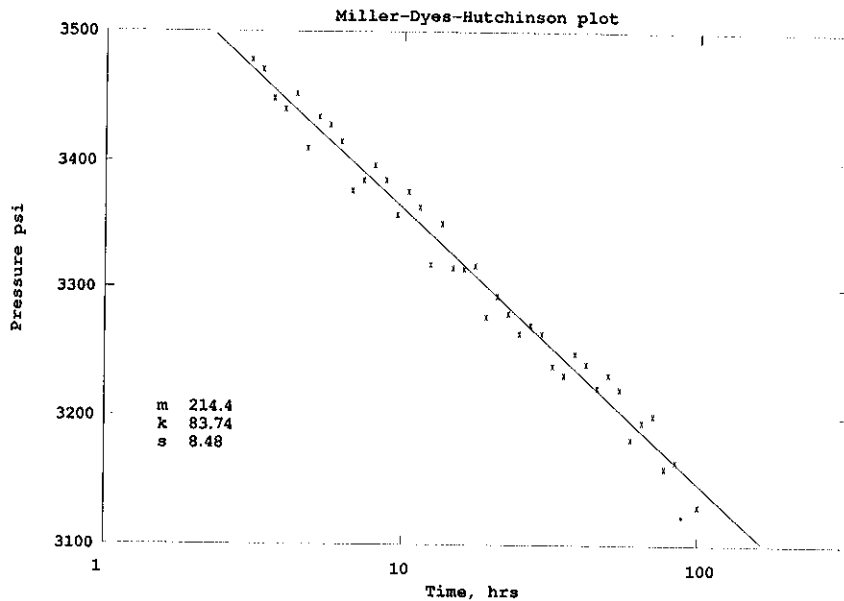


Figure 3.16

Since the data do not actually lie exactly in any straight line, there is some *uncertainty* as to whether the straight line is the correct one or not. If several people perform the fit graphically, then they are likely to obtain slightly different answers. Using regression, the answer will always be the same, but since the data is noisy perhaps under a different realization of the noise the answer would have been different. Hence we can say that although our answer is the most likely, due to the uncertainty in the data, there is a possibility that the true answer is different. There is high probability that the true answer is close to our best estimate, and low probability that it is far away. If we assume that the probability of a given answer is normally distributed about our best estimate, then we can recognize a "good" answer from a "bad" answer by the shape of the distribution (Fig. 3.17).

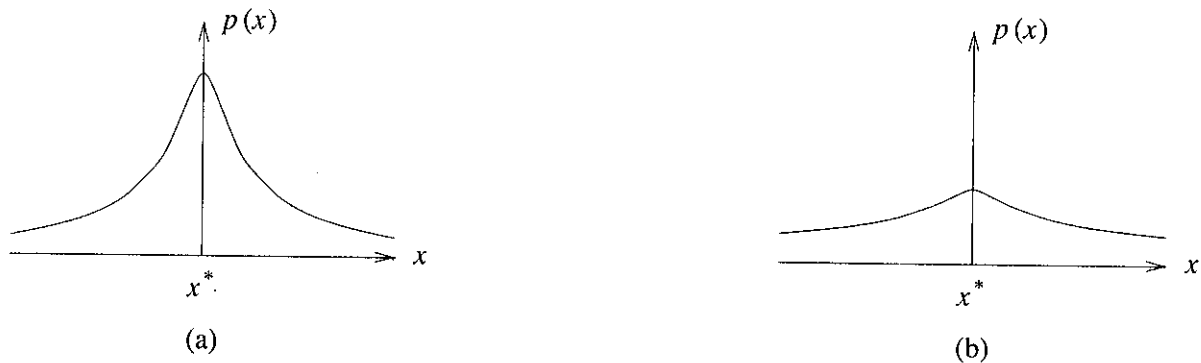


Figure 3.17

In Fig. 3.17(a), the probability that the true answer is close to x^* is high, and the probability that the answer is far from x^* is very small. Hence x^* is a "good" estimate. On the other hand, in Fig. 3.17(b), the true answer is almost as likely to have a value quite far from x^* as it is to have the value x^* itself. Hence x^* is a "bad" estimate in this case.

To specify the goodness of the estimate more quantitatively, we can define the confidence interval. The total area under the probability distribution curve is always 1.0, that is, there is 100% certainty that x will take a value somewhere between $-\infty$ and $+\infty$. However, if we restrict ourselves to 95% confidence,

then we can specify a much narrower range of values for which the included area under the curve is 0.95, as in Fig. 3.18.

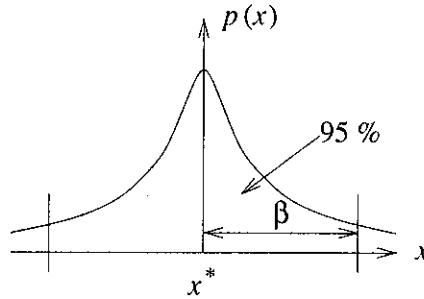


Figure 3.18

In this case we can say with 95% confidence of being right that the true value of x lies within the range

$$x^* - \beta < x < x^* + \beta \tag{3.6}$$

This range of values is known as the 95% confidence interval on the estimate value of x . There are various ways of specifying an answer together with its confidence interval, one would be to specify in terms of the absolute value of the range, for example $x^* \pm \beta$, while another would be to specify the range in terms of a percentage of the value of the parameter, for example $x^* \pm (100\beta/x^*)$ percent.

When using 95% confidence intervals to evaluate the goodness of fit of a nonlinear regression analysis of well tests, it is useful to define an *acceptable* estimate as one with a confidence interval that is 10% of the value itself. This definition is not useful for skin factor (since it can have value zero) or for initial reservoir pressure (since it can have large values). Table 3.2 summarizes the suggested limits on acceptable confidence ranges. The values in this table are based on a match of *pressure* -- when matching *pressure derivative* the acceptable confidence intervals can be roughly twice as wide.

Parameter	% Interval	Absolute Interval
k	10	-
C	10	-
ω	20	-
λ	20	-
r_e	10	-
x_f	10	-
s	-	1.0
p_i	-	1.0 (psi)

Table 3.2

The confidence interval is a function of the noise in the data, the number of data points, and the degree of correlation between the unknowns. As such, it is a useful indicator of whether the data is too noisy to confidently support the estimate obtained, and is also a good indicator of ambiguity (for example if the same fit could be obtained by changing the permeability estimate and making a compensating change in the skin estimate). No such indicators are possible with traditional graphical analysis, and in the past it was not possible to be assured as to how valid a given estimate was.

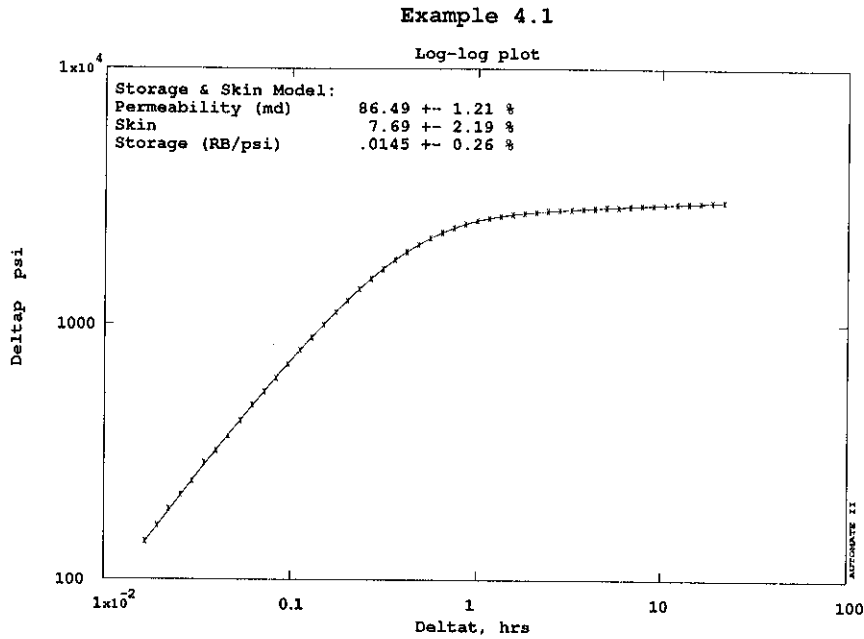


Figure 3.19a

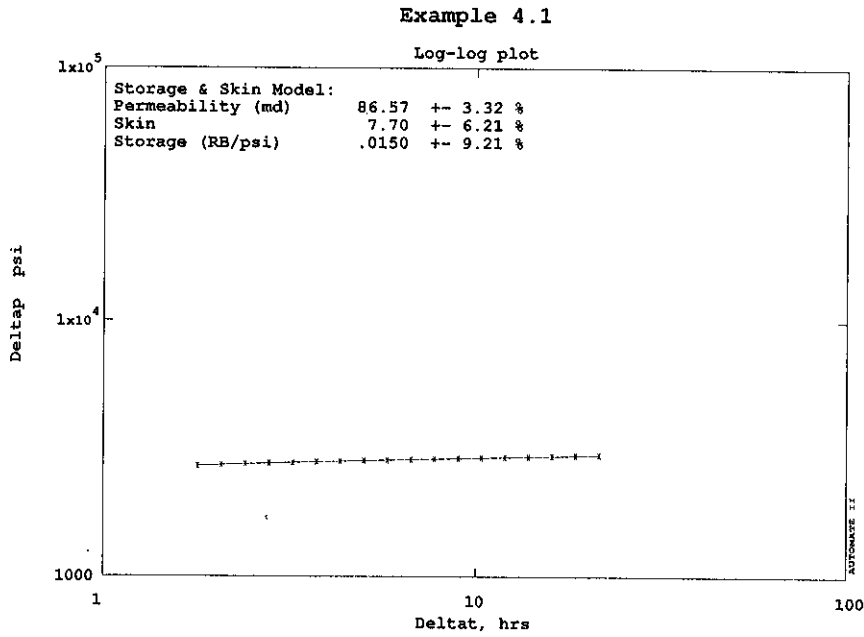


Figure 3.19b

In simple terms, there is reason to question the validity of a reservoir model if *any* of its parameters have confidence intervals which are wider than the acceptable range, however in practice, a less stringent condition may be used. If data is missing over a given flow regime (e.g. wellbore storage), then the confidence interval for this region will be wide. However, the answers that originate from the other flow regions (for which there is data) may have confidence intervals within the allowable range, and their estimated values are still acceptable. Figs. 3.19a and b illustrate this point -- removing the wellbore

storage dominated portion of the data results in a substantial widening of the confidence interval on the estimate of the wellbore storage parameter (Fig. 3.19b). The permeability and skin estimates are unchanged and their confidence intervals widen only somewhat since there are fewer data points in Fig. 3.19b.

On the other hand, matching a reservoir model that is inappropriate for the data should give confidence intervals that are unacceptable for most (or all) of the estimates, such as in Fig. 3.20.

Confidence intervals are also useful indicators that an apparently good match may in fact have insufficient data to be of significance (Fig. 3.21).

Examination of confidence intervals teaches us a lot about which variables are well determined in a well test, and which are not. For example, permeability can be found with a very high degree of confidence from a test that contains a long period of infinite acting radial flow (semilog straight line), but the double porosity parameters ω and λ are always much more indefinite, even when matching using pressure derivative (which is more sensitive to ω and λ than pressure itself).

In summary, confidence intervals are a powerful tool that provide interpretation information that is not available in traditional graphical well test analysis. To be able to discover the degree of significance of the answer is one of the primary advantages of computer-aided well test interpretation.

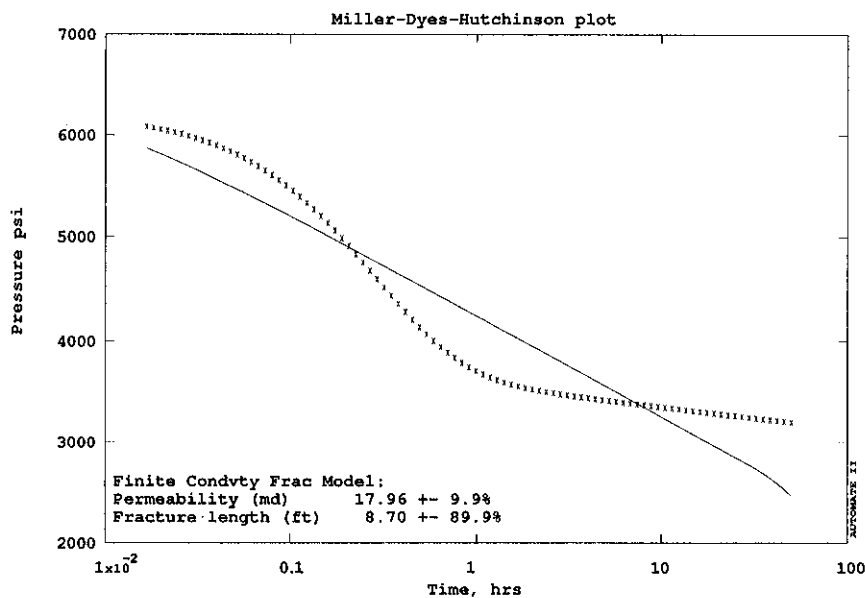


Figure 3.20

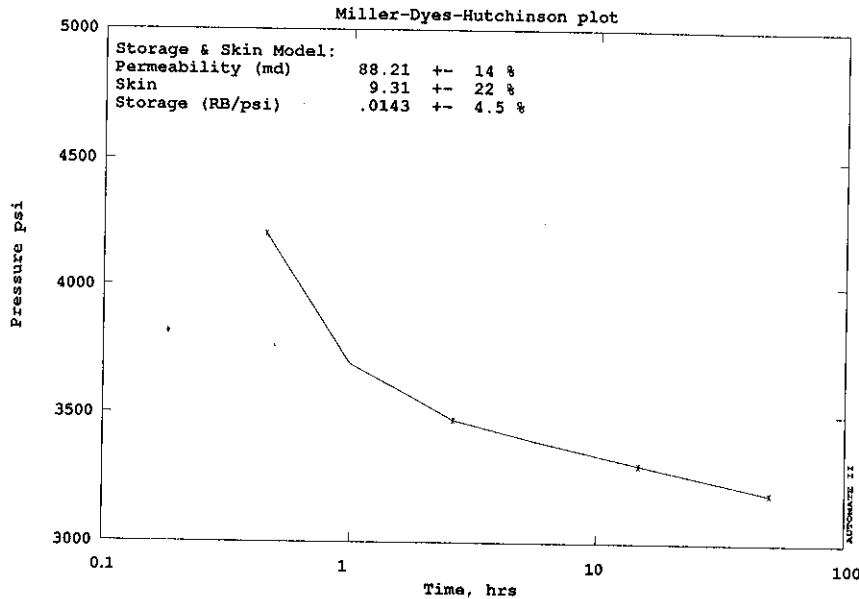


Figure 3.21

3.5.2 Initial Pressure

Due to the need to represent a complex reservoir model in a two-dimensional graphical form, traditional interpretation methods usually restrict the number of parameters that can be estimated, and fix the remainder. In particular, most type curves are based on representations of pressure drop rather than pressure itself:

$$\Delta p = p_i - p = \frac{141.2qB\mu}{kh} p_D(t_D) \quad (3.7)$$

Hence, the need to present a single graph of $p_D(t_D)$ to allow graphical analysis requires that we know the initial reservoir pressure, p_i , in advance. *This is an arbitrary requirement forced by the restrictions of graphical interpretation.* Nonlinear regression is not limited in this way, and is able to match pressure directly by treating the initial reservoir pressure p_i as an unknown variable. By treating p_i as an unknown, a nonlinear regression technique is able to make an estimate of the initial reservoir pressure that is consistent with the entire range of the data. By contrast, graphical type curve methods force an assumption of the value of the initial reservoir pressure based, for example, on the early time measurements -- as mentioned earlier such data may be in error, or may not represent an initial stable state in the reservoir. These assumptions in the graphical approach reduce the precision of estimates of initial pressure, and may also adversely affect the other reservoir parameter estimates.

Since computer-aided interpretation often uses standard graphical presentations for preliminary diagnosis and model selection, it is common to include standard approximations for the initial pressure (such as pressure just prior to opening for a drawdown test, or just prior to shut-in for a buildup test). These should normally be used for the graphical presentations only, and except in rare instances, it is almost always desirable to *release* the assumption of initial pressure during nonlinear regression. Initial

pressure is often a parameter that is usefully learned in a well test.

3.5.3 Multirate and Variable Rate Tests

In the same way that graphical analysis techniques require prior knowledge or assumption about the initial pressure value, they are similarly restricted to constant rate tests. Other than the practical necessity of maintaining a flow rate that can be registered, this limitation to constant rate is another restriction imposed by the necessities of the graphical techniques themselves. The entire concept of wellbore storage is required only to accommodate the fact that the sandface flow rate is not constant during the early part of the test. Estimating the wellbore storage coefficient has no inherent value of its own, and if the actual sandface flow rate could be measured and used in the analysis, then there would be no need to introduce wellbore storage into the problem at all. Modern downhole instruments have made reliable flow rate measurement a reality, and nonlinear regression provides a method of interpreting such information without imposing the constant rate restriction required for most graphical techniques. The same approach can also be used to include the effects of a series of different (constant) flow rates prior to or during the well test (Fig. 3.22). Such a "multirate" test would not require the use of a downhole flow meter, but the wellbore storage effect would always need to be included if such downhole data were not available. The pressure change during such a multirate test with nq different rates can be represented by superposition in time:

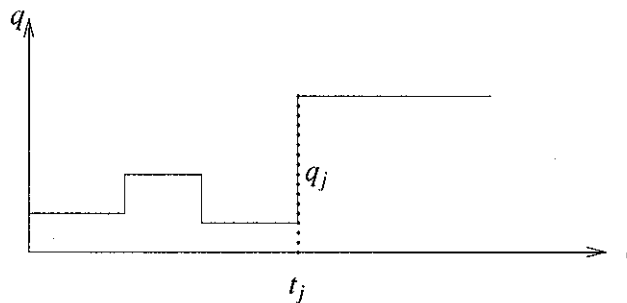


Figure 3.22

$$p(t) = p_i - \frac{141.2B\mu}{kh} \sum_{j=1}^{nq} (q_j - q_{j-1}) p_D(t_D - t_{Dj}), \quad t > t_j \quad (3.8)$$

where t_j is the time at which flow step q_j started. Continuously varying flow rate data can be used in exactly the same manner, treating each measured data point as a small "stairstep" of constant rate.

Nonlinear regression can accommodate such varying rate data just as easily as a constant rate test (although calculating the summation may take longer). In fact, incorporation of variable rate includes more information about the reservoir. Why is this so? Every measured pressure point contains *early time* reservoir response from the most recent flow rate change and *later time* response from earlier flow rate changes. Thus the reservoir pressure signal contains more indicators of early time behavior and late time behavior than a test conducted at constant rate (which has only one early time response and one late time response). Consider the example of a buildup test shown in Fig. 3.23 in which the well was shut in briefly to position the pressure bomb prior to the final closure.

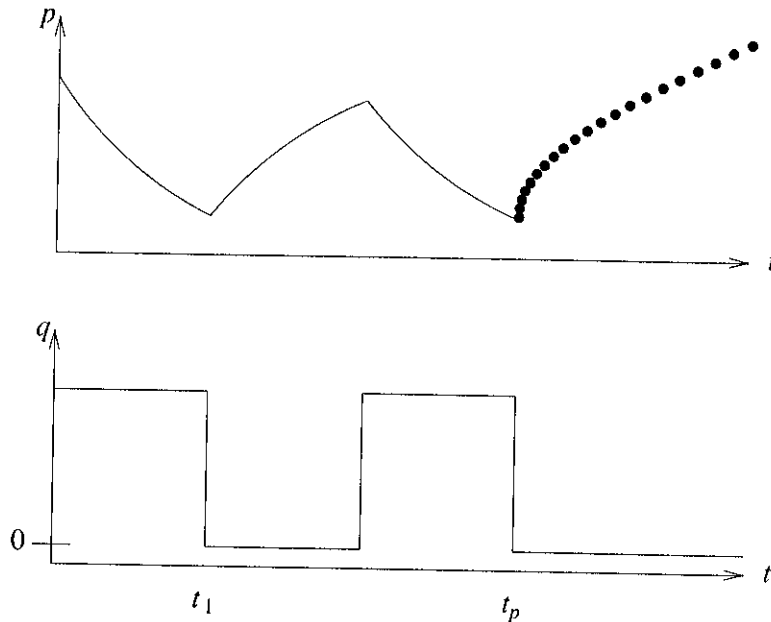


Figure 3.23

Traditional analysis would probably assume the pressure to be stabilized prior to the final shut-in, and would ignore the short closure. However, inclusion of the actual flow rate history is not only more accurate, it includes acknowledgement of the pressure response due to the earlier closure. Thus instead of the effective time of the test being Δt , it can in fact be considered to be $\Delta t + (t_p - t_1)$, even though pressure measurements did not start until time t_p . The effective length of the test is therefore longer than the actual measurement time that would have been analyzed (imprecisely) by traditional graphical techniques.

Consider a second example in which the flow rate was measured downhole in a gas well during shut-in (Fig. 3.24). Fig. 3.24 shows the real data which was presented by Guillot and Horne (1986). Due to wellbore storage effects, the sandface flow rate did not reach zero until about 20 minutes after the wellhead valve closed. At this time (20 min.) the reservoir was flowing at such a low rate that the flow rate tool (spinner) stopped rotating and indicated zero flow. Using nonlinear regression, together with the downhole flow rate data, it is possible to estimate the reservoir properties from only this 20 minutes of data, even though wellbore storage dominated this entire period (and later).

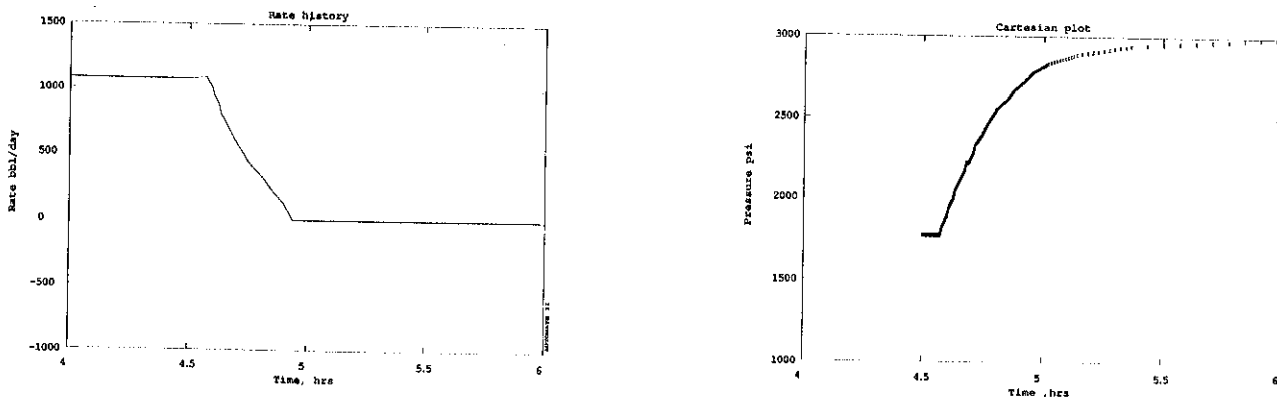


Figure 3.24

This is a particularly significant true life example in that it demonstrates how the use of downhole flow rate measurements and nonlinear regression made it possible to analyze 20 minutes of data in a test that would need to run for 8 hours to be interpretable by traditional techniques. Furthermore, using the same technique in a gas well test (Horne and Kuchuk, 1988), rate-dependent skin effect and absolute open flow potential (*AOF*) were estimated from a buildup test, even though traditional methodology requires a complex and time consuming isochronal test to determine these parameters. It is possible to estimate the rate-dependent skin effect since the reservoir is actually flowing into the wellbore throughout the afterflow (storage dominated) period. Having estimated the rate-dependent skin, it is straightforward to draw a deliverability diagram using the measured rate data and to extrapolate to determine the *AOF*.

Finally it should be noted that the use of simultaneous downhole pressure and flowrate measurements is unaffected by any complex wellbore phenomena such as changing wellbore storage or phase segregation ("humping effects"). As flow rate tools become more highly developed for use in multiphase environments, these techniques should become widely used.

3.6 Desuperposition

Despite the obvious advantages of variable rate analysis illustrated in the previous section, an obvious difficulty is that it is no longer possible to perform diagnosis by examining standard plots, since the familiar characteristics may not appear. For the purposes of diagnosis, a process of desuperposition is used to calculate the way the pressure response would have looked, had the flow rate been constant. Techniques of desuperposition require mathematical techniques that will not be described in detail here, but include constrained optimization (Kuchuk and Ayestaran, 1983) and Laplace transform techniques (Roumboutsos and Stewart, 1988). Mendes, Tygel and Correa (1989) provide a summary of approaches. Fig. 3.25 illustrates the extraction of a constant rate response from variable rate data.

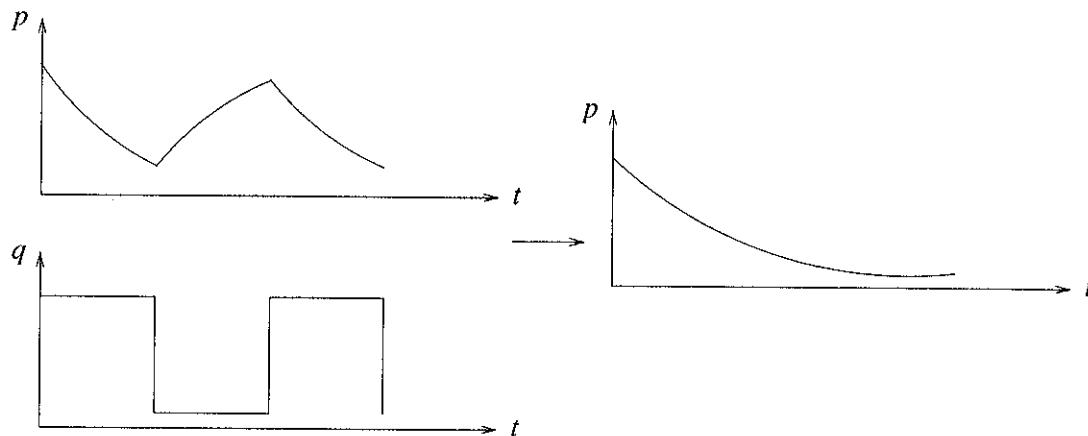


Figure 3.25

3.7 Interpretation Sequence

Having introduced the aspects of computer-aided interpretation separately, we can summarize the steps required in a typical test. These steps are illustrated pictorially in Fig. 3.26.

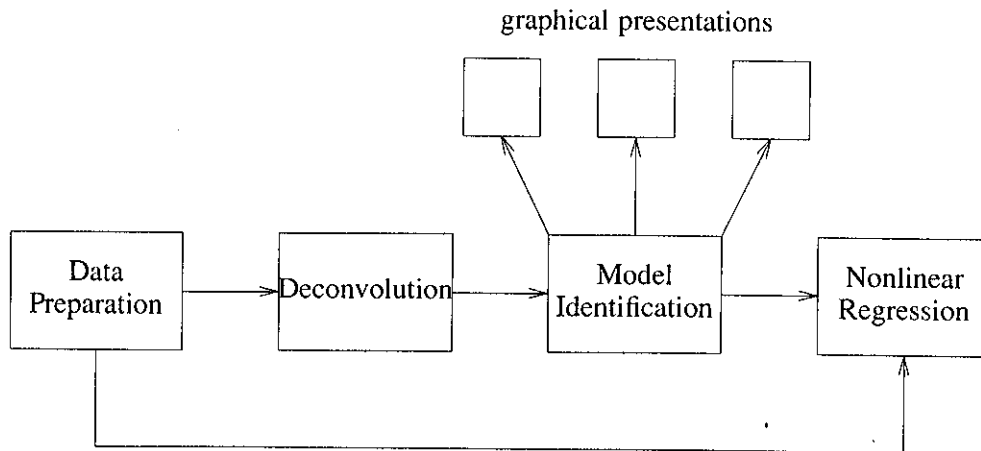


Figure 3.26

- (a) Data Preparation: Pressure and flow rate data are sampled to reduce their number, and datum shifted to correct early time inaccuracies (Section 3.4)
- (b) Deconvolution: The equivalent constant rate test response is extracted as an aid to diagnosis (Section 3.6)
- (c) Diagnosis and Model Identification: An appropriate reservoir model (or a number of possible candidates) is selected based upon identifiable characteristics (Section 3.3). A preliminary estimate of reservoir parameter values may be made to initiate nonlinear regression.
- (d) Nonlinear Regression: A best fit to the chosen model is obtained, and confidence intervals estimated (Section 3.5). Note that it is the original data which are used for nonlinear regression, not the deconvoluted data (which has had the useful flow rate information extracted from it).

It is worth noting that the overall procedure is general, since it is the same for all kinds of test: drawdown, buildup, injection, falloff, multirate and drillstem test (DST). The fact that nonlinear regression works as well with multirate tests as it does with constant rate tests avoids many of the specialized analyses made necessary by the restrictions required by traditional graphical techniques. Computer-aided interpretation is not only faster, more accurate and more widely applicable, it is also a good deal simpler.

3.8 Non-Ideality

The diffusive nature of pressure transmission in porous media means that small scale effects are hidden, and broad scale averaged properties most strongly influence a pressure transient response. Therefore a surprisingly large percentage of actual well tests really do respond in the manner suggested by the reservoir models (perhaps 70 to 80%). Nonetheless, there are physical and mechanical difficulties that can cause the pressure response to differ from that predicted by any reservoir model. These excursions can be due to gauge failure, wellbore transients (such as phase redistribution), unregistered flow changes, neglected reservoir mechanisms (such as segregated flow), human error during recording, etc. In some cases these non-idealities can lead to a response that is atypical in its entirety but in other cases there may be parts of the response that appear normal, and other parts that are strange (Fig. 3.27).

Such regions of abnormal response are of lesser importance in traditional graphical methods, which use only specific portions of the data. However, nonlinear regression techniques, which match the whole

data set, are sometimes adversely affected. In attempting to honor the abnormal data, a regression may be forced to misfit the normal part of the data (Fig. 3.28).

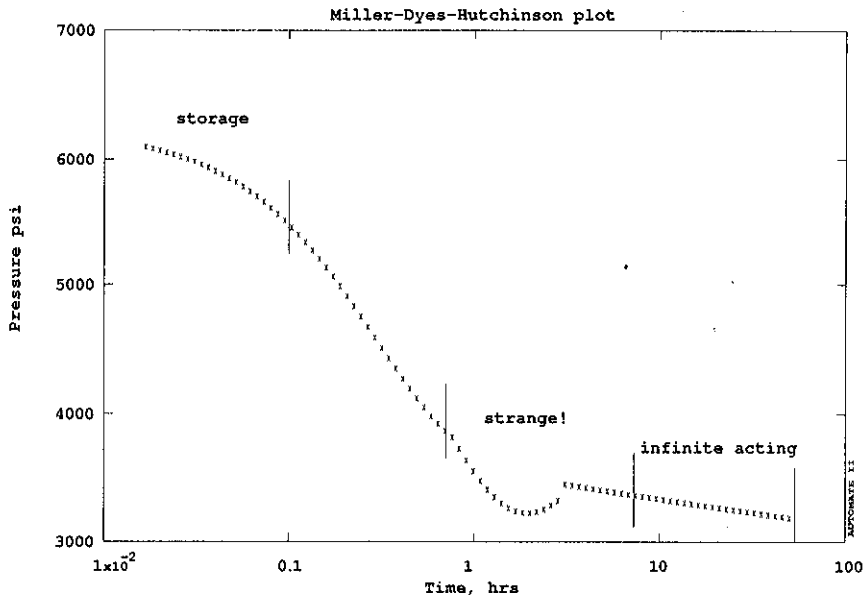


Figure 3.27

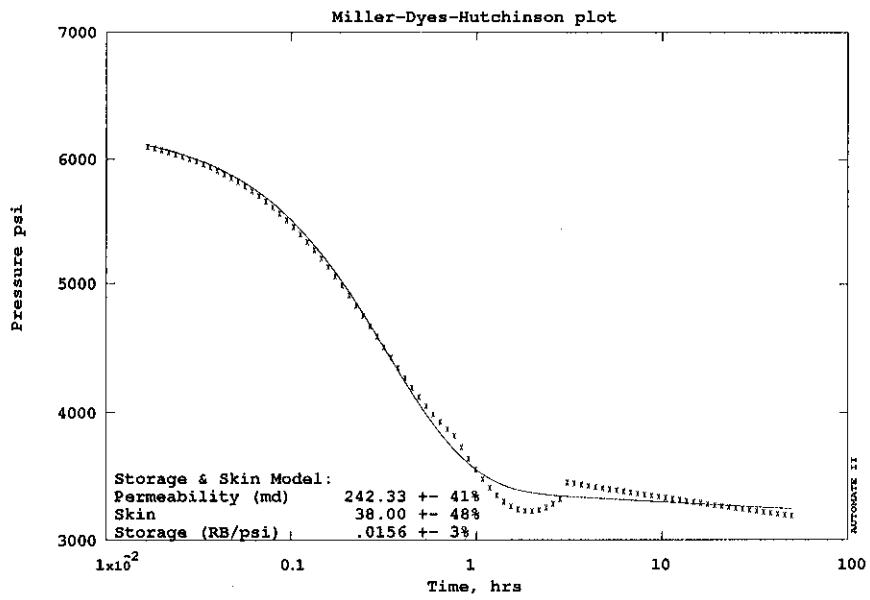


Figure 3.28

This may give rise to invalid estimates. In such cases it is important to recognize and *remove* the abnormal parts of the data, after which an automated analysis can determine those parameters for which it has appropriate ranges of data (Fig. 3.29).

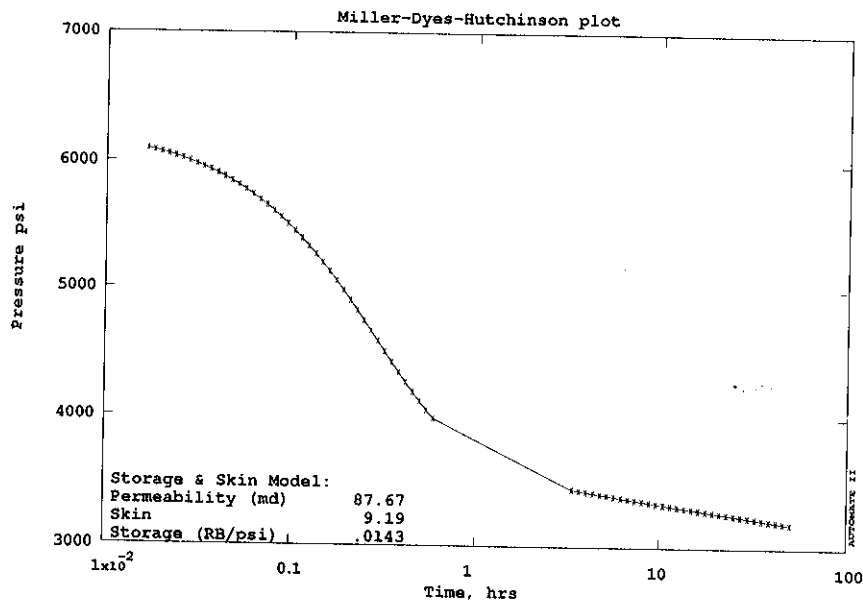


Figure 3.29

In the example illustrated here, the correct reservoir permeability of 87.67 md is only obtained when the abnormal data (probably due to phase redistribution) are removed.

Thus a valid nonlinear regression analysis may require the intervention of the interpretation engineer, and some reparation of the data.

3.9 References

- Bourdet, D., Whittle, T.M., Douglas, A.A., and Pirard, Y-M.: "A New Set of Type Curves Simplifies Well Test Analysis", *World Oil*, (May 1983), 95-106.
- Bourdet, D., Ayoub, J.A., and Pirard, Y-M.: "Use of the Pressure Derivative in Well Test Interpretation", *SPE Formation Evaluation*, (June 1989), 293-302.
- Economides, C.A, Joseph, J.A., Ambrose, R.W. and Norwood, C.: "A Modern Approach to Well Test Interpretation", paper 19814, presented at the 64th SPE Annual Technical Conference and Exhibition, San Antonio, TX, Oct 8-11, (1989), 429-444.
- Gringarten, A.C.: "Computer-Aided Well Test Analysis", paper SPE 14099 presented at the SPE International Meeting on Petroleum Engineering, Beijing, China, March 17-20, (1986).
- Guillot, A., and Horne, R.N.: Using Simultaneous Downhole Rate and Pressure Measurements to Improve Analysis of Well Tests", *SPE Formation Evaluation*, (1986), 217-226.

Horne, R.N., and Kuchuk, F.: "The Use of Simultaneous Flow Rate and Pressure Measurements to Replace Isochronal Gas Well Tests", *SPE Formation Evaluation*, (June 1988), 467-470.

Kuchuk, F., and Ayestaran, L.: "Analysis of Simultaneously Measured Pressure and Sandface Flow Rate in Transient Well Testing" paper 12177, presented at the 58th SPE Annual Technical Conference and Exhibition, San Francisco, CA, Oct 5-8, (1983).

Mendes, L.C.C., Tygel, M., and Correa, A.C.F.: "A Deconvolution Algorithm for Analysis of Variable Rate Well Test Pressure Data", paper 19815, presented at the 64th SPE Annual Technical Conference and Exhibition, San Antonio, TX, Oct 8-11, (1989), 445-459.

Roumboutsos, A., and Stewart, G.: "A Direct Deconvolution or Convolution Algorithm for Well Test Analysis", paper 18157, presented at the 63rd SPE Annual Technical Conference and Exhibition, Houston, TX, Oct 2-5, (1988).

4. INTERPRETATION EXAMPLES -- HOMOGENEOUS RESERVOIRS

This section illustrates the methodology of a well test interpretation by example, considering simple drawdown and buildup tests in homogeneous reservoirs. This kind of response is the most straightforward and "standard" behavior -- however, it is not of purely academic interest, since many real well tests do behave in this manner. More complex examples will be considered in later sections.

4.1 Drawdown Example

In this well test, a well was originally stable and shut in, within a reservoir at equilibrium. The well was then opened to flow at a constant rate, and the pressure drawdown monitored as a function of time. This is the kind of situation that would be seen in the initial production of a discovery in an otherwise unexploited field (although the data in this example have been generated artificially to demonstrate particular points).

The known reservoir data and the measured test data are listed in Table 4.1 of the Appendix.

4.1.1 Traditional Graphical Analysis

In a traditional graphical interpretation of a well test (in a simple, homogeneous reservoir) the following steps are commonly used:

- (a) Identify the various flow periods by looking at the data on derivative, and semilog plots.
- (b) Estimate individual reservoir parameters from the log-log and semilog plots.
- (c) Perform a type curve match to the log-log derivative type curve, and again estimate the reservoir parameters, checking for consistency with the prior estimates.

These same steps are likely to be taken as the preliminary stage of a computer-aided interpretation, as a means of evaluating the data, choosing a reservoir model and making a first estimate of the reservoir parameters.

4.1.1.1 Identifying Flow Periods

To begin with the first step, the data are displayed in a log-log presentation of the derivative ($t \cdot \partial p / \partial t$) and pressure (Fig. 4.1).

In the first log cycle, there is a clear indication of wellbore storage effect (unit slope). In the third log cycle, the derivative flattens out, indicative of infinite acting radial flow. The second log cycle, which lies between the two, is a transition period -- the "hump" in the pressure derivative is a feature that almost always comes at the end of a storage response. There are no other reservoir responses indicated -- no boundary effects after the infinite acting period, and no double porosity effects.

Before accepting the suggested interpretation model (storage followed by infinite acting radial flow), it is essential to make a consistency check. If the flattening region or the derivative is truly indicative of the current semilog straight line, then it should begin one and a half log cycles after the end of the unit slope period of the storage response. A check of Fig. 4.1 confirms that this is so. Hence we accept the preliminary evaluation of the reservoir model, and note for future use that the unit slope storage response ends at about 0.1 hours and the correct semilog straight line (infinite acting radial flow) begins at

about 2 hours. This attention to recognizing the start of the infinite acting period is important, since finding the correct semilog straight line is critical to achieving valid estimates of permeability, skin and reservoir pressure.

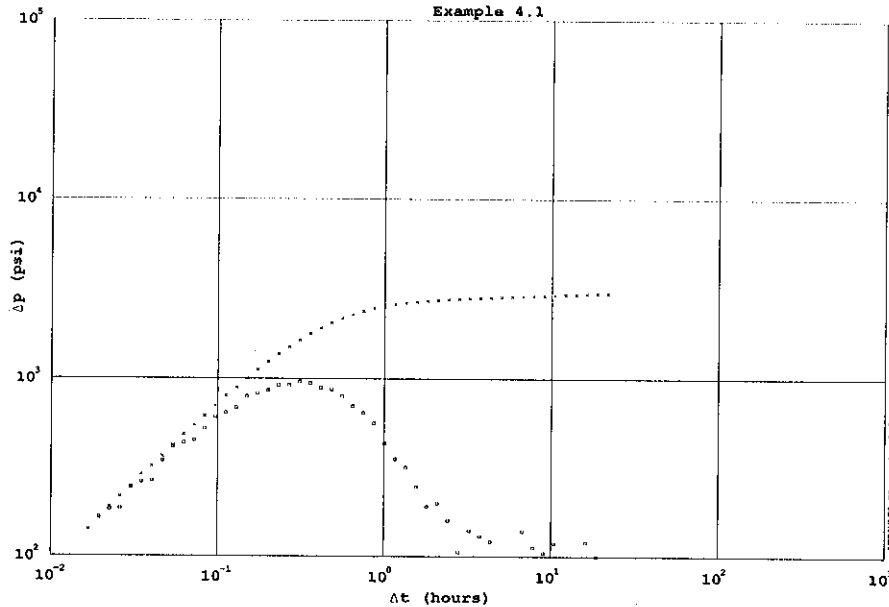


Figure 4.1

4.1.1.2 Estimating Parameters

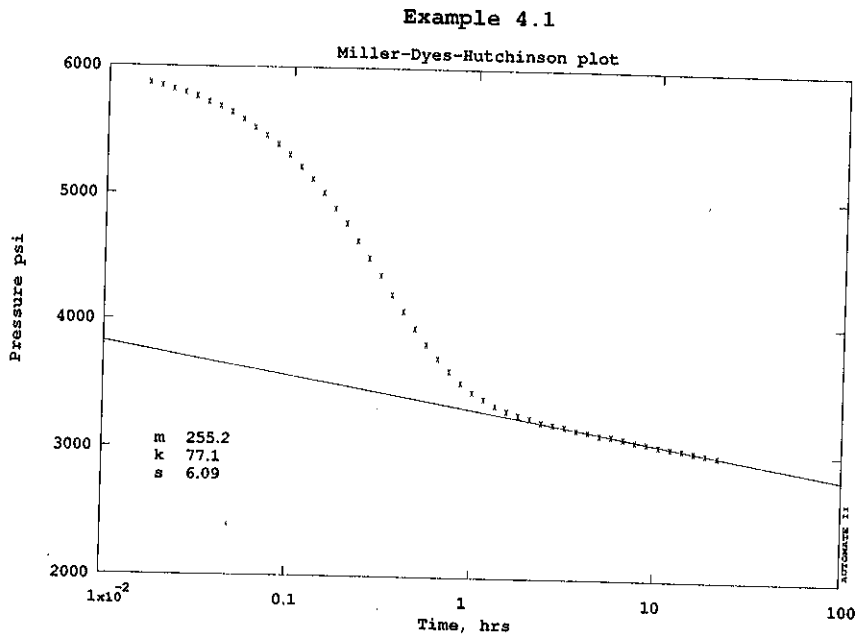
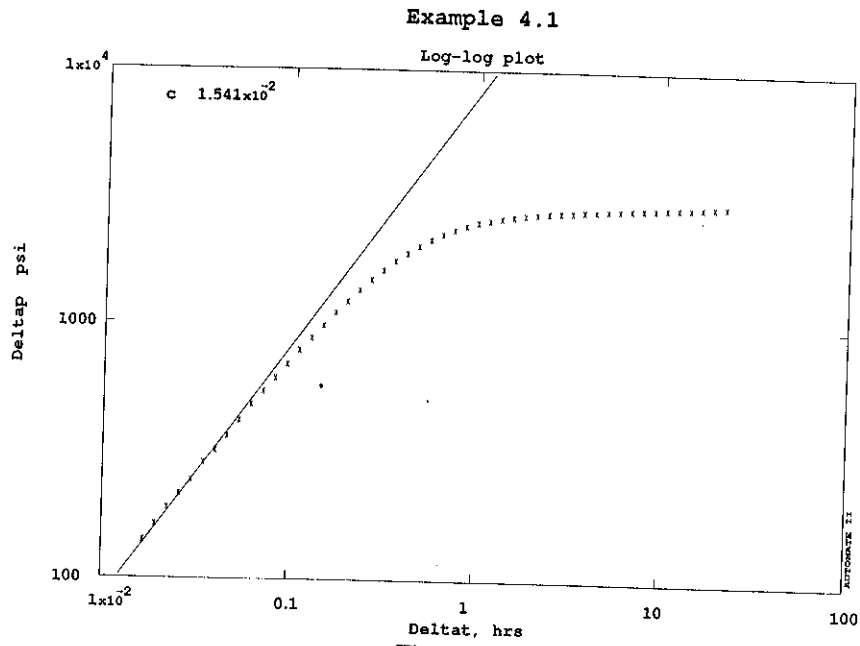
Moving on to the second step, the reservoir parameters are estimated. It is convenient to estimate the wellbore storage first, since this will serve again as a more precise indication of the time that wellbore storage ends. Fig. 4.2 shows the log-log plot of pressure drop ($p_i - p_{wf}(t)$ in this case) against production time with a unit slope line drawn through the early data.

From the equation of the unit slope straight line

$$(p_i - p) = \frac{0.234}{5.615} \frac{qB}{C} t \tag{4.1}$$

the storage coefficient C can be estimated from any point on the line. The estimated value of storage coefficient, C , is 0.0154 STB/psi. In Fig. 4.2 it appears that the data begin to move away from the unit slope line rather sooner than 0.1 hours. This emphasizes the fact that data in this storage period are measured only over a five minute time frame, and therefore, as discussed earlier, will be sensitive to time datum errors in the measured pressure data. This will be discussed later. Notice also that the appearance of the data is governed by the numerical value of initial reservoir pressure p_i . For this drawdown test, the value of p_i is the pressure measured downhole just before the well was opened to flow.

Moving on to the semilog graph of pressure $p_{wf}(t)$ against time (Fig. 4.3), a semilog straight line portion of data (starting at about 2 hours as expected) can be seen.



The slope of this line, m , allows us to estimate permeability, k , using the equation

$$m = -162.6 \frac{qB\mu}{kh} \tag{4.2}$$

$$kh = 162.6 \frac{qB\mu}{|m|} \quad (4.3)$$

and making use of prior estimates of thickness h . Thus

$$kh = 162.6 \frac{(2500)(1.21)(0.92)}{255.2} = 1773 \text{ md-ft}$$

$$k = 77.1 \text{ md (since } h = 23 \text{ ft)}$$

The skin factor, s , can be estimated from the intercept of the line

$$s = 1.151 \left[\frac{p_i - p_{1hr}}{|m|} - \log \frac{k}{\phi\mu c_t r_w^2} + 3.2274 \right] \quad (4.4)$$

taking careful note of the fact that the point p_{1hr} is a point on the semilog straight line and may not be a point in the data itself (in Fig. 4.3 the actual data point at time one hour [3465 psi] lies above the point on the semilog straight line used to determine the skin factor [3330 psi]). Thus the skin factor is estimated to be

$$s = 1.151 \left[\frac{6009 - 3330}{255.2} - \log \frac{77.1}{(0.21)(0.92)(8.72 \times 10^{-6})(0.41)^2} + 3.2274 \right] = 6.09$$

As a final consistency check, recall from Eq. (2.33) that the true reservoir response does not begin until a dimensionless time

$$t_D = C_D(60 + 3.5s) \quad (4.5)$$

In this case, C_D is 2033, so the value of t_D at which reservoir response begins is 1.653×10^5 or a real time of

$$t = t_D \frac{\phi\mu c_t r_w^2}{0.000264k} = 1.653 \times 10^5 \frac{(0.21)(0.92)(8.72 \times 10^{-6})(0.41)^2}{0.000264(77.1)} = 2.3 \text{ hrs}$$

This is more or less the time at which the data reach the semilog straight line on Fig. 4.3. Thus we have high confidence that we have correctly identified the semilog straight line.

At this point, we have used all of the identifiable periods (i.e., storage period, infinite acting period), and thus there are no further parameters than can be estimated. It is noted that the data lying in the transition period (the $1\frac{1}{2}$ log cycles from 0.1 hours to 2 hours) have not been used in any quantitative way. One of the advantages of a type curve match is that it matches the entire data set to the reservoir model, including the transition data as well.

4.1.1.3 Type Curve Match

Even though the reservoir parameters have already been estimated, there are several advantages in performing a type curve match. Whereas the semilog method and unit slope log-log line used only portions of the data, a type curve match uses the entire data set. This helps ensure consistency over the whole range of time, and also provides a mechanism to make use of the transition data which lies between the individual response periods.

In a log-log type curve, it is known that the p_D versus t_D curves (the reservoir model) will have exactly the same shape as the p_{wf} versus t data (the measurements during the well test). Thus the data are plotted on transparent three inch by three inch log-log graph paper (as in Fig. 4.1), to the same scale as the three inch log cycle type curve. The data are then laid over the type curves, and moved horizontally and vertically (keeping the axes parallel) until a match is achieved, as in Fig. 4.4.

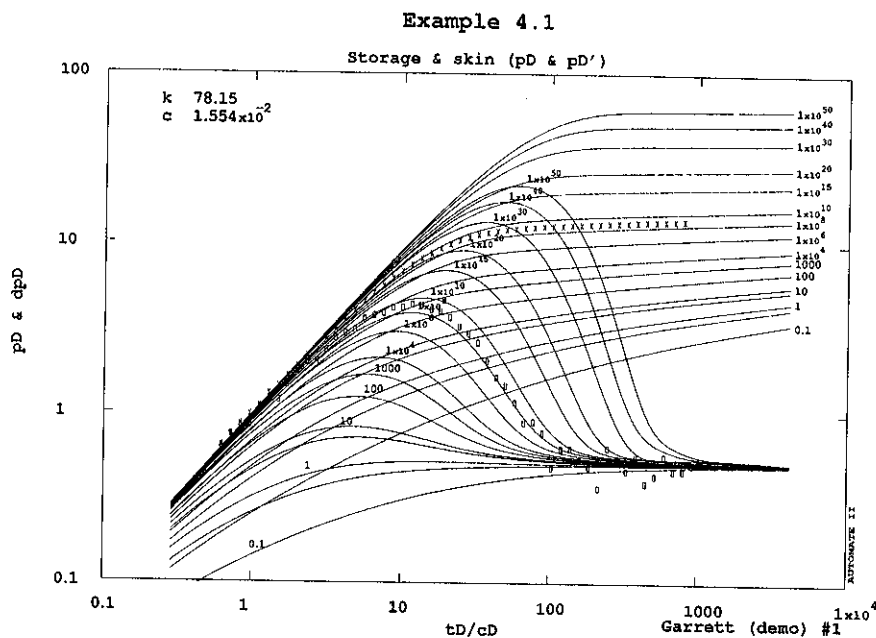


Figure 4.4

At the point of matching correspondence between p_D and Δp and between t_D and t has been achieved and the reservoir parameters can be estimated as described in Section 2.3. From Fig. 4.4 it is also possible to estimate skin factor s , by noting which of the various curves gives the best match, and reading the value of $C_D e^{2s}$ appropriate to that curve.

Looking at Fig. 4.4, we can choose any point to represent the correspondence between dimensional and dimensionless properties. For example, choosing the last data point at $t = 21.6$ hrs, $p_i - p_{wf} = 6009 - 2988.93 = 3020.07$ psi, we can read the corresponding values on the dimensionless axes to be $t_D/C_D = 800$ and $p_D = 13.67$.

Using the pressure match:

Recalling Eq. 2.3

$$p_D = \frac{kh}{141.2 qB\mu} (p_i - p_{wf}) \quad (4.6)$$

$$13.67 = \frac{k(23)}{141.2(2500)(1.21)(0.92)} (6009 - 2988.93)$$

$$k = 78.15 \text{ md}$$

Using the time match:

Recalling Eq. 2.4

$$t_D = \frac{0.000264 k t}{\phi\mu c_t r_w^2} \quad (4.7)$$

$$800 C_D = \frac{0.000264(78.15)(21.6)}{(0.21)(0.92)(8.72 \times 10^{-6})(0.41)^2}$$

$$\text{Hence, } C_D = 1960$$

Recalling Eq. 2.16

$$C_D = \frac{5.615 C}{2\pi\phi c_t h r_w^2} \quad (4.8)$$

$$C = 1960 \frac{2\pi(0.21)(8.72 \times 10^{-6})(23)(0.41)^2}{5.615}$$

$$\text{Hence, } C = 0.01554 \text{ STB/psi.}$$

We can also see that the best curve matched is at a value of $C_D e^{2s}$ around 5×10^8 , thus we can estimate skin factor s to be

$$C_D e^{2s} = 5 \times 10^8$$

$$e^{2s} = (5 \times 10^8) / 1960$$

$$\text{Hence, } s = 6.22$$

4.1.1.4 Comparison of Graphical Estimates

Table 4.1 compares the estimates of the parameters from the "slope matching" methods and from the type curve matching procedures.

Parameter	Slope matching	Type Curve
k (md)	77.1	78.15
s	6.09	6.22
C (STB/psi)	0.0154	0.0155

Table 4.1

In this case the estimates are extremely close, and therefore we gain confidence in our interpretation since we have demonstrated consistency between the semilog and log-log methods. Actually in this example the consistency is considerable better than would ever be possible with pencil and paper graphical methods, since the estimation here actually used computer-aided graph plotting and slope finding algorithms. It is a rather simple task for a computer to place the type curve match in exactly the location set by the slope fitting methods -- the human interpreter need only make a decision as to whether the match is good or not.

Log-log type curve matching is not as precise as semilog methods, since the log-log axes tend to hide inaccuracies at late time (large pressure drop). For example, if we calculate the model response using the recent estimates of the parameters, then we can compare this "customized" type curve with the data, as in Fig. 4.5.

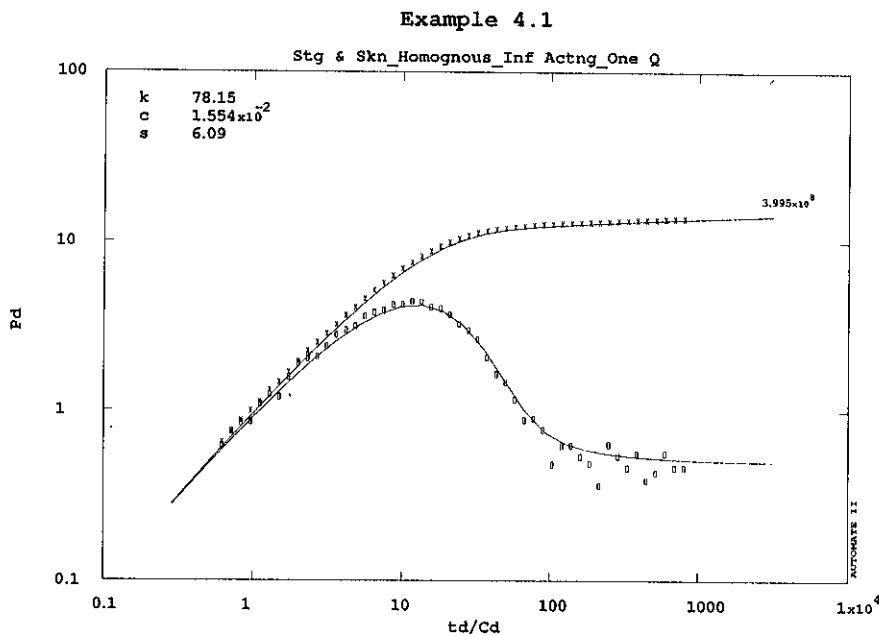


Figure 4.5

This step is sometimes referred to as simulation (not to be confused with numerical reservoir simulation) in that we have *simulated* the way the well test would have looked if our estimates were the correct answer.

Plotting the simulated test (or customized type curve) in log-log coordinates, as in Fig. 4.5, makes the match appear quite good. However, it must be remembered that a 1mm deviation of a data point from the (pressure) curve at late time means an actual error of about 200 psi, whereas the same deviation at early time means an actual error of only 5 psi. Thus a visually inspected type curve match in log-log coordinates tends to be imprecise at the place we need greatest definition, that is during the actual reservoir response. Plotting the same simulation in semilog coordinates (Fig. 4.6) shows that it is not such a good match after all, especially in the semilog straight line region.

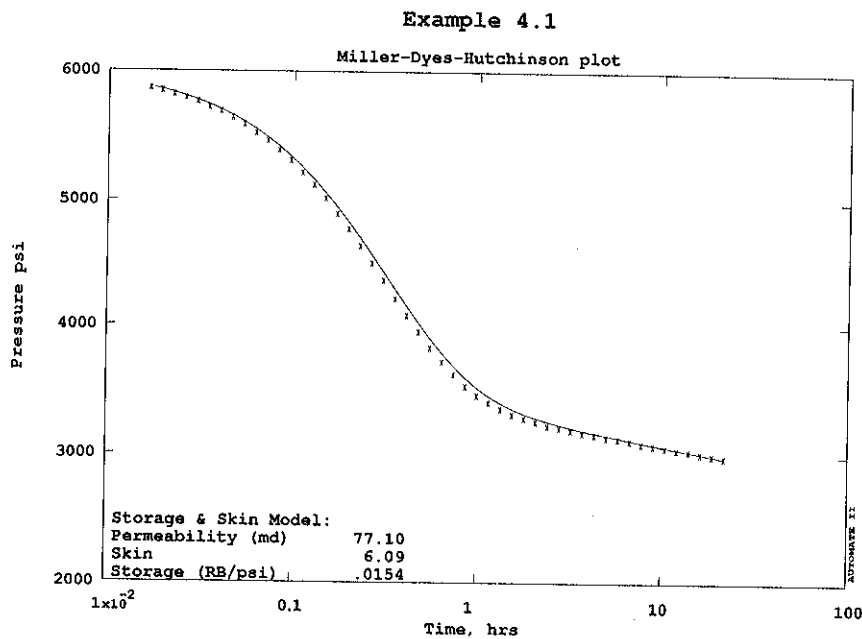


Figure 4.6

4.1.1.5 Time Shift Errors

As was discussed previously in Section 3.4.2, errors in registering the time at which the flow started can affect the early time data considerably. In this particular example, the storage period lasts only until about six minutes into the test, so a time error of only one minute can change the appearance of the log-log graph and hence the estimate of the wellbore storage coefficient. Fig. 4.7 shows the appearance of the data if time zero is shifted one minute earlier and Fig. 4.8 shows the appearance if it is shifted one minute later.

The unit slope straight line drawn in Figs. 4.7 and 4.8 is in the same location as that estimated for the original (correct) data, showing clearly how difficult it would be to correctly identify this line if the time datum was only one minute in error.

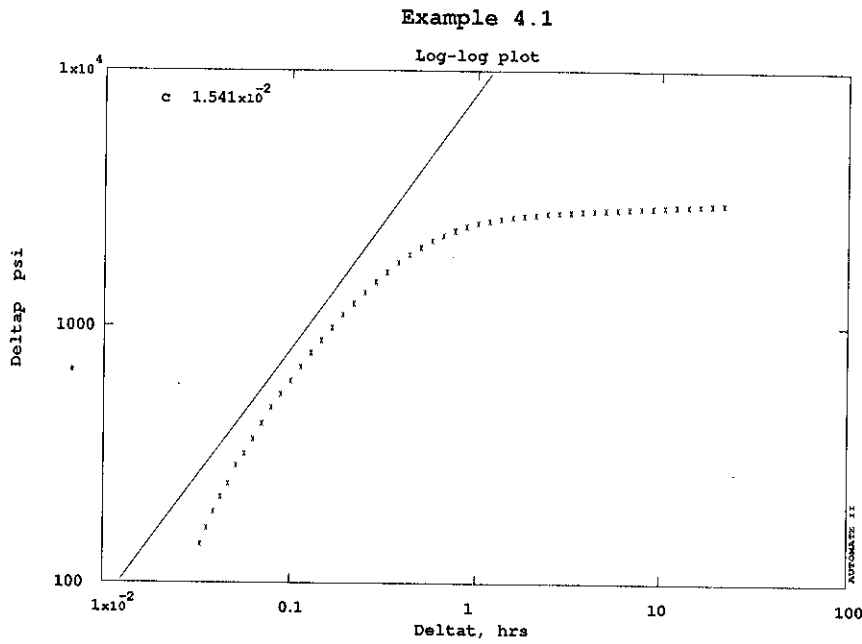


Figure 4.7

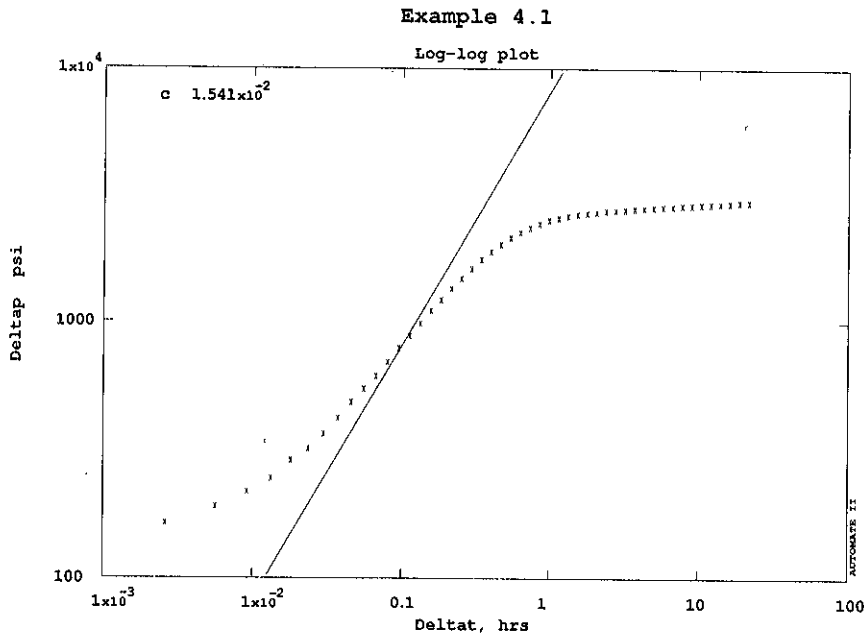


Figure 4.8

Luckily, the potential difficulty of time shift error (or pressure shift error, which has a similar effect) is overcome rather easily. Instead of insisting on that critical first data point ($t = 0, p = p_i$ in this example) we can ignore the measured value and calculate pressure p at time $t = 0$ by extrapolating back the

subsequent data points. Removing this one single data point makes the data appear much more conventional on the log-log plot, Fig. 4.9, even though the slightly incorrect data is still being used.

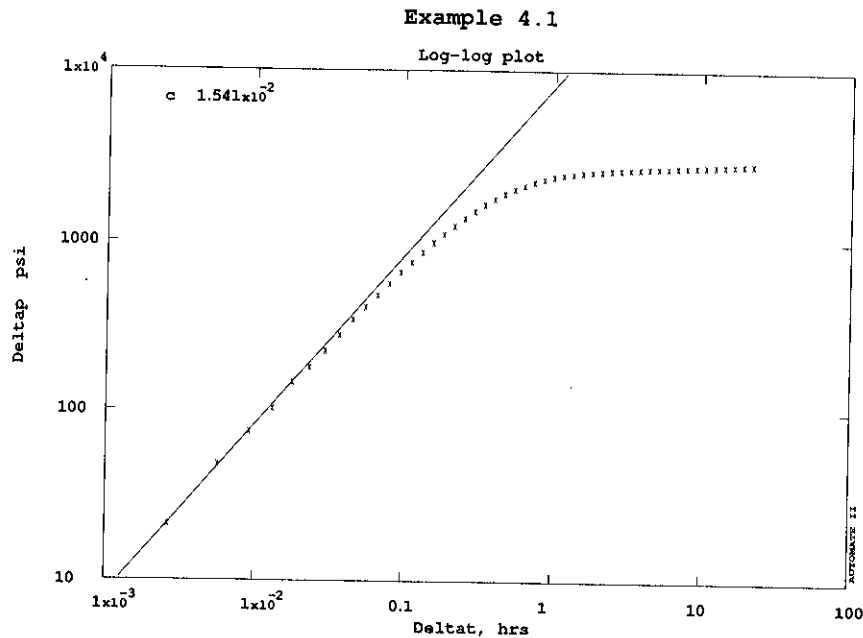


Figure 4.9

4.1.1.6 Confidence Intervals

The estimates obtained by graphical analysis (as listed earlier in Table 4.1) are about as close to the correct answer as a graphical analysis by hand is ever likely to come (since the test data in this example were artificially generated, the correct answer is actually known!). In fact, having used computer-assisted slope finding methods, these may be even better than can be achieved by eye. Nonetheless, using pencil and paper, different engineers will certainly obtain different estimates. Table 4.2 lists twenty different estimates of permeability obtained for this problem by a class of twenty petroleum engineering students. Discarding the highest and lowest values as probable outliers, the remaining estimates have a variation of about $\pm 10\%$.

<i>k</i> estimates				
80.10	81.52	73.43	78.11	82.35
75.07	75.35	70.08	82.76	77.44
74.44	76.93	79.86	75.31	87.86
75.11	76.71	76.14	81.81	74.34

Table 4.2

Thus within this human group, there is an uncertainty of $\pm 10\%$ as to the correct value of permeability. Note also that this is a rather clear example with good data -- with noisier data in a more complex situation the range of estimates will probably be wider. All this means that if a supervisor wanted to be reasonably sure of obtaining the best answer to within 10%, 20 engineers could be ordered to perform

independent interpretations. This of course would be ridiculously expensive, and still the degree of certainty could not be quantified.

Using the computer, we can calculate 95% confidence intervals, as described in Section 3.5.1. The intervals for our best graphical estimates are listed in Table 4.3.

Parameter	Estimate	Confidence Interval (absolute)	Confidence Interval (percent)
Permeability (md)	77.10	± 11.84	± 15.36%
Skin	6.090	± 1.890	± 31.04%
Storage (RB/psi)	.01541	± .5666×10 ⁻³	± 3.68%

Table 4.3

Within the criteria defined in Section 3.5.1 (Table 3.2) the confidence intervals are estimates of permeability, k , and skin factor, s , are beyond acceptable limits. Thus we cannot be sure (to within 95% confidence) that this answer is acceptable.

4.1.2 Nonlinear Regression

Using nonlinear regression, the computer can obtain the best fit match to the data, using the reservoir model that we have now identified (storage and skin, infinite acting reservoir, no boundary effect). The procedure requires a preliminary estimate of the unknown reservoir parameters, so the values obtained previously from the graphical analysis will be used. A (semilog) plot of the final match, Fig. 4.10, shows that a much closer match has been obtained, and Table 4.4 shows that the confidence intervals are now much narrower.

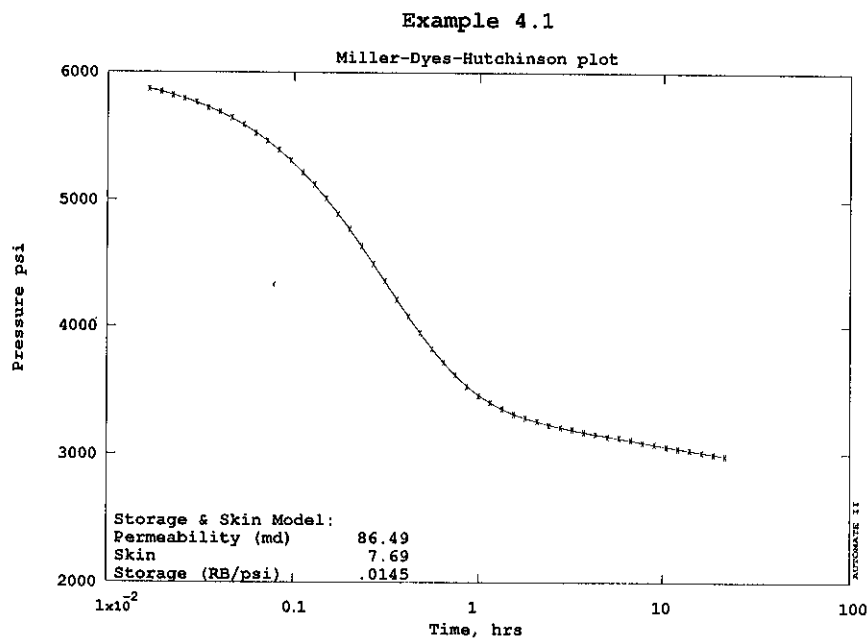


Figure 4.10

Parameter	Estimate	Confidence Interval (absolute)	Confidence Interval (percent)
Permeability (md)	86.49	± 1.046	± 1.21%
Skin	7.690	± .1687	± 2.19%
Storage (RB/psi)	.01453	± .3718 × 10 ⁻⁴	± .26%

Table 4.4

Even though nonlinear regression is sometimes known as automated type curve matching, it is important to recognize that the two are quite different. Nonlinear regression does not depend on log-log curve matching, and will minimize the deviation of the reservoir model from the data by an equivalent amount over all time ranges.

It might reasonably be questioned how nonlinear regression is affected by the time shifting error described in Section 4.1.1.5. Analyzing the data of Fig. 4.8 (which had a one minute time shift) results in a poor match, Fig. 4.11, although the wide confidence intervals, Table 4.5, warn us that the estimated answer is not acceptable.

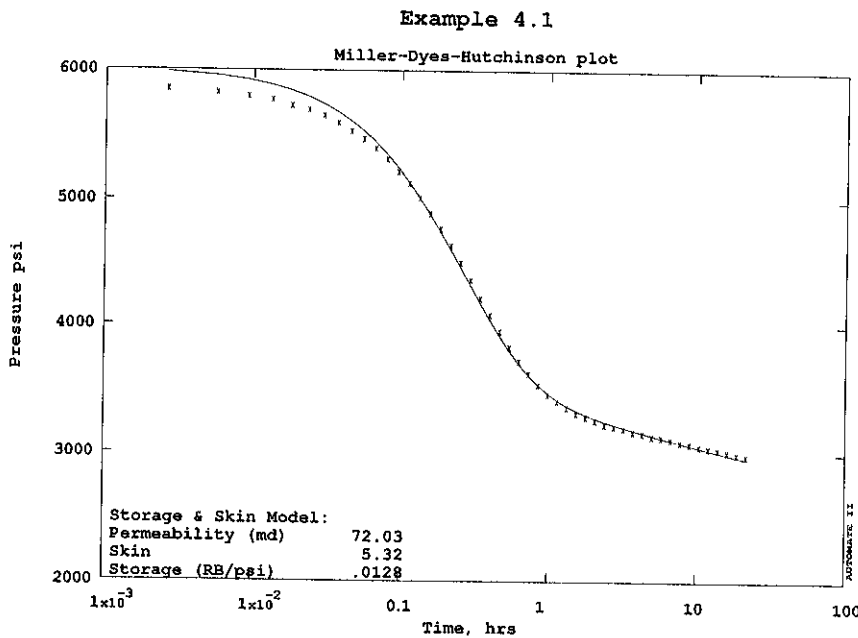


Figure 4.11

Parameter	Estimate	Confidence Interval (absolute)	Confidence Interval (percent)
Permeability (md)	72.03	± 12.16	± 16.88%
Skin	5.317	± 1.936	± 36.41%
Storage (RB/psi)	.01276	± .6173 × 10 ⁻³	± 4.84%

Table 4.5

The solution to this problem is much as it was in the graphical analysis, the first data point is removed, and the nonlinear regression routine is forced to match the initial pressure, p_i , in addition to k , s and C . In this case the answer is almost as before, with acceptable confidence intervals on all

parameters, Table 4.6.

Parameter	Estimate	Confidence Interval (absolute)	Confidence Interval (percent)
Permeability (md)	87.54	± 1.210	± 1.38%
Skin	7.146	± .1824	± 2.55%
Storage (RB/psi)	.01540	± .7084×10 ⁻⁴	± .46%
Init press (psi)	5869.	± 2.480	± .04%

Table 4.6

Although the permeability, k , and skin factor, s , estimates are almost the same as before, the storage coefficient, C , estimate might have been further away (although in this example the estimate of C is the same as before). If a different estimate had been obtained, this would be because it is the early time data that is most in error. Fortunately, C is not a parameter that we are actually interested in finding. The estimate of the initial reservoir pressure, p_i , is 5869 psia, whereas the true measured value was 6009 psia. This difference should serve as a warning as to the degree of accuracy to which p_i can be estimated, and the sensitivity of the estimate to the early time data in a single constant flow rate test. For reference, the extrapolated value of p_i that would be obtained graphically would be 5867 psia - - essentially the same value.

To obtain a more accurate estimate of the reservoir pressure, it is necessary to go back to data preparation, and shift the time values by the small increment required to straighten the unit slope storage line on the log-log graph.

4.1.3 Boundary Effects

In this example data set there is no evidence of any pressure transient caused by boundary effect. As time passes during the test, the pressure transient response at the well will reflect reservoir conditions at greater radius. Recall from Section 2.6.1 that for a closed circular reservoir, the boundary response begins at a dimensionless time t_{DA} of 0.1. Given that no such response was observable in the example data, we can ascertain that t_{DA} at time $t = 21.6$ hours (the last data point measured) must be smaller than 0.1. From this we can determine that the radius of investigation was less than the actual radius of the reservoir.

Putting this into numbers, the *area* of investigation can be determined from

$$t_{DA} = \frac{0.000264 k t}{\phi \mu c_t A} < 0.1 \quad (4.9)$$

$$\frac{0.000264(86.49)(21.6)}{(0.21)(0.92)(8.76 \times 10^{-6}) A} < 0.1$$

$$A > 2.93 \times 10^6 \text{ ft}^2$$

$$r_e > 965 \text{ ft}$$

From this estimate of the radius of investigation, we do not know where the actual reservoir boundaries are, but we have determined that they are at least 965 feet away. We have therefore been able to

place an approximate lower bound on the reservoir size. However it should be emphasized that this radius of investigation is a rather broad estimate of how far the test "sees" into the reservoir --the time at which the well pressure begins to be affected by the boundary may not be the time that the interpreter is able to notice the effect. It is possible that the reservoir could have a boundary closer than 965 feet, but that its influence is not strong enough to be noticeable. In practice, it is expedient to assume that the lower bound on reservoir size is rather smaller than the radius of investigation, perhaps using the value 600 ft in this example.

To estimate a boundary location with more precision, it is necessary to run a longer test. Table 4.7 lists an additional two days of pressure transient data beyond the original 21.6 hours of flow. Examination of the diagnostic plot (Fig. 4.12) reveals that there is an evident boundary effect, probably a pseudosteady state response.

t (hrs)	p (psia)
24.25	2939.3
26.37	2921.5
28.67	2902.3
31.17	2881.4
33.90	2858.7
36.86	2834.0
40.07	2807.2
43.57	2778.0
47.38	2746.2
51.51	2711.7
56.01	2674.2
60.90	2633.4
72	2540.7

Table 4.7

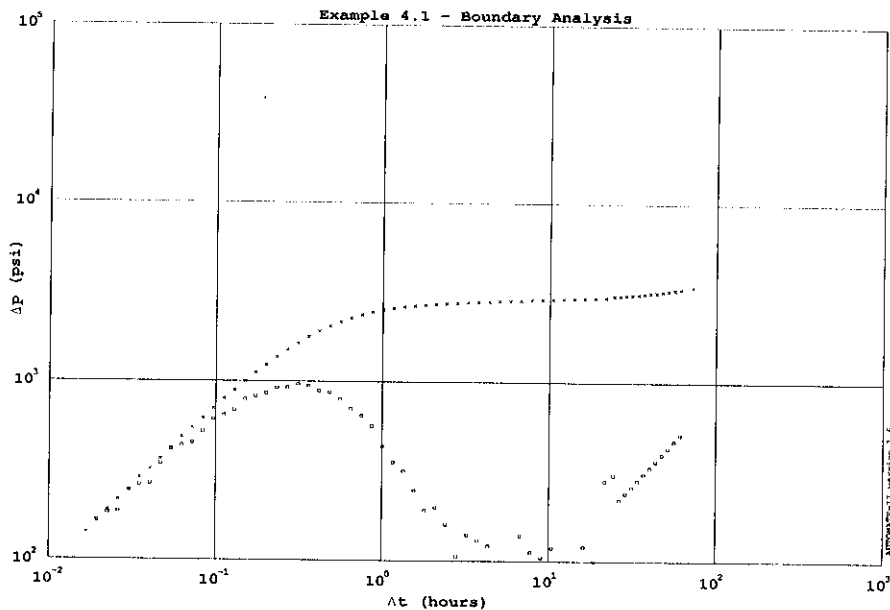


Figure 4.12

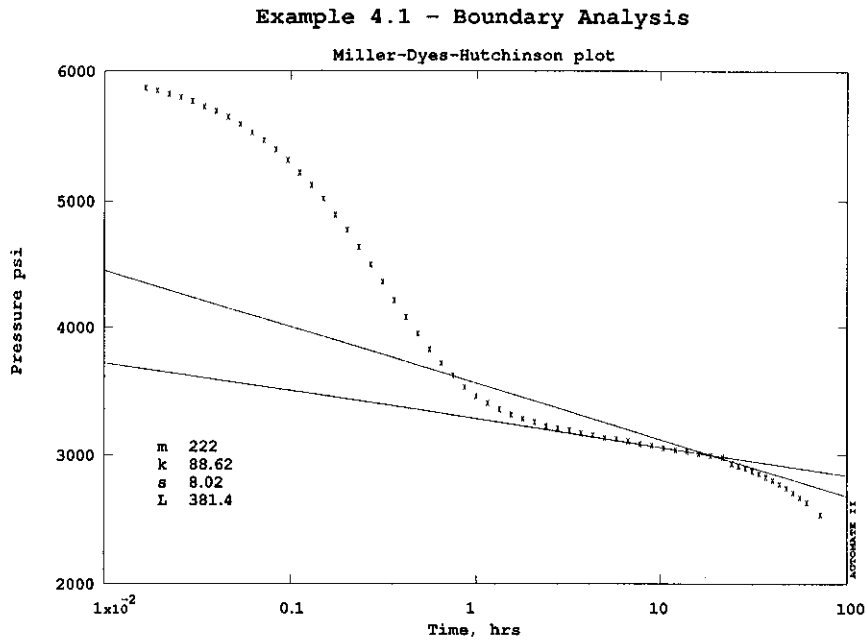


Figure 4.13

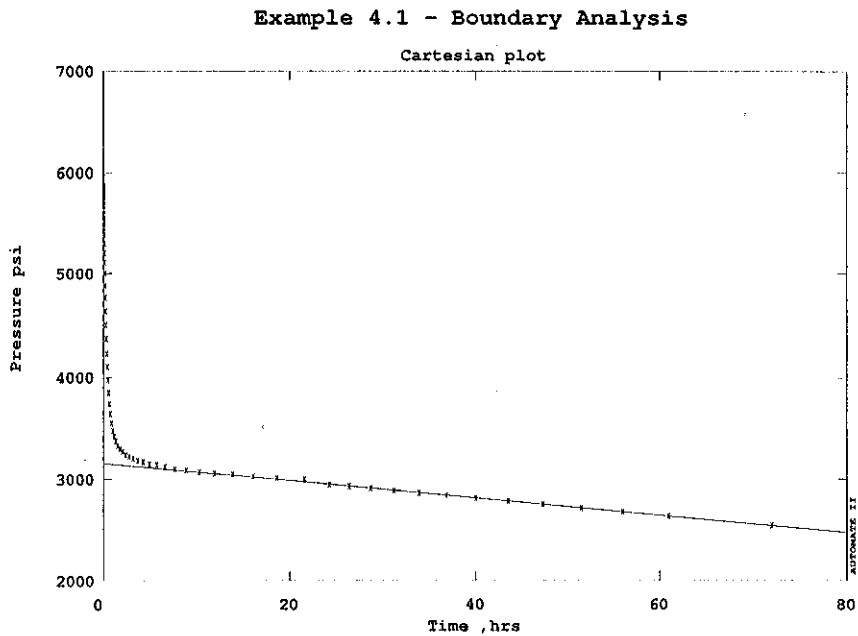


Figure 4.14

Notice that the departure from the earlier behavior is much more noticeable on the derivative plot than on the log-log pressure plot. Looking at the semilog plot (Fig. 4.13), we again see the boundary effect more clearly than on the log-log plot and also that the boundary response does not seem like that of a fault (doubling in slope). Based upon this observation, and on the earlier derivative view, we look at a

Cartesian plot of pressure against time (Fig. 4.14) which does show a straight line behavior characteristic of pseudosteady state.

It is important to note that it is easy to find "straight lines" on a Cartesian plot -- even when none are present. (For example, it is not difficult to imagine a straight line on a Cartesian plot, even with the original 21.6 hours of data). Therefore it is important that the pseudosteady state be clearly identified on the derivative and semilog plots, before it is drawn on the Cartesian plot. After observing the slope of the Cartesian straight line, $m_{Cartesian}$, to be 8.54 psi/hr the area of the reservoir can be estimated using Eq. 2.34:

$$m_{Cartesian} = \frac{0.2342 qB}{(\phi c_i h)A} \quad (4.10)$$

$$A = \frac{0.2342 qB}{\phi c_i h m_{Cartesian}} = \frac{0.2342(2500)(1.21)}{(0.21)(8.72 \times 10^{-6})(23)(8.54)}$$

$$A = 1.9697 \times 10^6 \text{ ft}^2; \quad r_e = 792 \text{ ft}$$

Notice that this is slightly less than the radius of investigation estimated previously (965 ft), emphasizing that it would have been wrong to treat 965ft as a lower bound on reservoir size, since we have now observed from the later data that the boundary response was already starting, except that it was not prominent enough to be noticeable. Checking the estimate in a simulation step (Fig. 4.15) confirms that the r_e estimate of 792 ft is consistent, and nonlinear regression refines the estimate (Fig. 4.16) and demonstrates that the confidence limits are within acceptable bounds (Table 4.8).

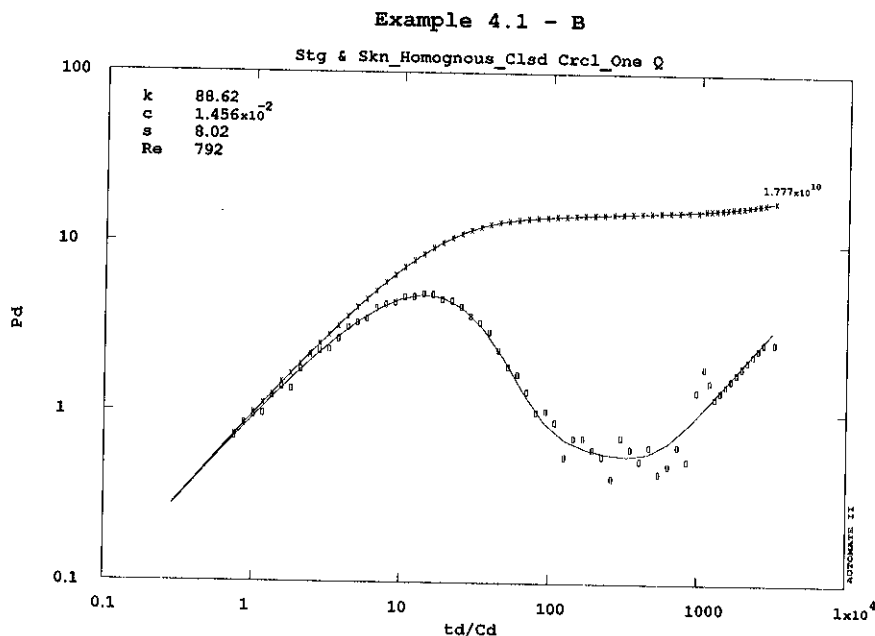
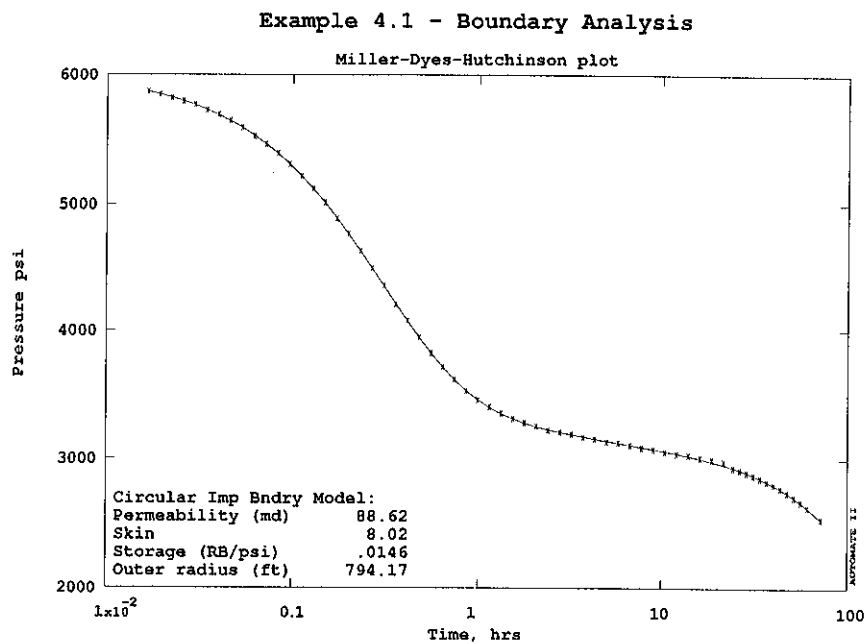


Figure 4.15



Parameter	Estimate	Confidence Interval (absolute)	Confidence Interval (percent)
Permeability (md)	88.62	± 1.759	± 1.98%
Skin	8.020	± .2832	± 3.53%
Storage (RB/psi)	.01456	± .5702×10 ⁻⁴	± .39%
Outer radius (ft)	794.2	± 5.541	± .70%

Table 4.8

The estimates of permeability and skin have changed somewhat, as we can see from the derivative plot (Fig 4.13) that the last part of the original semilog straight line has now been attributed to boundary effect. The confidence intervals have also grown slightly wider -- this is due to the fact that four parameters were matched, compared to the original three. It is generally not a good idea to place too much importance in relative sizes of confidence intervals, instead we are interested principally in whether they are within the acceptable range or not.

Before concluding our discussion of boundary effects we can compare our final interpretation with the responses that would have been observed under other reservoir boundary conditions. Fig. 4.17 shows the simulated responses for impermeable faults and constant pressure boundaries. Again notice how much easier the response is to recognize on the derivative plot, compared to the log-log pressure plot.

4.1.4 Ambiguity

In most well test analyses there is room for more than one interpretation, since the appearance of the data may be ambiguous. In many cases ambiguity is not a problem, since usually only one interpretation will be consistent with other known information (e.g., geology). In addition, investigation of the confidence intervals provides a useful tool for the recognition of ambiguity.

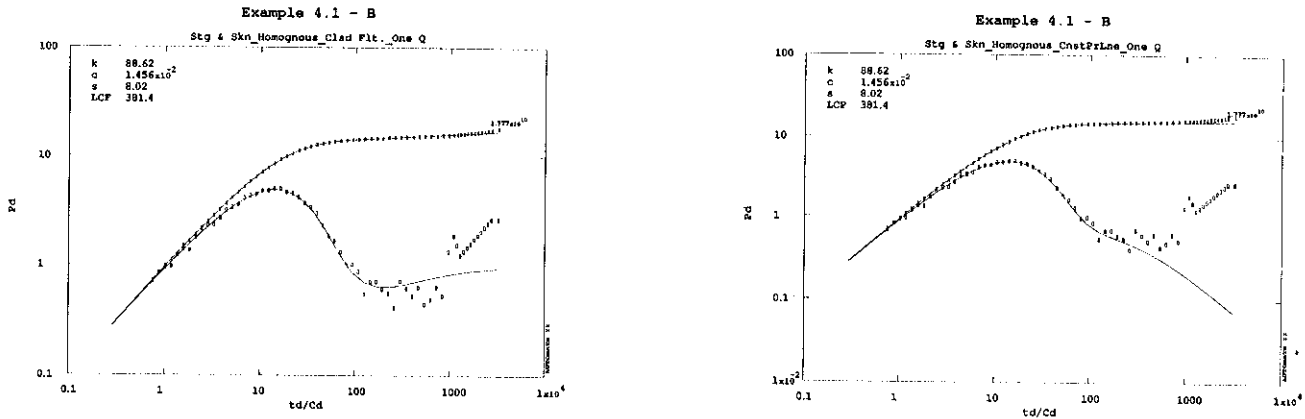


Figure 4.17

As an example, even the simple drawdown case considered in the preceding sections can permit alternative interpretations (with some imagination). Looking at the original 21.6 hour data set in a semi-log plot (shown previously in Fig. 4.3), we might imagine that the semilog straight line is already due to the boundary effect of an impermeable fault, and that its slope is in fact double that of the infinite acting semilog straight line (which would then be hidden in the storage dominated period). In this case the semilog interpretation would look as in Fig. 4.18.

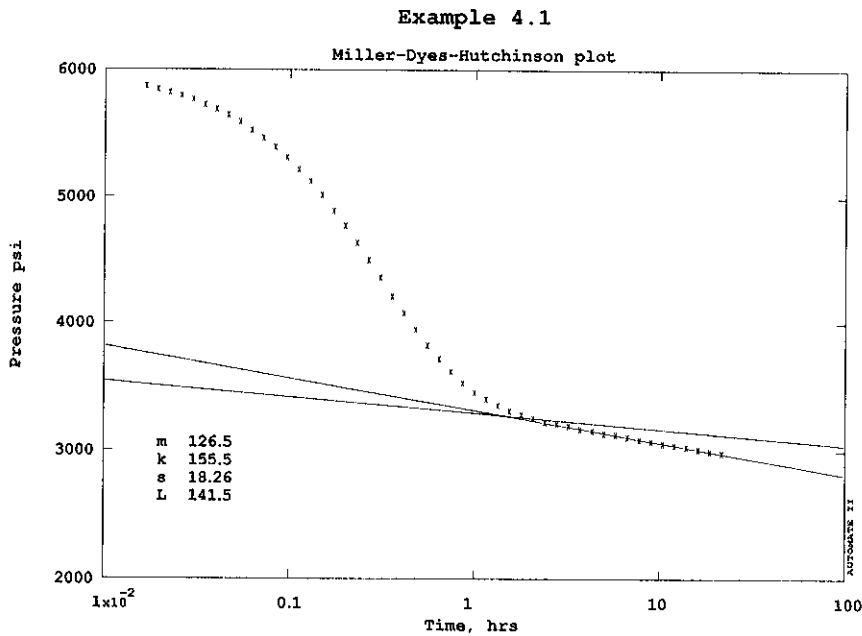


Figure 4.18

Starting with these estimates, we can obtain a very close looking match, Fig. 4.19, by nonlinear regression (if we start with the original estimates, nonlinear regression will force the supposed impermeable fault beyond the radius of investigation and converge to the same infinite acting solution as before).

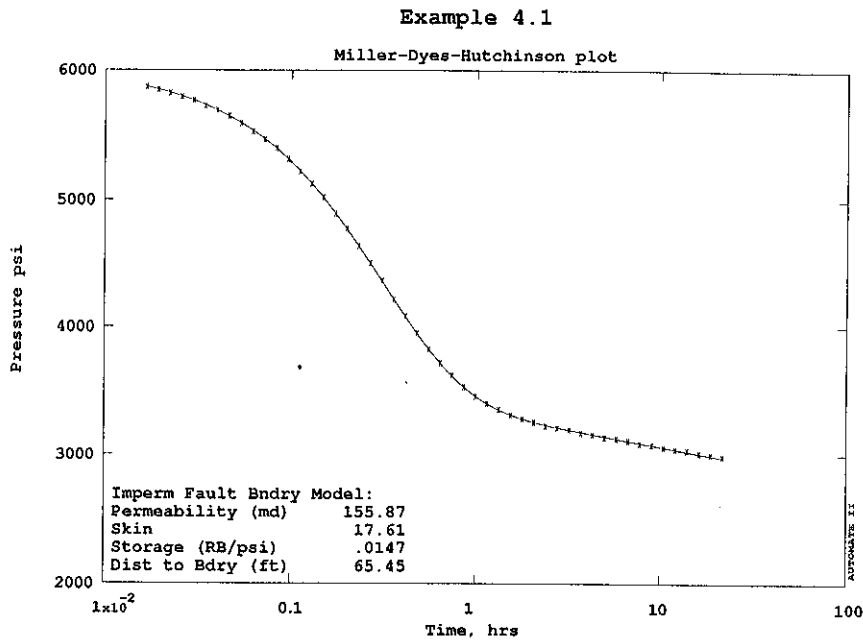


Figure 4.19

Fortunately, the confidence intervals (Table 4.9) warn us that the solution is not statistically significant, since the confidence interval on the fault distance is so large (168%) even though we have already ascertained that there is a long semilog period (which is all boundary effect under the interpretation being considered).

Parameter	Estimate	Confidence Interval (absolute)	Confidence Interval (percent)
Permeability (md)	155.9	± 10.94	± 7.02%
Skin	17.61	± .5455	± 3.10%
Storage (RB/psi)	.01472	± .8306×10 ⁻⁴	± .56%
Dist to Bdry (ft)	65.45	± 110.1	± 168.26%

Table 4.9

The reason for the wide confidence intervals is that, without any infinite acting period, the fault boundary could be at almost any location within the radius of investigation at the end of the storage period (even right at the well itself). On the basis of these unacceptable intervals, we would reject the interpretation. This is fortunate, since we would otherwise be in error (by a factor of two) in our estimates of permeability and skin factor. Consideration of the confidence intervals, and recognition of the correct starting point of the infinite acting semilog straight line, has rescued us from an invalid interpretation.

4.1.5 Truncated Data

As discussed in Section 3.5, nonlinear regression provides us with the capability to make estimates of reservoir parameters based on data in *transition* periods, thus allowing us to interpret well tests that

have been truncated even before reaching the infinite acting semilog straight line. For example, suppose our original drawdown had been cut off after only 1.55 hours by a failure of the pressure tool. In this case we know that the correct semilog straight line does not begin until around two hours, thus it would not be possible to do a traditional semilog analysis to estimate permeability and skin factor. We might be tempted to try a type curve match, however this is not a good idea since it is difficult to obtain a unique match, even with the derivative type curve, if the semilog straight line data are not present. Fig. 4.20 shows a reasonable looking type curve match, even though the parameter estimates are completely incorrect.

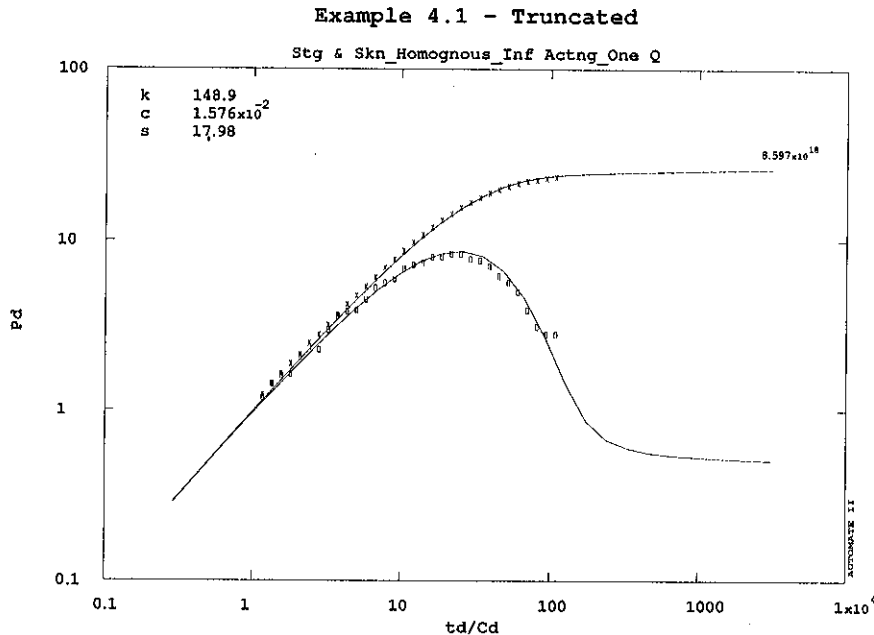


Figure 4.20

Using nonlinear regression, we can obtain a good match to this data (Fig. 4.21) even though it contains only storage dominated and transition data. The confidence intervals are all still within acceptable range (Table 4.10), and we can see from our original interpretation that the answers are correct.

Parameter	Estimate	Confidence Interval (absolute)	Confidence Interval (percent)
Permeability (md)	88.38	± 6.606	± 7.47%
Skin	7.979	± .9961	± 12.48%
Storage (RB/psi)	.01455	± .6520×10 ⁻⁴	± .45%

Table 4.10

The most impressive illustration of the power of the nonlinear regression technique can be seen in Fig. 4.22, which shows the correct semilog straight line drawn in a location based on the estimates of *k* and *s* from nonlinear regression. It is clear from this plot that *no part* of the actual data lies on the straight line. Nonlinear regression has been able to correctly ascertain the position of the straight line based on transition data alone.

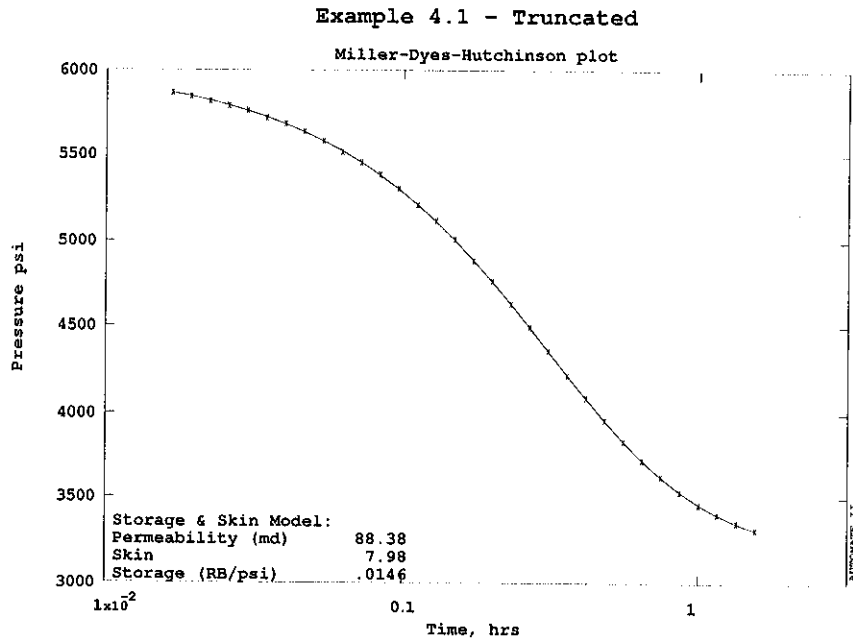


Figure 4.21

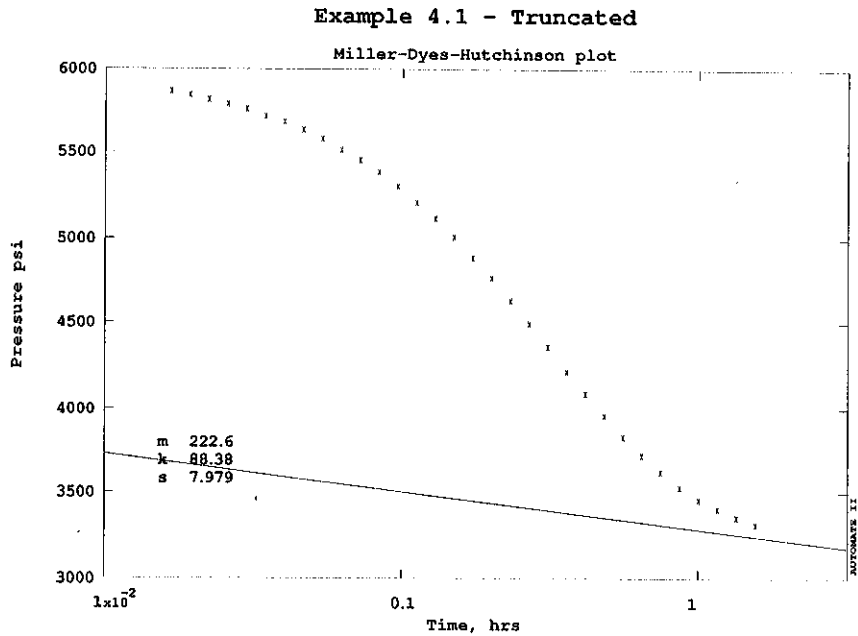


Figure 4.22

In this example, nonlinear regression would have allowed us to obtain the correct answer even if the test had been only 1½ hours long (compared to 21.6 hours in the original test) or would have saved us from having to rerun the test if the pressure tool had actually failed after 1½ hours. In either of these two situations, the expense of the well testing operation could be substantially reduced.

While discussing truncated data, it needs to be emphasized that not all truncated data can be interpreted in this way. If the data in our example were truncated still further, the confidence intervals would become so much broader that we could no longer rely on the estimate. Also, the objective of the test may have been to identify the reservoir model or to explore for reservoir limits - - in either case the full length of data would still be required. Nonetheless there are many routine well tests in producing fields that could be run for shorter time, if interpreted by nonlinear regression. There are also probably many older misdesigned tests or data sets truncated by tool failure that could be usefully interpreted using this approach.

4.1.6 Simultaneous Rate-Pressure Data

Improvements in measurement technology now make it possible to make simultaneous measurement of pressure and flow rate, although this is still problematic in multiphase wells. Flow rate measurement can either be made directly by a downhole flow meter, or indirectly by monitoring fluid levels in a downhole shut-off or DST tool. The advantage of knowing the sandface flow rate is that the wellbore storage effect is no longer of any consequence, and all of the measured pressure response is that of the reservoir rather than of the well. In general this means that more reservoir information can be obtained earlier in the test. However, some caution is necessary since the radius of influence at early time may be quite small, and the tested part of the reservoir may be only the skin damaged zone close to the well. Thus, although it may be possible in undamaged wells to analyze very short data, the likelihood of good interpretations in wells with skin damage is reduced. Rather than a means of interpreting shorter tests, use of simultaneous rate data should be seen as a way of obtaining more and less ambiguous information from a test of normal length.

To demonstrate the concept, as well as some of the difficulties, consider our same drawdown example test. Fig. 4.23 shows the flow rate history during the first 15 minutes of the drawdown (the eventual flow rate was 2500 STB/day).

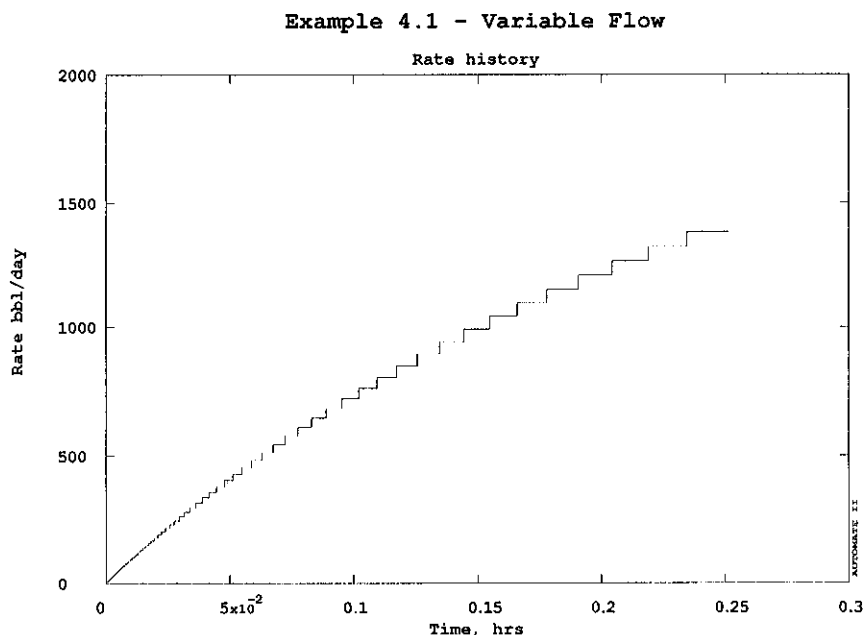


Figure 4.23

Fig. 4.24 shows the same period of pressure data, which lies more or less totally within the wellbore storage regime. Variable rate data can be "straightened" by desuperposition, to show an apparent semilog straight line in Fig. 4.25.

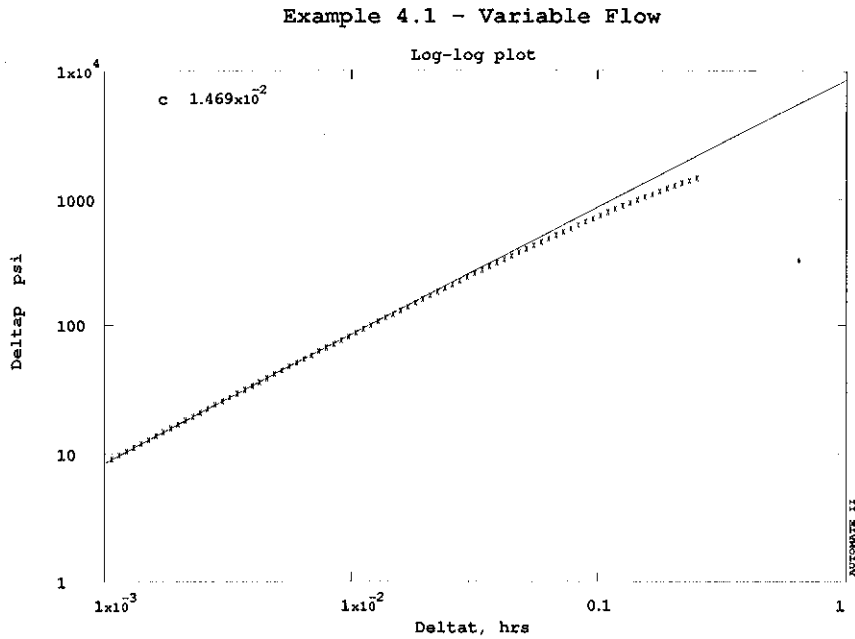


Figure 4.24

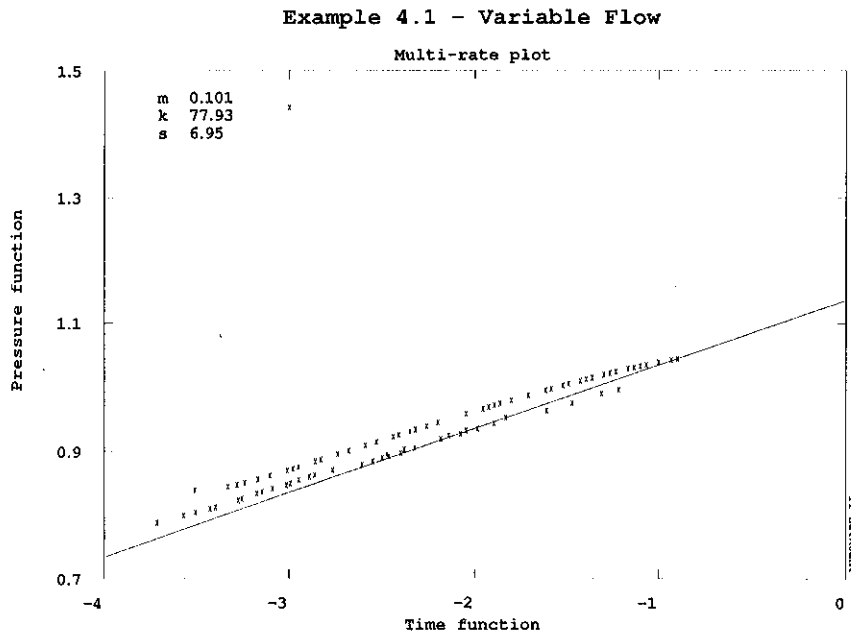


Figure 4.25

Desuperposition was discussed in Section 3.6. Using nonlinear regression, we can obtain estimates of k and s (C is no longer of significance) that are similar to the previous estimates. Using only 15 minutes of data, the estimates are obtained far from the semilog straight line they represent, Fig. 4.26.

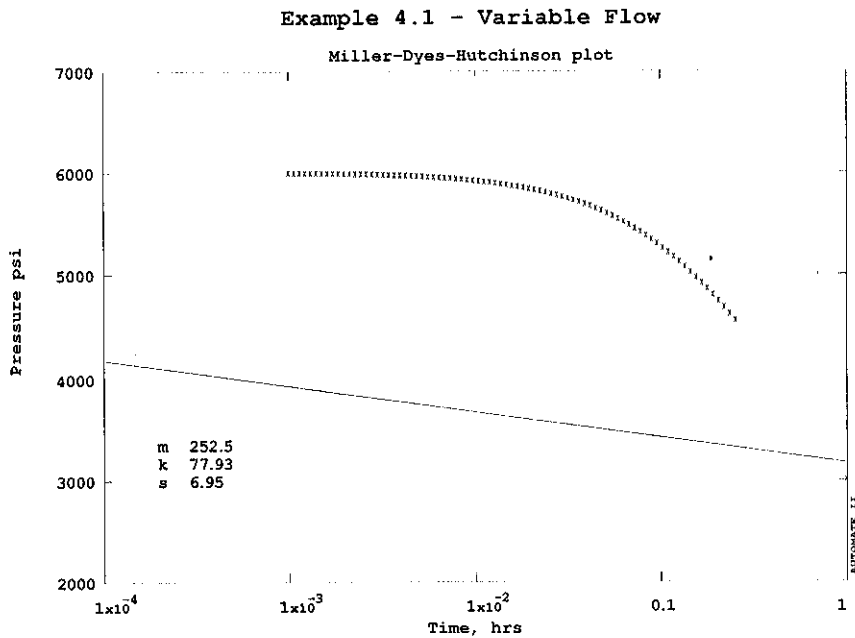


Figure 4.26

Even though the estimates are close to the (known) correct answers, the confidence intervals are wider than commonly acceptable. This is because of a very high correlation between k and s over this time interval since the pressure drop across the skin is a significant proportion of the total pressure drop. The radius of investigation during 15 minutes was only about 100 feet. Thus, over this period, the skin effect is dominant, making it more difficult to analyze the reservoir response. Thus in some ways we have avoided the storage effect, only to be trapped by the next non-reservoir effect in the sequence. This limits the extent to which short data can be analyzed, even with flow measurements, although the added advantages of flow measurement over normal test lengths are still major.

4.2 Buildup Example

In a buildup test, the well has been on production for some time prior to the test. The pressure measurement tool is lowered to the bottom of the well, and the well is shut in (in actuality the well may be shut in to install the pressure tool, then restarted, stabilized, and shut in again).

4.2.1 Test Without Boundary Effects

Fig. 4.27 shows the pressure and flow rate for an example test, with data listed in Table 4.2 in the Appendix. This example test shows a Horner straight line with slope $162.6 qB\mu/kh$, Fig. 4.28, and also shows apparently standard diagnosis using a (drawdown) derivative plot, Figure 4.29.

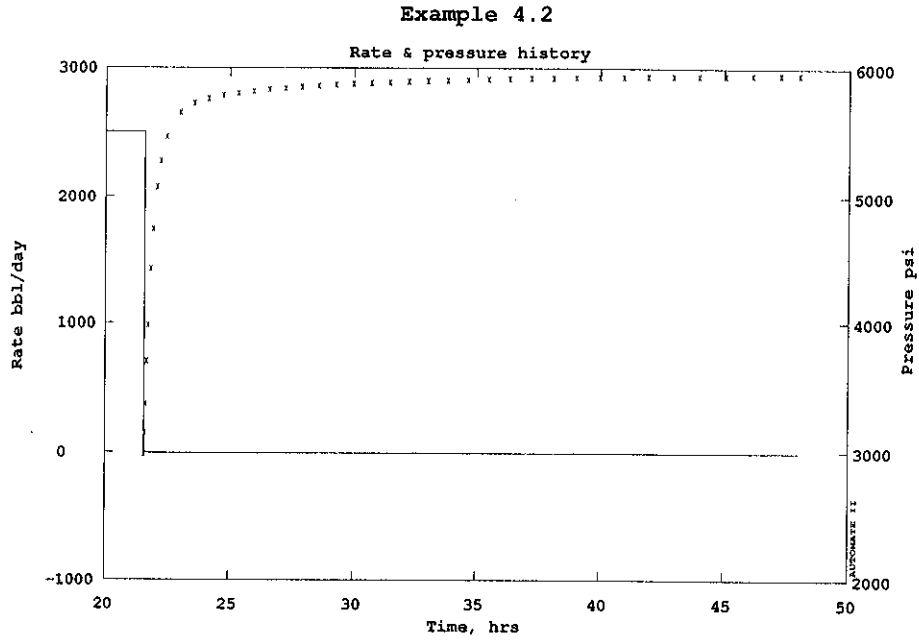


Figure 4.27

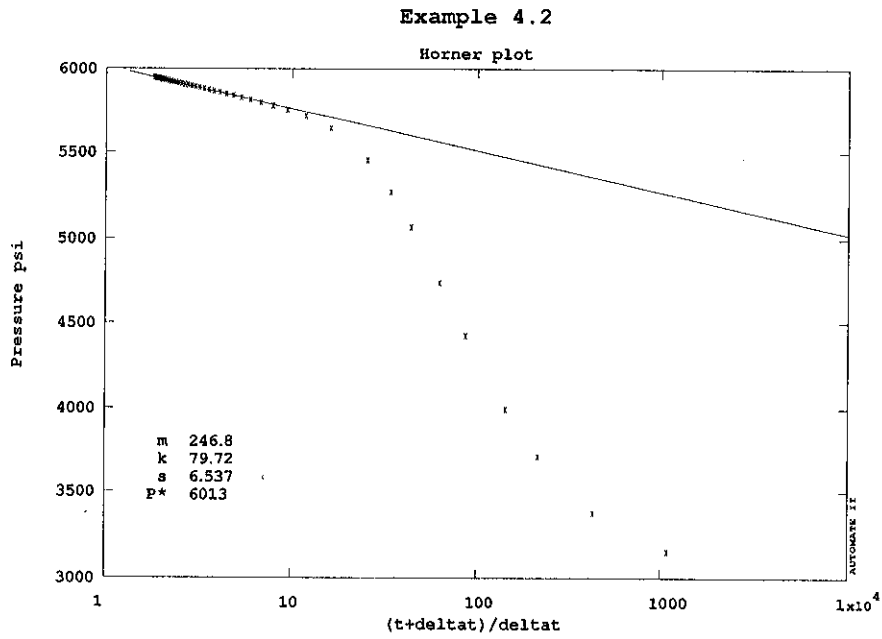


Figure 4.28

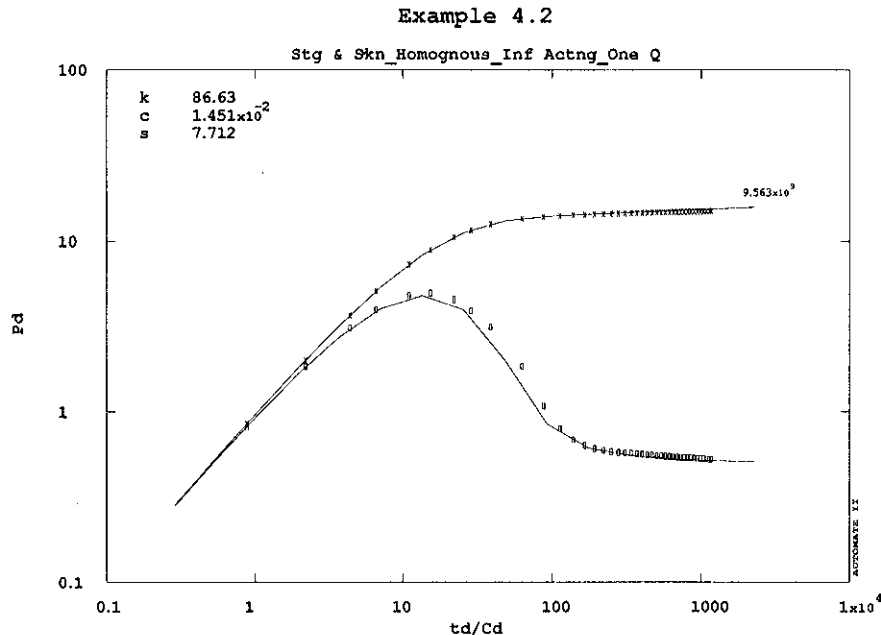


Figure 4.29

Nonetheless, it is actually incorrect to perform derivative diagnosis in this way, since the effects of the transient prior to the shut-in can change the slope of the derivative plot considerably. Traditionally, it has been assumed that drawdown type curves can be used for buildup if the shut in time is no longer than 20 to 30 percent of the producing, but this may not be valid if boundaries are present.

However, the example shown here shows no major distortions in shape, because there is no influence of any boundaries during the shut-in *nor during the preceding production*.

4.2.2 Effects of Boundaries

This is a key point regarding buildup tests. The measured response is characteristic not only of the time of the buildup itself, but also of the preceding drawdown. Thus the duration of the shut-in period may be much less than is required to reach a boundary response, but the drawdown transient, which has continued for much longer (and effectively continues during the buildup too), may be influenced by the drainage boundaries. This boundary effect will be superposed on the buildup behavior and may therefore be evident in the pressure response.

Consider for example a buildup in the well shown earlier in Example 4.1, if the well were to have been shut in after 21.6 hours. As seen earlier, no boundary effect was observed during the 21.6 hours drawdown period, although we determined from longer testing that a drainage area boundary existed at a distance of 800 feet, and that the influence of this boundary effect was significant within the 20 hours subsequent to the first 21.6 hours of drawdown. Therefore, the boundary effect will alter the appearance of a buildup test in which the well is shut in at 21.6 hours, even though no boundary effect was visible during the drawdown. The effect of the closed boundary is to flatten the Horner plot towards zero slope, Fig. 4.30, and to show an ever-decreasing derivative on the derivative plot, Fig. 4.31.

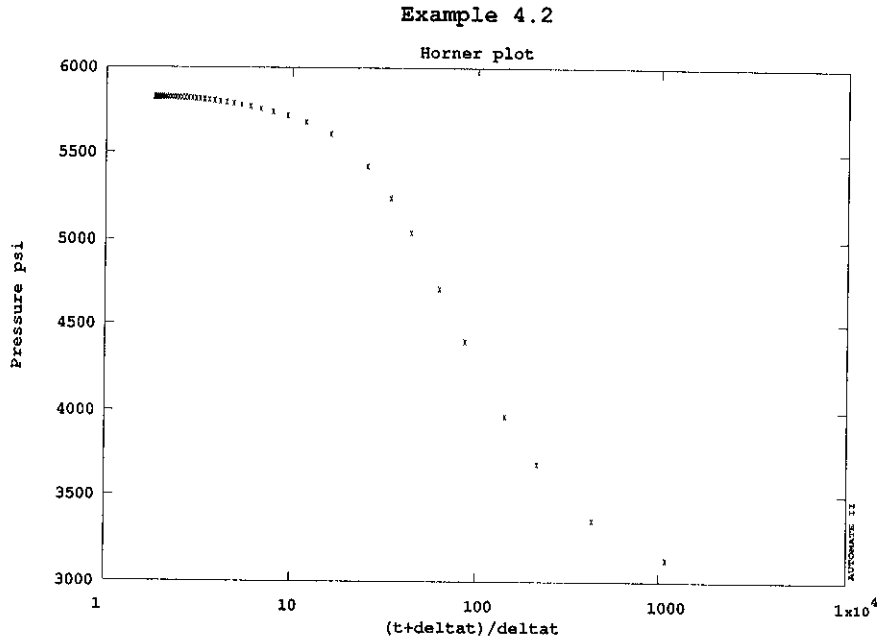


Figure 4.30

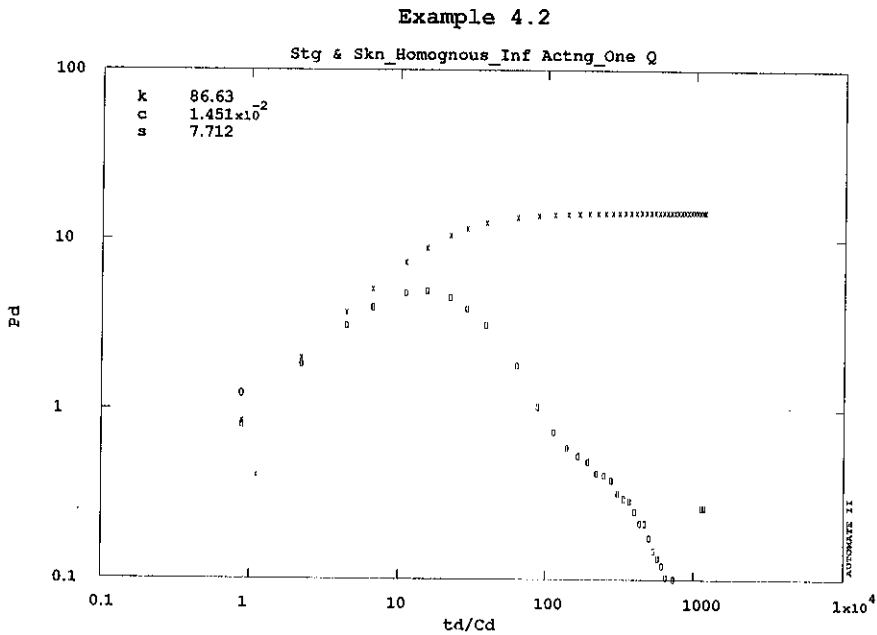
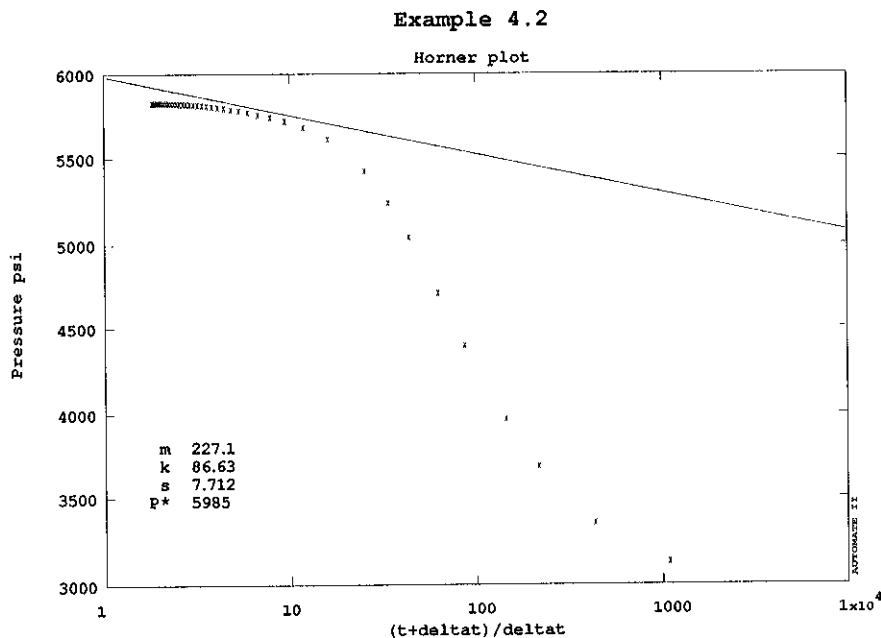


Figure 4.31

It is obviously wrong to try to diagnose this derivative plot as before, since it looks like the response of a system with a constant pressure boundary, although none is present.

The reason for this different appearance of the buildup plots is that the response consists of the summation (superposition) of the response to the change in flow rate at shut in, added to the response to the original change in flow rate when the well first started to flow. In the example shown in Figs. 4.30 and 4.31, the drawdown response has achieved pseudosteady state whereas the shut-in response is still infinite acting (with the beginning of a pseudosteady state towards the end). As a result of the summation of the two, the actual correct Horner straight line, Fig. 4.32, covers only a small portion of the data, and would probably be rather difficult to find by eye alone.



This emphasizes a major difficulty of interpreting buildup tests, since it is not only problematic to perform reservoir diagnosis, it is also more difficult to estimate the reservoir parameters. The problems are not seen when boundary effects are not present (such as in the example illustrated in Figs. 4.28 and 4.29), and can be minimal in some cases (for example if the drawdown has reached constant pressure boundary behavior, but the buildup has not).

The difficulty of recognizing the correct Horner slope is overcome by use of nonlinear regression, however the problem of reservoir diagnosis remains. It is not usually advisable to perform diagnosis on buildup data alone, unless the response has very clearly responded as if infinite acting. Desuperposition provides a hope for diagnosis, since it separates out the constant rate response.

It has often been found in traditional interpretation that the drawdown and buildup estimates of reservoir parameters were not the same. There are good physical reasons why this might occur (such as gas dissolution), however, once nonlinear regression became more commonly used it was discovered that in many cases the estimates from drawdown and buildup analyses were the same, and that it was the distortion of the Horner plot that caused an error in traditional estimation techniques.

4.2.3 Knowledge of p_{wf}

In the absence of wellbore storage effect, the buildup response is not affected by the skin effect, since the well is not actually flowing. Traditional analysis methods rely on the value of p_{wf} , the last pressure measured while the well was flowing, to estimate the skin factor s . If the logarithmic approximation to the infinite acting radial flow solution is used, then

$$\left[p_{ws}(t_p + \Delta t) - p_{wf}(t_p) \right] \frac{kh}{141.2 qB\mu} = \frac{1}{2} \left[\ln \frac{t_p \Delta t}{t_p + \Delta t} + 0.80907 + \ln \frac{0.000264 k}{\phi \mu c_i r_w^2} \right] + s \quad (4.11)$$

This is true for all points which lie on the semilog straight line (or its extrapolation). Traditionally, the value of p_{ws} at $\Delta t = 1$ hour has been used, so that

$$s = 1.151 \left[\frac{p_{1hr} - p_{wf}}{m} - \log \frac{kt_p}{(t_p + 1)\phi \mu c_i r_w^2} + 3.2274 \right] \quad (4.12)$$

where the Horner slope m is $162.6 qB\mu/kh$.

If Eq. 4.12 is used, it is seen that estimates of skin factors can be quite strongly dependent on the value of p_{wf} . This makes the traditional estimation process dependent on a single data point -- if this point is in error, then so too will be the estimate of the skin factor, s .

During nonlinear regression, skin factor is estimated differently, by matching the shape of the curve during the period of afterflow (wellbore storage) when the well is still flowing. This estimate uses more than a single data point, and is often more consistent with estimates of skin factor obtained during drawdown, however may be different from a traditional estimate obtained using the value of p_{wf} . In a mixed graphical and computer-aided interpretation of a buildup test, it may be necessary to make a choice between forcing the regression procedure to fit the model to the p_{wf} point exactly or to fit more generally with equal weighting to all pressure data points.

As an example, the Horner plot in Fig. 4.28 provided a traditional estimate of skin factor as 6.53, using a value of p_{wf} of 2989.4 psia. The second data point, less than a minute after shut in, was nearly 200 psi higher, indicating how rapidly pressure varies at this time, and how difficult it may be determining exactly when the well was shut. If a different value of p_{wf} is used, for example 2939.4 psi which is 50 psi different from the correct value, then the skin estimate changes to 6.86. The actual value of skin factor was 7.7, and this value is obtained by nonlinear regression, even if the wrong value of p_{wf} is used (provided the regression is not forced to pass through p_{wf} exactly).

4.2.4 Average Reservoir Pressure

One common objective for a shut-in test is to estimate the average reservoir pressure, which is expected to change as reservoir production occurs.

Finding the "initial" reservoir pressure p_i can be an integral part of nonlinear regression analysis, whether the test is drawdown or buildup type. In a buildup analysis, the estimated value of p_i obtained will be the estimate of average reservoir pressure. Even without nonlinear regression, the ability to "simulate" extended duration shut in tests makes it possible, in computer-aided interpretation, to extrapolate to the new reservoir pressure p_i , if the drainage shape is known or assumed. However, the traditional

methods will be described here for completeness.

The situation is straightforward if the actual initial pressure before production began is known, since the average reservoir pressure is then a simple matter of material balance, based on the equation for pseudosteady state behavior:

$$\frac{kh}{141.2qB\mu}(p_i - \bar{p}) = 2\pi t_{DA} \tag{4.13}$$

Notice that it is necessary to know the drainage area, and that no information from the actual well test is used (except the producing time).

If the initial p_i is unknown, which may be the case if the well has been in production for a long time, then a graphical technique due to Matthews, Brons and Hazebroek (1954) is used. An example of MBH plot is shown in Fig. 4.33.

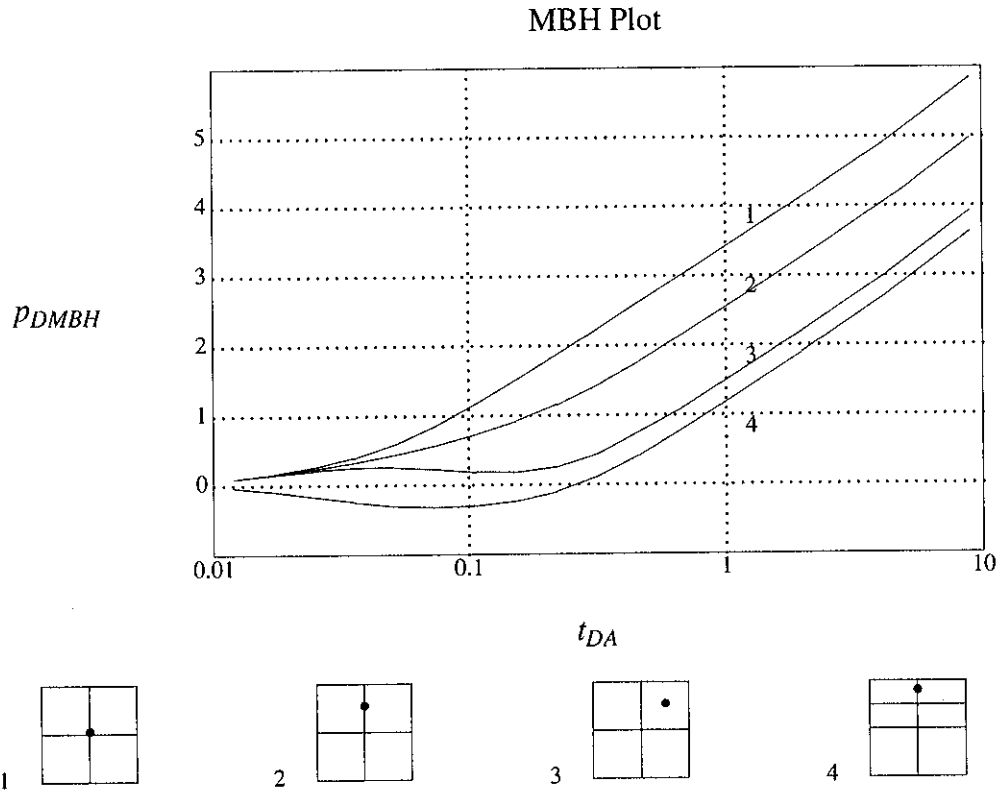


Figure 4.33

The procedure is to determine t_{DA} , using the value of producing time t_p , and an estimate or assumption of the drainage area. Next, the corresponding p_{DMBH} is read from the MBH plot (such as Fig. 4.33), making use of a prior estimate or assumption about the shape and/or configuration of the boundary. Finally, the value of average reservoir pressure, \bar{p} , is determined from the definition of p_{DMBH} :

$$p_{DMBH} = 2 \frac{kh}{141.2qB\mu}(p^* - \bar{p}) \tag{4.14}$$

$$p_{DMBH} = \frac{2.303(p^* - \bar{p})}{m} \quad (4.15)$$

where m is the slope of the Horner straight line, and p^* is the point at which the extension of the Horner straight line meets the axis $(t_p + \Delta t)/\Delta t = 1$, as in Fig. 4.34.

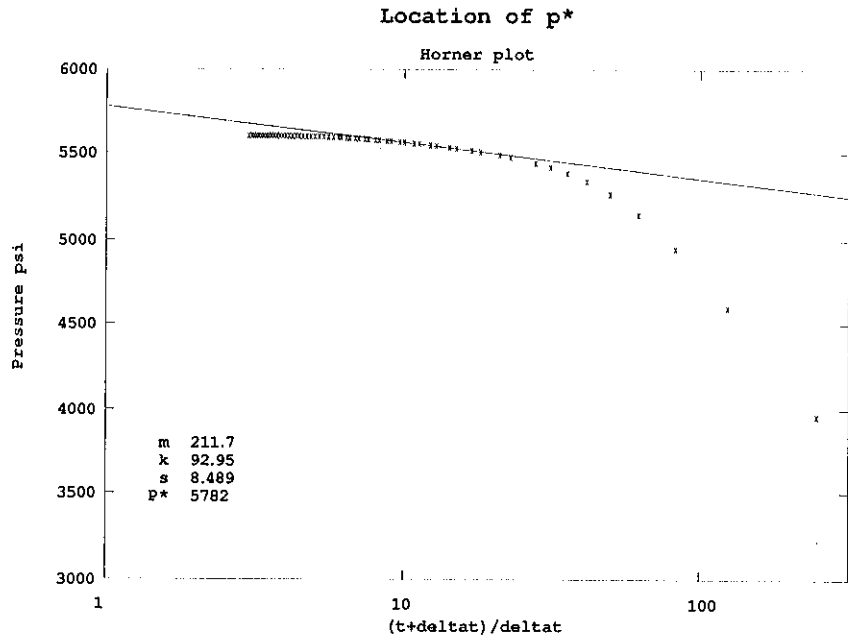


Figure 4.34

4.2.5 Treating Buildups as Drawdowns

As discussed earlier, it may be possible to treat a buildup the same as a drawdown if the preceding production time is three to five times as long as the period of shut in, although some care is required if boundary effects are present in either the drawdown or buildup responses. With computer-aided interpretation, it is not difficult to accommodate the full history of the production prior to the buildup, so the need or interest in using traditional drawdown analysis methods is much reduced.

A case of more practical interest is one in which the previous production history is unknown (perhaps due to collective production through a manifold, for example), and where the well has been in production for a long period of time. In such a case, any transient attributable to the production is likely to be very small during the duration of the buildup test. Thus the buildup test may be reasonably treated as if an injection of fluid at the rate $-q$ started at the time of the test, where q was the stabilized rate of production prior to shut in. Rather than include the production history back to the first flow of the well, it is adequate to treat the transient as if it had started just at the time of shut in.

4.3 References

Matthew, C.S., Brons, F., and Hazebroek, P.: "A Method for Determination of Average Reservoir Pressure in Bounded Reservoirs", *Transactions, AIME*, (1954), 201, 182-191.

5. EXAMPLE INTERPRETATIONS - FRACTURED WELLS

As discussed in Section 2.7, many wells are stimulated upon completion by hydraulic fracturing. Analysis of reservoirs that are penetrated by such wells almost always requires specific consideration of the effects of the fractures. Also, a common objective in testing fractured wells is to evaluate the effectiveness of the fracture treatment, and to estimate the length and conductivity of the fracture itself. Many hydraulically fractured wells display finite conductivity behavior, hence this type of analysis is a good way to start an interpretation if the well is known to be fractured.

5.1 Finite Conductivity Fracture Example

Table 5.1 in the Appendix lists the data from a drawdown test performed when a well was put into production following a fracture stimulation. Fig. 5.1 shows the diagnostic plot, indicating the absence of wellbore storage (which is unlikely in practice, but which serves the purpose of illustration in this example).

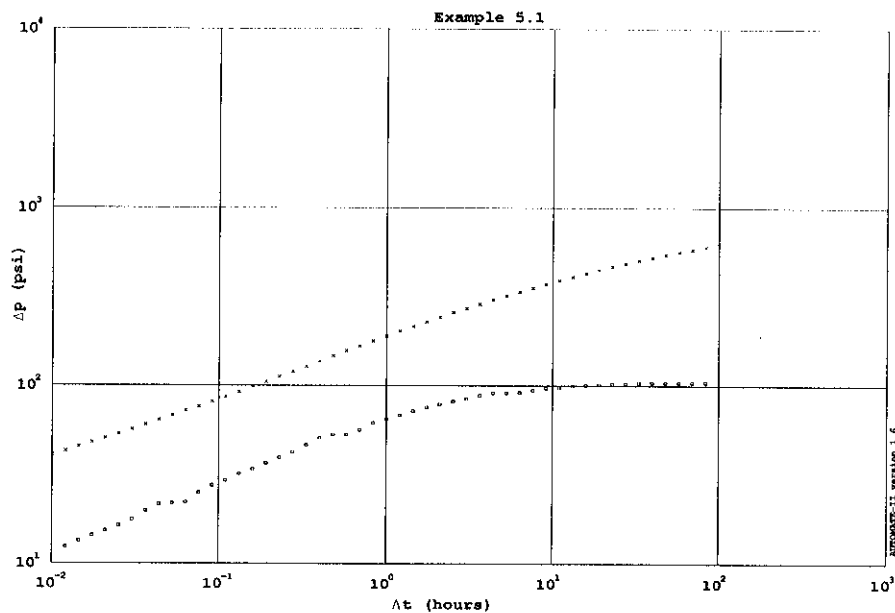


Figure 5.1

Since there is no unit slope (representing storage), and since the well is known to have been fractured, then it is worthwhile to look for fracture behavior on a log-log plot. Fig. 5.2 shows that there is a good match to the finite conductivity type curve, with a value of $(k_f w_f / k x_f)$ somewhat greater than 2π .

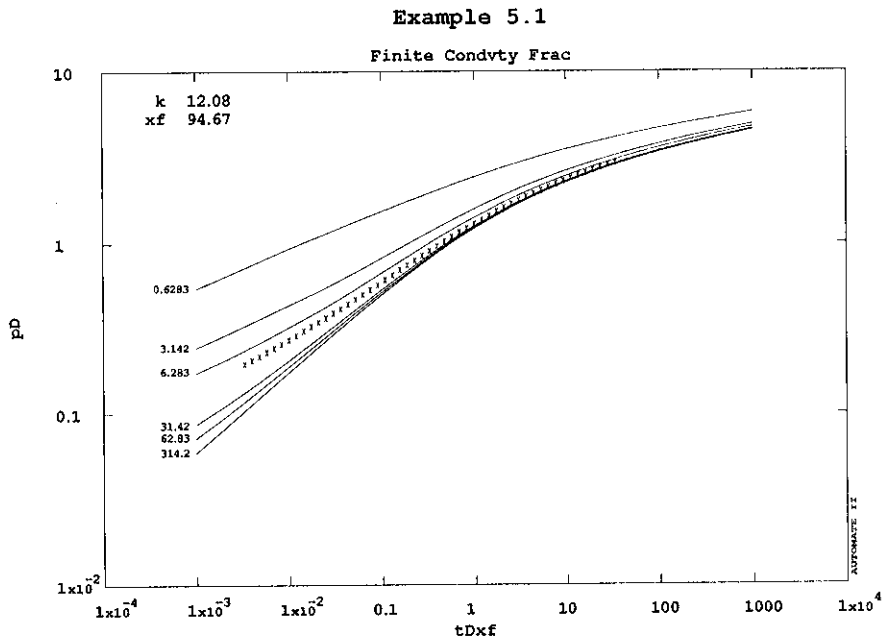


Figure 5.2

Match point (pressure): $\Delta p = 41.08 \text{ psi}$, $p_D = .197$

$$p_D = \frac{kh \Delta p}{141.2 q B \mu} = \frac{kh (41.08)}{141.2 (2000)(1.5)(.3)} = .197$$

$$kh = 609.5 \text{ md-ft}; k = 609.5/50 = 12.19 \text{ md}$$

Match point (time): $t = .01 \text{ hrs}$, $t_{Dxf} = 2.74 \times 10^{-3}$

$$t_{Dxf} = 2.74 \times 10^{-3} = \frac{0.000264 kh t}{\phi h \mu c_t x_f^2} = \frac{0.000264(609.5)(.01)}{(.24)(50)(.3)(.000148)x_f^2}$$

$$x_f = 105$$

Based upon the pressure and time match points, the permeability and fracture length are estimated to be about 12 md and 100 ft respectively.

A plot of pressure against fourth root of time, as suggested by Eq. 2.37, shows a straight line portion with a slope of $173.3 \text{ psia/hr}^{1/4}$, with intercept at the (known) value of p_i , 5200 psia (Fig. 5.3).

Since, from Eq. 2.37, we know that

$$p_D = \frac{2.451}{\sqrt{k_{fD} w_{fD}}} t_{Dxf}^{1/4} \tag{5.1}$$

Example 5.1

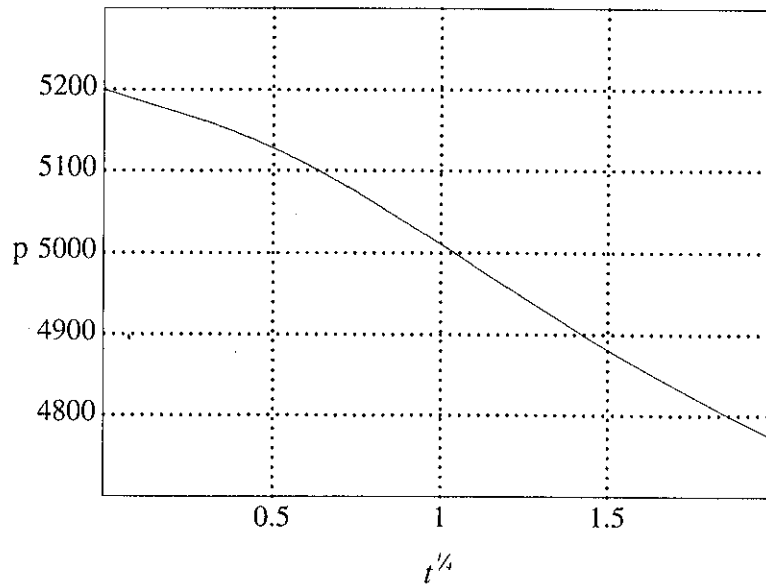


Figure 5.3

then

$$p = p_i - \frac{44.13qB\mu}{h(k_f w_f)^{1/2}(\phi\mu c_t k)^{1/2}} t^{1/2} \quad (5.2)$$

and the slope of the line p vs. $t^{1/2}$ is given by

$$m = - \frac{44.13qB\mu}{h(k_f w_f)^{1/2}(\phi\mu c_t k)^{1/2}} \quad (5.3)$$

Substituting the numbers and the slope observed in Fig. 5.3:

$$(k_f w_f)^{1/2} = - \frac{44.13(2000)(1.5)(0.3)}{(-173.3)(50)[(0.24)(0.3)(14.8 \times 10^{-6})(12.19)]^{1/2}}$$

Hence

$$k_f w_f = 5829.3 \text{ md-ft}$$

$$\frac{k_f w_f}{k x_f} = \frac{5829.3}{(12.19)(105)} = 4.55$$

Notice that the pressure behavior is not dependent on the length of the fracture during this bilinear flow period. The fracture length could, in principle, be estimated by locating the one half slope section of the log-log plot, however, as mentioned earlier, this half slope region is rarely present in real tests of finite conductivity fractures. The type curve match, relating values of real time t to dimensionless time $t_{D,f}$, is therefore the only way to estimate fracture length x_f .

Although permeability was also estimated by type curve matching in Fig. 5.2, as in unfractured reservoir analysis it is much better to calculate permeability by semilog analysis. Fig. 5.4 shows a semi-log (MDH) plot, with the straight line drawn. The slope of the line provides an estimate of permeability of 12.2 md. Notice that this same line provides an estimated skin factor of -4.66 (stimulated well).

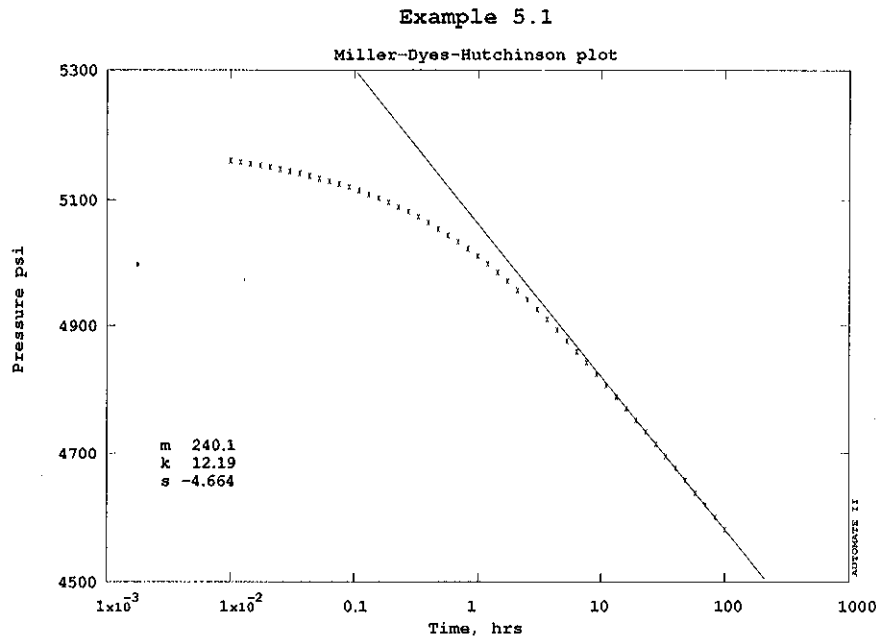


Figure 5.4

Finally, performing an automated match by nonlinear regression, the estimates are refined to $k = 20\text{md}$, $x_f = 105\text{ft}$, and $(k_f w_f)/(k x_f) = 10$, with good confidence intervals for all parameters, as well as a close visual match (Fig. 5.5).

Although this looks like a straightforward example, further examination reveals some pitfalls in the analysis of finite conductivity fractures. If we match the same data to the *infinite* conductivity fracture type curves (Fig. 5.6), then the match does not look as good (although it is still quite close).

However, if we allow the initial reservoir pressure p_i to be variable (since we have already observed that this can alter the slope of the early line), then a good match to the infinite conductivity fracture type curve can be obtained (Fig. 5.7), by changing the value of p_i by only 20 psia.

Finally, it should be noted that the presence of wellbore storage can also affect the ability to estimate fracture conductivity. The presence of even a moderate storage effect produces significant errors in the estimate of fracture conductivity (Fig. 5.8). However, the reservoir permeability is still well determined, as is the fracture half length x_f (in this case, since the storage effect does not overwhelm the entire fracture dominated portion of the response).

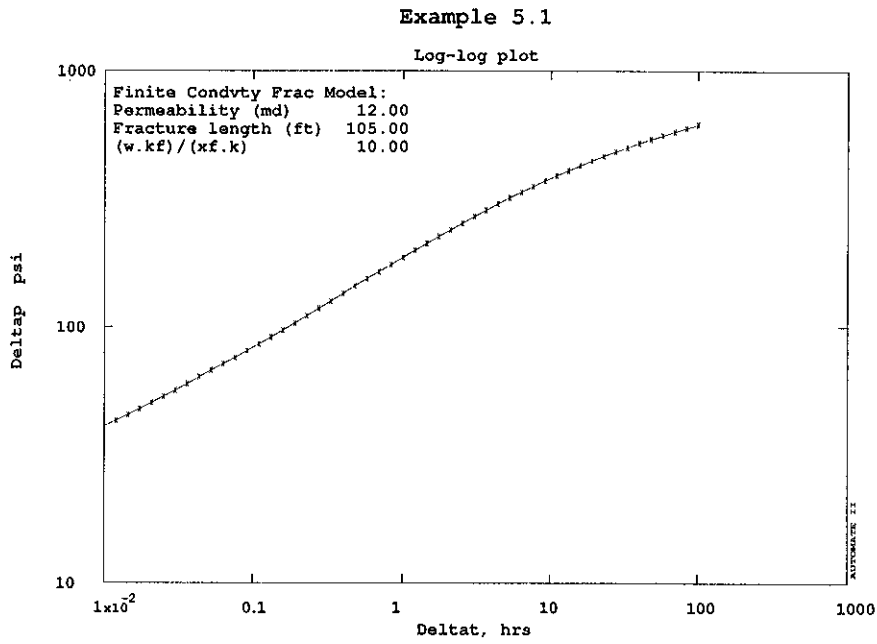


Figure 5.5

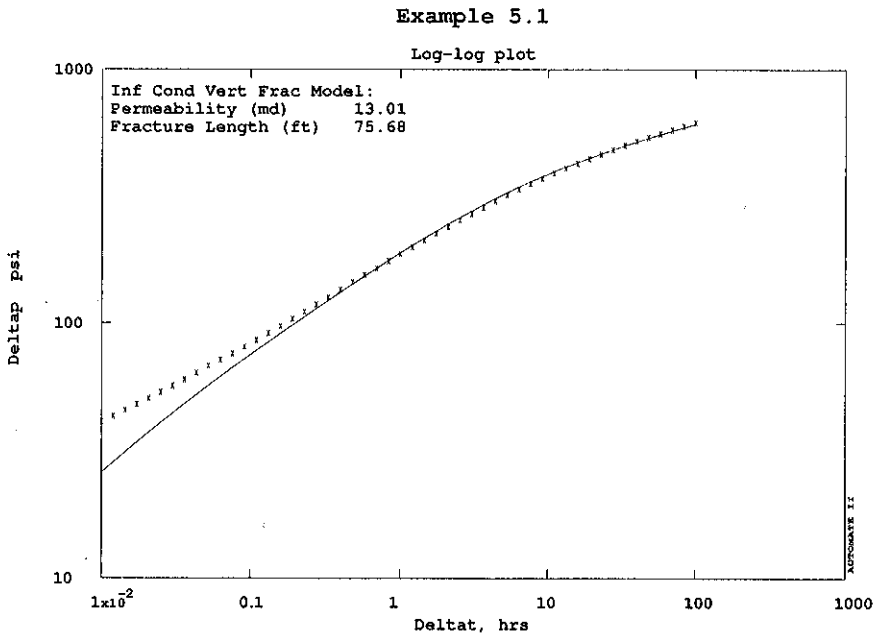


Figure 5.6

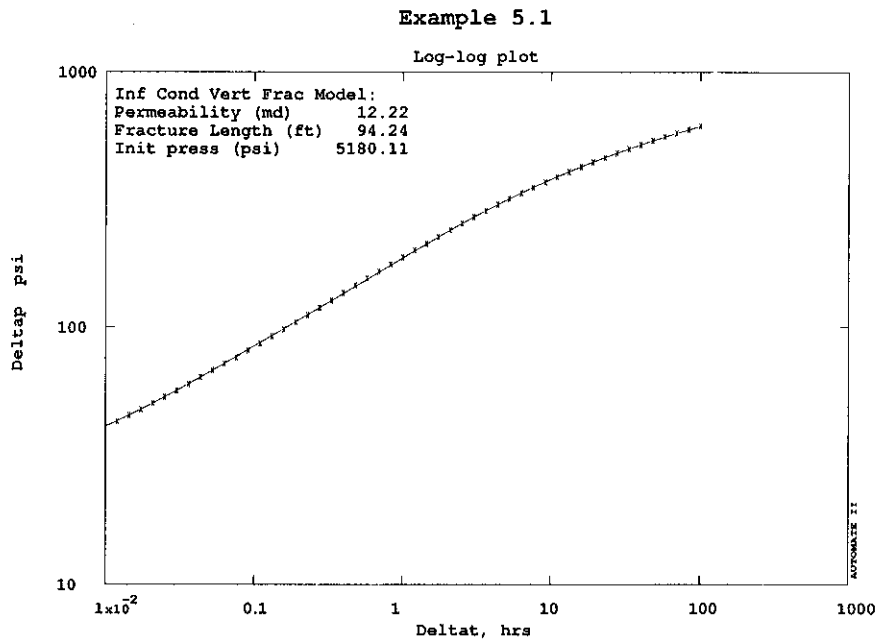


Figure 5.7

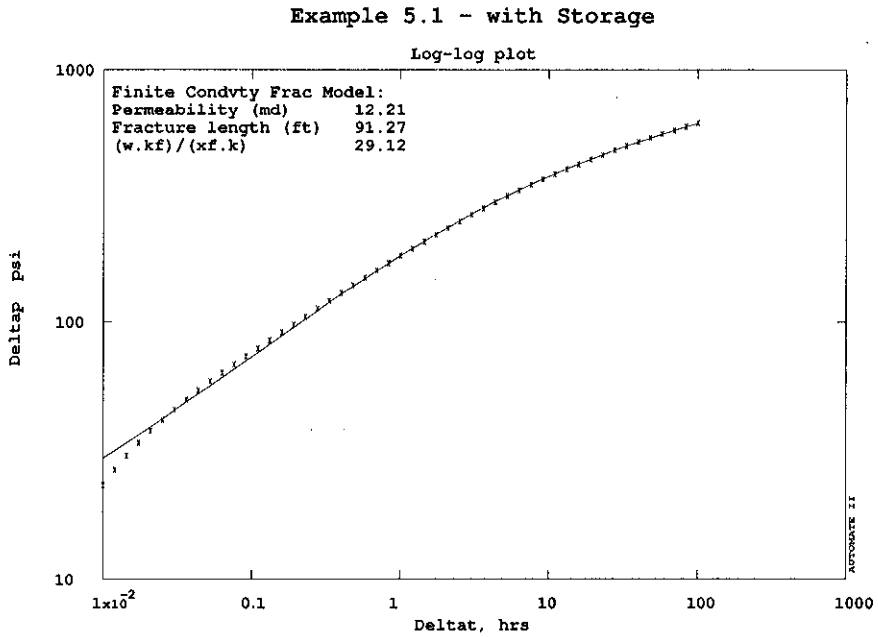


Figure 5.8

In conclusion, the interpretation of well tests in wells with finite conductivity fractures, such as those produced by hydraulic stimulation, requires careful consideration of the early data. In general, the fracture conductivity is not a very well determined parameter.

5.2 Infinite Conductivity Fracture Example

As can be seen from the finite conductivity fracture type curve, once the dimensionless fracture conductivity becomes large, the pressure transient behavior is indistinguishable from that of an infinite conductivity fracture, except at times that are so small that they cannot often be monitored in practice. Thus it is often simpler to treat highly conductive fractures as if they had infinite conductivity.

Table 5.2 in the Appendix lists the data from a drawdown test in a highly productive fractured well. This test is similar to Example 5.1 in almost every regard, except that it can be seen that the total pressure drawdown is 35 psi less (out of a total drawdown of about 600 psi) in this case.

Looking first at the finite conductivity fracture type curve (Fig. 5.9), it is seen that the data lie very close to the high conductivity lines, and in fact show no quarter slope behavior at all. Plotting a one half slope line on the log-log graph (Fig 5.10) shows a close representation of the early data. The data also fit well to the infinite conductivity type curve (Fig. 5.11), providing estimates of k and x_f from the match points.

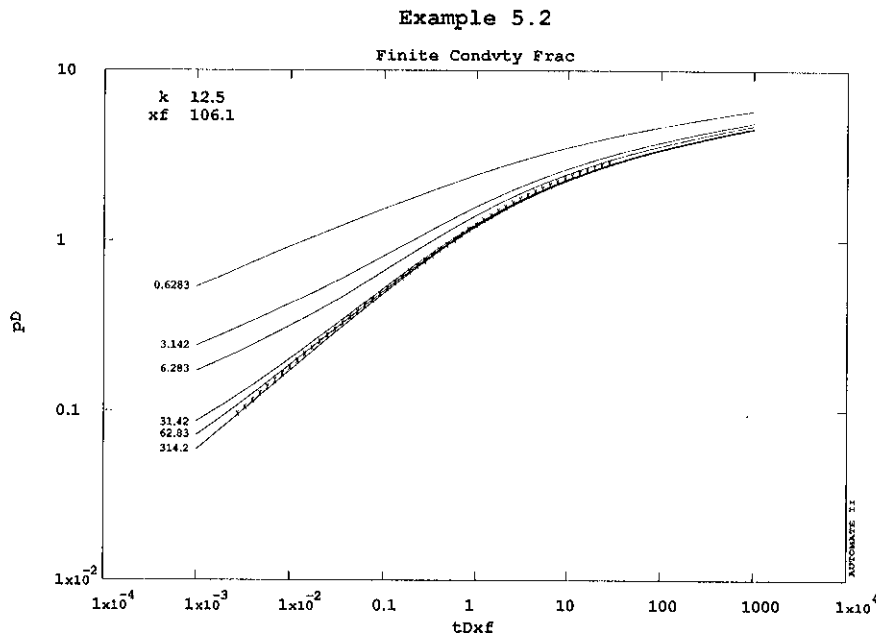


Figure 5.9

Match point (pressure): $\Delta p = 19.48 \text{ psi}$, $p_D = 9.368 \times 10^{-2}$

$$p_D = \frac{kh \Delta p}{141.2 q B \mu} = \frac{kh (19.48)}{141.2 (2000)(1.5)(.3)} = 9.368 \times 10^{-2}$$

$$kh = 611 \text{ md-ft}; k = 611/50 = 12.22 \text{ md}$$

Match point (time): $t = .01 \text{ hrs}$, $t_{Dxf} = 2.72 \times 10^{-3}$

$$t_{Dxf} = 2.72 \times 10^{-3} = \frac{0.000264 kh t}{\phi h \mu c_t x_f^2} = \frac{0.000264(611)(.01)}{(.24)(50)(.3)(.0000148)x_f^2}; x_f = 105.5 \text{ ft}$$

Based on the match to Figure 2.11, permeability k is estimated to be 12.22 md, and fracture length x_f is estimated to be 105.5 feet.

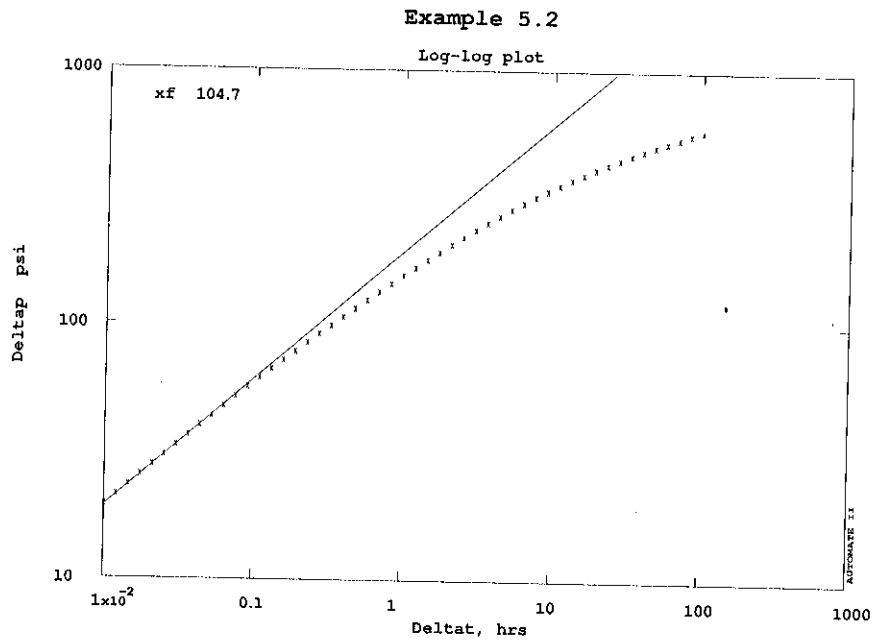


Figure 5.10

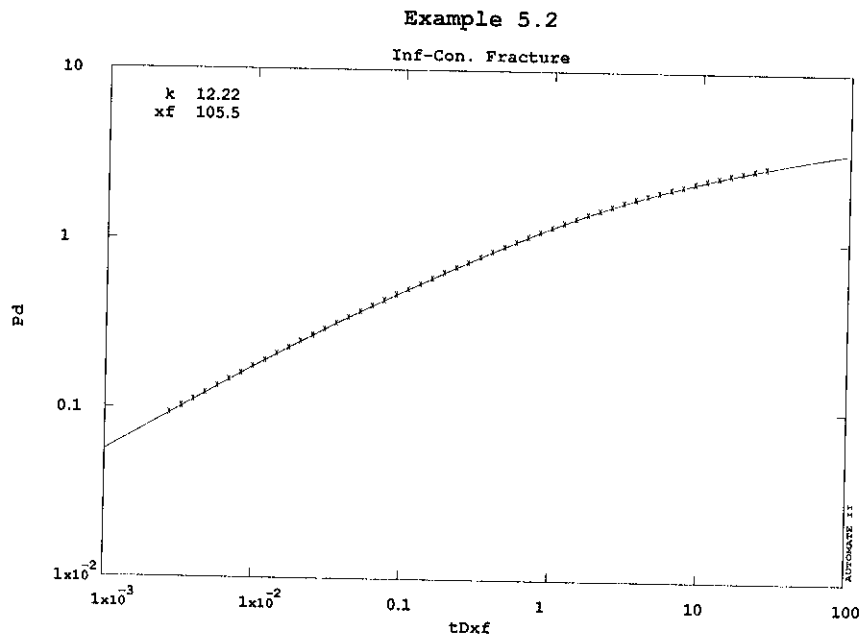


Figure 5.11

The estimates from the type curve match are confirmed and refined by nonlinear regression (Fig. 5.12).

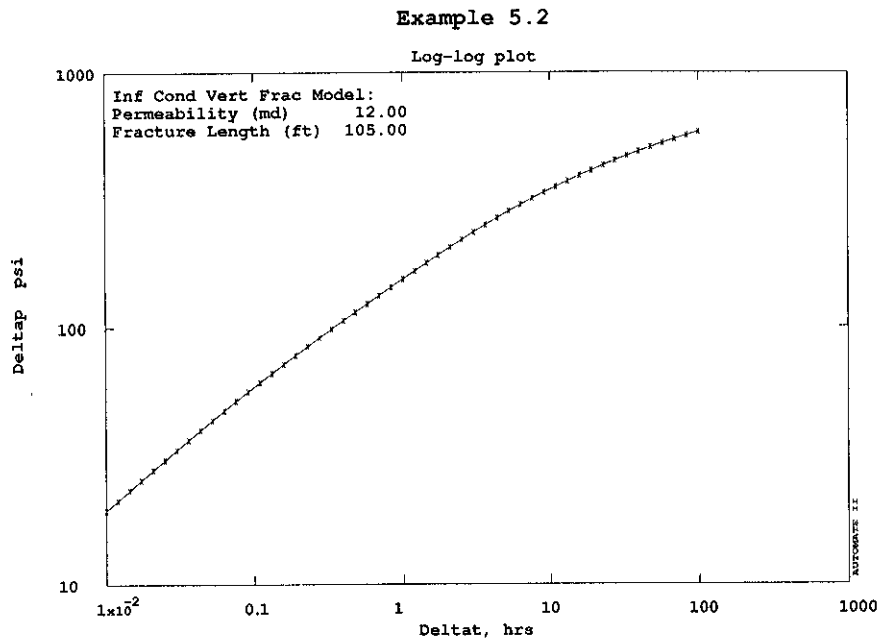


Figure 5.12

In spite of the fact that we are only using fracture type curves for this interpretation (and for Example 5.1), it is important to emphasize that the permeability is still determined from the *infinite acting radial flow* portion of the response. This part of the data fills the last part of this example data set, and is characterised by a semilog straight line (Fig. 5.13) and by a flat region in the derivative (Fig. 5.14).

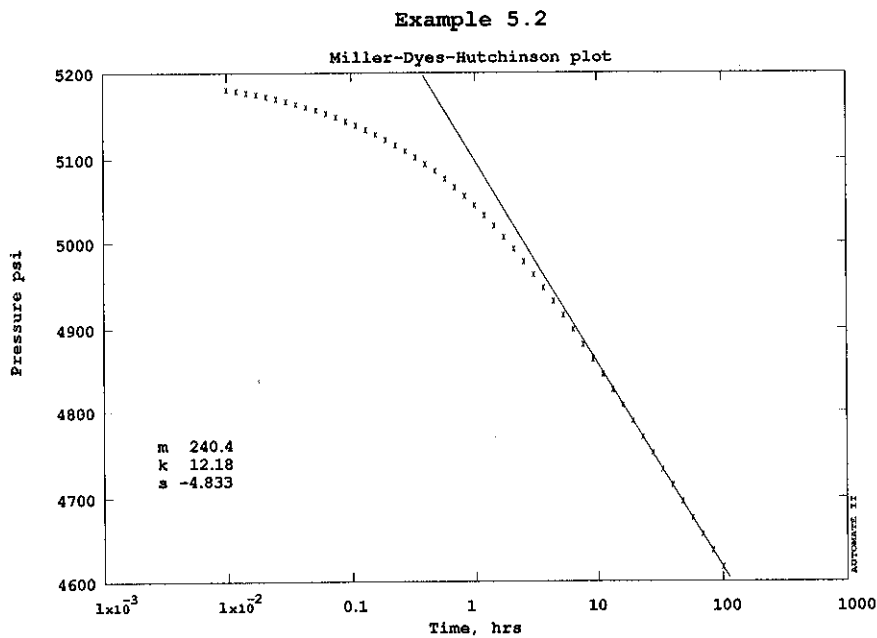


Figure 5.13

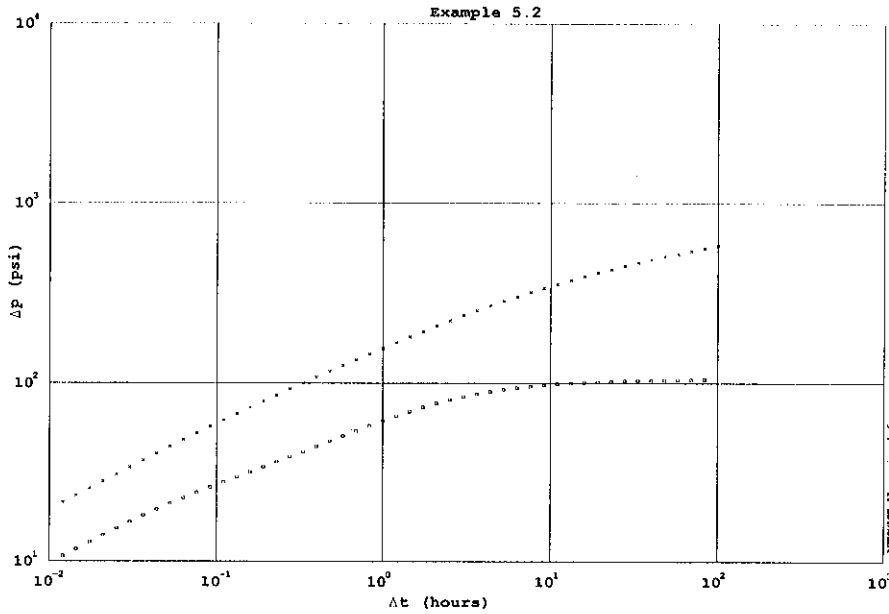


Figure 5.14

In the process of drawing the semilog straight line, it is seen that a negative skin factor of about -5 is estimated, representing a very highly stimulated well. With such a large stimulation, it is very common that the pressure transient behavior can look almost exactly like a normal storage and skin response for stimulated wells, without considering the fracture flow at all. For example, Fig. 5.15 shows a match of the example data to the storage and skin type curve. The poorer match at early time can be improved somewhat by allowing the estimate of the initial pressure p_i to vary by a few psi (Fig. 5.16).

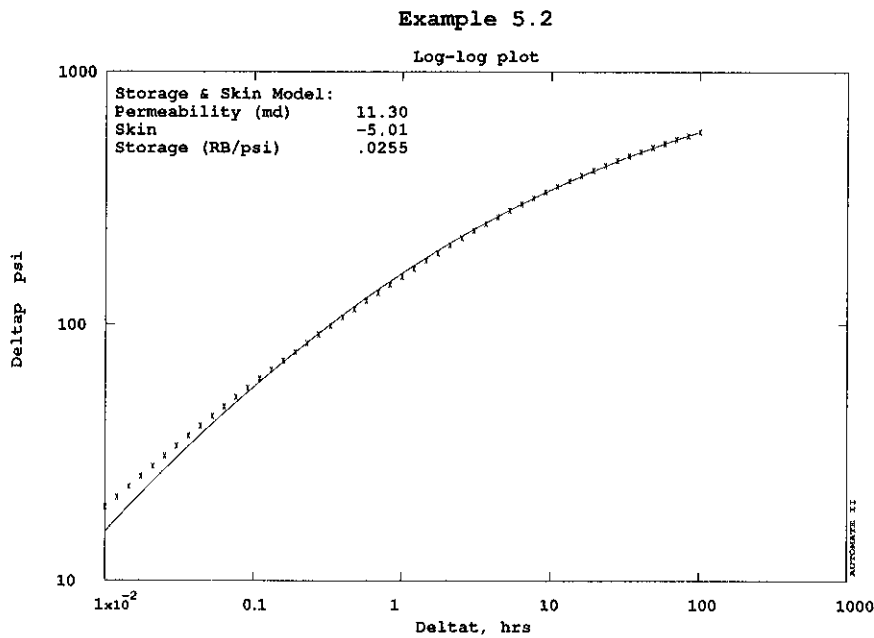


Figure 5.15

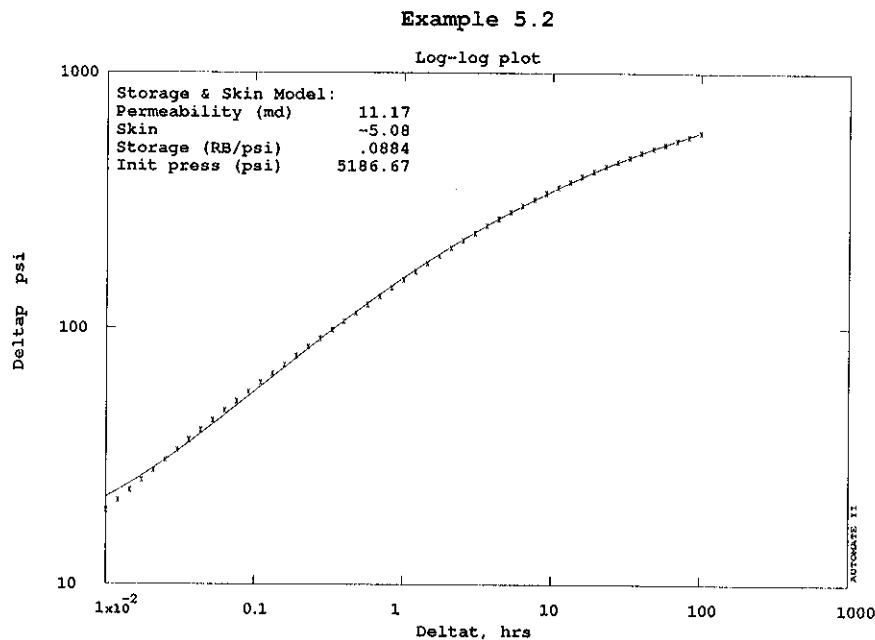


Figure 5.16

Confidence intervals reveal that all parameters except the wellbore storage coefficient were well determined (Table 5.1).

Parameter	Estimate	Confidence Interval (absolute)	Confidence Interval (percent)
Permeability (md)	11.17	$\pm .1462$	$\pm 1.31\%$
Skin	-5.083	$\pm .1913 \times 10^{-1}$	$\pm .38\%$
Storage (RB/psi)	$.8838 \times 10^{-1}$	$\pm .2910 \times 10^{-1}$	$\pm 32.93\%$
Init press (psi)	5187.	± 2.648	$\pm .05\%$

Table 5.1

Plotting the data on the storage and skin type curve (Fig 5.17) reveals why this so. For large negative values of skin factor s , the group $c_D e^{2s}$ takes small values, and the curves show little storage behavior in the usual form of a unit slope log-log line. This may also be true for wells with finite conductivity fractures (such as that in Example 5.1). In fact, it is even possible to match the infinite conductivity fracture type curve itself to the storage and skin type curve.

In summary, these two examples have demonstrated the use of type curves as a means of well test interpretation, in combination with semilog analysis. Reservoir permeability and fracture length can be estimated with good accuracy. Fracture conductivity is not as easy to determine in that it gives rise only to an early time effect, and in any case does not influence the pressure transient very strongly.

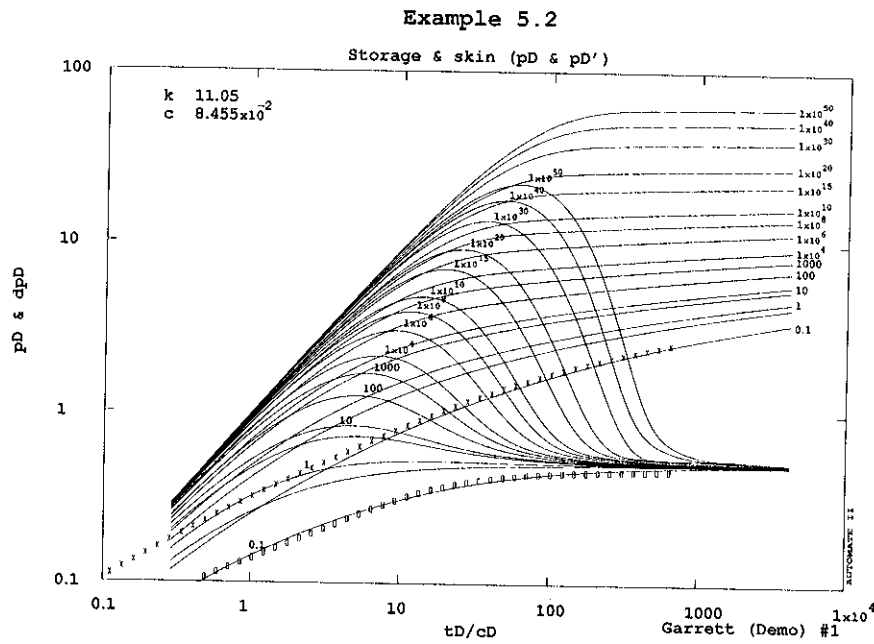


Figure 5.17

The use of type curves in these two examples also serves to emphasize the possibility of ambiguity when doing this kind of analysis. Sometimes more than one reservoir model may fit the data, and it is necessary for the interpretation engineer to make an intelligent evaluation of all information associated with the well (such as geological and geophysical data). Nonlinear regression requires the engineer to choose a model to be matched, although confidence intervals can often be useful to discriminate between model matches. In Example 5.2 here, the infinite conductivity fracture model match gave a better stimulated well model match, although in this case there is no real inconsistency between the two physical models (large fracture and highly stimulated well). Both models correctly estimated the reservoir permeability.

6. EXAMPLE INTERPRETATIONS - DOUBLE POROSITY RESERVOIRS

Double porosity effects occur frequently in naturally fractured reservoirs, and may also be found in formations with thin layering sequences. The pressure transients are characterized by the presence of two separate responses, one for the "primary" porosity (the rock matrix, or lower permeability layers), and the other for the "secondary" porosity (the fractures, or high permeability layers). This has been described earlier in Section 2.8. In this section, we will examine some examples of transients in double porosity reservoirs. Specifically, double porosity analysis is more complex than single porosity analysis, and may require special care to take account of the effects of storage, and of producing time in the case of buildups.

6.1 Drawdown Example

To illustrate the techniques of interpretation, the first example will consider a transient response without storage effect. This is unlikely in practice unless a downhole valve has been used, however serves the purpose of this example. The more realistic example, including storage, will be considered next. The data for this first example are listed in Table 6.1 of the Appendix.

Without the storage effect, the semilog (MDH) plot, Fig. 6.1, shows the expected pair of parallel straight lines.

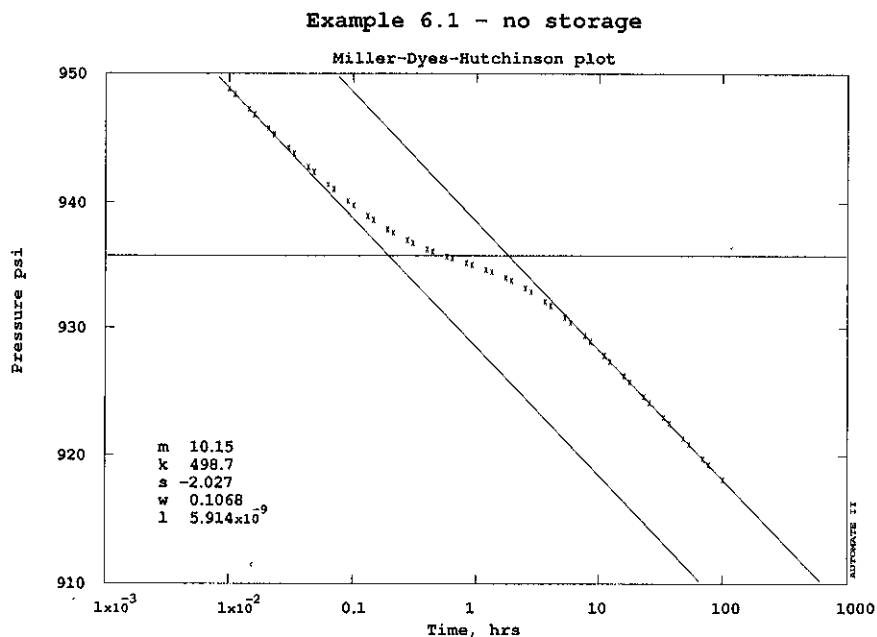


Figure 6.1

The permeability k_f of the *secondary* porosity (the fractures), can be found from the slope of either straight line, using Eq. 2.38:

$$k_f h = 162.6 \frac{q B \mu}{|m|} \quad (6.1)$$

Substituting values:

$$k_f(12) = 162.6 \frac{(1245)(1)(0.3)}{|-10.151|}$$

$$k_f = 500 \text{ md}$$

The skin effect s can be estimated as in a single porosity test, using the *later* semilog straight line, and substituting the value of p_{1hr} (935.6 from Fig. 6.1) in the equation:

$$s = 1.151 \left[\frac{p_i - p_{1hr}}{|m|} - \log \frac{k}{\phi \mu c_f r_w^2} + 3.2274 \right] \quad (6.2)$$

Substituting values:

$$s = 1.151 \left[\frac{1003 - 935.6}{|-10.151|} - \log \frac{500}{(0.033)(0.3)(3 \times 10^{-6})(0.29)^2} + 3.2274 \right] = -1.85$$

The skin effect could also be estimated from the slope of the first straight line, however must then be corrected by $+\frac{1}{2} \ln \omega$. Since ω is rather difficult to determine in many cases, and since the first straight line is often disguised by wellbore storage effects, it is usually better not use the first straight line to estimate skin unless the second straight line is not present (although in such a case, ω would be even more difficult to find).

The value of ω can be estimated from the semilog plot, by measuring the horizontal distance between the two semilog straight lines. Recall that ω reduces by a factor of ten for each log cycle between the two lines. From Fig. 6.1, it is seen that the lines are one log cycle apart, so the estimated value of ω is 0.1. To determine this estimate specifically, it is necessary only to pick two time values, t_1 and t_2 , one from each line at the same pressure level. ω is then found from:

$$\omega = \frac{t_1}{t_2} \quad (6.3)$$

where t_1 is a time point on the earlier straight line, and t_2 is on the later straight line.

λ may be estimated from the level of the horizontal line passing through the double porosity transition region. Finding the time at which the horizontal line meets the *later* semilog line (2 hrs in Fig. 6.1), λ can be found from:

$$t_D = \frac{1-\omega}{2\lambda} = \frac{0.000264 k_f t}{(\phi_f c_{fj} + \phi_m c_{mj}) \mu r_w^2} \quad (6.4)$$

$$\frac{1-0.1}{2\lambda} = \frac{0.000264(500)(2)}{(0.033)(3 \times 10^{-6})(0.3)(0.29)^2}$$

$$\lambda = 4.26 \times 10^{-9}$$

Examination of the derivative plot, Fig. 6.2, shows the "dip" caused by the double porosity transition, between the two flat regions representing the two semilog straight lines. The values of ω and λ can be estimated from the position of the minimum in this dip, using a procedure outlined by Bourdet et al (1989).

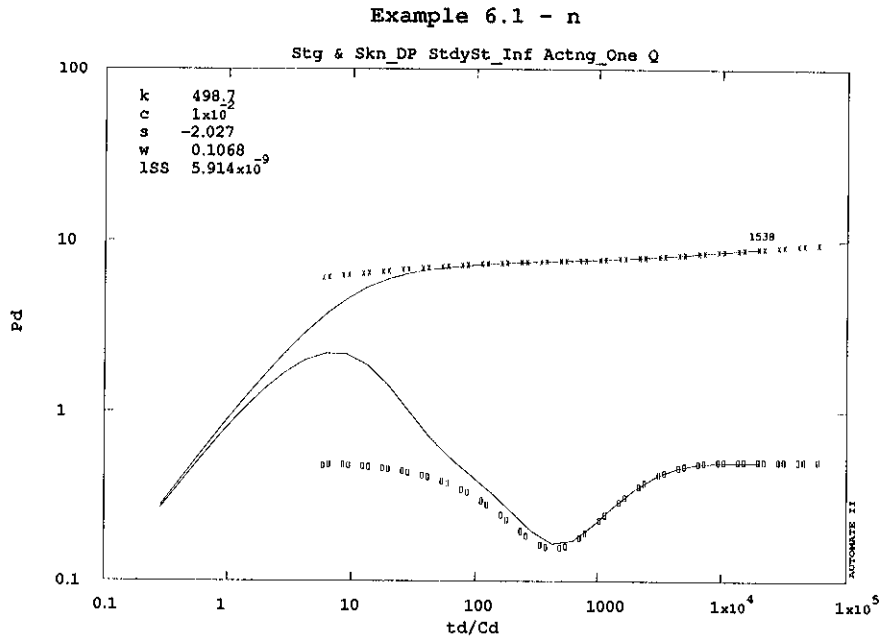


Figure 6.2

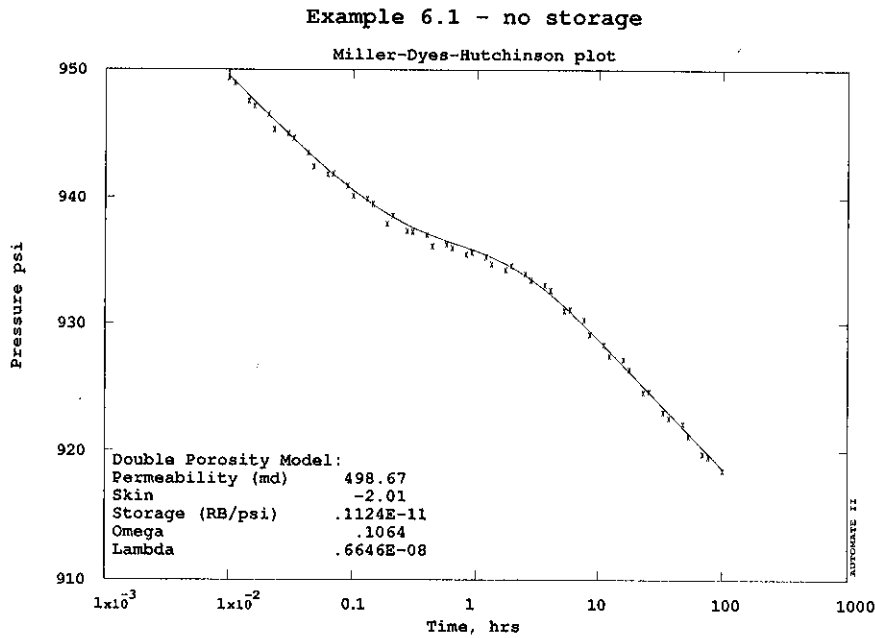


Figure 6.3

A nonlinear regression is able to obtain a good match to the data, Fig. 6.3, with acceptable confidence intervals, Table 6.1. It is interesting to note (and is quite commonly true) that the confidence

interval on ω is rather wide. This is because the data are noisy relative to the level of pressure change (only 30 psi between the second and last data points). Hence there is greater uncertainty as to the separation between the lines.

Parameter	Estimate	Confidence Interval (absolute)	Confidence Interval (percent)
Permeability (md)	498.7	± 16.84	$\pm 3.38\%$
Skin	-2.007	$\pm .2741$	$\pm 13.66\%$
Storage (RB/psi)	$.1124 \times 10^{-11}$	$\pm .3537 \times 10^{-17}$	$\pm .00\%$
Omega	.1064	$\pm .1742 \times 10^{-1}$	$\pm 16.37\%$
Lambda	$.6646 \times 10^{-8}$	$\pm .1110 \times 10^{-10}$	$\pm .17\%$

Table 6.1

Also shown earlier in Fig. 6.2 is a representation of a pressure response with only a very moderate storage effect ($C = 0.01$ RB/psi.). It is seen that such a storage effect would all but cover the first semilog straight line (the first flat portion on the derivative), although the "dip" characteristic of the double porosity transition would still be present and recognisable. This brings us to examine the difficulties introduced into the interpretation when storage is present.

Table 6.1 (a) in the Appendix lists the data from a modified form of Example 6.1, in which wellbore storage is present. Fig. 6.4 shows the semilog (MDH) plot, which is no longer useful for interpreting the double porosity effects since the earlier semilog straight line is not present (the lines drawn in Fig. 6.4 are in the correct position for illustration purposes only, they could not have been found from this plot). The later part of the transition is still present, allowing us to at least recognize that double porosity effects may be present.

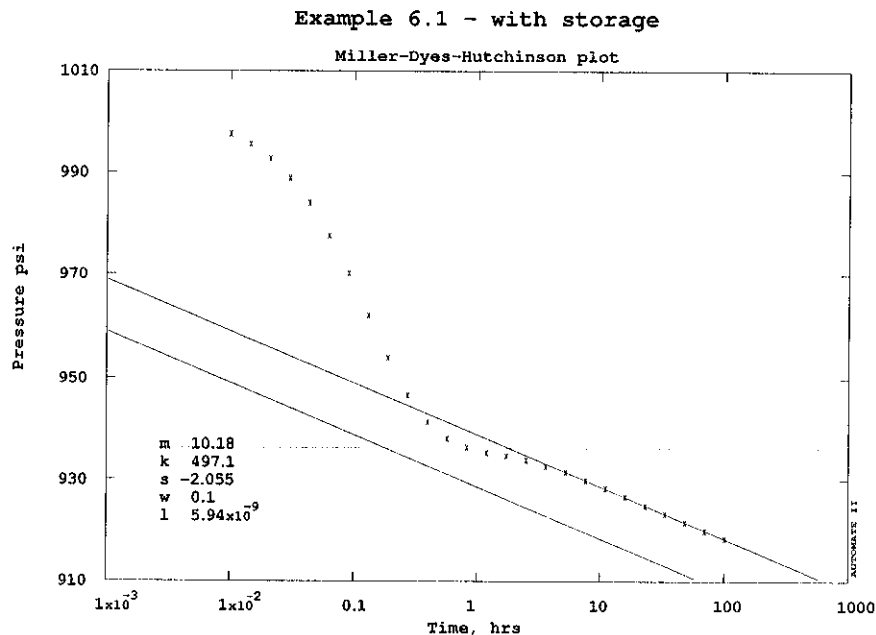


Figure 6.4

A derivative plot, Fig. 6.5, shows us the characteristic "dip", and the values of ω and λ can be estimated from the position of the minimum. However caution is required here -- the earlier presentation in Fig. 6.2 shows that the position of the minimum can be displaced by the wellbore storage effect. Thus

it is seen, not unexpectedly, that there is also difficulty in estimating ω and λ from the derivative plot when storage is present (we cannot expect to estimate a parameter whose influence has been hidden by the effect of another parameter, even though the derivative plot is more diagnostic in this regard than the semilog plot).

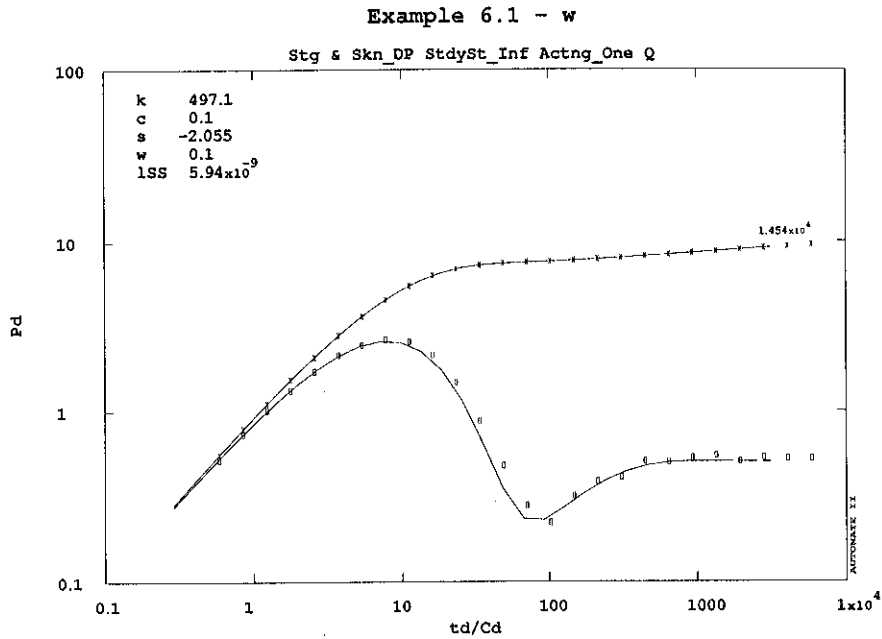


Figure 6.5

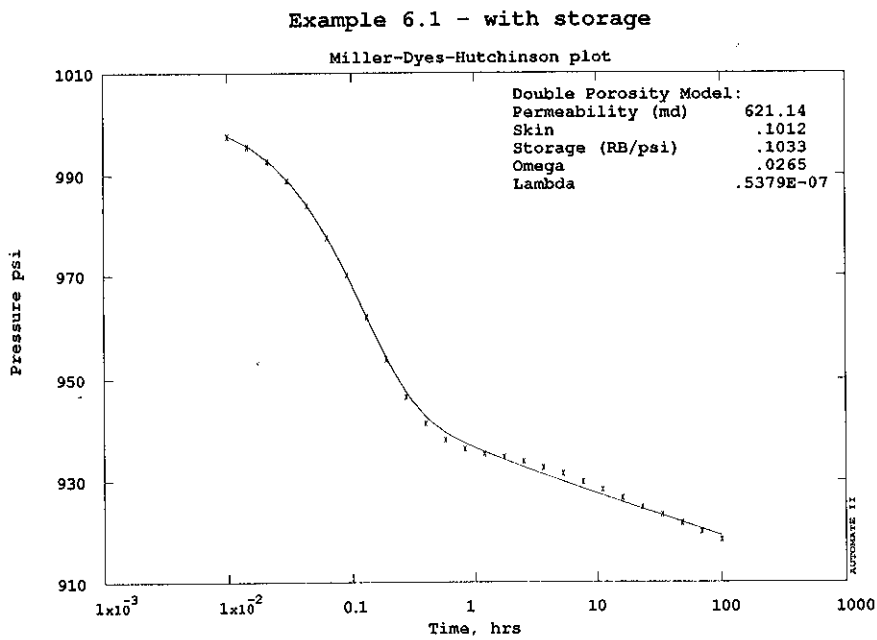


Figure 6.6

The same difficulty is found with nonlinear regression, even though this approach has the greatest precision we can achieve and can often obtain parameter estimates from transition regions. A nonlinear

regression match to the data shows very poor convergence, and the final match does not look good, Fig. 6.6. Luckily, the confidence intervals (Table 6.2) reveal that the match is unacceptable.

Parameter	Estimate	Confidence Interval (absolute)	Confidence Interval (percent)
Permeability (md)	621.1	± 51.11	$\pm 8.23\%$
Skin	.1012	$\pm .8223$	$\pm 812.65\%$
Storage (RB/psi)	.1033	$\pm .4783 \times 10^{-2}$	$\pm 4.63\%$
Omega	$.2654 \times 10^{-1}$	$\pm .1344$	$\pm 506.46\%$
Lambda	$.5379 \times 10^{-7}$	$\pm .3908 \times 10^{-9}$	$\pm .73\%$

Table 6.2

Just as the derivative plot shows more of the double porosity behavior than the semilog plot, we can achieve a better nonlinear regression in double porosity problems if we match to pressure derivatives instead of pressures, provided the data are of sufficient quality to provide smooth derivative values. Fig. 6.7 shows a greatly improved match when derivatives are used in the nonlinear regression, with much better confidence intervals (Table 6.3). Recall that the confidence intervals are always wider when derivatives are used, due to the greater noise in the derivative data. The intervals in Table 6.3 are therefore acceptable (although notice again that the interval on ω is marginal), and more importantly we have obtained the correct answers!

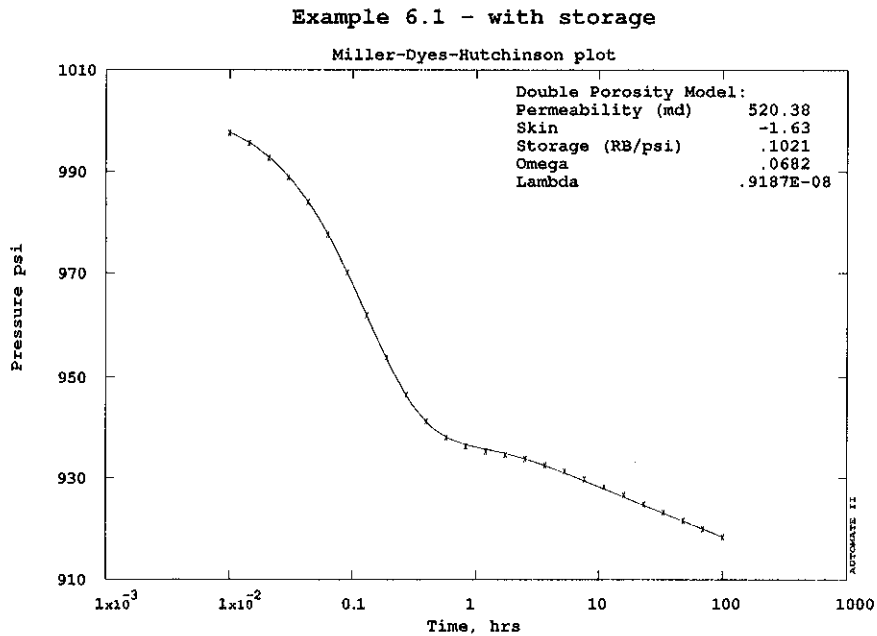


Figure 6.7

The use of pressure derivative matching by nonlinear regression is usually restricted to the double porosity models. This is because the nonlinear regression process is as sensitive to changes in the response as is the derivative plot, and since the use of the derivative in the regression adds noise to the data. In addition, it is not possible to "float" the value of the initial pressure p_i when using the derivative for matching -- we have seen in Sections 3.4.2 and 4.1.1.5 that it is often important to be able to do this. Thus there is little to gain by using the derivative, and often something to lose.

Parameter	Estimate	Confidence Interval (absolute)	Confidence Interval (percent)
Permeability (md)	520.4	± 16.17	± 3.11%
Skin	-1.632	± .2638	± 16.17%
Storage (RB/psi)	.1021	± .2028 × 10 ⁻²	± 1.99%
Omega	.6818 × 10 ⁻¹	± .3585 × 10 ⁻¹	± 52.58%
Lambda	.9187 × 10 ⁻⁸	± .2758 × 10 ⁻¹⁰	± .30%

Table 6.3

6.2 Buildup Example

We have seen earlier in Section 4.2, that buildup responses are more difficult to interpret, since their shape may be distorted by the transients that occurred (or *would have* occurred) in the preceding drawdown. Double porosity tests are particularly prone to this difficulty, since they include so many different features in their response (storage, double porosity transition, infinite acting radial flow, and boundary effect). Any of these may overlap the previous or subsequent feature depending on parameter values (for example, the response may go straight from double porosity transition to boundary effect). In addition, the part of the response that is superposed from the drawdown transient will depend on the length of the producing time. Thus for a short producing time, the first semilog straight line in the buildup response may be superposed on the first semilog straight line in the drawdown, while for a longer producing time it may be superposed on the transition instead.

As an example of the effect of producing time t_p , Fig. 6.8 shows the Horner plot for a test with producing time 50 hours. Fig. 6.9 shows a buildup that is the same in every way except that the producing time was reduced to 25 hours. The first case ($t_p = 50$) reaches the second straight line (which is on the left in a Horner plot), while the second case ($t_p = 25$) does not. Depending on the relative durations of the drawdown and buildup time, the Horner plot may show no second straight line at all in some cases.

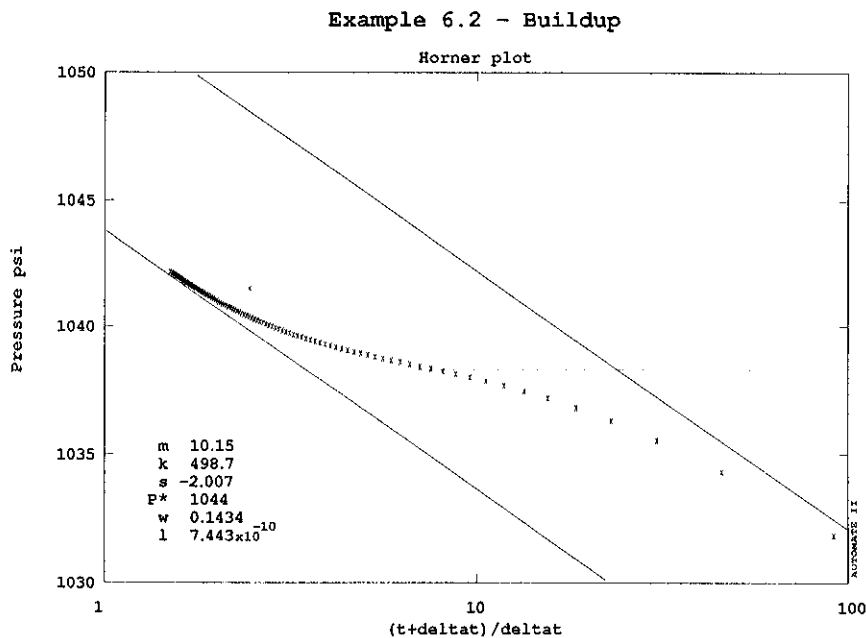


Figure 6.8

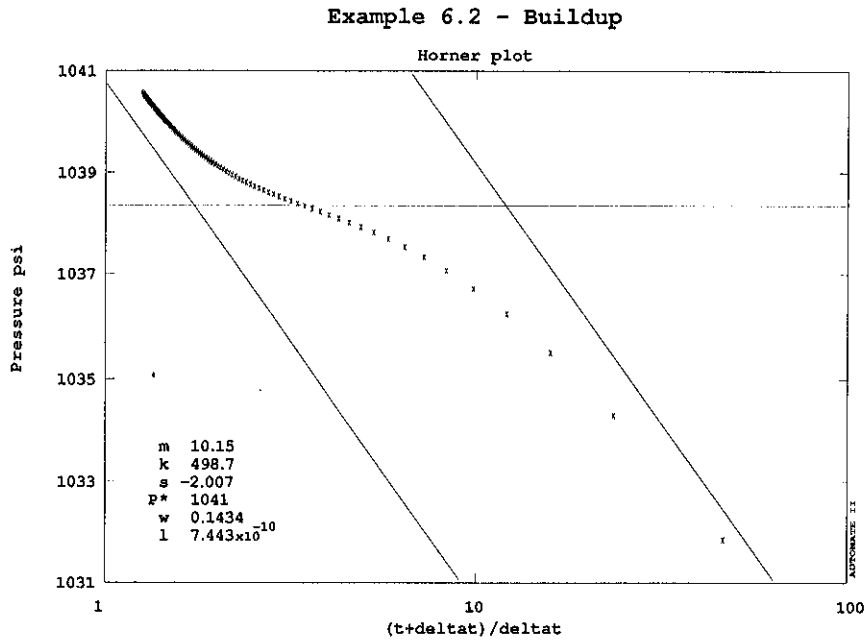


Figure 6.9

We shall examine the data shown in Fig. 6.9, with the producing time of 25 hrs. The data are listed in Table 6.2 in the Appendix. Clearly, the second straight line we would probably have drawn on the Horner plot would have given an incorrect estimate of ω and therefore also of λ . (The second straight line is shown on Fig. 6.9 in the correct position to illustrate this point).

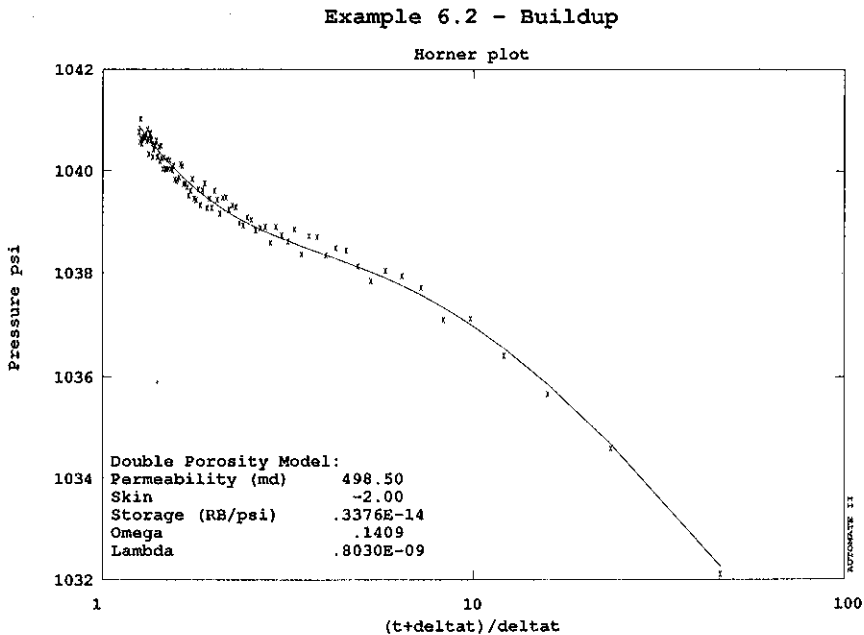


Figure 6.10

Nonetheless, as in the case of single porosity examples, nonlinear regression is unaffected by multiple rate superpositions (such as a buildup), and is able to match the buildup data as easily as drawdown

data (since there is no storage in this case). Fig. 6.10 shows a match to the data, and Table 6.4 lists the confidence intervals, which are all good (pressure matching was used in this case, since the data are too noisy to use the derivative). The answers obtained are correct.

Parameter	Estimate	Confidence Interval (absolute)	Confidence Interval (percent)
Permeability (md)	498.5	± 42.20	± 8.46%
Skin	-2.004	± .7226	± 36.07%
Storage (RB/psi)	$.3376 \times 10^{-14}$	± $.2023 \times 10^{-19}$	± .00%
Omega	.1409	± $.2367 \times 10^{-1}$	± 16.79%
Lambda	$.8030 \times 10^{-9}$	± $.3203 \times 10^{-12}$	± .04%

Table 6.4

From these examples we have seen that double porosity analysis is often more difficult than single porosity analysis. In particular, it is rather easy to obtain the wrong answer by analysing the dip in the derivative curve when storage is present. Nonlinear regression is helpful for this problem, however must also be applied with care. Nonlinear regression also provides a useful way of circumventing the effect of producing time in buildup tests.

Finally, it should also be noted that the double porosity parameters ω and λ are rather poorly estimated by any of these methods of analysis. Although we have been able to obtain the correct answers in these examples, there remains a greater uncertainty in the estimates of ω and λ than in the estimates of the other parameters.

6.3 References

Bourdet, D., Ayoub, J.A., and Pirard, Y-M.: "Use of the Pressure Derivative in Well Test Interpretation", *SPE Formation Evaluation*, (June 1989), 293-302.

7. EXAMPLE INTERPRETATIONS - INTERFERENCE TESTS

Interference testing differs from standard drawdown and buildup testing in that more than one well is used. One well (the "active" well) is put on production or injection, and another well (the "observation" well), which is not in production, is monitored for changes in pressure caused by operation of the first. The advantage of interference testing is that a much greater area of the reservoir is tested, providing estimates of reservoir properties between wells. In addition, the interference response is little affected by the complicating factors of wellbore storage and skin effect that make single well test interpretation more difficult. Furthermore, the nature of the response over distance makes it possible to estimate not only the reservoir transmissivity (kh), but also storativity ($\phi c_r h$). The disadvantage is that pressure drops can be very small over distance, and are affected by other operational variations in the field at large. Nonetheless, modern electronic gauges are quite capable of registering such small pressure drops (often less than 1 psi over days or even weeks), and thus interference testing is a useful method of proving up new discoveries. In new reservoirs, an interference test is not affected by other production in the field (since there is none) and serves to prove the existence of productive reservoir between the wells.

7.1 Single Well Pair Example

The following example is real data from a reservoir in which several wells were drilled over a wide spacing to explore the extent of the field. The producing well was 3353 feet from the observation well, and the pressure was monitored in the observation well when the production well was shut in after producing for 49 days. The test data are summarised in Table 7.1 in the Appendix, and illustrated in Fig. 7.1. Notice that the entire pressure change in the observation well, even over 16 days, was only about 1.5 psi.

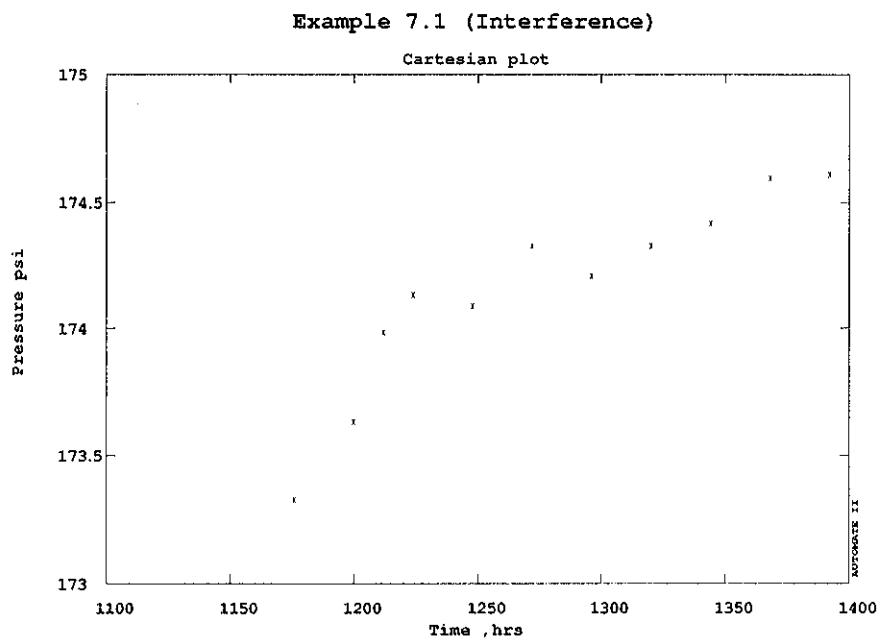


Figure 7.1

Even though an interference test still uses the same radial flow analysis as a single well test, the difference arises due to the effect of the radial distance at which the pressure is measured. The radial flow behavior in an infinite reservoir follows the exponential integral behavior:

$$p_D = -\frac{1}{2} Ei\left(-\frac{r_D^2}{4t_D}\right) \quad (7.1)$$

which for r_D of 1 (i.e. at the wellbore) follows a behavior that is very close to $\log(t)$ (described by Eq. 2.27). However in an interference test r_D can be large, giving rise to values of t_D/r_D^2 that will be small. Over this range, the exponential integral Ei no longer shows $\log(t)$ behavior. This is an advantage for the interpretation of interference tests, since the slope of a semilog straight line provides only one reservoir parameter estimate (kh). For small values of t_D/r_D^2 the semilog straight line develops into a curve, and it is possible to estimate both kh as well as $\phi c_r h$ by type curve matching or by nonlinear regression.

Fig. 7.2 shows a match to the exponential integral type curve (sometimes known as the line source type curve, or Theis curve). Using the pressure match point;

Match point (pressure): $\Delta p = .3087 \text{ psi}$, $p_D = .318$

$$p_D = \frac{kh \Delta p}{141.2 q B \mu} = \frac{kh (.3087)}{141.2 (38292.08)(1)(.115)} = .318$$

$$kh = 640400 \text{ md-ft}$$

Match point (time): $t = 24 \text{ hrs}$, $t_D/r_D^2 = .909$

$$t_D = .909 \times (3353/.33)^2 = \frac{0.000264 kh t}{\phi h \mu c_r r_w^2} = \frac{0.000264(640400)(24)}{\phi h (.115)(8.84 \times 10^{-6})(.33)^2} = 9.380337 \times 10^7$$

$$\phi h = 390.724 \text{ ft}$$

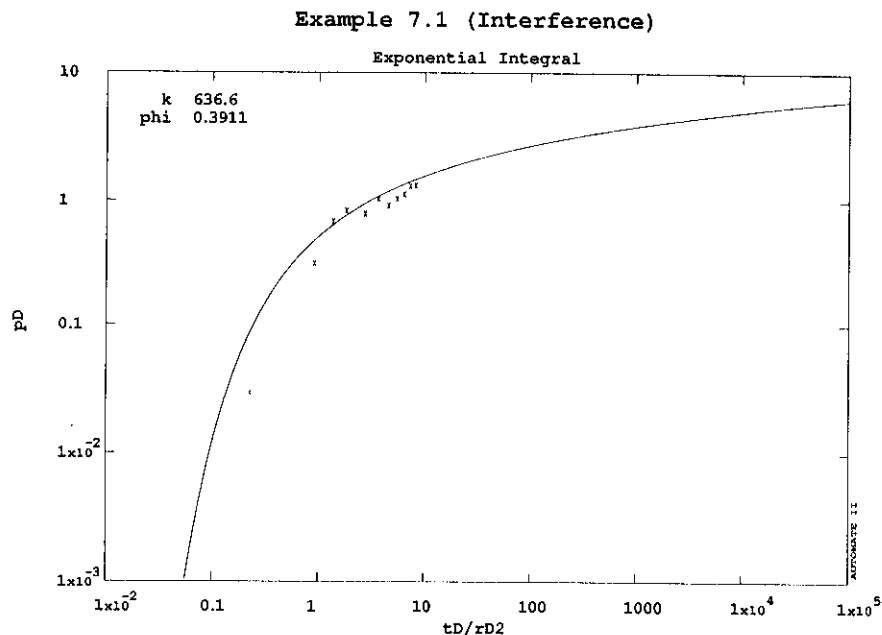


Figure 7.2

The porosity-thickness product ϕh is estimated to be 390 ft. With a circular area represented by the 3353 ft radius between the wells, ($353 \times 10^6 \text{ ft}^2$), the total estimated reservoir pore volume represented by

these two wells would be $1.38 \times 10^{10} \text{ ft}^3$. This is a very valuable parameter to have been able to estimate, as it bears directly on the reserve estimates for the field.

Nonlinear regression leads to similar estimates (Table 7.1). In this example the confidence intervals are very wide, mainly due to the few data as well as to the relative noise.

Parameter	Estimate	Confidence Interval (absolute)	Confidence Interval (percent)
kh (md-ft)	$.6404 \times 10^6$	$\pm .2505 \times 10^6$	$\pm 39.11\%$
ϕh (ft)	390.7	± 302.6	$\pm 77.46\%$
p_i (psi)	175.2	$\pm .3331$	$\pm .19\%$

Table 7.1

To check the consistency of the estimates, we can also look at the semilog (MDH or Horner) plot, since the later part of the data may reach to a semilog behavior (it need not necessarily always do so). Fig. 7.3 shows that it does in this case, and that the intercept of the line indicates a skin effect of zero, which must be the case if the interpretation is correct in using the radial flow model.

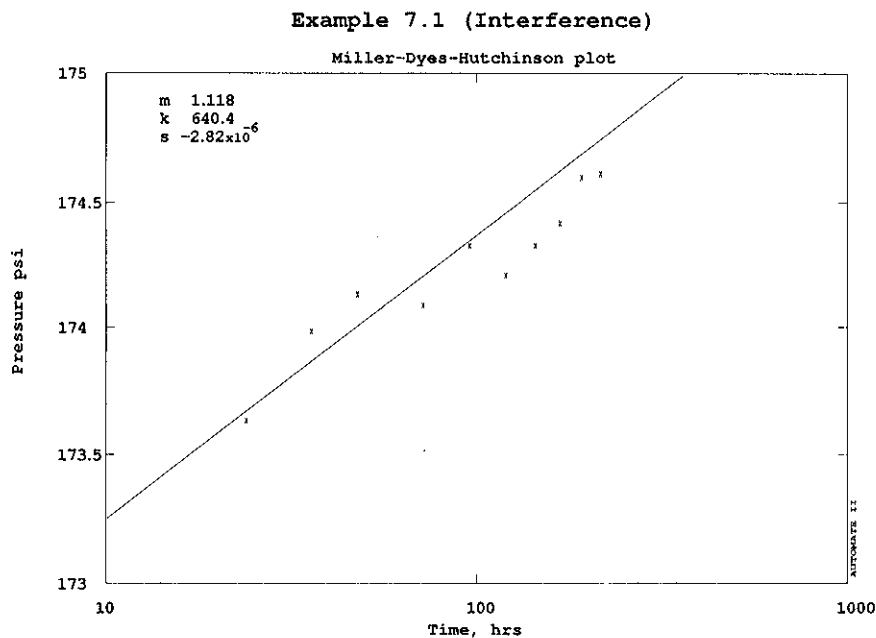


Figure 7.3

7.2 Multirate Example

From Example 7.1 it has been seen that an interference test provides very valuable during the evaluation of a reservoir, but that interpretation may be made more difficult since noise tends to mask the very small pressure changes. Considerable improvement to the interpretation can be made if more than one flow period is included in the data.

Example 7.2, with data listed in Table 7.2 of the Appendix, shows an interference test in which water was injected into the active well, and the pressure monitored in the observation well both during

the injection as well as during the subsequent falloff (this same example appears in Earlougher's 1977 well testing monograph, as Example 9.1). The continuation of monitoring after shut-in provides a longer set of data, and also provides a consistency check. Fig. 7.4 shows the flow rate in the active well, and Fig. 7.5 shows the corresponding response in the observation well.

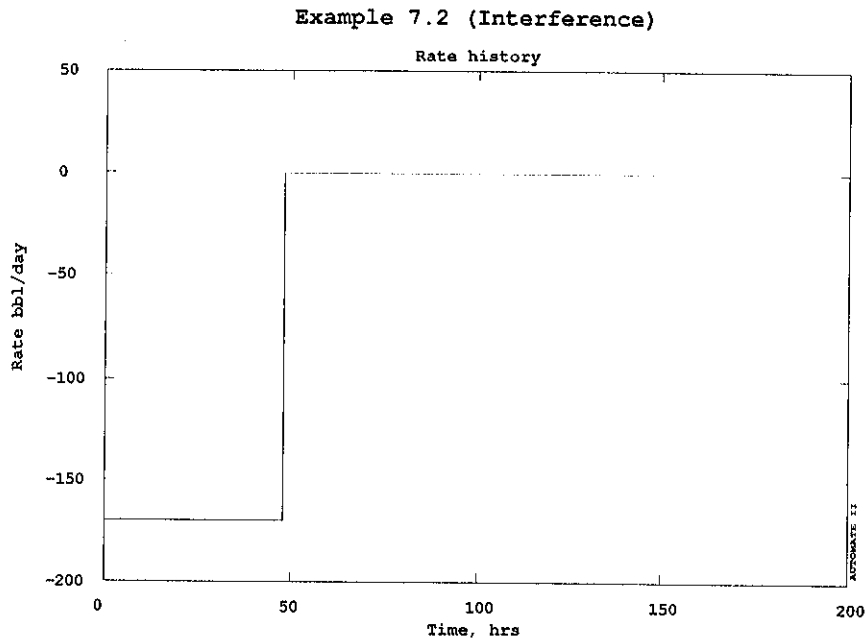


Figure 7.4

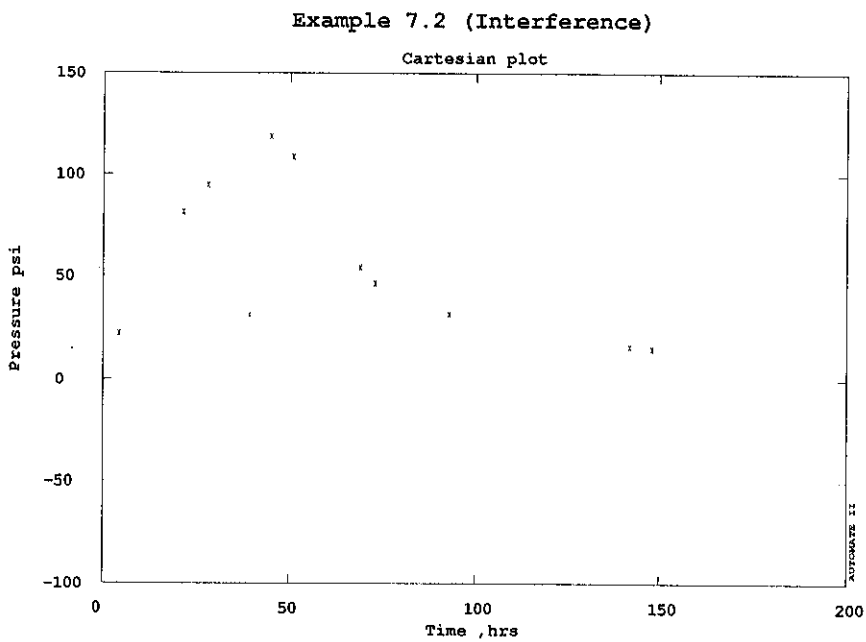


Figure 7.5

This data can be matched to a special form of the exponential integral or line source type curve developed by Henry J. Ramey, Jr., of Stanford University. This type curve (Fig. 7.6) includes both draw-down as well as buildup, and can be used to match both parts of the data at the same time.

Match point (pressure): $\Delta p = 22 \text{ psi}$, $p_D = .227$

$$p_D = \frac{kh \Delta p}{141.2 q B \mu} = \frac{kh (22)}{141.2 (170)(1)(1)} = .227$$

$$kh = 247.86 \text{ md-ft}$$

Match point (time): $t = 43.7 \text{ hrs}$, $t_D/r_D^2 = 4.558$

$$t_D = 4.558 \times (119/.25)^2 = \frac{0.000264 kh t}{\phi h \mu c_t r_w^2} = \frac{0.000264(247.86)(43.7)}{\phi h (1)(.000009)(.25)^2} = 1032781$$

$$\phi h = 4.922 \text{ ft}$$

Example 7.2 (Interference)

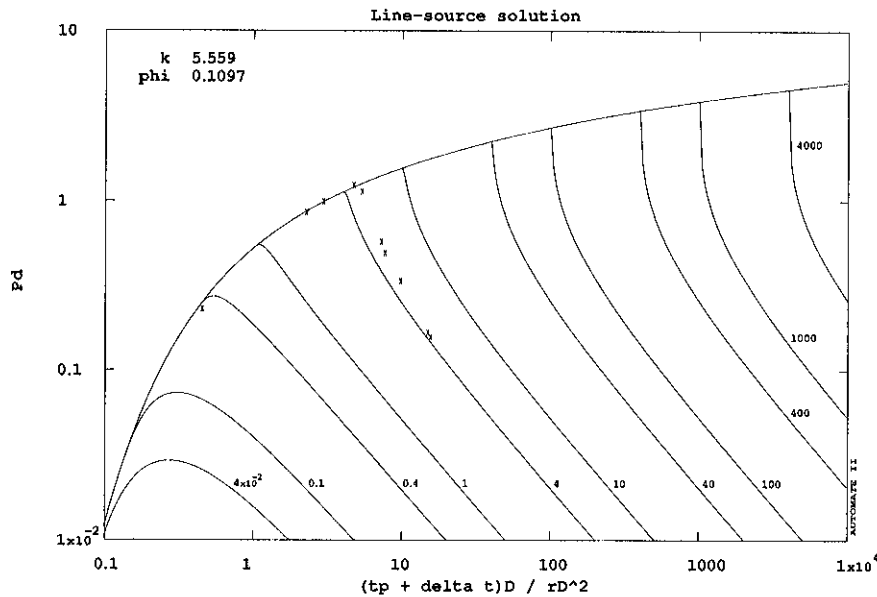


Figure 7.6

Nonlinear regression achieves a good match to both parts of the response at the same time (since nonlinear regression can accommodate any sequence of flow rates), and shows a good visual match (Fig 7.7) as well as acceptable confidence intervals (Table 7.2).

Parameter	Estimate	Confidence Interval (absolute)	Confidence Interval (percent)
kh (md-ft)	247.8	± 14.21	$\pm 5.73\%$
ϕh (ft)	4.922	$\pm .4936$	$\pm 10.03\%$

Table 7.2

Example 7.2 (Interference)

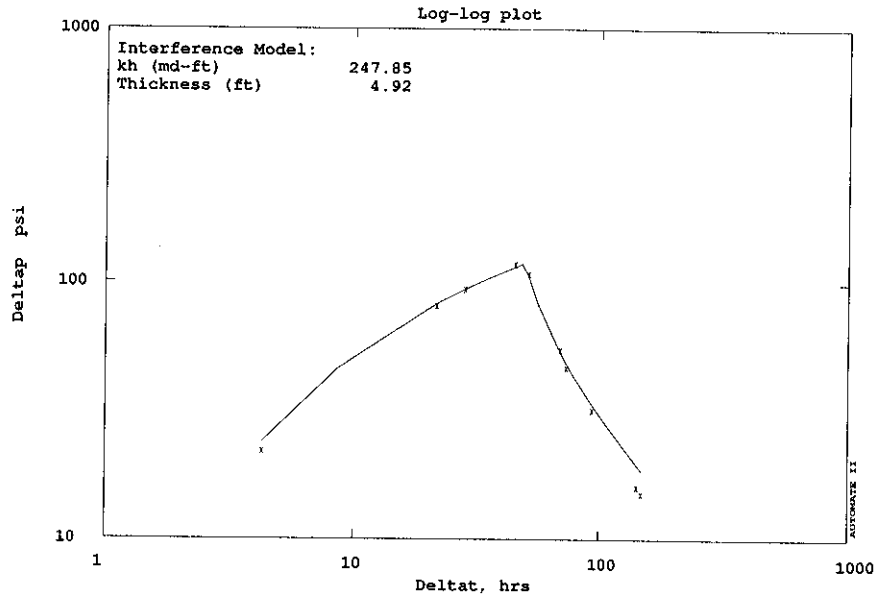


Figure 7.7

7.3 References

Earlougher, R.C., Jr.: "Advances in Well Test Analysis", Society of Petroleum Engineers Monograph 5, Dallas, TX, (1977).

8. GAS WELL TESTS

The analysis of gas well tests is made more complex by the fact that gas properties are strong functions of pressure, hence the equations governing pressure transmission through gases in a porous medium are nonlinear. Since all of the solutions derived for pressure transient analysis of liquid filled reservoirs are based on the slightly compressible pressure transmission equation (Eq. 2.2), it may seem at first as if none of these solutions would be applicable to the interpretation of gas well tests. Fortunately, by suitable definition of alternative variables, specifically the use of pseudopressure and pseudotime instead of pressure and time, most of the slightly compressible solutions can be modified for application to gas well test analysis.

8.1 Real Gas Pseudopressure and Pseudotime

The viscosity μ and compressibility c_g of real gases are strong functions of pressure, and it is not correct to apply the normal (slightly compressible) assumption when deriving the differential equations governing the pressure transients. However, if the gas is treated as obeying the real gas equation:

$$pV = znRT \quad (8.1)$$

then the governing differential equations can be linearised (approximately) by the definition of a variable termed the *real gas pseudopressure* by the workers who first defined it (Al-Hussainy and Ramey, 1966, and Al-Hussainy, Ramey and Crawford, 1966). The real gas pseudopressure is defined as:

$$m(p) = 2 \int_{p_0}^p \frac{p dp}{\mu z} \quad (8.2)$$

where the base pressure p_0 is an arbitrary pressure, usually at the lowest end of the range of pressures of interest during the test.

This definition of the real gas pseudopressure results in an equation governing pressure transmission as:

$$\frac{\partial^2 m(p)}{\partial r^2} + \frac{1}{r} \frac{\partial m(p)}{\partial r} = \frac{\Phi \mu c_t}{k} \frac{\partial m(p)}{\partial t} \quad (8.3)$$

This equation is linear with respect $m(p)$, except for the fact that the terms $\Phi \mu c_t/k$ are still functions of pressure (and therefore of pseudopressure). In practice, this remaining nonlinearity is not usually of consequence, and is often permissible to treat the equation as linear, substituting the values of viscosity μ and compressibility c_t defined at the initial reservoir pressure p_i (or at the highest pressure measured during the test if the initial reservoir pressure is not known). In cases where the gas compressibility variations with pressure are significant (such as may occur if the gas pressures are very low e.g. < 100 psia), the equations can be linearised further by the introduction of the pseudotime.

Pseudotime was introduced by Agarwal (1979) and its use described by Lee and Holditch (1982). Agarwal's pseudotime is defined as:

$$t_p = \int_0^t \frac{1}{\mu c_t} dt \quad (8.4)$$

However, the Agarwal definition of pseudotime is somewhat unintuitive to use, since it does not have units of time and therefore makes visual examination of the data plots more difficult. Recently, a new formulation for pseudopressure and pseudotime was introduced by Meunier, Kabir and Wittman (1987). These new normalized pseudofunctions allow the use of liquid flow solutions without special modification for gas flow, since the newer definitions have the same units as pressure and time. The Meunier *et al* definitions of normalized pseudopressure and normalized pseudotime are:

$$p_{pm} = p_i + \frac{\mu_i z_i}{p_i} \int_{p_i}^p \frac{p dp}{\mu z} \quad (8.5)$$

$$t_{pm} = \mu_i c_{t_i} \int_0^t \frac{1 dt}{\mu c_t} \quad (8.6)$$

By using the Meunier *et al* definitions of normalized pseudopressure and normalized pseudotime there is no need to modify any of the liquid analysis equations. Nonetheless, since the use of real gas pseudopressure (the original definition, given by Eq. 8.2) is traditional, the original application will be described here. Since it is usually not necessary to use pseudotime at all, the applications will be described here in terms of real time - in cases of low gas pressures, the Meunier *et al* normalized pseudotime can be used as a direct replacement of the time variable.

It is fortunate indeed that the pseudopressure transient equation (Eq. 8.3) is exactly the same as the pressure transient equation (Eq. 2.2) used for oil and water well transient analysis. This means that all of the liquid (slightly compressible) solutions can also be used for the analysis of gas well tests.

In the same manner as the dimensionless pressure was defined to nondimensionalise the differential equation, a dimensionless pseudopressure can also be defined for use with gas wells:

$$m_D = \frac{1.987 \times 10^{-5} kh T_{sc} [m(p_i) - m(p)]}{p_{sc} T q_{sc}} \quad (8.7)$$

where p_{sc} and T_{sc} are the pressure and temperature at standard conditions (usually 14.7 psia and 60 ° F or 520 ° R), and q_{sc} is the gas flow rate measure at standard conditions, measured in MCF/d. It is important to note that the temperatures in this equation, both T and T_{sc} are expressed in absolute units (° R), since they originate from the real gas equation.

The dimensionless time is defined the same as for liquid wells, however it should be remembered that viscosity μ and compressibility c_t are to be evaluated at initial reservoir pressure.

$$t_D = \frac{.000264 kt}{\phi(\mu c_t)_i r_w^2} \quad (8.8)$$

Once dimensionless variables are defined in this way, then m_D can replace p_D in any of the solutions or type curves developed for slightly compressible fluid transients.

8.2 Calculating Pseudopressures

To calculate pseudopressures from a set of pressure data, it is necessary to evaluate the integral expressed by Eq. 8.2. This is usually done numerically, since the properties may not be definable functions of pressure. The numerical integration is best done using a computer, and can be handled either by specially written programs, or by a spreadsheet approach. The steps involved are summarized in Table 8.1, which shows a spreadsheet calculation of the integral using input values of pressure p , viscosity μ , and z factor.

p (psia)	μ (cp)	z	Δp	$\frac{p}{\mu z}$	$(\frac{p}{\mu z})_{avg}$	$2\Delta p(\frac{p}{\mu z})_{avg}$	$m(p) (\frac{psia^2}{cp})$
14.7	0.01198	0.9987		1228.642			
200	0.01235	0.9839	185.3	16459.32	8843.984	3277580.	3277580.
400	0.01277	0.9686	200	32338.85	24399.09	9759636.	13037217
600	0.01319	0.9544	200	47662.41	40000.63	16000253	25759889
800	0.01362	0.9414	200	62393.40	55027.90	22011163	38011416
1000	0.01405	0.9296	200	76564.51	69478.96	27791584	49802748
1200	0.0145	0.9194	200	90013.72	83289.12	33315649	61107234
1400	0.01496	0.9107	200	102759.2	96386.50	38554603	71870253
1600	0.01542	0.9038	200	114805.6	108782.4	43512989	82067592
1800	0.01589	0.8986	200	126061.4	120433.5	48173414	91686403
2000	0.01636	0.8953	200	136545.7	131303.5	52521429	1.0069E8

Table 8.1: Real gas pseudopressure calculation

The integration uses the trapezoidal rule to evaluate:

$$m(p) = 2 \sum_{i=2}^n \frac{1}{2} [(\frac{p}{\mu z})_{i-1} + (\frac{p}{\mu z})_i] (p_i - p_{i-1}) \quad (8.9)$$

Figure 8.1 illustrates the nonlinearity of pseudopressure as a function of pressure, by plotting the data from Table 8.1.

8.3 Using Pseudopressure in Graphical Interpretation

After calculating the pseudopressure as described in the previous section, normal graphical interpretation can proceed exactly as when using pressure for liquid wells. However, due to the different definition of the variable, the calculation equations must be modified.

In semilog analysis (MDH or Horner) the slope of the semilog straight line during infinite acting behavior is given as:

$$m = \frac{5.794 \times 10^4 q_{sc} p_{sc} T}{khT_{sc}} \quad (8.10)$$

(Be careful not to be confused by the use of the symbol m for the slope; this is not the pseudopressure, which is always written $m(p)$). Eq. 8.10 is used as before, to estimate permeability-thickness kh . The

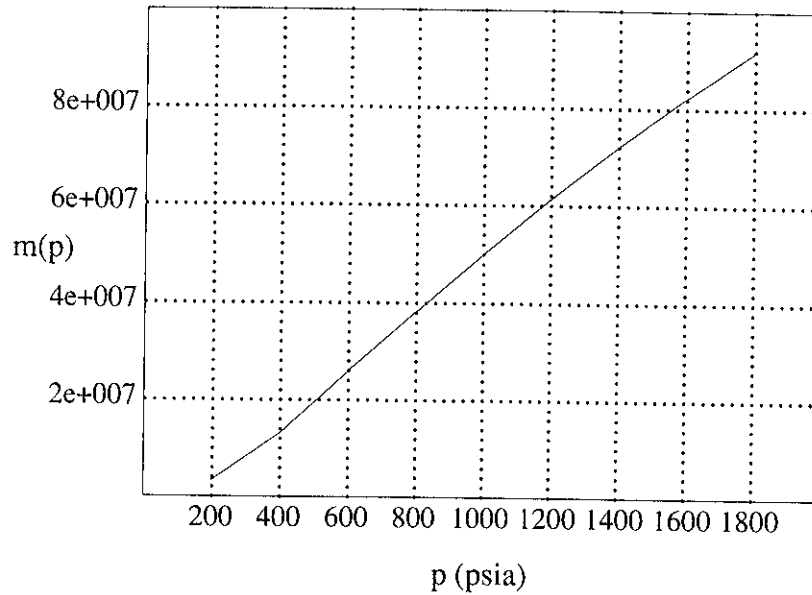


Figure 8.1

skin factor can be calculated from:

$$s = 1.151 \left[\frac{m(p_i) - m(p_{1hr})}{m} - \log \frac{k}{\phi(\mu c_t)_i r_w^2} + 3.2274 \right] \quad (8.11)$$

or for a Horner plot:

$$s = 1.151 \left[\frac{m(p_{1hr}) - m(p_{wf})}{m} - \log \frac{kt}{(t+1) \phi(\mu c_t)_i r_w^2} + 3.2274 \right] \quad (8.12)$$

Wellbore storage coefficient C can be evaluated from a point $[\Delta t, \Delta m(p)]$ on the unit slope, log-log line as:

$$C = \frac{83.39 p_{sc} T q_{sc} \Delta t}{T_{sc} \mu_i \Delta m(p)} \quad (8.13)$$

The dimensionless storage coefficient C_D is calculated from the estimate of C as before:

$$C_D = \frac{C}{2\pi \phi(c_t)_i h r_w^2} \quad (8.14)$$

Type curve matching is performed just as in the liquid well case, using the definitions of the dimensionless variables, Eqs. 8.7 and 8.8, to estimate kh . For example, if $m(p)$ is a pseudopressure data point, and m_D is the corresponding point on the type curve after matching, then:

$$kh = \frac{p_{sc} T q_{sc} m_D}{1.987 \times 10^{-5} T_{sc} m(p)} \quad (8.15)$$

For boundary analysis, m_D is used exactly as was p_D for liquid well cases. So, for example, during pseudosteady state the drainage area can be estimated by using:

$$m_D = 2\pi t_{DA} + \frac{1}{2} \ln \left[\frac{2.2458A}{C_A r_w^2} \right] + s \quad (8.16)$$

8.4 Rate Dependent Skin Effect

A remaining difficulty in gas well test interpretations lies in the non-linearity of the boundary conditions, and this is not easily overcome. The difficulty arises due to the "turbulent" or non-Darcy flow effects close to the wellbore, which appear as a rate-dependent skin (Muskat, 1946, Katz et al, 1959, Wattenbarger and Ramey, 1968). The total skin effect is thus comprised of a constant part s' together with a rate dependent part Dq_{sc} :

$$s = s' + Dq_{sc} \quad (8.17)$$

The constant part of the skin factor s' is due to the wellbore damage effect, while the rate dependent part is a function of the flow rate. To correctly identify the condition of the well, as well as to evaluate the absolute open flow potential (AOFP), it is clearly desirable to be able to separately evaluate the two different skin effects. It is this estimation of the rate dependent effect that requires gas wells to be tested at a variety of rates, using the well known flow-after-flow (Rawlins and Schellhardt, 1936), isochronal (Cullender, 1955) or modified isochronal tests (Katz et al, 1959, Aziz, 1967, and Brar and Aziz, 1978). Of these methods, only the modification of Brar and Aziz, 1978, avoids the necessity of running the test until flow stabilization is achieved. Thus all of these methods of interpretation require well tests of quite long duration. More recently, Meunier, et al (1987) showed how the inclusion of flow data into the analysis allows the test to be of much shorter duration. This important study demonstrated the advantages of including additional measurements into pressure transient tests as proposed earlier by Kucuk and Ayestaran (1985). Meunier, et al (1987) used a "rate-normalized quasipressure" to reduce the variable rate test to an equivalent single rate test. This idea permits such a test to be analyzed as if the test had been at constant rate. Unfortunately, the non-Darcy skin effect must be included as a correction in the Meunier et al (1987) "rate-normalized quasipressure", after which it is necessary to substitute values of the non-Darcy skin parameter by trial and error until a semilog straight line is obtained. There are two disadvantages in doing this: firstly the reservoir may show a response other than radial flow (double porosity or fracture flow would be common alternatives in tight gas reservoirs) and secondly the trial and error procedure is awkward to perform.

Nonlinear regression provides a more straightforward method of estimating the rate dependent skin factor D , as long as the well has been flowed at different rates during the test. In cases where a downhole flow measurement has been made, it has even been possible to estimate D and AOFP with a single rate test (Horne and Kuchuk, 1988).

8.5 Example Interpretation

Example 8.1 is a drawdown test in which a gas well was produced at five successively greater flow rates for four hours each. Figure 8.2 shows the pseudopressure as a function of time, and Fig. 8.3 shows the flow rate history.

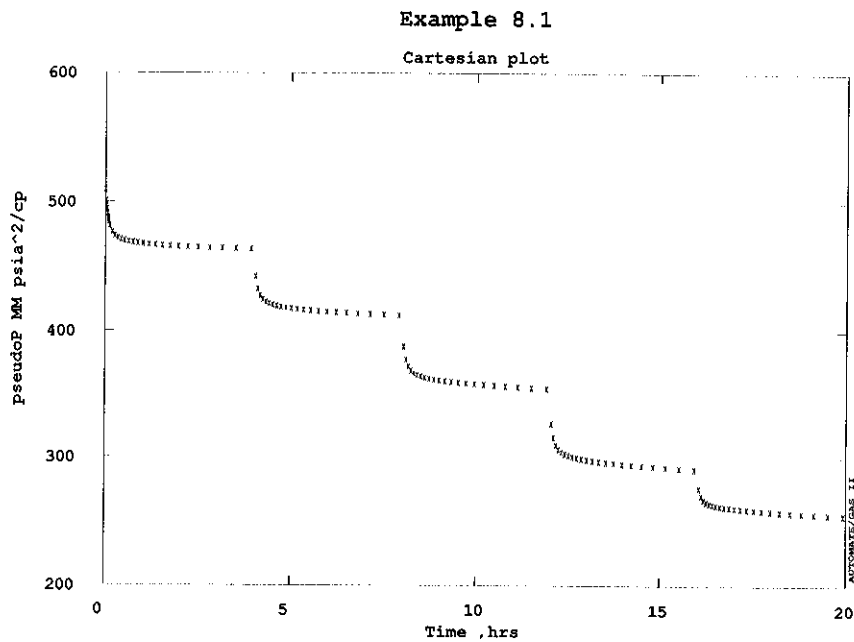


Figure 8.2

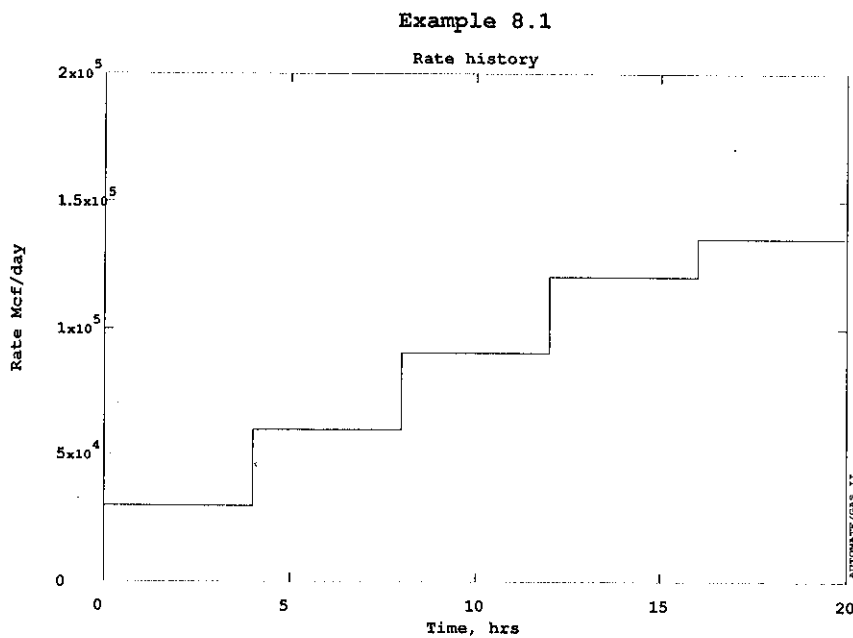


Figure 8.3

Analyzing the semilog plots is made more difficult by the need to specify a flow rate, while there were five different flow rates during the test. A multirate (rate convolution) plot, as in Fig. 8.4, illustrates the straight line portions of the data suggestive of infinite acting radial flow. However, the skin effect is seen to progressively increase with each increase in flow rate (compare the skin factor estimate of 1.669 from the first flow rate line in Fig. 8.4 with the estimate of 2.338 from the third flow rate line in Fig. 8.5). It is clear that there is a rate dependent skin effect in this case.

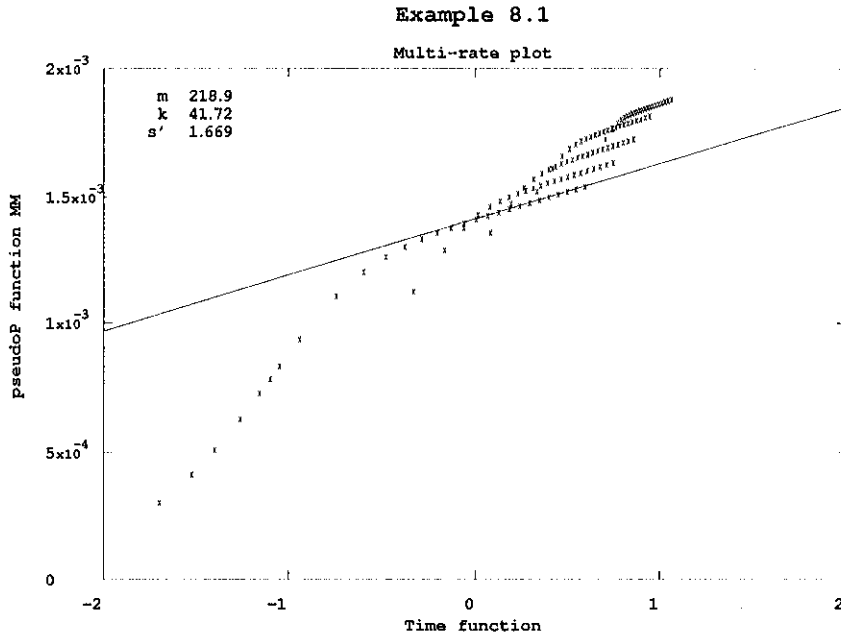


Figure 8.4

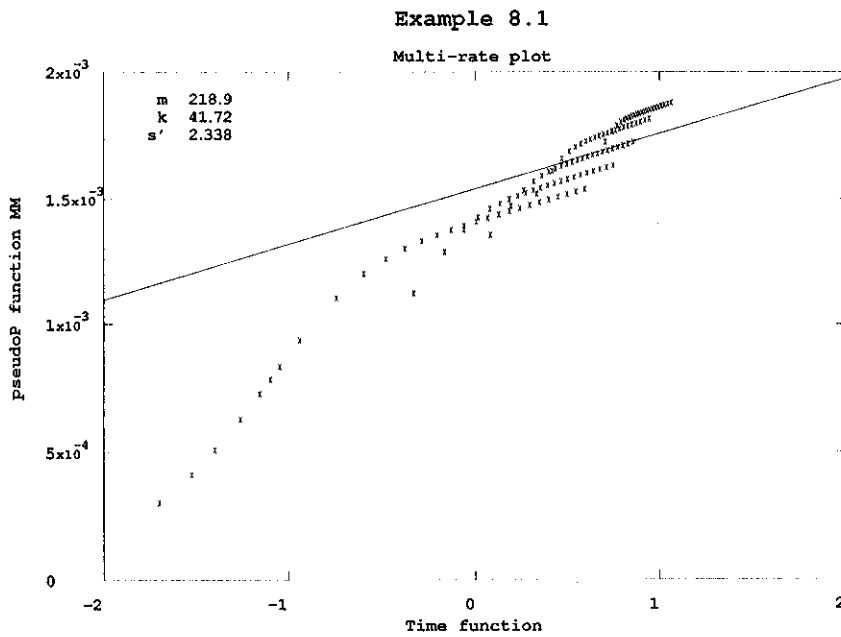


Figure 8.5

Nonlinear regression is the best way to analyse this data set, since the constant and rate dependent skin effects can be estimated from the consideration of all five flow rates together. Table 8.2 lists the parameter estimates and the confidence intervals, and Fig. 8.6 shows the match. For comparison, Fig. 8.7 shows a simulation of the test with the same permeability and constant skin factor values, but without the rate dependent skin effect. It is clear that the skin effect is different at each of the five flow rates.

Parameter	Estimate	Confidence Interval (absolute)	Confidence Interval (percent)
Permeability (md)	41.72	± 2.056	± 4.93%
Skin	1.295	± .3249	± 25.09%
Storage (SCF/psi)	5.440	± .2482	± 4.56%
Non-Darcy s (/MCF/d)	.1147E-04	± .9756E-06	± 8.50%

Table 8.2

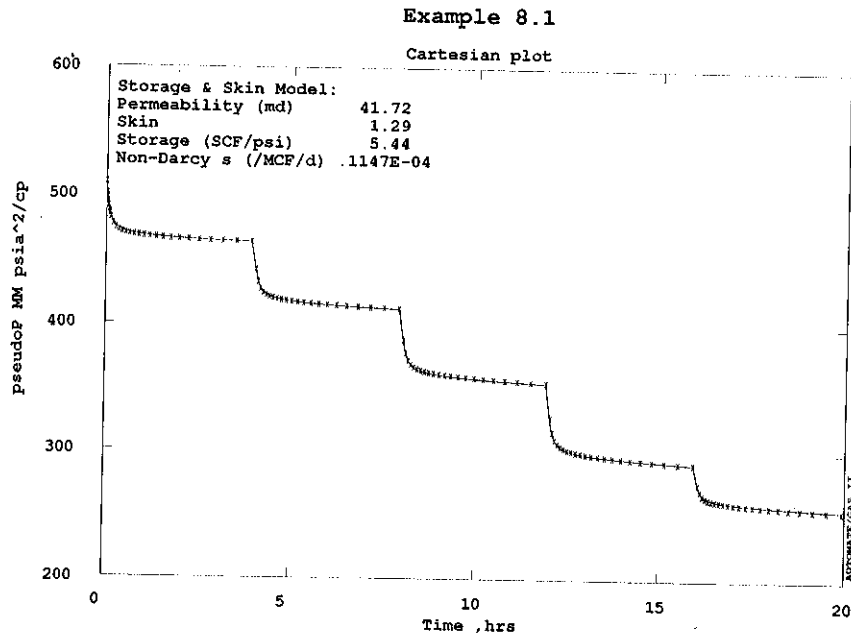


Figure 8.6

Once skin factor s and rate dependent skin factor D have been estimated in this way, the open flow potential (AOFPP) can be estimated by simulating a multirate test down to the minimum achievable well head pressure. The fact that pressures may not have stabilized during the actual test is of no consequence, since the simulated test can have individual flow periods as long as necessary to achieve stabilization.

The use of pseudopressure is not always necessary for proper interpretation. Fig. 8.8 shows a plot of pseudopressure against pressure for the data of this test. Since the relationship is almost completely linear, there would be little consequence if the analysis had used pressure directly. Table 8.3 shows the parameter estimates for the first flow period, based on a pressure analysis instead of a pseudopressure analysis.

Parameter	Estimate	Confidence Interval (absolute)	Confidence Interval (percent)
Permeability (md)	47.66	± .8293	± 1.74%
Skin	2.134	± .1304	± 6.11%
Storage (SCF/psi)	4.804	± .0377	± .78%

Table 8.3

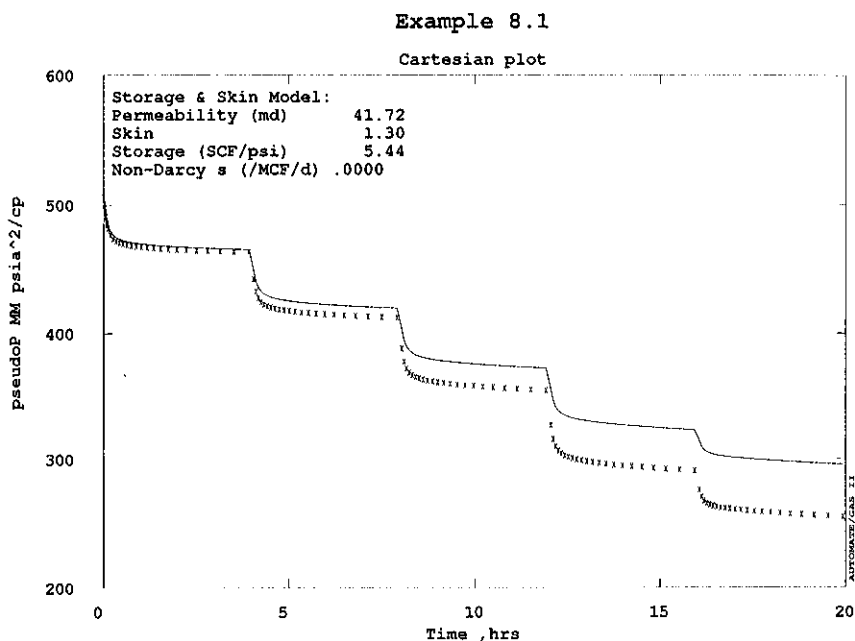


Figure 8.7

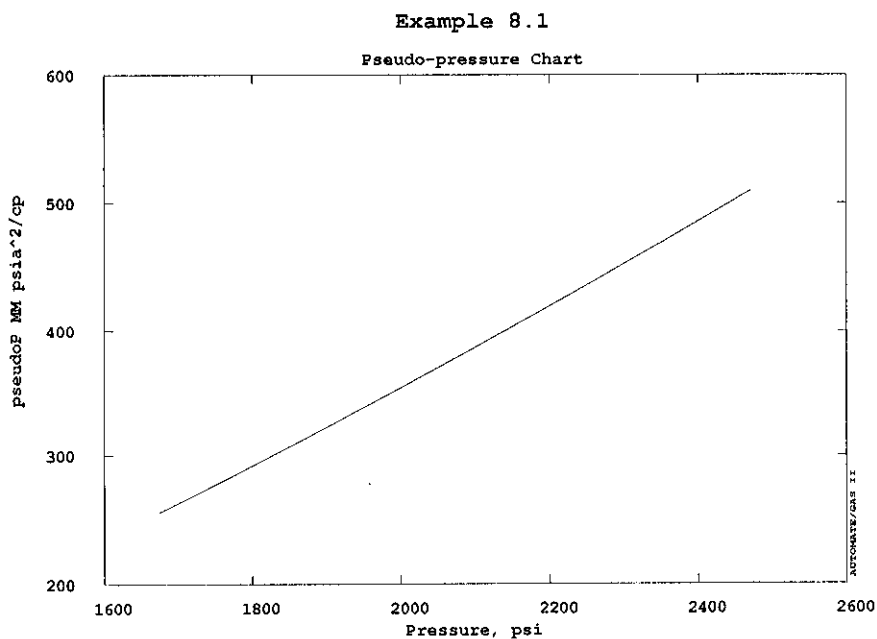


Figure 8.8

8.6 References

Agarwal, R. G.: "Real Gas Pseudotime - A New Function for Pressure Buildup Analysis of Gas Wells", paper SPE 8279 presented at the 1979 SPE Annual Technical Conference and Exhibition, Las Vegas,

Nevada, September 23-26, 1979.

Al-Hussainy, R. and Ramey, H. J. Jr.: "Application of Real Gas Flow Theory to Well Testing and Deliverability Forecasting", *J. Pet. Tech.* (May, 1966) 637-642, Trans., AIME, 237.

Aziz, K.: "Theoretical Basis of Isochronal and Modified Isochronal Back-Pressure Testing of Gas Wells", *J. Can. Pet. Tech.* (January-March, 1967) 20-22.

Brar, G. S. and Aziz, K.: "Analysis of Modified Isochronal Tests to Predict the Stabilized Deliverability Potential of Gas Wells Without Using Stabilized Flow Data", *J. Pet. Tech.* (February, 1978) 297-304.

Cullender, M. H.: "The Isochronal Performance Method of Determining the Flow Characteristics of Gas Wells", Trans., AIME 204, 137-142, 1955.

Horne, R.N., and Kuchuk, F.: "The Use of Simultaneous Flow Rate and Pressure Measurements to Replace Isochronal Gas Well Tests", *SPE Formation Evaluation*, (1988), 467-470.

Katz, D. L., Cornell, D., Kobayashi, R., Poettmann, F. H., Vary, J. A., Elenbaas, J. R. and Weinaug, C. F.: *Handbook of Natural Gas Engineering*, McGraw-Hill Book Co. Inc., New York, 1959.

Kucuk, F. and Ayestaran, L.: "Analysis of Simultaneously Measured Pressure and Sandface Flow Rate in Transient Well Testing", *J. Pet. Tech.* (February, 1985) 322-330.

Lee, W. J. and Holditch, S. A.: "Application of Pseudotime to Buildup Test Analysis of Low Permeability Gas Wells with Long-Duration Wellbore Storage Distortion", *J. Pet. Tech.* (December, 1982) 2877-2887.

Meunier, D., Kabir, C. S. and Wittmann, M. J.: "Gas Well Test Analysis: Use of Normalized Pressure and Time Functions", *SPE Formation Evaluation*, (Dec. 1987), 629-636.

Muskat, M.: *The Flow of Homogeneous Fluids*, J. E. McEdwards, Inc., Ann Arbor, Mich. (1946).

Rawlins, E. L. and Schellhardt, M. A.: "Backpressure Data on Natural Gas Wells and Their Application to Production Practices", U. S. Bureau of Mines, Monograph, 7, 1936.

Wattenbarger, R. A. and Ramey, H. J., Jr.: "Gas Well Testing with Turbulence, Damage and Wellbore Storage", *J. Pet. Tech.* (August, 1968) 877-887.

9. MULTIPHASE WELL TESTING

All of the preceding sections have examined the interpretation of tests of wells that produce single phase fluid - either oil, water or gas. In general, when more than one fluid phase flows in the reservoir at the same time, the multiphase interactions render the single phase flow equations invalid, and it may be necessary to develop new equations to specifically include the multiphase effects. Examples of situations in which this may arise are tests in solution gas drive reservoirs with well flowing pressures below the bubble point, or gas condensate reservoirs with well flowing pressures in the retrograde condensation region. When two or more phases flow simultaneously, the presence of one phase reduces the flow of the other, due to relative permeability effects. The result is that the effective permeabilities are functions of saturation, and therefore also of time. Since the total mobility is a combination of the separate phase mobilities, it follows that the net effective reservoir mobility will change during a well test and after it has been completed. To obtain useful interpretive results, these effects must be considered.

Several different approaches to analysis of multiphase well tests have been developed. The traditional approach is due to Perrine (1956) and Martin (1959). Their approach makes use of the concepts of total mobility and total compressibility, and is still widely used due to its straightforward application. However, Perrine's approach is known to be less reliable as gas saturations increase (Weller, 1966), and can underestimate the effective phase permeabilities (Chu, Reynolds and Raghavan, 1986). Ayan and Lee (1986) also found that Perrine's approach overestimated the skin effect in cases where flow was blocked by gas in the vicinity of the wellbore.

A second approach to multiphase well test analysis by Raghavan (1976 and 1986) makes use of specially defined pseudopressure that is analogous to the real gas pseudopressure derived for gas wells in Section 8. The definition of multiphase pseudopressure is:

$$m(p) = \int_0^p \frac{k_{ro}}{\mu_o B_o} dp' \quad (9.1)$$

This definition was used by Fetkovitch (1973) to define the productivity of wells:

$$q_o = \frac{kh}{141.2 (0.5 \ln t_D + 0.404 + s)} [m(p_i) - m(p_{wf})] \quad (9.2)$$

where

$$t_D = \frac{0.000264kt}{\phi \mu_o c_i r_w^2} \quad (9.3)$$

Application of the pseudopressure approach requires knowledge of the relative permeability curves appropriate for the reservoir. Aanonsen (1985a, 1985b) demonstrated that small inaccuracies in the relative permeability data can lead to greater inaccuracies in reservoir parameter estimates. This is a weakness of the pseudopressure approach, since in practice reservoir relative permeability data is quite difficult to obtain.

A third approach was described by Al-Khalifah, Aziz and Horne (1987), who developed a procedure that generalized the works of Perrine (1956), Martin (1959) and Fetkovitch (1973) by developing them from first principles. This approach is based on the use of pressure squared p^2 instead of pressure, and avoids the need to know the reservoir relative permeability behavior in advance. It has been successfully demonstrated for both high volatility and low volatility oil systems.

In this section, we will review first the traditional Perrine approach, since it still in common usage, and then describe the more general pressure squared approach of Al-Khalifah, Aziz and Horne (1987).

9.1 Perrine's Approach

The essence of traditional analysis of multiphase tests is the definition of total flow properties to replace the individual phase properties. The interpretation procedure uses the *total mobility* λ_t , and the total compressibility c_t , defined as follows:

$$\lambda_t = \frac{k_o}{\mu_o} + \frac{k_w}{\mu_w} + \frac{k_g}{\mu_g} \quad (9.4)$$

where the phase permeability is defined in terms of the relative permeability, typically

$$k_o = k k_{ro} \quad (9.5)$$

$$c_t = c_r + S_o c_o + S_w c_w + S_g c_g + \frac{S_o B_g}{5.615 B_o} \left[\frac{\partial R_s}{\partial p} \right] + \frac{S_w B_g}{5.615 B_w} \left[\frac{\partial R_{sw}}{\partial p} \right] \quad (9.6)$$

In the definition of total compressibility c_t , the last two terms on the right hand side of Eq. 9.6 represent the volume change due to gas dissolution upon pressure change. In practice, these terms are large (although the water-gas solution term is small relative to the oil-gas term), and can be the major contributor to the compressibility. This means that multiphase systems undergoing gas evolution from oil can have very large compressibilities, often larger than systems having only gas.

In the case of gas condensate reservoirs, the total compressibility is modified to take account of the formation of condensate:

$$c_t = c_r + S_o c_o + S_w c_w + S_g c_g + \left[\frac{\partial r_s}{\partial p} \right] + \frac{S_w B_g}{5.615 B_w} \left[\frac{\partial R_{sw}}{\partial p} \right] \quad (9.7)$$

where r_s is the volume of condensate liquid at reservoir conditions relative to the total pore volume (this is usually the same as oil saturation s_o).

The definition of total mobility and compressibility does not fully linearize the governing equations, and their use is subject to some assumptions.

1. Pressure gradients must be small.
2. Saturation gradients must be small.
3. Saturation changes during the duration of the test must be negligible.
4. Capillary pressure must be negligible.

Provided these conditions are satisfied, the methods and solutions developed for single phase well test applications can be used for multiphase well test interpretation. It is necessary to make suitable substitutions in the equations used for the analysis, being certain to use the multiphase definition of total compressibility and replacing terms in k/μ by the total mobility λ_t . It is also necessary to use the total fluid production rate as follows:

$$(qB)_t = q_o B_o + q_w B_w + [1000q_g - R_s q_o - R_{sw} q_w] \frac{B_g}{5.615} \quad (9.8)$$

For example, when performing type curve analysis, the definitions of dimensionless pressure and time are:

$$p_D = \frac{\lambda_r h}{141.2(qB)_t} \Delta p \quad (9.9)$$

$$t_D = \frac{0.000264 \lambda_r t}{\phi c_t r_w^2} \quad (9.10)$$

As another example, in semilog analysis, the slope of the infinite acting semilog straight line and the skin effect are given respectively by:

$$m = \frac{162.6(qB)_t}{\lambda_r h} \quad (9.11)$$

$$s = 1.151 \left[\frac{p_i - p_{1hr}}{m} - \log \frac{\lambda_r}{\phi c_t r_w^2} + 3.227 \right] \quad (9.12)$$

As a result of these definitions, the analysis procedure provides an estimate of total mobility λ_r rather than permeability directly. If the relative permeabilities of the reservoir are known, then the separate phase mobilities can be estimated from the fractional flow curves, for example:

$$\frac{\lambda_w}{\lambda_o} = f_w(s_w) \quad (9.13)$$

and

$$\frac{\lambda_g}{\lambda_o} = f_g(s_g) \quad (9.14)$$

Alternatively, the calculation can use the phase relative permeabilities k_{ro} , k_{rw} and k_{rg} directly, making use of Eqs. 9.4 and 9.5. In either method, it is necessary to know the saturations of each of the phases in the reservoir. This may present something of a difficulty since the saturations originally measured by logging will be different from those under the conditions of the well test. Saturations may also vary during the test and will be different at different distances from the well. Bøe, Skjæveland and Whitson (1981) developed an expression that relates saturation to pressure during drawdown in solution gas reservoirs. This expression may be used to estimate saturations for use in Eqs. 9.13 and 9.14.

Absolute reservoir permeability can also be estimated from λ_r by substituting the relative permeability values in the expanded form of Eq. 9.4:

$$\lambda_r = k \left[\frac{k_{ro}}{\mu_o} + \frac{k_{rw}}{\mu_w} + \frac{k_{rg}}{\mu_g} \right] \quad (9.15)$$

9.2 Pressure Squared Approach

As discussed by Al-Khalifah, Aziz and Horne (1987), the equations governing multiphase pressure transients during a well test can be reduced to the following equation in terms of pressure squared:

$$\frac{\partial^2 p^2}{\partial r^2} + \frac{1}{r} \frac{\partial p^2}{\partial r} = \frac{\phi c_t}{\lambda_t} \frac{\partial p^2}{\partial t} \quad (9.16)$$

This equation holds only provided the group of parameters $k_o/(\mu_o B_o)$ is a linear function of pressure:

$$\frac{k_o}{\mu_o B_o} = ap \quad (9.17)$$

In practice, this is often approximately true (Handy, 1957, Fetkovich, 1973, Al-Khalifah, Aziz and Horne, 1987).

Using these expressions, a new set of equations can be developed for interpretation. For example, the equation describing the infinite acting (semilog straight line) behavior can be written:

$$p_i^2 - p_{wf}^2 = \frac{325.1 q_o}{a h} \left[\log t + \log \left[\frac{\lambda_t}{\phi c_t r_w^2} \right] - 3.227 + 0.868s \right] \quad (9.18)$$

The skin factor can be found from:

$$s = 1.151 \left[\frac{p_i^2 - p_{1hr}^2}{m} - \log \frac{\lambda_t}{\phi c_t r_w^2} + 3.227 \right] \quad (9.19)$$

where m is the slope of the infinite acting semilog straight line on the plot of pressure squared p^2 against the log of time.

After finding the slope of the infinite acting semilog straight line, the parameter a can be estimated, and used with Eq. 9.17 to estimate the oil phase permeability k_o . The question remains as to which value of pressure should be associated with the estimated value of a . Al-Khalifah, Aziz and Horne (1987) showed that if the average pressure during the infinite acting period is used, then the permeability calculated is the same as that of Perrine's approach (which usually underestimates oil permeability). As an alternative, it was proposed that a be evaluated at a higher pressure, specifically at initial reservoir pressure p_i for drawdown tests, and at average reservoir pressure \bar{p} for buildup tests. Thus for drawdown tests, a would be given by:

$$a = \left[\frac{k_o}{\mu_o B_o} \right]_i \frac{1}{p_i} \quad (9.20)$$

and oil phase permeability would therefore be given by:

$$k_o = \frac{325.2 q_o p_i (\mu_o B_o)_i}{m h} \quad (9.21)$$

For buildup tests, the expression for oil phase permeability would be:

$$k_o = \frac{325.2 q_o \bar{p} (\bar{\mu}_o \bar{B}_o)_i}{m h} \quad (9.22)$$

Al-Khalifah, Aziz and Horne (1987) showed that Eqs. 9.21 and 9.22 gave good estimates of oil phase permeability for tests involving oils of both high and low volatility. However, in cases of large drawdowns in tests with oils of low volatility, it was found to be necessary to use a lower pressure for the evaluation of a , otherwise the oil permeability was somewhat overestimated.

After estimating oil phase permeability k_o , water and gas phase permeabilities can be estimated in the same manner discussed in Section 9.1, using Eqs. 9.13 and 9.14. Absolute reservoir permeability k can be estimated as before, using Eq. 9.15. Again, relative permeability data and knowledge of the phase saturations are required.

9.3 References

Aanonsen, S.I.: "Nonlinear Effects During Transient Fluid Flow in Reservoirs as Encountered in Well Test Analysis," Dr. Scient. dissertation, Univ. of Bergen, Norway, 1985a.

Aanonsen, S.I.: "Application of Pseudotime to Estimate Average Reservoir Pressure", paper SPE 14256 presented at the 60th Annual SPE Technical Conference and Exhibition, Las Vegas, NV, Sept. 22-25, 1985b.

Al-Khalifah, A.A., Aziz, K., and Horne, R.N.: "A New Approach to Multiphase Well Test Analysis", paper SPE 16473 presented at the 62nd Annual SPE Technical Conference and Exhibition, Dallas, TX, Sept. 27-30, 1987.

Bøe, A., Skjæveland, S.M., and Whitson, C.S.: "Two-Phase Pressure Transient Test Analysis", paper SPE 10224 presented at the 56th Annual SPE Technical Conference and Exhibition, San Antonio, TX, Oct. 5-7, 1981.

Chu, W.C., Reynolds, A.C., Jr., and Raghavan, R.: "Pressure Transient Analysis of Two-Phase Flow Problems", *SPE Formation Evaluation*, (April 1986).

Handy, L.L.: "Effect of Local High Gas Saturations on Productivity Indices", *Drill. and Prod. Prac.*, API (1957)

Martin, J.C.: "Simplified Equations of Flow in Gas Drive Reservoirs and the Theoretical Foundation of Multiphase Buildup Analysis", *Trans.*, AIME (1959), 216, 309-311.

Perrine, R.L.: "Analysis of Pressure Buildup Curves", *Drill. and Prod. Prac.*, API (1956), 482-509.

Raghavan, R.: "Well Test Analysis for Multiphase Flow", paper SPE 14098 presented at the SPE International Meeting on Petroleum Engineering, Beijing, China, March 17-20, 1986.

Raghavan, R.: "Well Test Analysis: Wells Producing by Solution Gas Drive", *Soc. Petr. Eng. J.*, (Aug. 1976), 1966-208.

Weller, W.T.: "Reservoir Performance During Two-Phase Flow", *J. Pet. Tech.*, (Feb. 1966), 240-246.

10. DESIGNING WELL TESTS

As described in Section 1, a well test is intended to meet specific reservoir analysis objectives. To meet the required objectives, a test must be properly designed. An improperly planned test is not only a fruitless expense, it also fails to provide the desired reservoir data. In some cases, it may not be possible to attain the required objectives at all, and in other cases special equipment may need to be ordered in advance and transported to the wellsite. For all these reasons, it is clearly essential to carefully consider what the test is to achieve, and how it is to be performed to successfully reach those goals.

Effective well test design requires consideration of which operational variables affect the estimates of which reservoir variables. For the most part, the operational variables under the control of the engineer are the flow rate and the duration of the test. A choice must also be made as to the type of test to be carried out. This section is divided into three parts, consideration of the effects of flow rate and time, specification of the test duration, and appraisal of the flow rate.

10.1 Variable Dependency

Which variables depend on which? Understanding this concept is of assistance in planning the test. In designing the operation, there are two major considerations; (a) will the reservoir parameter to be estimated affect the well pressure in a significant enough way that the effect will be detectable with the tools available to measure it, and the tools available to analyze the response, and (b) will the test be of sufficient length for the response to be seen.

We have seen in earlier sections, mainly Section 2, that different parts of the pressure response begin and end at certain times. These are summarised again here (in the order they would appear in an optimum case):

End of wellbore storage effect (Eq. 2.22):

$$t_D = C_D(0.041 + 0.02 s) \quad (10.1)$$

Start of semilog straight line, either single porosity or secondary part of double porosity (from Eq. 2.23):

$$t_D = C_D(60 + 3.5 s) \quad (10.2)$$

End of secondary porosity semilog-straight line in a double porosity reservoir:

$$t_D = \frac{\omega(1 - \omega)}{6.6 \lambda} \quad (10.3)$$

End of double porosity transition:

$$t_D = \frac{1.2(1 - \omega)}{\lambda} \quad (10.4)$$

End of infinite acting behavior (semilog straight line) -- depends on reservoir shape and boundary configuration (see Table 2.1), for *circular bounded reservoirs*:

$$t_{DA} = 0.1 \quad (10.5)$$

Start of pseudosteady state -- also depends on reservoir shape and boundary configuration (see Table 2.1), for *circular bounded reservoirs*:

$$t_{DA} = 0.1 \quad (10.6)$$

The important feature to recognise about these start and end times is that they can all be expressed in terms of dimensionless time t_D or t_{DA} . This means that they are affected by mobility k/μ , storativity $\phi c_i h$ and transmissivity kh , *but not by flow rate*. Thus for any given reservoir, the transition times will occur at a specific moment, regardless of the rate at which the well is flowing.

The pressure response may be estimated by looking at specific models, but for illustration, we can look at the infinite acting response (Eq. 2.27):

$$p_{wf} = p_i - 162.6 \frac{qB\mu}{kh} \left[\log t + \log \frac{k}{\phi\mu c_i r_w^2} + 0.8686s - 3.2274 \right] \quad (10.7)$$

From this equation, it is seen that the magnitude of the pressure drop depends on the group of variables $qB\mu/kh$. Thus the pressure drop is directly proportional to the flow rate (and will always be so for single phase reservoirs). Deciding on a flow rate change to induce for the purpose of the test is not really an issue, since it is usually best to produce as large a response as practical, to be as sure as possible to obtain a recognizable set of characteristic responses. However it is necessary to determine in advance whether the likely pressure changes will be sufficient to be able to interpret the test adequately.

Nonetheless, we can see from Eq. 10.7 that the amount of the pressure change is only indirectly dependent on the storativity of the reservoir $\phi c_i h$. This means that reservoirs with high storativity will experience the same pressure drop as reservoirs with low storativity, although the times at which the pressure drop is reached will be very different.

10.2 Test Duration

The overall period of time for which the test must be conducted has to be sufficient to be assured of reaching that part of reservoir response that is of interest. For example, if the objective of the test is to evaluate the effectiveness of an acidization treatment in removing skin damage, then it is necessary to obtain sufficient data past the end of the storage transition to be assured of recognising the correct semi-log straight line. Specifically, if we need an entire log cycle of infinite acting response, then the test would have to run for a time of at least (using Eq. 10.2):

$$t_D \geq 10 \times C_D (60 + 3.5 s) \quad (10.8)$$

If, on the other hand, it was required to estimate the drainage radius of the well, then we would need to observe a sufficient duration of pseudosteady state response, again perhaps a log cycle. Assuming the drainage area to circular, we could use Eq. 10.6 to specify:

$$t_{DA} \geq 1 \quad (10.9)$$

Another consideration when examining test times is whether one part of the pressure response will overlap another. Perhaps the required part of the response will be disguised by a less diagnostic effect. For example, it is conceivable that a well with a large storage effect (such as caused by falling liquid level), in a relatively small reservoir, could exhibit a pressure transient that went from storage response directly to pseudosteady state. It could do this (in a circular reservoir) if:

$$C_D(60 + 3.5 s) \geq 0.1 \frac{A}{r_w^2} \quad (10.10)$$

In such a case, the well would be difficult to interpret for permeability k and skin factor s if the wellbore storage coefficient were greater than:

$$C_D \geq \frac{A}{r_w^2} \frac{0.1}{(60 + 3.5 s)} \quad (10.11)$$

In real dimensions, the storage coefficient C in STB/psi must be less than (using Eq. 2.16):

$$C \leq \frac{2\pi\phi c_f h A}{5.615} \frac{0.1}{(60 + 3.5 s)} \quad (10.12)$$

If the wellbore storage is measured or estimated to be larger than this, then it will be pointless to conduct the well test unless the storage effect can be reduced or overcome (for example by using a downhole shutoff or by measuring flow rates down hole).

A similar consideration can be made to determine whether storage effects will make it impossible to interpret double porosity effects, as will occur if:

$$C_D(60 + 3.5 s) \geq \frac{\omega(1 - \omega)}{6.6 \lambda} \quad (10.13)$$

10.3 Flow Rate Considerations

As discussed in Section 10.1, the amount of the pressure change is directly proportional to the flow rate in all but a few special cases. Thus it is necessary to determine whether the maximum flow rate change attainable will provide sufficient pressure change over the part of the response most diagnostic of the reservoir parameters of interest. For example, a highly permeable reservoir may have only very small pressure change during the semilog straight line period of its response -- if this change is so small as to be adversely influenced by measurement noise, then it will be difficult to obtain good estimates of the permeability. Example 7.1 showed data from a real well test example where this was the case.

Since the pressure change is also a function of the reservoir permeability and fluid viscosity, and since the level of measurement noise depends on type of instrument used, it is difficult to prescribe a set of equations to evaluate whether the available flow will be sufficient. The best approach, especially in a computer-aided interpretation environment, is to "simulate" the test with prospective values of the reservoir parameters, and then examine the simulated data to see whether it is able to provide valid estimates of the required parameters or not. Some caution is required however, since "perfect" data can often provide answers over restricted data ranges, whereas real data will not. Thus it is necessary to collect more data than may be suggested from a simulated set of data, especially since it is also necessary to include

contingencies and uncertainties.

Finally, it should also be noted that a well test in a computer-aided system of data acquisition and processing may be interpreted at the same time the test is being carried out, either at the wellsite or by using remote data transmission. Thus it is feasible to "redesign" the test before terminating the measurements, thereby saving the need for a retest while still meeting the original goals of the reservoir analysis.

11. CALCULATING PROPERTIES

In order to use most of the methods described within this book, it is necessary to first obtain numerical values for fluid and rock properties such as formation volume factor B_o and total system compressibility c_t . Sometimes these parameters have been measured directly in the laboratory by core or PVT analysis, but often it is necessary to estimate them. This section discusses methods of estimation, so that the required oil, gas, water and rock properties can be determined if they are not otherwise available. These estimation techniques are based upon observations and correlations developed by many authors. Many of the correlations described here have been collected in a book by McCoy (1983).

11.1 Oil Properties

The oil properties required for most well test applications are formation volume factor B_o , viscosity μ_o , and compressibility c_o (which is included into the calculation of total compressibility c_t). These parameters are functions of the reservoir pressure and temperature, the separator pressure and temperature, the gas/oil ratio and gas gravity, the API density of the oil, and depend on whether the reservoir pressure is above or below the bubble point.

Following the sequence of calculations described by McCoy (1983), the first step is to correct the observed gas gravity to separator conditions:

$$\gamma_{gs} = \gamma_g \left[1 + 5.912 \times 10^{-5} API T_s \frac{\ln \left[\frac{p_s}{114.7} \right]}{2.3026} \right] \quad (11.1)$$

where γ_{gs} = gas gravity corrected to separator conditions
 γ_g = observed gas gravity (air = 1)
 API = observed oil API gravity
 T_s = separator temperature ($^{\circ}$ F)
 p_s = separator pressure (psia)

The second step is to calculate the bubble point pressure p_{bp} in psia, based upon the observed gas oil ratio GOR in SCF/STB, and the reservoir temperature T_R in $^{\circ}$ R:

$$\text{For } API \leq 30, \quad p_{bp} = \left[\frac{GOR}{0.0362 \gamma_{gs} e^{\frac{25.724 API}{T_R}}} \right]^{\frac{1}{1.0937}} \quad (11.2)$$

$$\text{For } API > 30, \quad p_{bp} = \left[\frac{GOR}{0.0178 \gamma_{gs} e^{\frac{23.931 API}{T_R}}} \right]^{\frac{1}{1.1870}} \quad (11.3)$$

The third step is to calculate the equilibrium gas/oil ratio R_y in SCF/STB:

$$\text{For } API \leq 30, \quad R_y = 0.0362 \gamma_{gs} p^{1.0937} e^{\frac{25.724 API}{T_R}} \quad (11.4)$$

$$\text{For } API > 30, \quad R_s = 0.0178 \gamma_{gs} p^{1.1870} e^{\frac{23.931 API}{T_R}} \quad (11.5)$$

In calculations that require a value of the reservoir *dissolved* gas/oil ratio GOR_{res} , the value of observed GOR is used if reservoir pressure is greater than bubble point pressure ($p > p_{bp}$). If reservoir pressure is less than bubble point ($p < p_{bp}$), then the equilibrium gas/oil ratio R_s is used for GOR_{res} .

The fourth step is to calculate the oil compressibility c_o (/psi) at or above the bubble point:

$$c_o = \frac{-2433 + 5 GOR + 17.2 T_F - 1180 \gamma_{gs} + 12.61 API}{10^5 p} \quad (11.6)$$

$$\begin{aligned} \text{where } T_F &= \text{reservoir temperature (}^\circ\text{F)} \\ p &= \text{reservoir pressure (psia)} \end{aligned}$$

The fifth step is to calculate the oil viscosity. Different equations are used depending on whether the oil is above or below the bubble point. It is first necessary to calculate viscosity of the "dead oil" (gas free oil) μ_{od} in cp:

$$\mu_{od} = 10^x - 1 \quad (11.7)$$

where

$$x = 10^{3.0324 - 0.02023 API} T_F^{-1.163}$$

After which the viscosity of the "live oil" at or below the bubble point μ_{ob} in cp is given by:

$$\mu_{ob} = 10.715 (GOR_{res} + 100)^{-0.515} \mu_{od}^x \quad (11.8)$$

where

$$x = 5.44 (GOR_{res} + 150)^{-0.338}$$

The viscosity of the "live oil" above the bubble point μ_o in cp is given by:

$$\mu_o = \mu_{ob} \left[\frac{p}{p_{bp}} \right]^x \quad (11.9)$$

where

$$x = 2.6 p^{1.187} e^{-0.0000898 p - 11.513}$$

Finally the oil formation volume factor is calculated. At or below the bubble point, B_{ob} is given by:

$$\begin{aligned} \text{For } API \leq 30, \quad B_{ob} &= 1 + 1.751 \times 10^{-5} (T_F - 60) \left[\frac{API}{\gamma_{gs}} \right] \\ &+ \left[4.677 \times 10^{-4} - 1.811 \times 10^{-8} (T_F - 60) \left[\frac{API}{\gamma_{gs}} \right] \right] GOR_{res} \end{aligned} \quad (11.10)$$

$$\begin{aligned} \text{For } API > 30, \quad B_{ob} = 1 + 1.100 \times 10^{-5} (T_F - 60) \left[\frac{API}{\gamma_{gs}} \right] \\ + \left[4.670 \times 10^{-4} + 1.377 \times 10^{-9} (T_F - 60) \left[\frac{API}{\gamma_{gs}} \right] \right] GOR_{res} \end{aligned} \quad (11.11)$$

The oil formation volume factor above the bubble point B_o in RB/STB is given by:

$$B_o = B_{ob} e^{c_o(p_{bp} - p)} \quad (11.12)$$

11.2 Gas Properties

The gas properties required for most well test applications are formation volume factor B_g , viscosity μ_g , and compressibility c_g (which is included into the calculation of total compressibility c_t). These parameters are functions of the reservoir pressure and temperature, the critical (or pseudocritical) pressure and temperature, the gas gravity, and the concentrations of the gas impurities N_2 , CO_2 and H_2S .

The first step is to determine the pseudocritical pressure p_{pc} in psia and temperature T_{pc} in °R from the gas gravity γ_g , using Standing's correlation:

For California gases:

$$p_{pc} = 677 + 15 \gamma_g - 37.5 \gamma_g^2 \quad (11.13)$$

$$T_{pc} = 168 + 325 \gamma_g - 12.5 \gamma_g^2 \quad (11.14)$$

For condensate gases:

$$p_{pc} = 706 - 51.7 \gamma_g - 11.1 \gamma_g^2 \quad (11.15)$$

$$T_{pc} = 187 + 330 \gamma_g - 71.5 \gamma_g^2 \quad (11.16)$$

If unknown, gas gravity can also be calculated from measured values of critical pressure p_c in psia and temperature T_c in °R if these are available:

$$\gamma_g = \frac{1}{2} \left[\frac{T_c - 175.59}{307.97} - \frac{p_c - 700.55}{47.94} \right] \quad (11.17)$$

If the gas contains impurities, corrections should be made using the Wichert-Aziz correction e °F (Wichert and Aziz, 1972):

$$e = 120(y_{CO_2} + y_{H_2S})^{0.9} - 120(y_{CO_2} + y_{H_2S})^{1.6} + 15(y_{H_2S}^{0.5} - y_{H_2S}^4) \quad (11.18)$$

$$p_c^* = \frac{p_c(T_c - e)}{T_c + y_{H_2S}(1 - y_{H_2S})e} \quad (11.19)$$

$$T_c^* = T_c - e \quad (11.20)$$

$$\begin{aligned} \text{where } y_{CO_2} &= CO_2 \text{ content (decimal)} \\ y_{H_2S} &= H_2S \text{ content (decimal)} \\ T_c^* &= \text{corrected critical temperature (}^\circ R\text{)} \\ p_c &= \text{corrected critical pressure (psia)} \end{aligned}$$

Having estimated or obtained the pseudocritical or critical properties, it is necessary to calculate the reduced pressure and temperature, p_r and T_r , as follows:

$$p_r = \frac{p}{p_{pc}} \quad (11.21)$$

$$T_r = \frac{T_R}{T_{pc}} \quad (11.22)$$

The reduced density is calculated iteratively using Newton's method, and used to estimate the z factor with the procedure described by Dranchuk, Purvis and Robinson (1974) to evaluate the Standing and Katz (1942) relations:

$$\rho_r^{k+1} = \rho_r^k - \frac{f(\rho_r^k)}{f'(\rho_r^k)} \quad (11.23)$$

where

$$f(\rho_r) = a\rho_r^6 + b\rho_r^3 + c\rho_r^2 + d\rho_r + e\rho_r^3(1 + f\rho_r^2) \exp[-f\rho_r^2] - g \quad (11.24)$$

$$f'(\rho_r) = 6a\rho_r^5 + 3b\rho_r^2 + 2c\rho_r + d + e\rho_r^2(3 + f\rho_r^2[3 - 2f\rho_r^2])\exp(-f\rho_r^2) \quad (11.25)$$

$$\begin{aligned} \text{where } a &= 0.06423 \\ b &= 0.5353T_r - 0.6123 \\ c &= 0.3151T_r - 1.0467 - 0.5783/T_r^2 \\ d &= T_r \\ e &= 0.6816/T_r^2 \\ f &= 0.6845 \\ g &= 0.27p_r \\ \rho_r^0 &= 0.27 p_r/T_r \end{aligned}$$

Then

$$z = \frac{0.27 p_r}{\rho_r T_r} \quad (11.26)$$

The gas compressibility is calculated next, from the expression:

$$c_g = \frac{1}{p_c p_r \left[1 + \frac{p_r}{z} \frac{\partial z}{\partial p_r} \right]} \quad (11.27)$$

where

$$\frac{\partial z}{\partial p_r} = \frac{1}{p_r T_r} \left[5a p_r^5 + 2b p_r^2 + c p_r + 2e p_r^2 \left(1 + f p_r^2 - f^2 p_r^4 \right) \exp(-f p_r^2) \right] \quad (11.28)$$

and where a, b, c, d, e, f are as in Eqs. 11.24 and 11.25.

The next step is the calculation of gas viscosity, μ_g . This is done in two stages, first the Carr, Kobayashi and Burrows (1954) gas viscosity μ_{g1} is determined, after which the equation of Dempsey (1965) is used for the final result.

$$\begin{aligned} \mu_{g1} = & (1.709 \times 10^{-5} - 2.062 \times 10^{-6} \gamma_g) T_F + 8.188 \times 10^{-3} - 6.15 \times 10^{-3} \log \gamma_g \\ & + y_{N_2} [8.48 \times 10^{-3} \log \gamma_g + 9.59 \times 10^{-3}] \\ & + y_{CO_2} [9.08 \times 10^{-3} \log \gamma_g + 6.24 \times 10^{-3}] \\ & + y_{H_2S} [8.49 \times 10^{-3} \log \gamma_g + 3.73 \times 10^{-3}] \end{aligned} \quad (11.29)$$

$$\begin{aligned} \ln \left(T_r \frac{\mu_g}{\mu_{g1}} \right) = & a_0 + a_1 p_r + a_2 p_r^2 + a_3 p_r^3 \\ & + T_r [a_4 + a_5 p_r + a_6 p_r^2 + a_7 p_r^3] \\ & + T_r^2 [a_8 + a_9 p_r + a_{10} p_r^2 + a_{11} p_r^3] \\ & + T_r^3 [a_{12} + a_{13} p_r + a_{14} p_r^2 + a_{15} p_r^3] \end{aligned} \quad (11.30)$$

$$\begin{aligned} a_0 &= -2.46211820 \\ a_1 &= 2.97054714 \\ a_2 &= -2.86264054 \times 10^{-1} \\ a_3 &= 8.05420522 \times 10^{-3} \\ a_4 &= 2.80860949 \\ a_5 &= -3.49803305 \\ a_6 &= 3.60373020 \times 10^{-1} \\ a_7 &= -1.04432413 \times 10^{-2} \\ a_8 &= -7.93385684 \times 10^{-1} \\ a_9 &= 1.39643306 \\ a_{10} &= -1.49144925 \times 10^{-1} \\ a_{11} &= 4.41015512 \times 10^{-3} \\ a_{12} &= 8.39387176 \times 10^{-2} \\ a_{13} &= -1.86408848 \times 10^{-1} \\ a_{14} &= 2.03367881 \times 10^{-2} \\ a_{15} &= -6.09579263 \times 10^{-4} \end{aligned}$$

Finally, the gas formation volume factor B_g (reservoir ft³/SCF) is calculated using reservoir pressure p , reservoir temperature T_R in °R, and the z factor calculated previously:

$$B_g = 0.02829 \frac{z T_R}{p} \quad (11.31)$$

11.3 Water Properties

The water properties required for most well test applications are formation volume factor B_w , viscosity μ_w , and compressibility c_w (which is included into the calculation of total compressibility c_t). These parameters are functions of the reservoir pressure and temperature, as well as the salinity of the water.

Starting first with the water compressibility c_w (/psi):

$$c_{w1} = \left[a + bT_F + cT_F^2 \right] 10^{-6} \quad (11.32)$$

$$\begin{aligned} \text{where } a &= 3.8546 - 0.000134 p \\ b &= -0.01052 + 4.77 \times 10^{-7} p \\ c &= 3.9267 \times 10^{-5} - 8.8 \times 10^{-10} p \end{aligned}$$

Correcting for the salinity $NaCl$ (in percent, 1% = 10,000 ppm):

$$c_w = c_{w1} \left[1 + NaCl^{0.7} \left[-0.052 + 0.00027 T_F - 1.14 \times 10^{-6} T_F^2 + 1.121 \times 10^{-9} T_F^3 \right] \right] \quad (11.33)$$

The water formation volume factor, B_w in RB/STB, is determined from:

$$B_w = \left[a + b p + c p^2 \right] S_{c1} \quad (11.34)$$

where for gas-free water,

$$\begin{aligned} a &= 0.9947 + 5.8 \times 10^{-6} T_F + 1.02 \times 10^{-6} T_F^2 \\ b &= -4.228 \times 10^{-6} + 1.8376 \times 10^{-8} T_F - 6.77 \times 10^{-11} T_F^2 \\ c &= 1.3 \times 10^{-10} - 1.3855 \times 10^{-12} T_F + 4.285 \times 10^{-15} T_F^2 \end{aligned}$$

and for gas-saturated water,

$$\begin{aligned} a &= 0.9911 + 6.35 \times 10^{-6} T_F + 8.5 \times 10^{-7} T_F^2 \\ b &= -1.093 \times 10^{-6} - 3.497 \times 10^{-9} T_F + 4.57 \times 10^{-12} T_F^2 \\ c &= -5 \times 10^{-11} + 6.429 \times 10^{-13} T_F - 1.43 \times 10^{-15} T_F^2 \end{aligned}$$

and where the salinity correction factor S_{c1} is given by:

$$\begin{aligned} S_{c1} = 1 + NaCl \left[5.1 \times 10^{-8} p + (5.47 \times 10^{-6} - 1.96 \times 10^{-10} p) (T_F - 60) \right. \\ \left. + (-3.23 \times 10^{-8} + 8.5 \times 10^{-13} p) (T_F - 60)^2 \right] \end{aligned} \quad (11.35)$$

The water viscosity μ_w in cp is given by:

$$\mu_w = S_{c2} S_p 0.02414 \times 10^{446.04 / (T_R - 252)} \quad (11.36)$$

where the salinity correction, S_{c2} , pressure correction, S_p , are given respectively by:

$$S_{c2} = 1 - 0.00187NaCl^{0.5} + 0.000218NaCl^{2.5} + (T_F^{0.5} - 0.0135T_F) (0.00276NaCl - 0.000344NaCl^{1.5}) \quad (11.37)$$

$$S_p = 1 + 3.5 \times 10^{-12} p^2 (T_F - 40) \quad (11.38)$$

11.4 Rock Properties

The rock properties required for most well test applications are porosity ϕ and compressibility c_r (which is included into the calculation of total compressibility c_t). In general, it is better to use direct measurements of these properties, since there are no widely accepted correlations for them. Since experimental observations have wide scatter, there is little expectation that measurements from one reservoir will necessarily apply to another reservoir (or even a different part of the same reservoir).

However, in cases where compressibility measurements are unavailable, c_r can be estimated from experimental observations summarized by Newman (1973). These observations are provided here in the form of correlations, although there was considerable scatter in the original data. It is important to note that porosity in these correlations is given as a decimal number between 0.0 and 1.0.

For consolidated limestones:

$$c_r = \exp \left[4.026 - 23.07 \phi + 44.28 \phi^2 \right] \times 10^{-6} / psi \quad (11.39)$$

For consolidated sandstones:

$$c_r = \exp \left[5.118 - 36.26 \phi + 63.98 \phi^2 \right] \times 10^{-6} / psi \quad (11.40)$$

For unconsolidated sandstones (for $\phi \geq 0.2$):

$$c_r = \exp \left[34.012 [\phi - 0.2] \right] \times 10^{-6} / psi \quad (11.41)$$

These three correlations are illustrated in Fig. 11.1.

11.5 Total Properties

The final calculation is of the total compressibility c_t . For single phase flow, c_t is given by:

$$c_t = c_r + S_o c_o + S_w c_w + S_g c_g \quad (11.42)$$

where S_o , S_w and S_g are the reservoir oil, water and gas saturations respectively.

For multiphase flow in the reservoir, c_t is given by Eq. 9.6, repeated here:

$$c_t = c_r + S_o c_o + S_w c_w + S_g c_g + \frac{S_o B_g}{5.615 B_o} \left[\frac{\partial R_s}{\partial p} \right] + \frac{S_w B_g}{5.615 B_w} \left[\frac{\partial R_{sw}}{\partial p} \right] \quad (11.43)$$

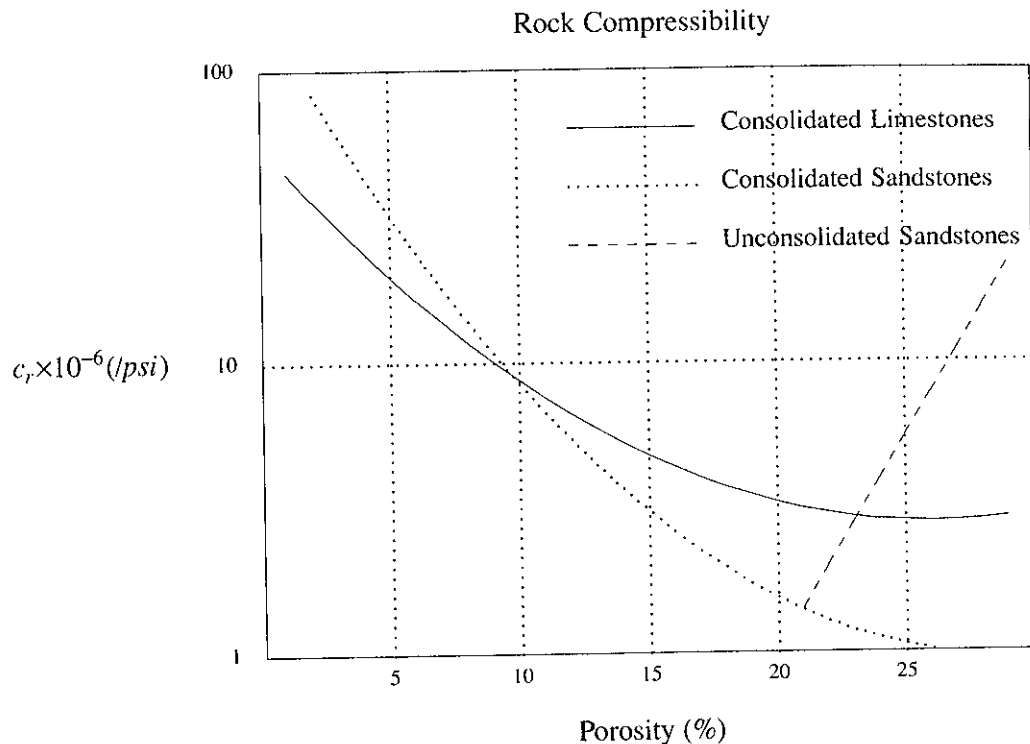


Figure 11.1

Finally, it is worth noting that it is usual to use the *drilled radius* for the wellbore radius r_w . The actual effective wellbore radius depends considerably on the type of well completion and on the condition of the well, however the use of drilled hole radius provides a consistent way of specifying r_w .

References

- Beal, C.: "The Viscosity of Air, Water, Natural Gas, Crude Oil and Associated Gases at Oil Field Temperatures and Pressures," *Transactions AIME*, (1946), 94-115.
- Beggs, H.D., and Robinson, J.R.: "Estimating the Viscosity of Crude Oil Systems", *J. Pet. Tech.*, (Sept. 1975), 1140-1141.
- Carr, N.L., Kobayashi, R., and Burrows, D.B.: "Viscosity of Hydrocarbon Gases Under Pressure", *Transactions AIME*, (1954), 263-272.
- Chew, J.N., and Connally, C.A.: "A Viscosity Correlation for Gas-Saturated Crude Oils", *Transactions AIME*, (1959), 23-25.
- Dempsey, J.R.: "Computer Routine Treats Gas Viscosity as a Variable", *Oil & Gas Journal*, (August 1965), 141.
- Dranchuk, P.M., Purvis, R.A., and Robinson, D.B.: "Computer Calculations of Natural Gas Compressibility Factors Using the Standing and Katz Correlation", Institute of Petroleum Technical Series, No. IP-74-008, (1974).
- Lee, A.L., Gonzales, M.H., and Eakin, B.E.: "The Viscosity of Natural Gases", *J. Pet. Tech.*, (August

1966), 997-1000.

McCoy, R.L.: "Microcomputer Programs for Petroleum Engineers: 1. Reservoir Engineering and Formation Evaluation", Gulf Publishing Co., Houston, (1983).

Meehan, D.N.: "A Correlation for Water Compressibility", *Petroleum Engineer*, (Nov. 1980), 125-126.

Meehan, D.N.: "Estimating Water Viscosity at Reservoir Conditions", *Petroleum Engineer*, (July 1980), 117-118.

Newman, G.H.: "Pore-Volume Compressibility of Consolidated, Friable, and Unconsolidated Rocks Under Hydrostatic Loading," *J. Pet. Tech.*, (1973), 129-134.

Numere, D., Brigham, W.E., and Standing, M.B.: "Correlations for Physical Properties of Petroleum Reservoir Brines", Stanford University Petroleum Research Institute, (Nov. 1977), 8-16.

Standing, M.B.: "Volumetric and Phase Behavior of Oil Field Hydrocarbon Systems", SPE reprint, 8th edition, (1977)

Standing, M.B., and Katz, D.L.: "Density of Natural Gases", *Transactions AIME*, (1942), 140-144.

Vasquez, M., and Beggs, H.D.: "Correlations for Fluid Physical Property Predictions", *J. Pet. Tech.*, (June 1980), 968-970.

Wichert, E., and Aziz, K.: "Calculating Z's for Sour Gases", *Hydrocarbon Processing*, (May 1972), 51

Example 4.1

WELL TEST ANALYSIS REPORT
Example 4.1

FLUID PROPERTIES			
Bo, bbl/STB	1.21	Viscosity, cp	0.92
Ct, 10 ⁻⁶ psi	8.72		
RESERVOIR PROPERTIES			
Porosity	0.21	Formation Thickness, ft	23
Wellbore Radius, ft	0.401		
WELL TEST INFORMATION			
Type of Test	Drawdown	Date of test	01/01/90
Directory/Path	D:	Main Data file	examp41.mai
Pressure Data file	examp41.prs	Rate Data file	examp41.flr
WELLBORE ESTIMATES			
Storage, bbl/psi	1.541e-2	Cd	2033
CDe2s	3.962e8	Skin Factor	6.09
DeltaP across skin, psi	1350	Pwf, psi	2989
Flow Efficiency	0.5531		
RESERVOIR ESTIMATES			
Permeability, md	77.1	Semi-log slope, 'm'	255.2
Parameter name	cd.e ² s	Parameter value	1e10
BOUNDARY ESTIMATES			
Duration of Trans., hrs	21.6	Radius of Invest., ft	1006
PRESSURE ESTIMATES			
p*, psia	6009	p bar, psia	6009
COMMENTS			

WELL TEST ANALYSIS REPORT
 Example 4.1
 RATE AND PRESSURE DATA

RATE HISTORY

T of start	STB/day
0.00000	2500.00

PRESSURE HISTORY

T, hrs	P, psia	DeltaT	DeltaP
0.00000	6009.00		
0.00000	6009.00	0.00000	0.00000
0.01670	5867.82	0.01670	141.179
0.01933	5845.93	0.01933	163.074
0.02237	5819.44	0.02237	189.565
0.02590	5792.50	0.02590	216.502
0.02997	5765.01	0.02997	243.991
0.03469	5720.90	0.03469	288.096
0.04016	5688.36	0.04016	320.644
0.04648	5642.92	0.04648	366.079
0.05380	5587.43	0.05380	421.572
0.06227	5521.66	0.06227	487.339
0.07207	5459.70	0.07207	549.301
0.08342	5389.75	0.08342	619.250
0.09655	5306.48	0.09655	702.519
0.11176	5211.11	0.11176	797.894
0.12935	5117.79	0.12935	891.213
0.14972	5009.74	0.14972	999.256
0.17330	4886.13	0.17330	1122.88
0.20058	4769.13	0.20058	1239.87
0.23217	4635.16	0.23217	1373.84
0.26872	4501.08	0.26872	1507.92
0.31103	4365.85	0.31103	1643.15
0.36001	4219.70	0.36001	1789.30
0.41669	4089.84	0.41669	1919.16
0.48230	3960.16	0.48230	2048.84
0.55824	3835.59	0.55824	2173.41
0.64614	3727.20	0.64614	2281.80
0.74788	3630.08	0.74788	2378.92
0.86564	3538.77	0.86564	2470.23
1.00194	3465.23	1.00194	2543.77
1.15970	3411.56	1.15970	2597.44
1.34230	3361.60	1.34230	2647.40
1.55366	3318.80	1.55366	2690.20
1.79829	3289.38	1.79829	2719.62
2.08144	3263.02	2.08144	2745.98
2.40918	3231.28	2.40918	2777.72

2.78852	3216.27	2.78852	2792.73
3.22758	3200.34	3.22758	2808.66
3.73579	3175.40	3.73579	2833.60
4.32401	3162.30	4.32401	2846.70
5.00485	3139.87	5.00485	2869.13
5.79289	3133.46	5.79289	2875.54
6.70502	3114.87	6.70502	2894.13
7.76076	3092.78	7.76076	2916.22
8.98274	3081.99	8.98274	2927.01
10.3971	3062.07	10.3971	2946.93
12.0342	3047.29	12.0342	2961.71
13.9291	3037.98	13.9291	2971.02
16.1223	3018.23	16.1223	2990.77
18.6608	3002.85	18.6608	3006.15
21.6000	2988.93	21.6000	3020.07

Example 4.2

WELL TEST ANALYSIS REPORT
Example 4.2

FLUID PROPERTIES			
Bo, bbl/STB	1.21	Viscosity, cp	0.92
Ct, 10 ⁻⁶ psi	8.72		
RESERVOIR PROPERTIES			
Porosity	0.21	Formation Thickness, ft	23
Wellbore Radius, ft	0.401		
WELL TEST INFORMATION			
Type of Test	Build-up	Date of test	01/01/90
Directory/Path	D:	Main Data file	examp42.mai
Pressure Data file	examp42x.prs	Rate Data file	examp42.flr
WELLBORE ESTIMATES			
Storage, bbl/psi	1.451e-2	Cd	1915
CDe2s	9.563e9	Skin Factor	7.712
DeltaP across skin, psi	1521	Pwf, psi	2989
Flow Efficiency	0.4964		
RESERVOIR ESTIMATES			
Permeability, md	86.63	Semi-log slope, 'm'	227.1
Eff. Producing T, hrs	21.6	Parameter name	cd.e^2s
Parameter value	1e10		
BOUNDARY ESTIMATES			
Duration of Trans., hrs	26.4	Radius of Invest., ft	1179
R of closed circle, ft	801.4		
PRESSURE ESTIMATES			
p*, psia	6009	p bar, psia	6009
COMMENTS			

WELL TEST ANALYSIS REPORT
Example 4.2
RATE AND PRESSURE DATA

RATE HISTORY

T of start	STB/day
0.00000	2500.00
21.6000	0.00000

PRESSURE HISTORY

T, hrs	P, psia	DeltaT	(T+dT)/dT	DeltaP
21.6000	2989.39			
21.6200	3156.31	0.02000	1080.98	166.917
21.6500	3384.61	0.05000	433.007	395.221
21.7000	3715.46	0.10000	216.999	726.068
21.7500	3994.55	0.15000	145.000	1005.16
21.8500	4431.29	0.25000	87.4000	1441.90
21.9477	4740.80	0.34773	63.1174	1751.41
22.1000	5068.25	0.50000	44.2000	2078.85
22.2500	5273.46	0.65000	34.2308	2284.07
22.4798	5461.40	0.87984	25.5499	2472.01
23.0249	5650.05	1.42485	16.1595	2660.65
23.5831	5722.05	1.98307	11.8922	2732.66
24.1548	5760.09	2.55483	9.45457	2770.70
24.7404	5785.22	3.14045	7.87800	2795.83
25.3403	5804.13	3.74027	6.77499	2814.74
25.9546	5819.42	4.35463	5.96024	2830.03
26.5839	5832.31	4.98389	5.33396	2842.92
27.2284	5843.45	5.62840	4.83768	2854.06
27.8885	5853.25	6.28854	4.43482	2863.85
28.5647	5861.97	6.96468	4.10136	2872.57
29.2572	5869.81	7.65722	3.82087	2880.42
29.9665	5876.91	8.36654	3.58171	2887.52
30.6931	5883.39	9.09306	3.37544	2894.00
31.4372	5889.33	9.83720	3.19575	2899.94
32.1994	5894.81	10.5994	3.03786	2905.42
32.9800	5899.87	11.3800	2.89806	2910.48
33.7796	5904.58	12.1796	2.77345	2915.19
34.5986	5908.96	12.9986	2.66172	2919.57
35.4374	5913.06	13.8374	2.56099	2923.67
36.2966	5916.90	14.6966	2.46973	2927.51
37.1766	5920.51	15.5766	2.38670	2931.12
38.0779	5923.91	16.4779	2.31085	2934.51
39.0011	5927.11	17.4011	2.24130	2937.72
39.9466	5930.14	18.3466	2.17733	2940.75
40.9151	5933.01	19.3151	2.11830	2943.61
41.9071	5935.73	20.3071	2.06367	2946.33

42.9231	5938.31	21.3231	2.01299	2948.92
43.9637	5940.76	22.3637	1.96585	2951.37
45.0296	5943.10	23.4296	1.92191	2953.71
46.1213	5945.33	24.5213	1.88087	2955.94
47.2395	5947.46	25.6395	1.84245	2958.07
48.0000	5948.82	26.4000	1.81818	2959.43

Horner producing time = 21.6



L

Example 5.1

WELL TEST ANALYSIS REPORT
Example 5.1

FLUID PROPERTIES			
Bo, bbl/STB	1.5	Viscosity, cp	0.3
Ct, 10 ⁻⁶ psi	14.8		
RESERVOIR PROPERTIES			
Porosity	0.24	Formation Thickness, ft	50
Wellbore Radius, ft	0.4		
WELL TEST INFORMATION			
Type of Test	Drawdown	Directory/Path	D:
Main Data file	examp51.mai	Pressure Data file	examp51.prs
Rate Data file	examp51.flr		
WELLBORE ESTIMATES			
Fracture half width, ft	105	Skin Factor	-4.664
DeltaP across skin, psi	-972.4	Pwf, psi	4581
Flow Efficiency	2.571		
RESERVOIR ESTIMATES			
Permeability, md	2.19	Semi-log slope, 'm'	240.1
Parameter name	(w.kf)/(xf.k)	Parameter value	10
BOUNDARY ESTIMATES			
Duration of Trans., hrs	100	Radius of Invest., ft	1082
PRESSURE ESTIMATES			
p*, psia	5200	p bar, psia	5200
COMMENTS			

02-05-1990

WELL TEST ANALYSIS REPORT
 Example 5.1
 RATE AND PRESSURE DATA

RATE HISTORY

T of start	STB/day
0.00000	2000.00

PRESSURE HISTORY

T, hrs	P, psia	DeltaT	DeltaP
0.00000	5200.00		
0.00000	5200.00	0.00000	0.00000
0.01000	5158.92	0.01000	41.0771
0.01202	5156.72	0.01202	43.2808
0.01445	5154.35	0.01445	45.6519
0.01738	5151.78	0.01738	48.2212
0.02089	5149.04	0.02089	50.9580
0.02512	5146.12	0.02512	53.8809
0.03020	5142.97	0.03020	57.0342
0.03631	5139.58	0.03631	60.4189
0.04365	5135.63	0.04365	64.3750
0.05248	5131.60	0.05248	68.4009
0.06310	5127.57	0.06310	72.4258
0.07586	5123.43	0.07586	76.5742
0.09120	5118.33	0.09120	81.6689
0.10965	5113.23	0.10965	86.7651
0.13183	5107.44	0.13183	92.5581
0.15849	5101.36	0.15849	98.6362
0.19055	5094.81	0.19055	105.193
0.22909	5087.72	0.22909	112.281
0.27542	5080.12	0.27542	119.879
0.33113	5072.01	0.33113	127.994
0.39811	5062.96	0.39811	137.041
0.47863	5053.14	0.47863	146.859
0.57544	5043.32	0.57544	156.676
0.69183	5033.51	0.69183	166.494
0.83176	5022.50	0.83176	177.502
1.00000	5010.74	1.00000	189.258
1.20226	4998.50	1.20226	201.505
1.44544	4985.55	1.44544	214.449
1.73780	4971.89	1.73780	228.113
2.08930	4957.68	2.08930	242.319
2.51189	4942.91	2.51189	257.086
3.01995	4927.61	3.01995	272.394
3.63078	4911.77	3.63078	288.226
4.36516	4895.03	4.36516	304.973
5.24808	4878.17	5.24808	321.825

6.30957	4861.32	6.30957	338.676
7.58578	4844.35	7.58578	355.646
9.12011	4826.47	9.12011	373.528
10.9648	4808.59	10.9648	391.410
13.1826	4790.31	13.1826	409.694
15.8489	4771.89	15.8489	428.108
19.0546	4753.29	19.0546	446.711
22.9087	4734.54	22.9087	465.460
27.5423	4715.66	27.5423	484.338
33.1131	4696.68	33.1131	503.323
39.8107	4677.57	39.8107	522.428
47.8630	4658.38	47.8630	541.624
57.5440	4639.18	57.5440	560.820
69.1831	4619.98	69.1831	580.016
83.1764	4600.70	83.1764	599.296
100.000	4581.37	100.000	618.629

Example 5.2

WELL TEST ANALYSIS REPORT

Example 5.2

FLUID PROPERTIES			
Bo, bbl/STB	1.5	Viscosity, cp	0.3
Ct, 10 ⁻⁶ psi	14.8		
RESERVOIR PROPERTIES			
Porosity	0.24	Formation Thickness, ft	50
Wellbore Radius, ft	0.4		
WELL TEST INFORMATION			
Type of Test	Drawdown	Directory/Path	D:
Main Data file	examp52.mai	Pressure Data file	examp52.prs
Rate Data file	examp52.flr		
WELLBORE ESTIMATES			
Fracture half width, ft	105	Pwf, psi	4616
Flow Efficiency	1		
RESERVOIR ESTIMATES			
Permeability, md	12	Semi-log slope, 'm'	243.9
Parameter name	(w.kf)/(xf.k)	Parameter value	136.5
BOUNDARY ESTIMATES			
Duration of Trans., hrs	100	Radius of Invest., ft	1074
PRESSURE ESTIMATES			
p*, psia	5200	p bar, psia	5200
COMMENTS			

02-05-1990

WELL TEST ANALYSIS REPORT
 Example 5.2
 RATE AND PRESSURE DATA

RATE HISTORY

T of start	STB/day
0.00000	2000.00

PRESSURE HISTORY

T, hrs	P, psia	DeltaT	DeltaP
0.00000	5200.00		
0.00000	5200.00	0.00000	0.00000
0.01000	5180.52	0.01000	19.4839
0.01202	5178.64	0.01202	21.3638
0.01445	5176.58	0.01445	23.4229
0.01738	5174.32	0.01738	25.6782
0.02089	5171.85	0.02089	28.1450
0.02512	5169.16	0.02512	30.8398
0.03020	5166.22	0.03020	33.7759
0.03631	5163.03	0.03631	36.9668
0.04365	5159.57	0.04365	40.4258
0.05248	5155.84	0.05248	44.1641
0.06310	5151.81	0.06310	48.1909
0.07586	5147.48	0.07586	52.5200
0.09120	5142.84	0.09120	57.1631
0.10965	5137.87	0.10965	62.1318
0.13183	5132.56	0.13183	67.4438
0.15849	5126.88	0.15849	73.1172
0.19055	5120.83	0.19055	79.1719
0.22909	5114.37	0.22909	85.6348
0.27542	5107.47	0.27542	92.5332
0.33113	5100.10	0.33113	99.8979
0.39811	5092.23	0.39811	107.768
0.47863	5083.82	0.47863	116.183
0.57544	5074.81	0.57544	125.185
0.69183	5065.18	0.69183	134.817
0.83176	5054.88	0.83176	145.121
1.00000	5043.87	1.00000	156.127
1.20226	5032.14	1.20226	167.858
1.44544	5019.68	1.44544	180.320
1.73780	5006.49	1.73780	193.506
2.08930	4992.61	2.08930	207.394
2.51189	4978.05	2.51189	221.947
3.01995	4962.88	3.01995	237.121
3.63078	4947.13	3.63078	252.866
4.36516	4930.87	4.36516	269.126
5.24808	4914.15	5.24808	285.847

6.30957	4897.02	6.30957	302.975
7.58578	4879.54	7.58578	320.458
9.12011	4861.75	9.12011	338.251
10.9648	4843.69	10.9648	356.309
13.1826	4825.40	13.1826	374.596
15.8489	4806.92	15.8489	393.078
19.0546	4788.28	19.0546	411.724
22.9087	4769.49	22.9087	430.511
27.5423	4750.58	27.5423	449.416
33.1131	4731.58	33.1131	468.420
39.8107	4712.49	39.8107	487.508
47.8630	4693.33	47.8630	506.665
57.5440	4674.12	57.5440	525.882
69.1831	4654.85	69.1831	545.147
83.1764	4635.55	83.1764	564.454
100.000	4616.21	100.000	583.795

Example 6.1

WELL TEST ANALYSIS REPORT
Example 6.1 - no storage

FLUID PROPERTIES			
Bo, bbl/STB	1	Viscosity, cp	0.3
Ct, 10 ⁻⁶ psi	3		
RESERVOIR PROPERTIES			
Porosity	3.33e-2	Formation Thickness, ft	12
Wellbore Radius, ft	0.29		
WELL TEST INFORMATION			
Type of Test	Drawdown	Main Data file	examp61.mai
Pressure Data file	examp61a.prs	Rate Data file	examp61.flr
WELLBORE ESTIMATES			
Storage, bbl/psi	1.124e-12	Cd	9.962e-6
CDe2s	1.799e-7	Skin Factor	-2.007
DeltaP across skin, psi	-17.69	Pwf, psi	918.5
Flow Efficiency	1.209		
RESERVOIR ESTIMATES			
Permeability, md	498.7	Semi-log slope, 'm'	10.15
Omega	0.1064	Lambda	6.646e-9
BOUNDARY ESTIMATES			
Duration of Trans., hrs	100	Radius of Invest., ft	4.128e4
PRESSURE ESTIMATES			
p*, psia	1003	p bar, psia	1003
COMMENTS			

02-03-1990

WELL TEST ANALYSIS REPORT
 Example 6.1 - no storage
 RATE AND PRESSURE DATA

RATE HISTORY

T of start	STB/day
0.00000	1245.00

PRESSURE HISTORY

T, hrs	P, psia	DeltaT	DeltaP
0.00000	1003.18		
0.00000	1003.18	0.00000	0.00000
0.01000	949.359	0.01000	53.8167
0.01111	948.954	0.01111	54.2224
0.01445	947.546	0.01445	55.6299
0.01606	947.113	0.01606	56.0630
0.02089	946.487	0.02089	56.6886
0.02322	945.291	0.02322	57.8855
0.03020	944.966	0.03020	58.2104
0.03356	944.596	0.03356	58.5802
0.04365	943.456	0.04365	59.7196
0.04851	942.387	0.04851	60.7893
0.06310	941.773	0.06310	61.4032
0.07012	941.839	0.07012	61.3369
0.09120	940.853	0.09120	62.3232
0.10136	940.085	0.10136	63.0909
0.13183	939.847	0.13183	63.3287
0.14651	939.445	0.14651	63.7307
0.19055	937.911	0.19055	65.2650
0.21177	938.539	0.21177	64.6367
0.27542	937.355	0.27542	65.8214
0.30609	937.299	0.30609	65.8770
0.39811	937.060	0.39811	66.1165
0.44244	936.173	0.44244	67.0033
0.57544	936.320	0.57544	66.8565
0.63952	936.049	0.63952	67.1270
0.83176	935.523	0.83176	67.6535
0.92439	935.702	0.92439	67.4744
1.20226	935.339	1.20226	67.8366
1.33615	934.784	1.33615	68.3917
1.73780	934.319	1.73780	68.8568
1.93132	934.651	1.93132	68.5248
2.51189	934.029	2.51189	69.1466
2.79161	933.515	2.79161	69.6606
3.63078	933.140	3.63078	70.0359
4.03510	932.724	4.03510	70.4525
5.24808	931.118	5.24808	72.0580

5.83250	931.190	5.83250	71.9862
7.58578	930.434	7.58578	72.7421
8.43053	929.262	8.43053	73.9140
10.9648	928.436	10.9648	74.7403
12.1858	927.551	12.1858	75.6252
15.8489	927.292	15.8489	75.8836
17.6139	926.503	17.6139	76.6725
22.9087	924.681	22.9087	78.4950
25.4598	924.773	25.4598	78.4027
33.1131	923.135	33.1131	80.0410
36.8006	922.671	36.8006	80.5051
47.8630	922.204	47.8630	80.9716
53.1930	921.223	53.1930	81.9529
69.1831	919.822	69.1831	83.3537
76.8873	919.606	76.8873	83.5704
100.000	918.530	100.000	84.6462

Example 6.1 (a)

WELL TEST ANALYSIS REPORT
Example 6.1 - with storage

FLUID PROPERTIES			
Bo, bbl/STB	1	Viscosity, cp	0.3
Ct, 10 ⁻⁶ psi	3		
RESERVOIR PROPERTIES			
Porosity	3.33e-2	Formation Thickness, ft	12
Wellbore Radius, ft	0.29		
WELL TEST INFORMATION			
Type of Test	Drawdown	Directory/Path	C:
Main Data file	examp61b.mai	Pressure Data file	examp61b.prs
Rate Data file	examp61.flr		
WELLBORE ESTIMATES			
Storage, bbl/psi	0.1021	Cd	9.05e5
CDe2s	3.46e4	Skin Factor	-1.632
DeltaP across skin, psi	-13.78	Pwf, psi	918.3
Flow Efficiency	1.163		
RESERVOIR ESTIMATES			
Permeability, md	520.4	Semi-log slope, 'm'	9.725
Omega	6.818e-2	Lambda	9.187e-9
BOUNDARY ESTIMATES			
Duration of Trans., hrs	100	Radius of Invest., ft	4.217e4
PRESSURE ESTIMATES			
p*, psia	1003	p bar, psia	1003
COMMENTS			

02-03-1990

WELL TEST ANALYSIS REPORT
 Example 6.1 - with storage
 RATE AND PRESSURE DATA

RATE HISTORY

T of start	STB/day
0.00000	1245.00

PRESSURE HISTORY

T, hrs	P, psia	DeltaT	DeltaP
0.00000	1002.61		
0.00000	1002.61	0.00000	0.00000
0.01000	997.664	0.01000	4.94751
0.01445	995.634	0.01445	6.97723
0.02089	992.771	0.02089	9.83954
0.03020	988.992	0.03020	13.6188
0.04365	984.125	0.04365	18.4858
0.06310	977.709	0.06310	24.9016
0.09120	970.368	0.09120	32.2431
0.13183	962.072	0.13183	40.5393
0.19055	953.743	0.19055	48.8680
0.27542	946.352	0.27542	56.2586
0.39811	941.058	0.39811	61.5531
0.57544	937.854	0.57544	64.7574
0.83176	936.121	0.83176	66.4901
1.20226	935.123	1.20226	67.4878
1.73780	934.516	1.73780	68.0948
2.51189	933.647	2.51189	68.9638
3.63078	932.406	3.63078	70.2055
5.24808	931.280	5.24808	71.3310
7.58578	929.681	7.58578	72.9298
10.9648	928.121	10.9648	74.4897
15.8489	926.529	15.8489	76.0824
22.9087	924.734	22.9087	77.8770
33.1131	923.194	33.1131	79.4167
47.8630	921.528	47.8630	81.0829
69.1831	919.857	69.1831	82.7545
100.000	918.287	100.000	84.3243

Example 6.2

WELL TEST ANALYSIS REPORT
Example 6.2 - Buildup

FLUID PROPERTIES			
Bo, bbl/STB	1	Viscosity, cp	0.3
Ct, 10 ⁻⁶ psi	3		
RESERVOIR PROPERTIES			
Porosity	3.33e-2	Formation Thickness, ft	12
Wellbore Radius, ft	0.29		
WELL TEST INFORMATION			
Type of Test	Build-up	Main Data file	examp62.mai
Pressure Data file	examp62.prs	Rate Data file	examp62.flr
WELLBORE ESTIMATES			
Storage, bbl/psi	3.376e-15	Cd	2.992e-8
CDe2s	5.437e-10	Skin Factor	-2.004
DeltaP across skin, psi	-17.67	Pwf, psi	962.7
Flow Efficiency	1.223		
RESERVOIR ESTIMATES			
Permeability, md	498.5	Semi-log slope, 'm'	10.15
Eff. Producing T, hrs	25	Omega	0.1409
Lambda	8.03e-10		
BOUNDARY ESTIMATES			
Duration of Trans., hrs	100	Radius of Invest., ft	4.127e4
PRESSURE ESTIMATES			
p*, psia	1042	p bar, psia	1042
COMMENTS			

02-04-1990

WELL TEST ANALYSIS REPORT
 Example 6.2 - Buildup
 RATE AND PRESSURE DATA

 RATE HISTORY

T of start	STB/day
0.00000	1245.00
25.0000	0.00000

 PRESSURE HISTORY

T, hrs	P, psia	DeltaT	(T+dT)/dT	DeltaP
25.0000	962.393			
25.5523	1031.83	0.55233	46.2628	69.4420
26.1108	1034.27	1.11077	23.5069	71.8810
26.6754	1035.49	1.67538	15.9220	73.0989
27.2462	1036.23	2.24622	12.1298	73.8420
27.8234	1036.73	2.82336	9.85470	74.3391
28.4069	1037.08	3.40689	8.33807	74.6920
28.9969	1037.35	3.99686	7.25491	74.9529
29.5933	1037.55	4.59335	6.44265	75.1540
30.1964	1037.70	5.19642	5.81100	75.3120
30.8062	1037.83	5.80616	5.30577	75.4400
31.4226	1037.94	6.42263	4.89249	75.5469
32.0459	1038.03	7.04592	4.54815	75.6370
32.6761	1038.11	7.67608	4.25687	75.7160
33.3132	1038.18	8.31321	4.00726	75.7859
33.9574	1038.24	8.95738	3.79100	75.8489
34.6087	1038.30	9.60867	3.60182	75.9059
35.2671	1038.35	10.2671	3.43495	75.9590
35.9329	1038.40	10.9329	3.28668	76.0090
36.6060	1038.45	11.6060	3.15406	76.0569
37.2865	1038.49	12.2865	3.03475	76.1020
37.9746	1038.54	12.9746	2.92684	76.1450
38.6703	1038.58	13.6703	2.82879	76.1880
39.3736	1038.62	14.3736	2.73930	76.2289
40.0847	1038.66	15.0847	2.65731	76.2690
40.8037	1038.70	15.8037	2.58191	76.3080
41.5306	1038.74	16.5306	2.51234	76.3470
42.2656	1038.78	17.2656	2.44797	76.3849
43.0086	1038.81	18.0086	2.38822	76.4219
43.7599	1038.85	18.7599	2.33263	76.4590
44.5195	1038.89	19.5195	2.28077	76.4949
45.2874	1038.92	20.2874	2.23229	76.5309
46.0639	1038.96	21.0639	2.18687	76.5670
46.8489	1038.99	21.8489	2.14422	76.6020
47.6426	1039.03	22.6426	2.10411	76.6360
48.4450	1039.06	23.4450	2.06632	76.6710

49.2564	1039.10	24.2564	2.03066	76.7050
50.0766	1039.13	25.0766	1.99694	76.7380
50.9060	1039.17	25.9060	1.96503	76.7720
51.7445	1039.20	26.7445	1.93477	76.8050
52.5923	1039.23	27.5923	1.90605	76.8370
53.4494	1039.26	28.4494	1.87875	76.8690
54.3160	1039.29	29.3160	1.85278	76.9009
55.1922	1039.33	30.1922	1.82803	76.9330
56.0781	1039.36	31.0781	1.80443	76.9641
56.9737	1039.39	31.9737	1.78189	76.9949
57.8792	1039.42	32.8792	1.76036	77.0250
58.7948	1039.45	33.7948	1.73976	77.0550
59.7204	1039.48	34.7204	1.72004	77.0850
60.6563	1039.51	35.6563	1.70114	77.1140
61.6025	1039.54	36.6025	1.68301	77.1430
62.5592	1039.56	37.5592	1.66562	77.1719
63.5265	1039.59	38.5265	1.64890	77.2010
64.5044	1039.62	39.5044	1.63284	77.2289
65.4931	1039.65	40.4931	1.61739	77.2560
66.4928	1039.68	41.4928	1.60251	77.2840
67.5034	1039.70	42.5034	1.58819	77.3100
68.5253	1039.73	43.5253	1.57438	77.3370
69.5584	1039.76	44.5584	1.56106	77.3630
70.6030	1039.78	45.6030	1.54821	77.3890
71.6591	1039.81	46.6591	1.53580	77.4150
72.7269	1039.83	47.7269	1.52381	77.4400
73.8064	1039.86	48.8064	1.51223	77.4650
74.8979	1039.88	49.8979	1.50102	77.4890
76.0014	1039.91	51.0014	1.49018	77.5140
77.1172	1039.93	52.1172	1.47969	77.5380
78.2452	1039.95	53.2452	1.46953	77.5610
79.3858	1039.98	54.3858	1.45968	77.5840
80.5389	1040.00	55.5389	1.45014	77.6070
81.7047	1040.02	56.7047	1.44088	77.6299
82.8835	1040.05	57.8835	1.43190	77.6520
84.0752	1040.07	59.0752	1.42319	77.6740
85.2801	1040.09	60.2801	1.41473	77.6950
86.4984	1040.11	61.4984	1.40651	77.7170
87.7301	1040.13	62.7301	1.39853	77.7380
88.9753	1040.15	63.9753	1.39078	77.7580
90.2344	1040.17	65.2344	1.38323	77.7790
91.5074	1040.19	66.5074	1.37590	77.7990
92.7944	1040.21	67.7944	1.36876	77.8181
94.0956	1040.23	69.0956	1.36182	77.8380
95.4112	1040.25	70.4112	1.35506	77.8570
96.7414	1040.27	71.7414	1.34847	77.8760
98.0862	1040.29	73.0862	1.34206	77.8940
99.4459	1040.31	74.4459	1.33581	77.9130
100.821	1040.32	75.8206	1.32973	77.9310
102.211	1040.34	77.2105	1.32379	77.9479
103.616	1040.36	78.6158	1.31800	77.9660
105.037	1040.38	80.0366	1.31236	77.9830
106.473	1040.39	81.4730	1.30685	77.9999
107.925	1040.41	82.9254	1.30148	78.0161

109.394	1040.43	84.3938	1.29623	78.0330
110.878	1040.44	85.8784	1.29111	78.0490
112.379	1040.46	87.3794	1.28611	78.0650
113.897	1040.47	88.8970	1.28122	78.0800
115.431	1040.49	90.4313	1.27645	78.0960
116.983	1040.50	91.9826	1.27179	78.1110
118.551	1040.52	93.5511	1.26723	78.1260
120.137	1040.53	95.1368	1.26278	78.1411
121.740	1040.55	96.7401	1.25842	78.1550
125.000	1040.58	100.000	1.25000	78.1830

Horner producing time = 25

Example 7.1

WELL TEST ANALYSIS REPORT
Example 7.1 (Interference)

FLUID PROPERTIES			
Bo, bbl/STB	1	Viscosity, cp	0.115
Ct, 10 ⁻⁶ psi	8.84		
RESERVOIR PROPERTIES			
Porosity	1	Formation Thickness, ft	1000
Wellbore Radius, ft	0.33		
WELL TEST INFORMATION			
Type of Test	Interference	Directory/Path	D:
Main Data file	examp71.mai	Pressure Data file	examp71.prs
Rate Data file	examp71.flr		
WELLBORE ESTIMATES			
Pwf, psi	173.3	Flow Efficiency	1
RESERVOIR ESTIMATES			
Permeability, md	640.4	Semi-log slope, 'm'	1.118
Eff. Producing T, hrs	1176		
BOUNDARY ESTIMATES			
Duration of Trans., hrs	384	Radius of Invest., ft	1.574e4
PRESSURE ESTIMATES			
p*, psia	175.2	p bar, psia	175.2
COMMENTS			

WELL TEST ANALYSIS REPORT
Example 7.1 (Interference)
RATE AND PRESSURE DATA

RATE HISTORY

T of start	STB/day
144.000	23518.4
576.000	23301.1
1008.00	38292.1
1176.00	0.00000

PRESSURE HISTORY

T, hrs	P, psia	DeltaT	DeltaP
1176.00	173.328		
1176.00	173.328	0.00000	0.00000
1200.00	173.636	24.0000	0.30870
1212.00	173.989	36.0000	0.66150
1224.00	174.136	48.0000	0.80850
1248.00	174.092	72.0000	0.76440
1272.00	174.327	96.0000	0.99960
1296.00	174.210	120.000	0.88200
1320.00	174.327	144.000	0.99960
1344.00	174.415	168.000	1.08780
1368.00	174.592	192.000	1.26421
1392.00	174.607	216.000	1.27890

Example 7.2

WELL TEST ANALYSIS REPORT
Example 7.2

FLUID PROPERTIES			
Bo, bbl/STB	1	Viscosity, cp	1
Ct, 10 ⁻⁶ psi	9		
RESERVOIR PROPERTIES			
Porosity	1	Formation Thickness, ft	45
Wellbore Radius, ft	0.25		
WELL TEST INFORMATION			
Type of Test	Interference	Date of test	09/18-85
Directory/Path	D:	Main Data file	examp72.mai
Pressure Data file	examp72.prs	Rate Data file	examp72.flr
RESERVOIR ESTIMATES			
Permeability, md	5.508	Semi-log slope, 'm'	111.5
Eff. Producing T, hrs	48		
BOUNDARY ESTIMATES			
Duration of Trans., hrs	48	Radius of Invest., ft	173.4
PRESSURE ESTIMATES			
p bar, psia	0		
COMMENTS			

02-05-1990

WELL TEST ANALYSIS REPORT
Example 7.2
RATE AND PRESSURE DATA

RATE HISTORY

T of start	STB/day
0.00000	-170.000
48.0000	0.00000

PRESSURE HISTORY

T, hrs	P, psia	DeltaT	DeltaP
0.00000	0.00000		
0.00000	0.00000	0.00000	0.00000
4.30000	22.0000	4.30000	22.0000
21.6000	82.0000	21.6000	82.0000
28.2000	95.0000	28.2000	95.0000
45.0000	119.000	45.0000	119.000
51.0000	109.000	51.0000	109.000
69.0000	55.0000	69.0000	55.0000
73.0000	47.0000	73.0000	47.0000
93.0000	32.0000	93.0000	32.0000
142.000	16.0000	142.000	16.0000
148.000	15.0000	148.000	15.0000

Example 8.1

WELL TEST ANALYSIS REPORT (GAS)

Example 8.1

FLUID PROPERTIES			
Gas Specific Gravity	0.7	Bg, bbl/Mscf	1.063
Viscosity, cp	1.68e-2	Ct, 10 ⁻⁶ psi	539.7
Pseudo-critical T, R	383	Pseudo-critical P, psi	664.4
RESERVOIR PROPERTIES			
Porosity	0.25	Formation Thickness, ft	100
Wellbore Radius, ft	0.333		
WELL TEST INFORMATION			
Type of Test	Multi-rate	Directory/Path	D:
Main Data file	examp81.mai	Pressure Data file	examp81.prs
Rate Data file	examp81.flr		
Pseudo-Pressure file			examp81.psp
WELLBORE ESTIMATES			
Storage, bbl/psi	0.9688	Cd	578.6
CDe2s	1.417e4	Skin Factor	1.599
DeltaP across skin, psi	130.4	Pwf, psi	1673
Flow Efficiency	0.8366		
RESERVOIR ESTIMATES			
Permeability, md	41.72	Semi-log slope, 'm'	93.93
BOUNDARY ESTIMATES			
Duration of Trans., hrs	19.93	Radius of Invest., ft	612.8
PRESSURE ESTIMATES			
p*, psia	2471	z at p*	0.7515
p bar, psia	2471	z	0.7515
p/z, psia	3288		
COMMENTS			

WELL TEST ANALYSIS REPORT (GAS)
 Example 8.1
 RATE AND PRESSURE DATA

RATE HISTORY

T of start	MSCF/day
0.00000	30000.0
4.00000	60000.0
8.00000	90000.0
12.0000	120000.
16.0000	135000.

PRESSURE HISTORY

T, hrs	P, psia	m(P)	DeltaT	Deltam(P)
0.00000		5.0903E+08		
0.00000	2471.23	5.0903E+08	0.00000	0.00000
0.02000	2444.39	4.9991E+08	0.02000	9.1161E+06
0.03000	2434.60	4.9659E+08	0.03000	1.2435E+07
0.04000	2426.10	4.9371E+08	0.04000	1.5319E+07
0.05500	2415.32	4.9007E+08	0.05500	1.8962E+07
0.07000	2406.47	4.8708E+08	0.07000	2.1952E+07
0.08000	2401.45	4.8538E+08	0.08000	2.3649E+07
0.09000	2397.01	4.8388E+08	0.09000	2.5149E+07
0.11550	2387.82	4.8078E+08	0.11550	2.8249E+07
0.18205	2373.07	4.7581E+08	0.18205	3.3214E+07
0.25526	2364.62	4.7297E+08	0.25526	3.6059E+07
0.33578	2359.36	4.7120E+08	0.33578	3.7829E+07
0.42436	2355.77	4.7000E+08	0.42436	3.9032E+07
0.52179	2353.11	4.6910E+08	0.52179	3.9923E+07
0.62897	2351.00	4.6839E+08	0.62897	4.0633E+07
0.74687	2349.21	4.6779E+08	0.74687	4.1232E+07
0.87656	2347.64	4.6727E+08	0.87656	4.1758E+07
1.01921	2346.22	4.6679E+08	1.01921	4.2233E+07
1.17614	2344.92	4.6636E+08	1.17614	4.2671E+07
1.34875	2343.70	4.6595E+08	1.34875	4.3081E+07
1.53862	2342.54	4.6556E+08	1.53862	4.3468E+07
1.74749	2341.44	4.6519E+08	1.74749	4.3837E+07
1.97723	2340.38	4.6484E+08	1.97723	4.4191E+07
2.22996	2339.36	4.6449E+08	2.22996	4.4533E+07
2.50796	2338.38	4.6416E+08	2.50796	4.4864E+07
2.81375	2337.42	4.6384E+08	2.81375	4.5185E+07
3.15013	2336.48	4.6353E+08	3.15013	4.5499E+07
3.52014	2335.57	4.6322E+08	3.52014	4.5806E+07
3.92715	2334.67	4.6292E+08	3.92715	4.6106E+07
4.05500	2270.32	4.4146E+08	4.05500	6.7564E+07
4.11550	2240.92	4.3172E+08	4.11550	7.7305E+07
4.18205	2225.06	4.2648E+08	4.18205	8.2549E+07

4.25526	2215.89	4.2346E+08	4.25526	8.5562E+07
4.33578	2210.12	4.2156E+08	4.33578	8.7463E+07
4.42436	2206.12	4.2025E+08	4.42436	8.8778E+07
4.52179	2203.09	4.1925E+08	4.52179	8.9774E+07
4.62897	2200.62	4.1844E+08	4.62897	9.0585E+07
4.74687	2198.50	4.1774E+08	4.74687	9.1284E+07
4.87656	2196.59	4.1712E+08	4.87656	9.1912E+07
5.01922	2194.83	4.1654E+08	5.01922	9.2492E+07
5.17614	2193.17	4.1599E+08	5.17614	9.3039E+07
5.34875	2191.58	4.1547E+08	5.34875	9.3560E+07
5.53862	2190.04	4.1496E+08	5.53862	9.4062E+07
5.74749	2188.54	4.1448E+08	5.74749	9.4552E+07
5.97724	2187.08	4.1400E+08	5.97724	9.5032E+07
6.22996	2185.63	4.1352E+08	6.22996	9.5505E+07
6.50796	2184.20	4.1305E+08	6.50796	9.5973E+07
6.81375	2182.78	4.1259E+08	6.81375	9.6438E+07
7.15013	2181.36	4.1213E+08	7.15013	9.6901E+07
7.52014	2179.95	4.1166E+08	7.52014	9.7364E+07
7.92715	2178.54	4.1120E+08	7.92715	9.7826E+07
8.05500	2104.10	3.8699E+08	8.05500	1.2203E+08
8.11550	2072.27	3.7674E+08	8.11550	1.3228E+08
8.18205	2055.03	3.7122E+08	8.18205	1.3781E+08
8.25526	2045.02	3.6802E+08	8.25526	1.4100E+08
8.33578	2038.67	3.6600E+08	8.33578	1.4303E+08
8.42436	2034.24	3.6458E+08	8.42436	1.4445E+08
8.52180	2030.85	3.6350E+08	8.52180	1.4553E+08
8.62897	2028.06	3.6261E+08	8.62897	1.4642E+08
8.74687	2025.63	3.6184E+08	8.74687	1.4719E+08
8.87656	2023.42	3.6114E+08	8.87656	1.4789E+08
9.01921	2021.36	3.6048E+08	9.01921	1.4854E+08
9.17614	2019.40	3.5986E+08	9.17614	1.4917E+08
9.34875	2017.50	3.5926E+08	9.34875	1.4977E+08
9.53862	2015.65	3.5867E+08	9.53862	1.5036E+08
9.74749	2013.82	3.5809E+08	9.74749	1.5093E+08
9.97723	2012.01	3.5752E+08	9.97723	1.5151E+08
10.2300	2010.21	3.5695E+08	10.2300	1.5208E+08
10.5080	2008.40	3.5638E+08	10.5080	1.5265E+08
10.8138	2006.59	3.5580E+08	10.8138	1.5323E+08
11.1501	2004.77	3.5522E+08	11.1501	1.5380E+08
11.5201	2002.93	3.5464E+08	11.5201	1.5439E+08
11.9271	2001.07	3.5405E+08	11.9271	1.5498E+08
12.0550	1913.95	3.2682E+08	12.0550	1.8220E+08
12.1155	1878.85	3.1605E+08	12.1155	1.9297E+08
12.1820	1859.77	3.1023E+08	12.1820	1.9879E+08
12.2553	1848.64	3.0688E+08	12.2553	2.0215E+08
12.3358	1841.55	3.0474E+08	12.3358	2.0429E+08
12.4244	1836.57	3.0323E+08	12.4244	2.0579E+08
12.5218	1832.74	3.0208E+08	12.5218	2.0695E+08
12.6290	1829.56	3.0112E+08	12.6290	2.0791E+08
12.7469	1826.77	3.0028E+08	12.7469	2.0875E+08
12.8766	1824.22	2.9952E+08	12.8766	2.0951E+08
13.0192	1821.82	2.9880E+08	13.0192	2.1023E+08
13.1761	1819.52	2.9811E+08	13.1761	2.1091E+08
13.3488	1817.28	2.9744E+08	13.3488	2.1158E+08

13.5386	1815.08	2.9679E+08	13.5386	2.1224E+08
13.7475	1812.89	2.9614E+08	13.7475	2.1289E+08
13.9772	1810.71	2.9548E+08	13.9772	2.1354E+08
14.2300	1808.53	2.9483E+08	14.2300	2.1420E+08
14.5080	1806.32	2.9417E+08	14.5080	2.1485E+08
14.8138	1804.09	2.9351E+08	14.8138	2.1552E+08
15.1501	1801.84	2.9284E+08	15.1501	2.1619E+08
15.5201	1799.54	2.9215E+08	15.5201	2.1688E+08
15.9271	1797.21	2.9145E+08	15.9271	2.1757E+08
16.0550	1746.37	2.7650E+08	16.0550	2.3253E+08
16.1155	1727.02	2.7086E+08	16.1155	2.3817E+08
16.1821	1716.45	2.6782E+08	16.1821	2.4121E+08
16.2553	1710.21	2.6602E+08	16.2553	2.4301E+08
16.3358	1706.13	2.6485E+08	16.3358	2.4418E+08
16.4244	1703.18	2.6400E+08	16.4244	2.4503E+08
16.5218	1700.82	2.6332E+08	16.5218	2.4571E+08
16.6290	1698.79	2.6274E+08	16.6290	2.4629E+08
16.7469	1696.95	2.6220E+08	16.7469	2.4682E+08
16.8766	1695.20	2.6170E+08	16.8766	2.4732E+08
17.0192	1693.51	2.6122E+08	17.0192	2.4781E+08
17.1761	1691.84	2.6074E+08	17.1761	2.4828E+08
17.3487	1690.17	2.6027E+08	17.3487	2.4876E+08
17.5386	1688.49	2.5979E+08	17.5386	2.4924E+08
17.7475	1686.78	2.5930E+08	17.7475	2.4972E+08
17.9772	1685.03	2.5881E+08	17.9772	2.5022E+08
18.2300	1683.23	2.5830E+08	18.2300	2.5073E+08
18.5079	1681.38	2.5777E+08	18.5079	2.5125E+08
18.8137	1679.48	2.5723E+08	18.8137	2.5180E+08
19.1501	1677.51	2.5667E+08	19.1501	2.5235E+08
19.5201	1675.47	2.5609E+08	19.5201	2.5293E+08
19.9272	1673.36	2.5549E+08	19.9272	2.5353E+08

INDEX

- | | | | |
|---------------------------------------|---------|--------------------------------------|-------------|
| 1 ½ log cycle rule | 51,68 | duration of test | 143 |
| absolute open flow potential (AOF) . | 131,134 | effective wellbore radius | 11,153 |
| active well | 121 | exponential integral | 19,121 |
| Agarwal equivalent time | 42 | falloff test | 5 |
| ambiguity | 1,84 | fault boundary | 25 |
| aquifer | 25 | finite conductivity fracture | 27 |
| average reservoir pressure | 96,97 | example | 100-105 |
| bilinear flow | 27 | flow efficiency | 13 |
| example | 102 | fracture conductivity | 102,103,106 |
| boundaries | 20 | fracture length | 26 |
| drawdown example | 80 | examples | 101,106 |
| buildup example | 93-95 | fractured wells | 26 |
| buildup test | 4 | gas properties | 148 |
| example | 91-99 | gas wells | 127-137 |
| as drawdown | 98 | example | 131 |
| in dual porosity | 118 | graphical characteristics | 43-47 |
| circular boundary | 26 | half slope | 26,44 |
| closed boundary | 21 | heterogeneities | 2 |
| conductivity | 2 | homogeneous reservoirs (examples) . | 68-69 |
| confidence intervals | 55-59 | Horner plot | 41 |
| acceptable range | 57 | Horner time | 41 |
| example | 77 | hydraulic diffusivity | 7 |
| consistent units | 9 | impulse and response | 7 |
| constant pressure boundary | 25 | infinite acting flow | 19,21,52 |
| constant rate | 43 | infinite conductivity fracture | 28 |
| damaged zone | 10 | example | 106-111 |
| Darcy's Law | 7 | initial pressure | 43,60 |
| data preparation | 52,64 | injection test | 4 |
| data sampling | 53 | interference test | 5 |
| datum pressure | 54, 96 | example | 121-126 |
| decline curves | 3 | interporosity flow | 32 |
| deconvolution (see desuperposition) | | inverse problem | 1 |
| deliverability | 1,19 | least squares | 55 |
| derivative matching | 117 | line source | 121 |
| derivative plot | 43-49 | mathematical models | 7 |
| desuperposition | 63,64 | MBH plot | 97 |
| diagnostic plot (see derivative plot) | | MDH plot (see semilog plot) | |
| differentiation interval | 49-51 | multiphase flow | 137-141 |
| diffusion | 2,3 | non-Darcy skin | 131 |
| diffusion equation | 7 | non-ideality | 64-66 |
| dimensionless variables | 8 | nonlinear regression | 55,64,78 |
| double porosity | 31 | observation well | 121 |
| example | 112-120 | oil properties | 146 |
| drainage area | 83 | oilfield units | 8 |
| drawdown test | 3 | Perrine's approach | 138 |
| example | 68-91 | pressure match | 73,122 |
| drill stem test (DST) | 6 | pressure squared | 140 |
| dual porosity (see double porosity) | | primary porosity | 127 |

pseudopressure	127
normalized	128
calculating	129
pseudosteady state	21
pseudotime	127
normalized	128
quarter slope (see bilinear flow)	
radial flow	19,21,28,44
radius of investigation	80,83
Ramey, H.J., Jr.	125
rate dependent skin	131
rectangular boundaries	39
relative permeability	139
reservoir description	2
rock properties	152
secondary porosity	31,112
semilog analysis	70
semilog plot	20
shape factor	22,23,24
simulation	75
skin effect	10
example	12
skin factor	10
negative	12
example	71
slightly compressible assumption	7
slightly compressible equation	7
steady state	25
storage coefficient (wellbore)	13,69,115,144
storativity	22
storativity ratio ω	32
superposition	36
in space	36
in time	39
test design	142-145
Theis curve	121
time datum	54,75
time match	73,122
total properties	152
transition period	22
truncated data	86
type curve match	71,72
type curves	9
uniform flux fracture	30
variable rate	43,61-63,89,124
water properties	151
wellbore radius	153
wellbore storage	13,69,115,144
example	16
characteristic	44

